The University of Hull

Use of $Mg(OH)_2$ Particles as Stabilisers in Pickering Emulsions

being a Thesis submitted for the degree of
MSc (by Research) Chemistry
at the University of Hull

by

Daniel J. Turner
BSc (University of Hull)

September 2017

Risk Assessment

All experiments were carried out in accordance with the University of Hull's Health and Safety guidelines. A full COSHH and risk assessment was carried out for each new experiment, signed by the undertaking student, supervisor and the Departmental safety officer (Dr. Tom McCreedy) before any practical work started.

Acknowledgment

I would like to thank Prof. Bernard P. Binks for his extensive supervision and AkzoNobel (Sweden) for their funding of this MSc (by Research) course. I would like to thank Dr. Magnus Jonsson and Dr. Anna Larsson Kron personally for their industrial supervision.

I also wish to express my gratitude to Dr. Timothy Prior (X-ray powder diffraction), Mr. Anthony Sinclair (SEM) and Miss Ann Lowry (SEM).

Abstract

Twenty-six different samples of magnesium hydroxide particles were formed from various reactants and under varied reaction conditions. The morphologies of the different magnesium hydroxide samples were assessed via SEM and TEM and their zeta potentials were also measured. The particles were also characterised by XRD and FT-IR. The majority of the samples were of around 150-250 nm in diameter and had either a rod-like morphology or were platelets. However, some rod-like samples grew much larger, being around 2 μm in length. Zeta potential of the samples did not greatly vary and for each of the twenty-six samples; zeta potential was in the range of 15 mV ±6 mV.

Isooctane–in–water and methyl methacrylate–in–water emulsions were produced from the samples of magnesium hydroxide. Isooctane–in–water emulsions had much better long-term stability than MMA-in-water emulsions, which underwent complete phase separation very quickly; the most stable MMA-in-water emulsion destabilised within a week. The long-term stability of MMA-in-water emulsions improved upon the addition of an electrolyte, but the emulsions destabilised within a month. Factors such as particle concentration, presence of electrolyte and temperature were varied for isooctane–in–water emulsions. Emulsions containing isooctane and MMA as the oil phase were also prepared, with varied fractions of each oil. The greater the fraction of isooctane when in mixtures with MMA, the more stable the subsequent emulsion. Contact angle measurements were conducted on brucite, raw magnesium hydroxide, proving magnesium hydroxide is hydrophilic.

Contents

1. Introduction

1.1 Magnesium hydroxide literature review

1.1.1 Background information and uses of magnesium hydroxide

Magnesium hydroxide is a non-toxic, non-corrosive, porous and thermally stable material which has tendencies to form a number of different nanostructures [1]. It is thought that nanotechnology will radically transform many industries and industrial processes in the near future.

Solid magnesium hydroxide comprising of Mg^{2+} and OH^- ions in a 1:2 ratio forms when these species are involved in a reaction together. Most commonly, a reaction such as this involves a magnesium salt and a base such as sodium, potassium or ammonium hydroxide, although, any compound containing a hydroxide species can be used.

$$Mg^{2+}_{(aq)} + 2\ OH^-_{(aq)} \rightarrow Mg(OH)_{2\ (s)} \qquad (1)$$

Magnesium hydroxide also occurs naturally in the mineral form of brucite. Brucite, discovered by Archibald Bruce, was first described in 1824. Brucite adopts the space group P-3m1 and has a number of different crystal habits, including tabular crystals, platy masses and a fibrous variety called nemalite. A sample of raw brucite can be observed in Figure 1.

Figure 1. Nemalite, the fibrous form of brucite [2].

$Mg(OH)_2$ has a number of uses in industry and also in health products. For example, suspensions of magnesium hydroxide in water are used as antacids, in deodorants and to treat canker sores. $Mg(OH)_2$ can be also used in laxatives as the magnesia suspension acts to draw fluids from the body to the bowels. Magnesium hydroxide is a smoke suppressor and a fire retardant due to its endothermic decomposition at around 330 ^oC, as outlined below.

$$Mg(OH)_2\ (s) \rightarrow MgO\ (s) + H_2O\ (g) \qquad (2)$$

The heat absorbed by the above reaction delays the ignition of the fuel and the steam produced acts to dilute combustible gases and prevents oxygen from feeding the flame. Thus each aspect of the fire triangle is retarded [3,4]. In industry, magnesium hydroxide powder is used as an alkali to neutralise acidic wastewaters and as a fire retardant in plastics, roofing and coatings [5].

Nanostructures of $Mg(OH)_2$ are currently being investigated to determine their suitability as the solid component in oil -in-water Pickering emulsions. The paper by Tan et al.[6] is the only current article discussing the use of magnesium hydroxide as a Pickering emulsifier. Upon gathering information from past studies, it is apparent that the crystals of magnesium hydroxide produced in any reaction are strongly affected by the conditions in which their synthesis is undertaken. [6-39]. Temperature, pH, concentrations of reactants and duration of reaction are all important factors to consider when carrying out a reaction to produce $Mg(OH)_2$. Different conditions resulting in different nanostructures of $Mg(OH)_2$ shall be discussed in this literature review. Different morphologies of magnesium hydroxide nanocrystals shall also be observed. The ageing process of $Mg(OH)_2$ shall be considered in this literature review.

1.1.2 Structures of magnesium hydroxide found in literature

A number of different types of reactions have been used to synthesise magnesium hydroxide crystals. Precipitation reactions [6-8, 11, 12, 28, 40], hydrothermal/ solvothermal techniques [9, 10, 15, 18, 20, 23, 30-32, 34], liquid- solid arc discharge and microwave assisted synthesis [19, 25] have all been used as novel techniques in the synthesis of magnesium hydroxide nanoparticles. Many of the above techniques lead to different morphologies of magnesium hydroxide. Although traditional $Mg(OH)_2$ has a hexagonal structure, there are a number of different possible morphologies of magnesium hydroxide available. For example, nanorods [1, 14, 18, 20, 36], nanoflowers [10, 26, 38], nanofibers [19], nanotubes [23] and nanoneedles [35] have all been synthesised in past studies as well as standard, hexagonal platelets [17, 33]. A number of the available morphologies are shown in Figure 2.

Figure 2. SEM and TEM micrographs of magnesium hydroxide particles formed in past experiments. (a) [33] and (b) [17] represent traditional magnesium hydroxide as they show hexagonal platelet structures. (c) represents magnesium hydroxide nanofibers [19], (d) is a magnesium hydroxide nanoflower [10], (e) is a TEM image of platelet like magnesium hydroxide particles which are not hexagonal [7] and (f) shows how irregular the morphology of magnesium hydroxide can be [8].

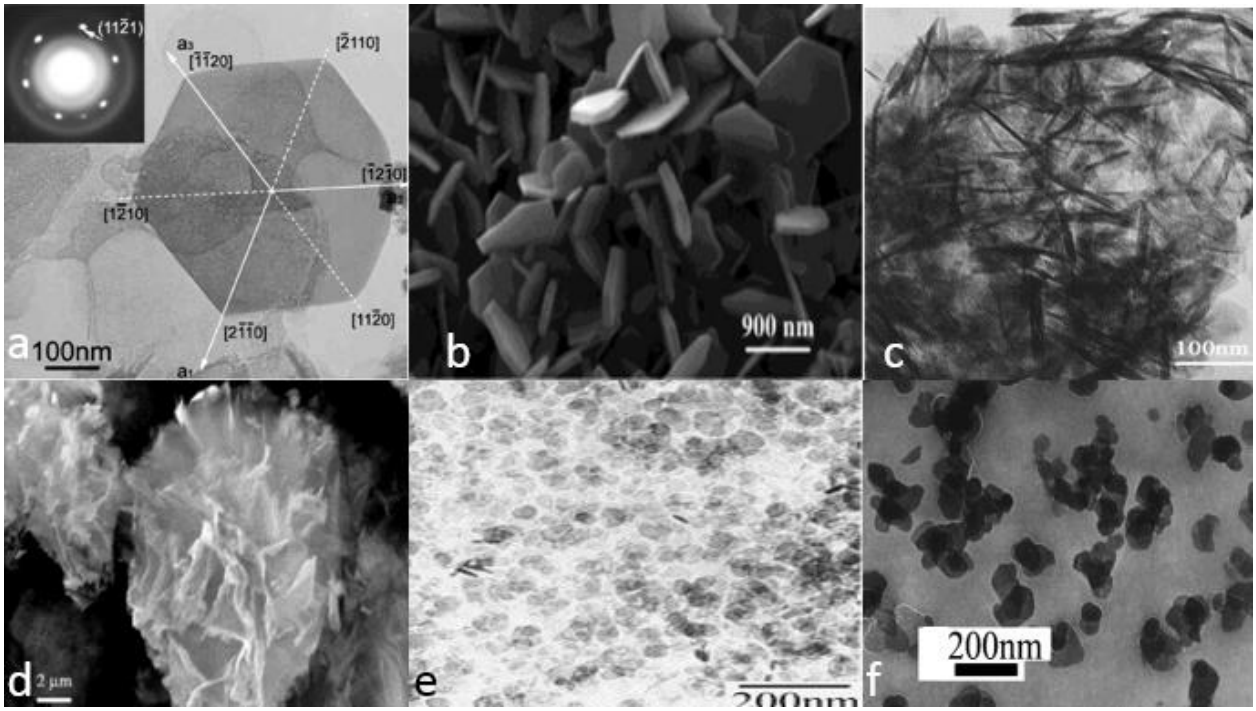

It has been difficult to find a correlation between reaction conditions and morphology of particles produced. Very similar conditions can form different products and some reactions yield a mixture of morphologies. For example, in work by Lv *et al.* [7], both lamellar and rod-like magnesium hydroxide particles are the product of one reaction. However, in an almost identical reaction conducted by Henrist *et al.*[12], only lamellar particles were produced. The magnesium hydroxide particles of Henrist *et al.* [12] also had a much greater diameter on average than the product of Lv *et al.* [7], shown in figure 3.

Figure 3. (a) Mixture of lamellar and needle-like magnesium hydroxide particles synthesised from ammonia and magnesium chloride, via a precipitation reaction, at 20 ^{o}C. [7]. (b) The lamellar produced by Henrist *et al.*[12] in a precipitation reaction between magnesium chloride and ammonia conducted at 25 ^{o}C.

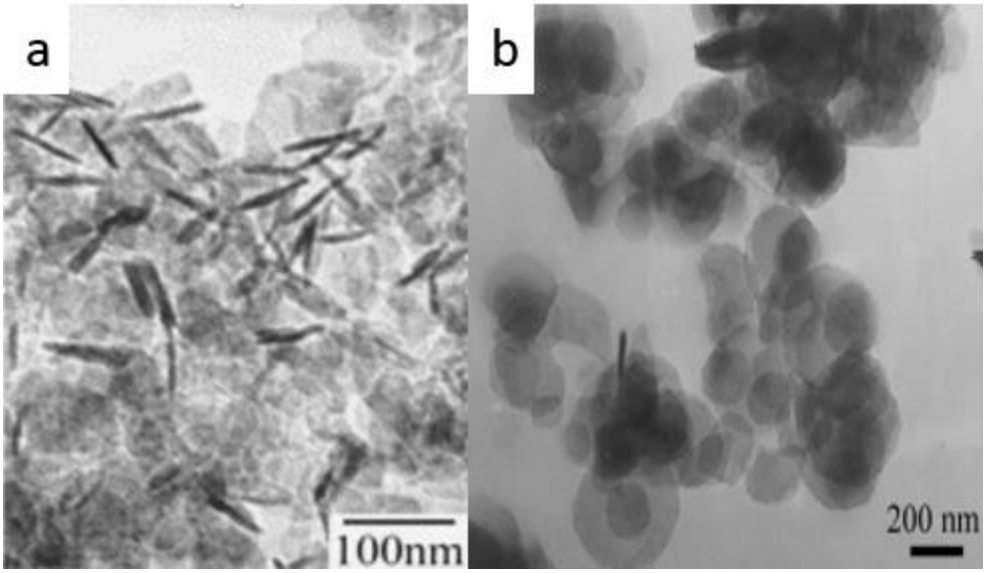

Another notable contradiction in the literature regarding the synthesis of magnesium hydroxide is when using sodium hydroxide as the base. Henrist *et al.* [12] state that the use of a strong base as a reactant will lead to globular, spherical structures due to reaction pH levels being very high and promoting aggregation of particles, as in figure 4. However, Lv *et al.* [7] successfully produced magnesium hydroxide crystals with lamellar and rod-like structures. Sodium hydroxide was also used to form magnesium hydroxide particles in the work of Tan *et al.*[6] and again the product was lamellar particles.

Figure 4. An SEM micrograph of the magnesium hydroxide particles formed by Henrist *et al.* [12] from sodium hydroxide and magnesium chloride.

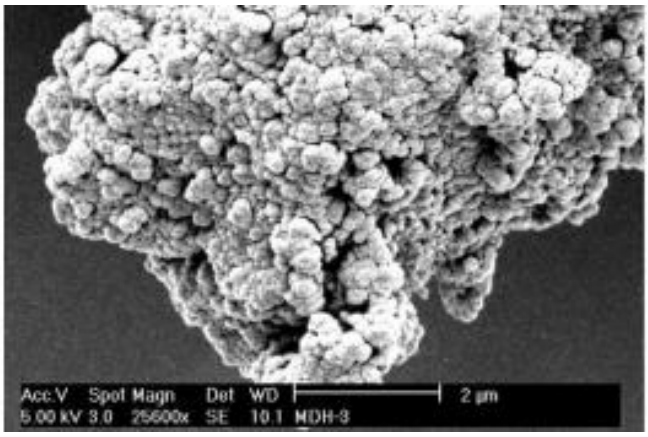

The vast quantity of different morphologies magnesium hydroxide is capable of adopting suggests that much more extensive research is required in order to understand exactly why magnesium hydroxide forms different morphologies under different reaction conditions [23]. Despite the fact there are many different morphologies available for magnesium hydroxide, X-ray diffraction patterns show that they each stem from a hexagonal unit structure which arise due to the octahedral complexes magnesium hydroxide forms, shown in Figure 5 (a).

The octahedral structures of magnesium hydroxide anions are involved in a growth mechanism, outlined in Figure 5, which leads to a product with a hexagonal crystal structure. The growth mechanism begins when a condensation reaction occurs between two hydrides belonging to two adjacent magnesium hydroxide octahedral structures, a growth unit is formed, as shown in figure 5 (a). In figure 5 (b), growth units begin to “pile up”.

Figure 5. Growth mechanism and formation process of standard magnesium hydroxide unit cells. Adapted from the work of Wu *et al.*[23] Dark spheres = Mg, light spheres = OH.

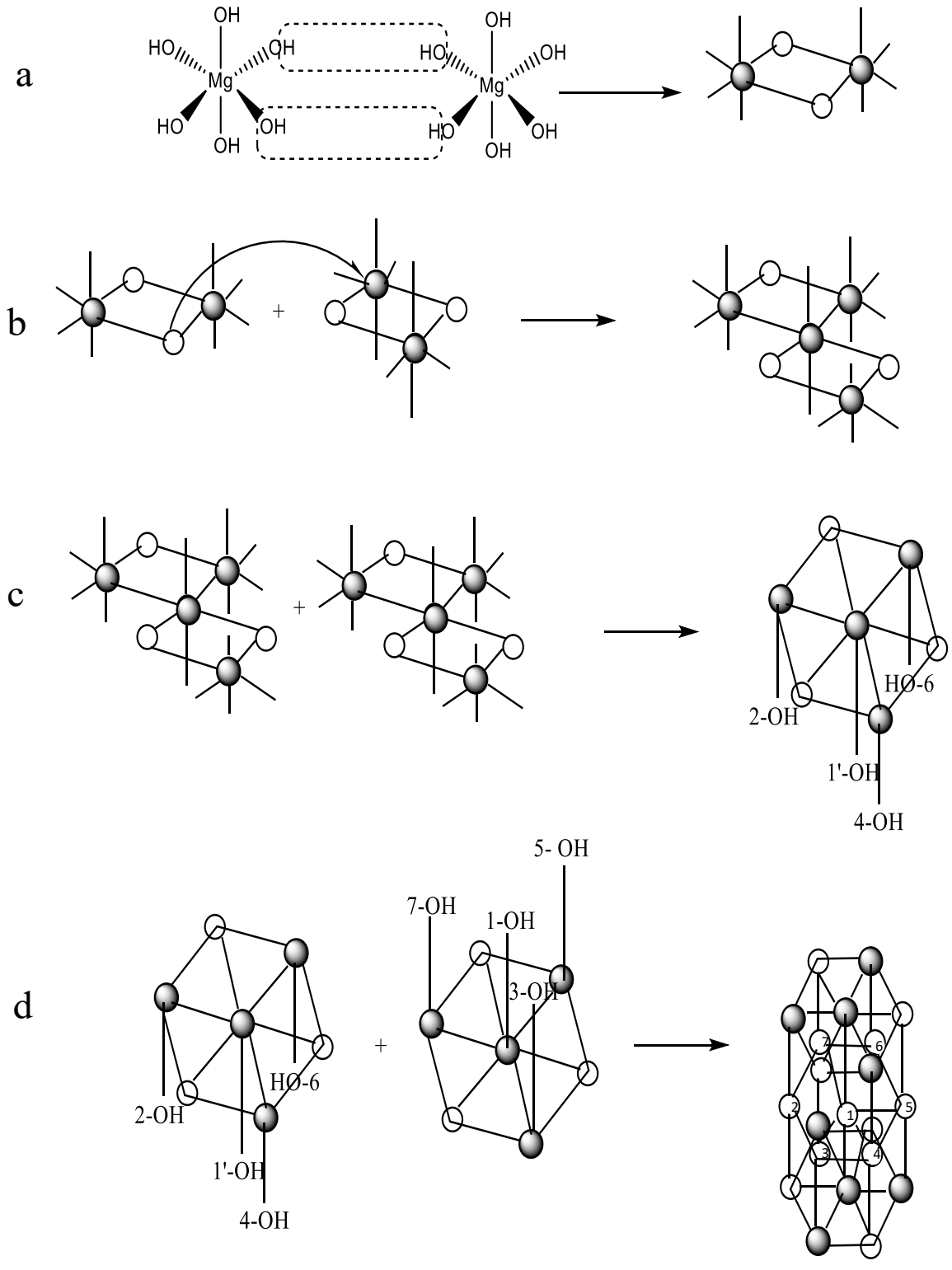

1.1.3 How reaction conditions can affect magnesium hydroxide morphology

There are many different synthesis routes which have been used to synthesise magnesium hydroxide particles. However, the precipitation of magnesium hydroxide and the reaction conditions affecting the morphology of magnesium hydroxide particles produced in this way are of great interest. A useful paper for noting how the conditions and reactants used affect the crystals formed is by Henrist *et al*.[12]. In this paper, temperature was varied, counter ion to magnesium in the magnesium salt used was varied and both a strong and weak base were used, meaning structures formed from different OH^- concentrations and pH levels were also observed. In the experiment outlined in this article, the samples were obtained by reacting a magnesium salt (0.75 mol/l) with a base (1.50 mol/l) at a controlled temperature. Both reactants were simultaneously added at 3 ml/ min into an ultrasonicated vessel, containing alkaline water (450 ml, pH 10). Once reacted, the precipitate was allowed to age in the mother liquor at synthesis temperature for one day, and at room temperature for a following two days. Vigorous stirring was applied throughout. The solid phase was then recovered via centrifugation (3500 rpm) and washed with slightly alkaline water. The samples were then air dried at 60 ^oC.

Table 1. Summary of the different methods of producing magnesium hydroxide crystals used in ref. 12 and shows the different morphologies produced.

Sample	Magnesium Salt	Base	Temperature (^oC)	Morphology
1	$MgCl_2$	NaOH	60	Large aggregates
2	$MgCl_2$	NH_4OH	60	Platelet- like (aggregated)
3	$MgCl_2$	NH_4OH	25	Circular platelets
4	$Mg(NO_3)_2$	NH_4OH	25	Circular platelets

5	$MgSO_4$	NH_4OH	25	Randomly tangled particles
6	$MgCl_2$	NH_4OH	10	Circular platelets
7	$MgCl_2$	NH_4OH	47	Circular platelets

For experiment 1, as shown in Table 1, sodium hydroxide was used to synthesise the magnesium hydroxide crystals. Sodium hydroxide is a strong base and therefore will fully dissociate, yielding more OH^- ions than the weak base ammonium hydroxide. A high OH^- concentration led to pH levels exceeding pH 13. It is documented that the isoelectric point of magnesium hydroxide is around pH 12 which means that the net residual electric charge on the surface of the magnesium hydroxide particles formed is expected to be negative. Na^+ ions, which were also of a high concentration, were attracted to the developing crystals during nucleation, hindering the entry of magnesium ions and, in turn, inhibiting crystal growth resulting in very small particles.

In the formation of sample 2, ammonium hydroxide was used as the base which led to the pH of the suspension being around pH 10, lower than the isoelectric point of magnesium hydroxide in water. This means the crystals being formed are now positively charged, and the adsorption of cations is no longer favoured. The ammonium ions do not interfere in the same way sodium ions did when the base source was NaOH, because ammonium ions are larger and are not readily adsorbed onto the crystal facets. OH^- ions adsorb onto the basal plane of the forming crystals (a plane parallel to horizontal axis) which promotes the edgewise growth of particles. Platelets with an apparent high surface area to volume ratio were the result of this reaction, with intergrowth of crystals, and the particles from experiment 2 are much larger than those formed in experiment 1. Sample 2 also has an increased nucleation rate due to high reaction temperatures. This leads to small, not well defined nuclei which agglomerate to form larger

particles, as Na^+ ions do not inhibit crystal growth during the precipitation of sample 2 as in sample 1 [12].

Sample 3, which was formed from magnesium chloride and ammonium hydroxide at room temperature, had much smaller particles than sample 2 and apparently larger particles than in sample 1. It is suggested that this could be due to the rate of nucleation in experiment 3 being slower than in experiment 1 and 2. This meant small crystals were not formed and the crystals did not need to agglomerate to compensate for a fast nucleation time. Experiments 3-5 were all used to note the influence of using different counter ions in the magnesium salt used on the magnesium hydroxide crystals formed. Sample 3 used $MgCl_2$ as the magnesium source. Using chloride ions to counter the Mg^{2+} ions is the most common method of producing magnesium hydroxide. Experiment 4 used $Mg(NO_3)_2$ as the magnesium salt. The product from experiment 4 was similar to that produced in experiment 3. Both samples contain de-agglomerated, circular platelets with similar diameter (~ 350 nm). The particles of sample 5 appear to be of a larger size compared to those in sample 3 and 4. However, the morphology looks slightly different and the platelets look thinner and are not as spherical. A possible explanation offered by Henrist *et al.* is that the sulfate ions from magnesium sulfate have weak basic properties, in turn, increasing the supersaturation of OH^- ions in the solution and increasing the rate of nucleation, in a similar way seen in the synthesis of sample 2. SEM micrographs of the magnesium hydroxide particles formed by Henrist *et al.*[12] are shown in Figure 6.

Figure 6. (a) SEM micrograph of magnesium hydroxide sample 1, synthesised from NaOH and $MgCl_2$ at 60 ^oC. (b) SEM micrograph of magnesium hydroxide sample 2, synthesied from NH_4OH and $MgCl_2$ at 60 ^oC. (c) SEM micrograph of magnesium hydroxide sample 3, synthesised from NH_4OH and $MgCl_2$ at room temperature. (d) SEM micrograph of magnesium hydroxide sample 4, synthesised from NH_4OH and $Mg(NO_3)_2$ at room temperature. (e) SEM micrograph of magnesium hydroxide sample 5, synthesised from NH_4OH and $MgSO_4$ at room temperature. (f) TEM micrograph of magnesium hydroxide sample 3. Each reaction was stoichiometric with sonication [12].

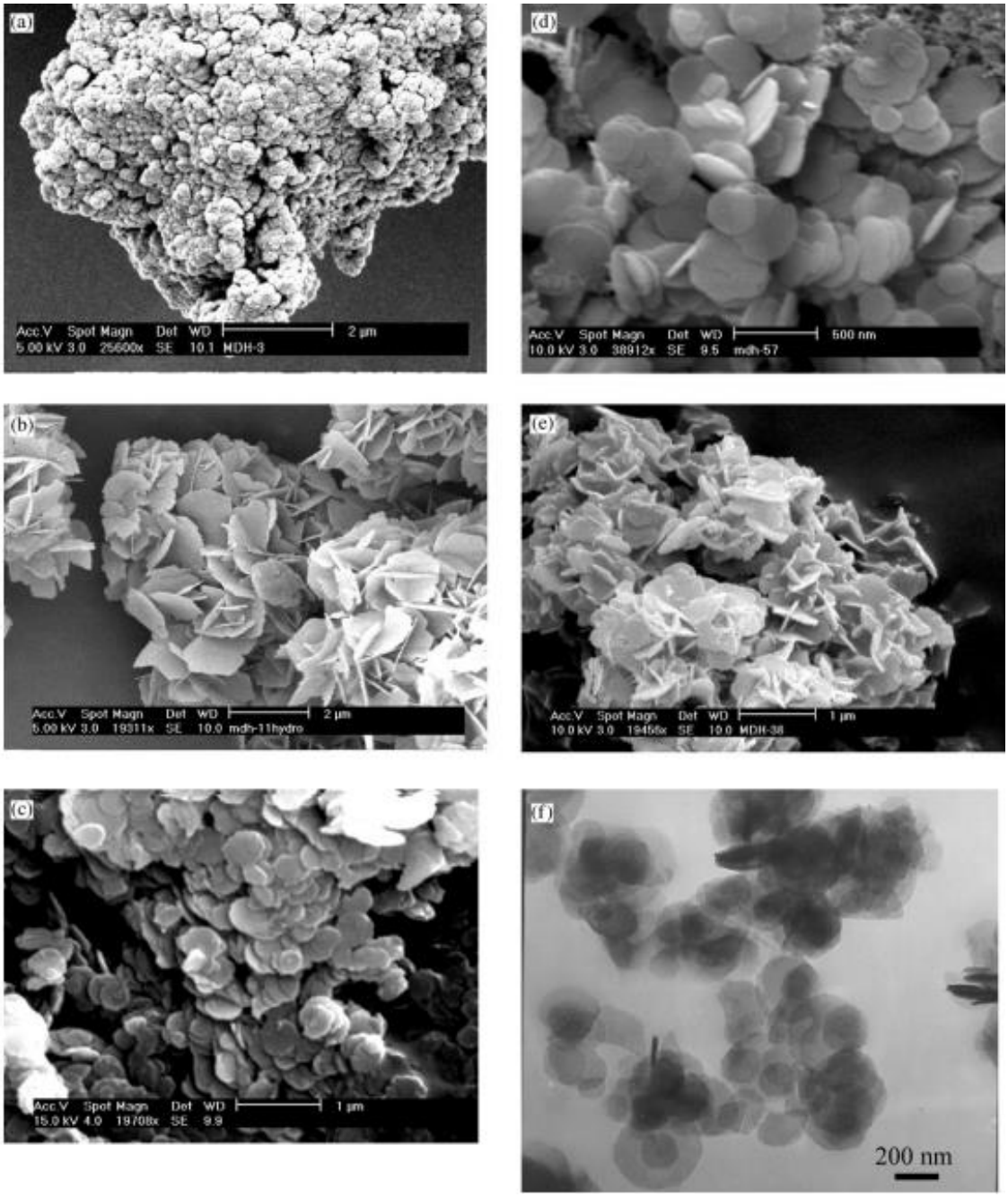

Henrist *et al.*[12] also carried out an experiment to see how reaction temperature affected the size and morphology of magnesium hydroxide particles. It has been noted through observations of the particles of sample 2 and 3 that at temperatures of around 60 ^{o}C, particles with a greater diameter were formed. However, from 10 ^{o}C to 47 ^{o}C, little variation in morphology, size and size distribution curve for these samples is observed, shown if Figure 7.

Figure 7. Size distribution curves for magnesium hydroxide particles formed at various temperatures, obtained with the use of a Malvern Mastersizer Hydro2000S granulometer[12].

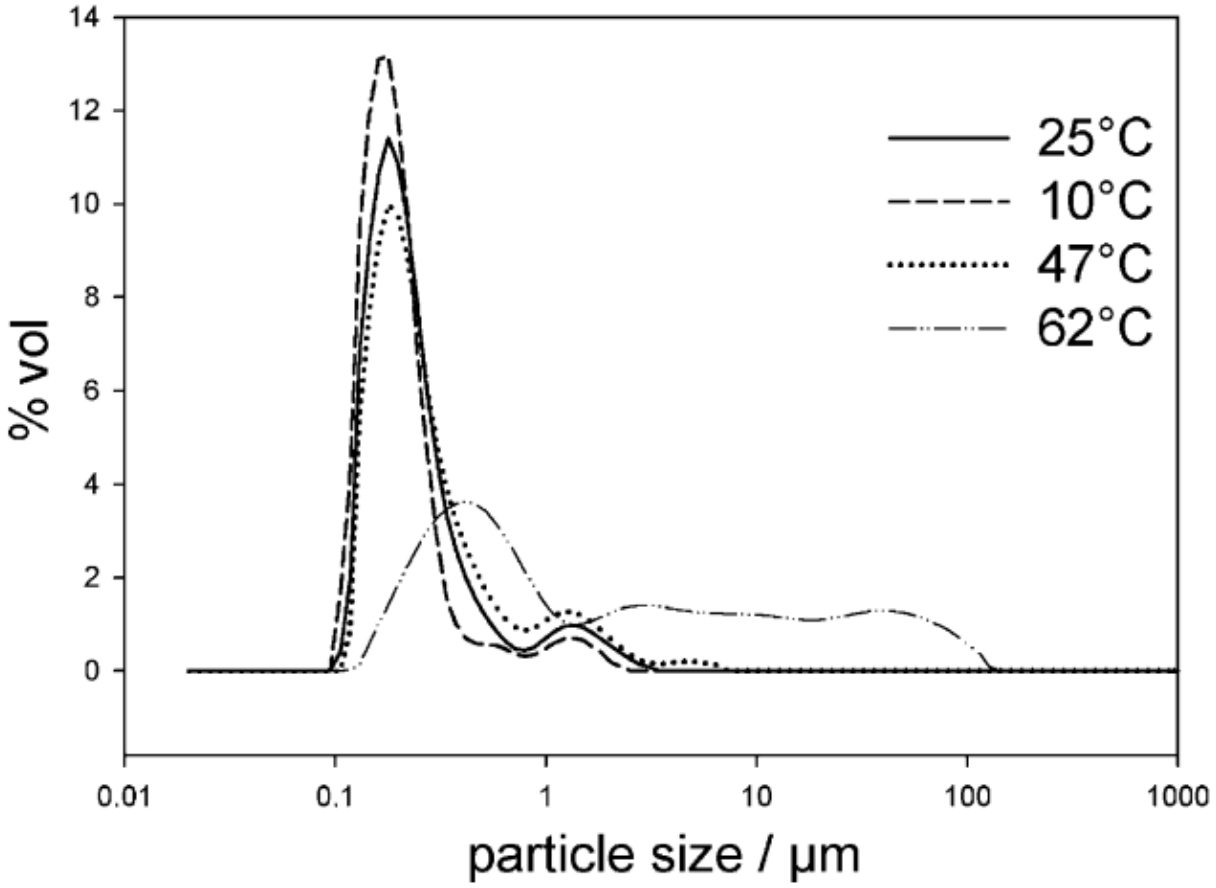

Figure 7 shows the sample formed at 62 ^{o}C has a greater average particle size (diameter) and also a greater size distribution than the samples formed at lower temperatures. From 10 ^{o}C to 50 ^{o}C, reaction temperature does not appear to have a great effect on sample morphology or size. The instrument used to assess particle size distribution in this study, the Malvern Mastersizer Hydro2000S utilises dynamic light scattering in order to measure particle size and assumes that all particles are perfect spheres. In the case that particles are not spherical, the data gathered may indicate the sample is more polydisperse than it actually is, particularly if the particles have faces of different lengths.

The work of Lv *et al.*[7] also notes that reaction temperature has an effect on particle morphology. The temperatures in this study were lower than the reaction temperatures quoted in Henrist *et al.* [12]. In the article by Lv *et al.*[7] at temperatures of 2 ^{o}C, magnesium hydroxide had a needle-like morphology with a very small surface area. As temperature was increased to 10 ^{o}C, a rod-like morphology is observed and upon further increase in temperature to 20 ^{o}C, lamellar and rod-like particles form. This suggests that at temperatures below 20 ^{o}C, crystal growth is not equal in all planes. The temperature of reaction can also affect the crystallinity of the magnesium hydroxide particles produced, see Figure 8. Where (a) has been formed at a higher temperature and is more crystalline.

Figure 8. An XRD pattern produced by $Mg(OH)_2$ crystals formed at different temperatures, but the same pH (9.5), (a) 115 ^{o}C and (b) 95 ^{o}C. [10]

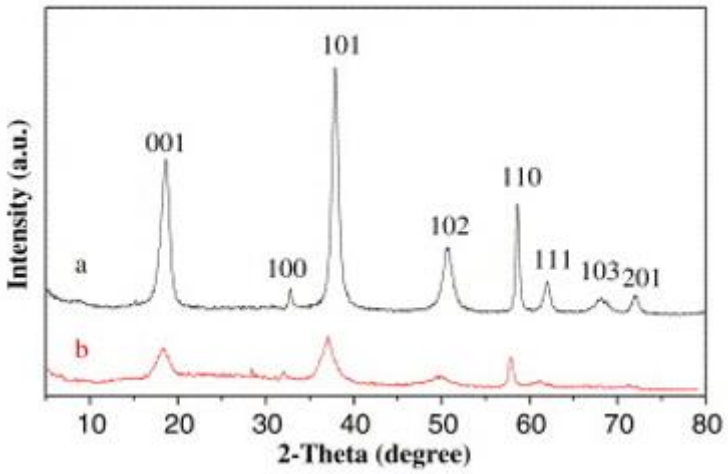

1.1.4 Ageing of $Mg(OH)_2$

It has been documented in a number of research papers, most notably in work by Mullin *et al.* [40], that Ostwald ripening is a major factor in the ageing of $Mg(OH)_2$ particles. The objective of their paper was to identify causes behind the ageing of magnesium hydroxide crystals and to further explore the nature of the ageing process. To achieve this, magnesium chloride (200 ml) and sodium hydroxide (200 ml) were added to each other rapidly at 25 ^{o}C and left to react for 24 hours. Three different concentrations of the reactants, in stoichiometric ratio were used, giving $Mg(OH)_2$ concentrations of 12.5 mol m^{-3}, 25 mol m^{-3} and 50 mol m^{-3} respectively after reaction. The precipitating solution was agitated with a four blade paddle impeller located in the centre of the reaction vessel. After the addition of $Mg(OH)_2$ and NaOH, 50 ml samples

were removed with the use of a pipette at fixed times to allow precipitate surface area and particle size distribution to be measured after certain times. Ostwald ripening is the dissolution of small crystals and the re-deposition of the dissolved species on the surface of the larger crystals present in the system.[42, 43]. Ostwald ripening occurs because the equilibrium solubility increases as the size of the crystal decreases. This means the solution can become deficient in small crystals during precipitation but remain supersaturated with respect to larger crystals. Having a low concentration of small crystals and supersaturated with large crystals leads to the smaller crystals dissolving at the surface of the larger crystals. Larger crystals are more energetically favoured than smaller crystals. Whilst it is more kinetically favourable for many small crystals to form, large crystals are thermodynamically favourable.

There are a number of methods which can be undertaken to reduce and prevent Ostwald ripening. For example, Mullin *et al.*[44] suggest that agitating a solution with $Mg(OH)_2$ forming a uniform precipitate would decrease agglomeration and in turn the ageing process. Ostwald ripening can be minimised by reducing the particle size distribution in the system. A sample of magnesium hydroxide displaying monodispersity should prevent Ostwald ripening from occurring as there would be no small particles to be deposited onto the larger particles if the particles were uniform. A study by Wu *et al.*[41] discusses the synthesis and characterisation of superfine magnesium hydroxide displaying monodispersity.

In this study, magnesium chloride hexahydrate, $MgCl_2.6H_2O$, was used as the Mg^{2+} source and $NH_3.H_2O$ was used as the OH^- source. Hydrogen peroxide, H_2O_2, was used to treat the resultant magnesium hydroxide particles. The magnesium chloride hexahydrate (152.3 g) and hydrogen peroxide (2 ml) were dissolved in a water/ acetone (20/80, v/v) mixture in a 1000 mL round-bottom flask, the concentration of Mg^{2+} was fixed at 1.5 mol/l. The ammonia solution was fed into the reaction via a peristaltic pump. The reaction temperature and ageing time were maintained at 25 ^oC and 2.5 hours respectively. During the reaction and the ageing process vigorous stirring was applied and a white solid was eventually obtained from the mother liquor.

Figure 9. Size distribution of $Mg(OH)_2$ particles present in the product synthesised in distilled water [41].

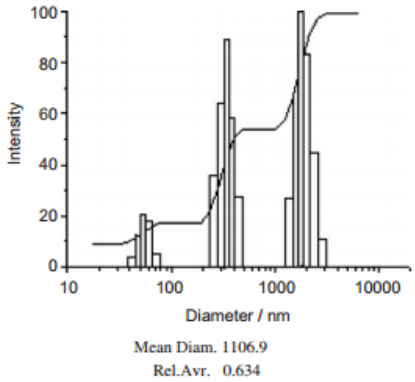

Figure 10. Size distribution of $Mg(OH)_2$ particles synthesised in a water/ acetone (20/80, v/v) solvent [41].

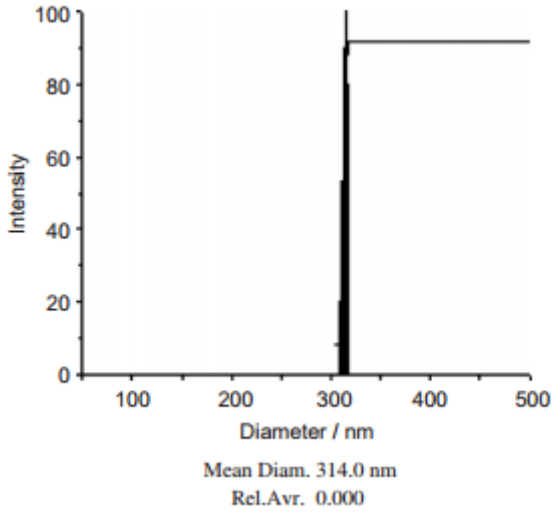

As Figure 9 and Figure 10 indicate, the size distribution of $Mg(OH)_2$ crystals is much greater in the control sample, where the solvent was water, than in the other synthesised sample, where the solvent was water/ acetone, (20/80, v/v). The average diameter of the particles produced was also reduced from 1106.9 nm to 314.0 nm. The monodispersity present in the synthesised sample is thought to be due to pH value and supersaturation. The acetone speedily diluted the

$NH_3.H_2O$ which contributed to a lower ionic product. The acetone decreased the effective concentration of the OH^- and Mg^{2+} ions and led to lower supersaturation.

1.1.4 $Mg(OH)_2$ as a Pickering emulsifier

In the paper by Tan *et al.*[6] magnesium hydroxide was used as a Pickering emulsifier for emulsions of liquid paraffin and water (1:1 volume). In this study, it was shown that magnesium hydroxide can act as a successful Pickering emulsifier in this particular system, closely binding to the interface of oil droplets. In this study, magnesium hydroxide particles encapsulated emulsion droplets, acting as a steric barrier and aiding in the prevention of coalescence of droplets and, in turn, increasing the stability of the emulsion. See Figure 11 which indicates the presence of particles at the water-oil interface.

Figure 11. Confocal fluorescence microscope images of paraffin droplets in a continuous aqueous phase. The red colour on the micrograph indicates the presence of the magnesium hydroxide particles at the liquid-liquid interface surrounding the paraffin droplets [6].

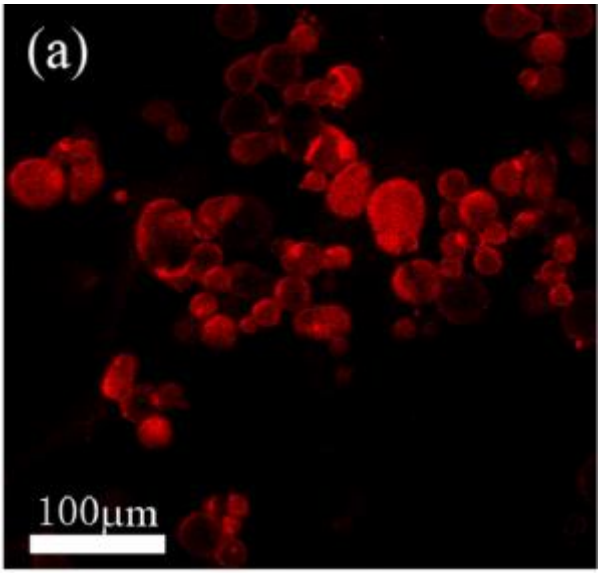

In the experiment resulting in the above micrograph, the magnesium hydroxide particles were fluorescently labelled and confocal laser scanning microscopy was used to assess the emulsions formed. Cryo-SEM could have been used as an alternative to view how the particles had adsorbed at the liquid- liquid interface.

In terms of the relationship between the concentration of magnesium hydroxide particles and the stability of the emulsion, the results in this experiment follow a slightly different trend to what is expected. It has been recognised in many emulsion systems that as concentration of

emulsifier increases, the stability of the emulsions initially increase and the mean droplet diameter decreases. However, beyond a certain concentration of emulsifier, the stability and mean droplet diameter remain constant.

The results of this particular study are in agreement with the above trend in terms of an initial increase in concentration of magnesium hydroxide (0.01 – 1 wt.%) leads to an increase in emulsion stability and a decrease in droplet size. Above 1 wt. %, the mean droplet size and stability of the emulsion did not level off, they began to increase and decrease respectively. This is unusual behaviour for Pickering emulsions. This effect is outlined in figure 12.

Figure 12. Emulsion volume as a function of [$Mg(OH)_2$], collected 48 hours after emulsion formation [6].

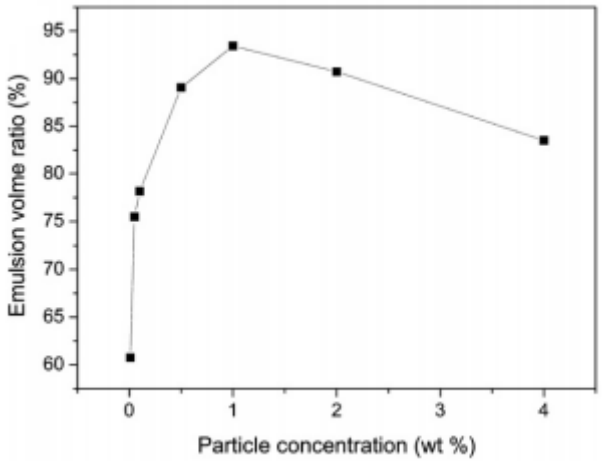

The aim of the study by Tan *et al.*[6] was to observe the behaviour of magnesium hydroxide particles as an emulsifier at different pH levels. The study concluded that at pH 9.5 or below, the emulsion would destabilise and phase separate. However, at pH levels exceeding 9.5, magnesium hydroxide particles acted as successful Pickering emulsifiers. This indicates that magnesium hydroxide particles are pH dependent when used as an emulsifier.

There is very limited literature with regards to magnesium hydroxide particles and their use as Pickering emulsifiers and no paper to compare the work of Tan *et al*. to [6]. It will be interesting to investigate this topic further.

1.2 Pickering emulsions

1.2.1 Emulsions and Pickering emulsions

An emulsion is a thermodynamically unstable mixture of two immiscible phases, such as oil and water, stabilised by emulsifiers. Energy is required in order for an emulsion to form, outlined in the following equation [45],

$$\Delta G = \Delta A \gamma_{12} \qquad (3)$$

where ΔG is the associated free energy, ΔA is the change in interfacial area and γ_{12} is the interfacial tension between phases 1 and 2.

In an emulsion, droplets of one liquid phase are dispersed within another continuous liquid phase. During homogenization, both phases are turned into droplets, the phase which has the droplets that coalesce at a faster rate will be the eventual continuous phase. Without an emulsifier, the emulsion would soon destabilise as the droplets would fuse together and complete phase separation is expected to occur due to the immiscibility and difference in density of the two phases. Possible emulsifiers include surfactants [46-50], polymers [51, 52], proteins [53, 54] and solid particles [55, 56]. Emulsions can either be described as oil-in-water (o/w) or water-in-oil (w/o). In o/w emulsions, oil droplets are dispersed in water. In w/o droplets, water droplets are dispersed in oil. There are a number of methods used to distinguish between the two kinds of emulsions. One of which being the drop test, where drops of emulsion are deposited into a container of water and a container of the oil used. If the drop disperses in the water, the emulsion is o/w and vice versa. Another method which is widely used to identify the classification of an emulsion is to assess electrical conductivity.

Pickering emulsions are those stabilised solely by solid particles [56], stemming from the early work of Ramsden [57] and Pickering [58]. Pickering emulsions generally possess a higher stability to coalescence than emulsions stabilised by surfactants as the solid particles have a higher energy of attachment and are held very strongly at the interface. This means they are ideal for use in stabilising emulsions over a long period of time. The minimum energy required to remove a stabilising particle from the interface is given by equation [59],

$$\Delta G_d = \pi \gamma_{ow} r^2 (1 - |\cos\theta|)^2 \qquad (4)$$

where ΔG_d is the energy required to detach a particle from the liquid interface, γ is interfacial tension, r is radius of the particles and θ is contact angle.

Therefore, as radius of the particle and surface tension at oil-water interface increase, and as the three-phase contact angle nears 90 °, the energy required to remove the particle from the interface increases.

Contact angle indicates wettability of a particle which is the ability of a liquid to maintain contact with a solid. Particles which have a contact angle of around 90 ° are well wetted by both the water phase of the emulsion and the oil phase, meaning they are roughly equally submerged in the two phases. Generally speaking, for hydrophilic particles, $\theta_{ow} < 90$ ° which means a large portion of the particle shall remain submerged by the water phase of an emulsion. For hydrophobic particles, $\theta_{ow} > 90$ ° meaning a large portion of the particle shall remain submerged by the oil phase of an emulsion. Figure 13 illustrates the way in which a particle may be positioned at an oil – water interface [59,60].

Figure 13. (a) Position of a spherical particle at an oil-water interface with $\theta_{ow} < 90$ ° (left), $\theta_{ow} = 90$ ° (centre) and $\theta_{ow} > 90$ ° (right). (b) Predicts the position of a hydrophilic (left) and a hydrophobic (right) particle at a curved oil – water interface. Taken from Ref. 60.

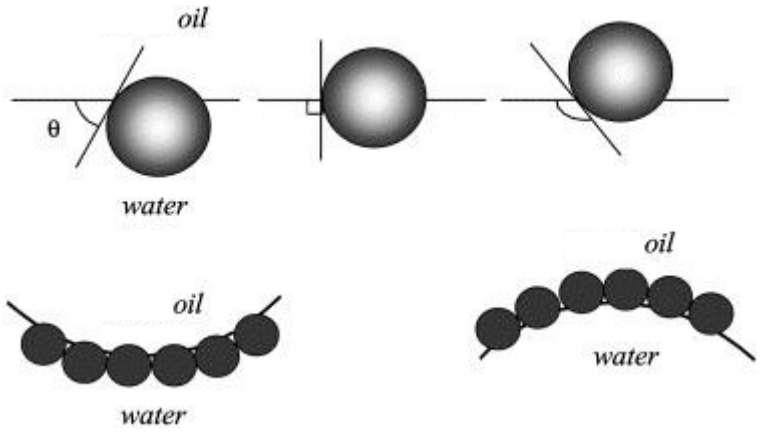

If particles are too hydrophilic/ hydrophobic, they will be unable to stabilise an emulsion as they remain completely submerged by the phase they are so strongly attracted to.

Contact angle and wettability of a particle by a liquid is one of the major factors in determining the type of emulsion formed in terms of o/w or w/o as shown in Figure 14.

Figure 14. Pickering emulsion stabilised by hydrophobic solid particles (θ > 90º, W/O) (a) and a Pickering emulsion stabilised by hydrophilic solid particles (θ < 90º, O/W) (b).

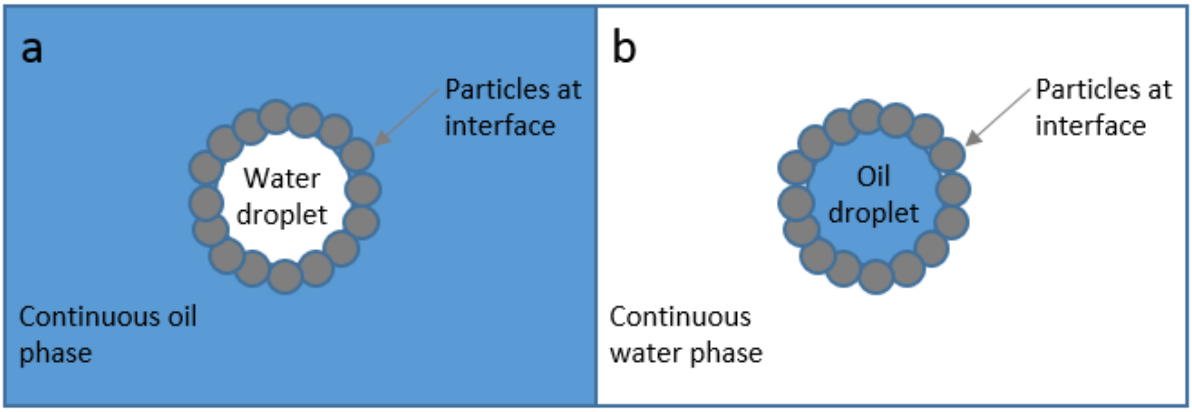

Contact angles can be determined with the use of Young's equation [61],

$$\gamma_{GS} = \gamma_{SL} + \gamma_{LG} \cos \theta \qquad (5)$$

where γ is interfacial tension, θ is contact angle and s, l and g are solid liquid or gas respectively. (Figure 15).

Figure 15. Notation of the three phase boundaries of a drop of liquid deposited onto a solid surface when gas is the third phase.

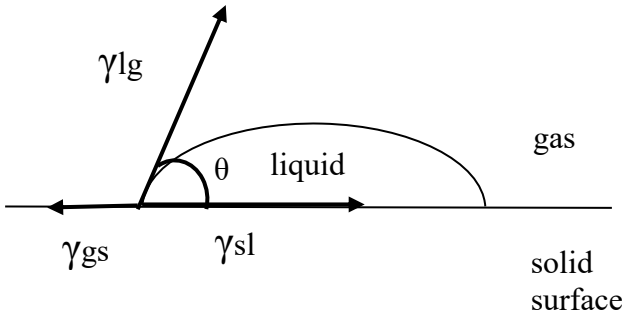

In a three-phase contact, the drop spreads along the solid interface creating a new liquid-solid interface and reducing the original solid-gas interface, until it is no longer energetically favourable to do so [62, 63]. Energy is gained by reducing the air-solid interface.

Contact angles are dependent on cohesive forces between the molecules in the liquid and the adhesive forces between the liquid and the solid surface. If the liquid which is deposited onto the solid surface is water, and the solid surface consists of polar groups, strong adhesive forces will arise and lead to a small contact angle as the water wets the solid. This indicates that the solid surface in question is hydrophilic. Therefore, a hydrophobic solid surface is made up of

non-polar groups and will give rise to a contact angle of above 90 °. If contact angle < 5 °, complete wetting has occurred.

Advancing and receding contact angle measurements can be measured. An advancing contact angle is the maximum contact angle possible without increasing the solid-liquid interfacial area. To achieve the advancing contact angle, the volume of the drop is increased dynamically. A receding contact angle is the minimum contact angle possible without decreasing the solid-liquid interfacial area, which is achieved by reducing the volume of the drop dynamically. The difference in values between an advancing contact angle and a receding contact angle is known as hysteresis, which can arise due to chemical heterogeneity of the surface and roughness of the surface [63].

1.2.2 Aging mechanisms of emulsions

Emulsion stability is considered in terms of droplet number, droplet size and also the fraction of oil phase and water phase which remains within the emulsion. There are a number of different aging mechanisms which lead to the destabilisation and breakdown of emulsions. An emulsion can be subject to more than one of these mechanisms at any given time. According to the Derjaguin Landau Verwey Overbeek theory, outlined in Figure 16, an emulsion will become unstable when attractive van der Waals forces between droplets overcome the repulsive electrostatic forces [64].

Figure 16. Graphical representation of the DLVO theory for two emulsion drops in their continuous phase [65].

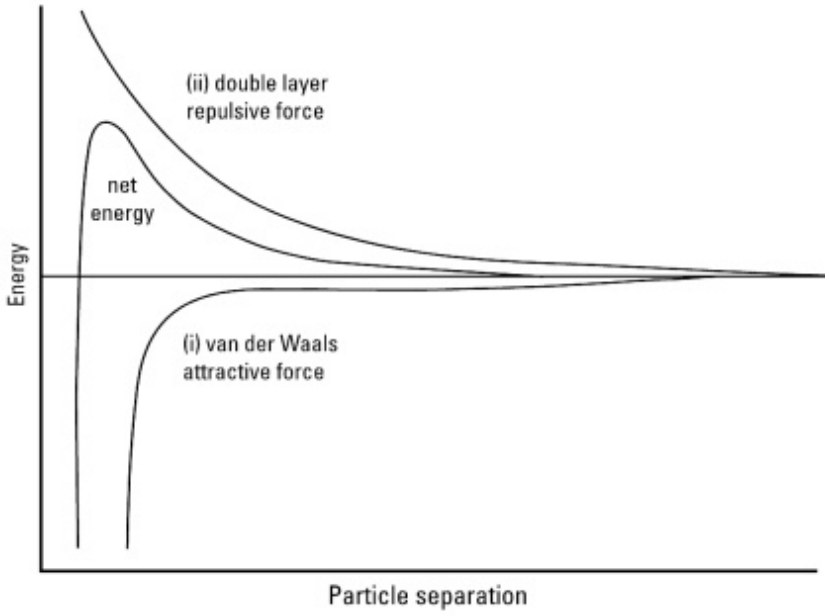

One example of the destabilisation of emulsions is coalescence. Coalescence sees two or more droplets combine to produce a single larger droplet. In coalescence, the thin film of continuous phase separating droplets rupture due to the droplets approaching each other [69]. In an o/w emulsion, coalescence is the binding of oil droplets and subsequent liberation of oil from the emulsion. The forces leading to the thinning and eventual rupture of this film have been discussed in previous articles [66-68].

Creaming is also a very common form of aging in emulsions and is mainly due to gravity affecting the system [69]. In o/w systems, water is liberated from the system due to differences in density between the phases. Normally, the water is more dense than the emulsion and oil phases and the water will collect at the bottom of the container. Creaming can be reduced by decreasing the density difference between the phases, decreasing droplet size or increasing the viscosity of the continuous phase. This can be achieved by increasing particle concentration. Creaming is reversible, unlike coalescence.

Flocculation is an aging mechanism which sees droplets gather together to form aggregates. There is a net attraction between droplets. Although the droplets form aggregates, a thin layer between droplets remains and therefore the droplets are still separate structures [70].

Ostwald ripening is a thermodynamically favourable process which can occur when the droplets in an emulsion are polydisperse. In an o/w emulsion, smaller oil droplets are more soluble in water than the larger oil droplets. Once smaller droplets have dissolved, the molecules make their way through the continuous phase to a larger oil droplet and adsorb onto it. This process leads to the system containing less small oil droplets and the larger droplets in the system becoming larger. Ostwald ripening can be combatted with the use of a disperse phase which is less soluble in the continuous phase [71].

Figure 17 shows each of the instability methods emulsions can undergo.

Figure 17. The various destabilisation mechanisms which act on emulsions. Taken from Ref. 72.

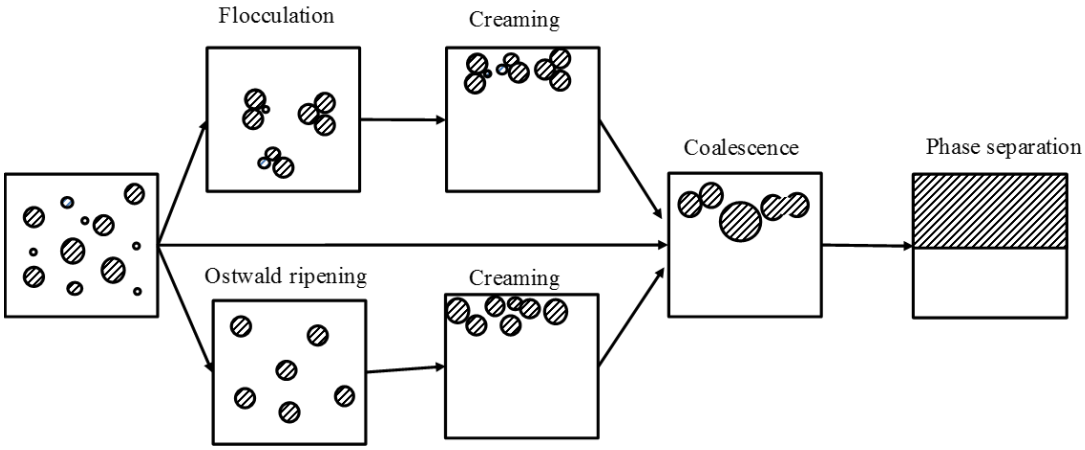

1.2.3 Methods of activating highly hydrophilic particles

There are methods which can be used to activate highly hydrophilic particles, which do not adsorb to oil – water interfaces spontaneously [73]. Many of these methods involve reducing the surface charge of the particles, which in turn decreases electrostatic repulsion between particles and therefore encourages floc formation. For example, electrolytes have been used to improve emulsion stability to coalescence [74 – 78]. Studies have shown that despite an initial increase in stability to coalescence, at high concentrations of added salt, flocs form which are too large, leading to less stable emulsions possibly due to decreased adsorption of large flocs at the oil-water interface. The salt can either be added to the aqueous phase of the emulsion or the oil phase. When an oil-soluble salt is used, the salts dissociate to produce oppositely charged ions to the stabilising particles, reducing the repulsion between particles and allowing particles to pack closely at the interface. The oppositely charged ions in the oil phase can lead to the stabilising particles partially submerging in the oil phase [79] as shown in Figure 18.

Figure 18. Illustration of the effect of the presence of ions in the oil phase possessing an opposite charge to the hydrophilic particles. (a) No added salt, therefore no oppositely charged ions. (b) Added salt, system contains added ions. Adapted from the work of Xu *et al.* [79].

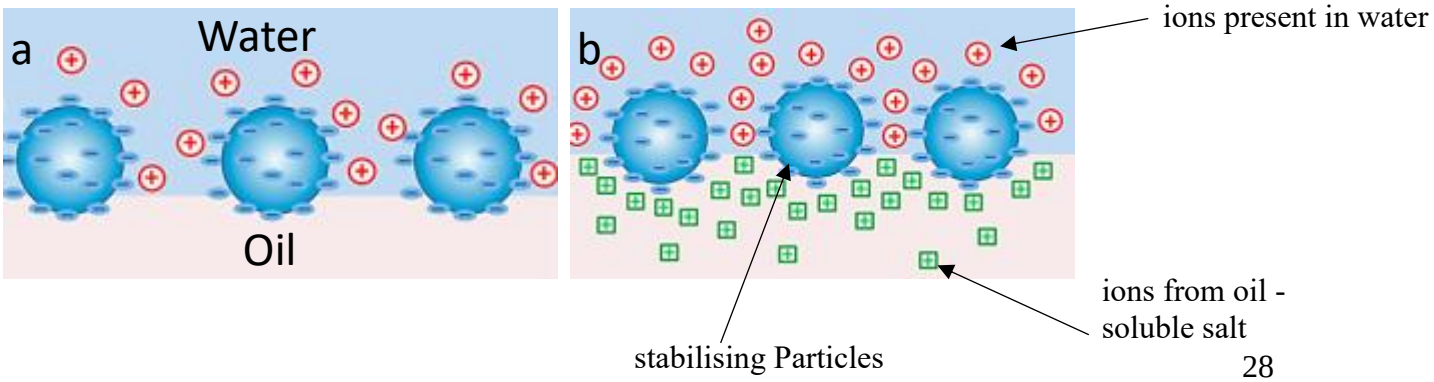

Another method which may be used to activate highly hydrophilic particles is to vary pH. The work of Amalvy *et al.* notes how sterically-stabilised polystyrene latex particles are affected by pH levels [80]. The hydrophilicity of particles with ionisable surface groups will be different at different pH values. This is because as pH levels near the isoelectric point of the particles, they will be less strongly charged and repel each other less strongly. They will begin to agglomerate and pack closely at the oil-water interface.

Short- chain alcohol molecules can be also be used to reduce the surface charge of stabilising particles. This was evident in the work of Younan *et al.* which noted the effect the presence of alcohol molecules had on citrate coated gold nanoparticles [81]. It is thought that the alcohol molecules displaced the citrate ions on the surface of the gold nanoparticles. This reduced the electrostatic repulsion between the gold particles and allowed them to form a gold film at the water-1,2-dichloroethane interface, seen in Figure 19.

Figure 19. Gold film with yellow reflectance forming from citrate-coated gold nanoparticles, at a water and 1,2-dichloroethane interface. From the work of Younan *et al* [81].

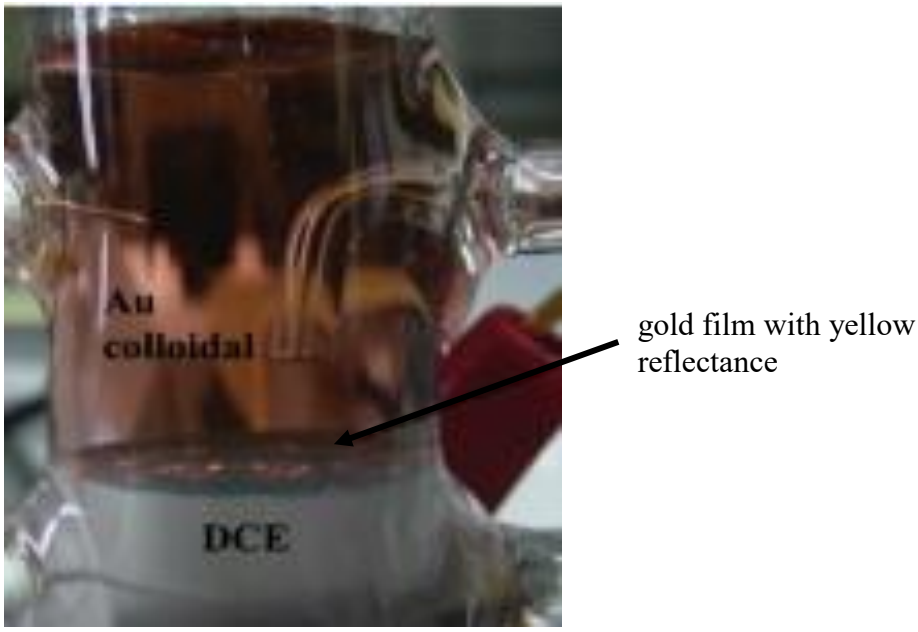

The addition of oppositely charged particles has also been used to reduce electrostatic repulsion between highly hydrophilic, emulsifying particles. For example, Binks *et al.* used a mixture of positively charged and negatively charged silica particles to form emulsions [82]. The oppositely charged particles formed heteroaggregates which reduced the net charge of the particles, rendering them more hydrophobic. Positive/ negative silica particles were unable to stabilise emulsions alone as they were too hydrophilic. A similar outcome is observed when oppositely

charged polymers are mixed and when oppositely charge surfactants are added [83-85]. It is also possible to reduce hydrophilicity of particles by dissolving functional oil in the aqueous phase of the emulsion, which in turn form hydrogen bonds with the particle surface, acting to decrease the surface charge of the particles [86].

1.3 Aims of project

The aim of this project was to form magnesium hydroxide particles under various reaction conditions and then determine how successful they are as Pickering emulsifiers in oil-in water systems.

This was achieved by varying the following conditions in the synthesis of magnesium hydroxide samples; reactant concentration, reaction temperature, reaction time, extent of agitation, counter ion to Mg^{2+} and strong/weak base were all varied. The samples were analysed via XRD and FT-IR and their size and morphology was assessed by SEM and TEM. Aqueous magnesium hydroxide dispersions were prepared in order to measure zeta potential.

In order to determine how successful each magnesium hydroxide sample was as a Pickering emulsifier, emulsions of isooctane-water, methyl methacrylate-water and isooctane + methyl methacrylate-water were formed from each of the samples. In the preparation of emulsions, concentration of magnesium hydroxide, storage temperature, concentration of added electrolyte and fraction of isooctane in oil when in mixtures with MMA were all varied.

Such emulsions are used industrially in the suspension polymerisation of polymer microspheres which encapsulate organic compounds. When heated, the organic compounds boil and the microsphere expands.

2 Experimental

2.1 Materials

The water in this experiment was purified with the use of an Elga Prima reverse osmosis unit and treated with a Milli-Q reagent system, until a resistivity of 10 – 18 M Ω cm was reached. In the synthesis of magnesium hydroxide, the two OH^- sources used were sodium hydroxide pellets (purity >98 %) and ammonium hydroxide solution (≥99.99 %) both purchased from Sigma – Aldrich. The three Mg^{2+} sources used were magnesium chloride hexahydrate (purity >99 %), magnesium nitrate hexahydrate (purity 99 %) and magnesium sulfate hexahydrate (purity > 99 %), which were also purchased from Sigma-Aldrich. Sodium chloride (purity >99 %) was purchased from Fisher Chemicals. When measuring contact angles, raw brucite purchased from Treasure Mountain Mining, U.S. was used. Isooctane (purity >99 %, density 0.6958 g/cm^3 at 22 ^{o}C) and methyl methacrylate (purity >99 %, density 0.9509 g/cm^3 at 17.5 ^{o}C) were used as the oil phase of the emulsions formed in this experiment, purchased from Fisher Chemicals and Sigma-Aldrich respectively. The structures of both isooctane and MMA are shown in Figure 20.

Figure 20. Chemical structures of (a) isooctane and (b) methyl methacrylate.

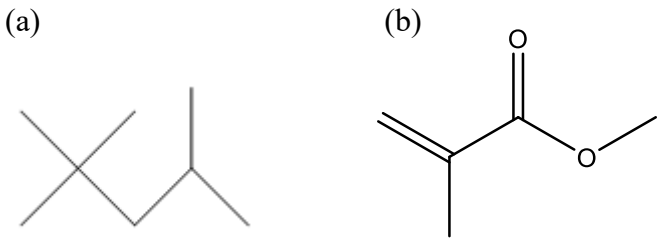

2.2 Methods

2.2.1 Synthesis of magnesium hydroxide samples

Mg^{2+} containing solutions and OH^- containing solutions were prepared with the use of Milli- Q water. Volumes and masses were measured accurately with the use of pipettes and an analytical balance respectively. Each reacting solution was of 60 cm^3 in volume and were clear and colourless in appearance.

When synthesising magnesium hydroxide samples, a basic solution was added to a magnesium containing solution from a burette at around 10 cm^3 min^{-1}. The reaction was allowed to occur at room temperature for 2.5 hours with agitation from a magnetic stirrer bar (560 rpm), unless otherwise specified. Each reaction took place in a round bottom flask. Upon formation of magnesium hydroxide, the reaction mixture turned cloudy and viscous.

During this experiment, samples of magnesium hydroxide were produced via different synthetic routes and under different reaction conditions. Variables in this experiment included the concentrations of reacting solutions (samples 1-5, 16-20), source of Mg^{2+} (samples 1, 9, 10, 14 and 15), base used (1 and 16), reaction temperature (samples 1, 6, 7, 8, 21, 22 and 23), extent of agitation during reaction (samples 1, 11, 12, 24 and 25) and rate of addition of the two reactants (samples 1, 13 and 26) as shown in table 2. The latter half of the syntheses explores how reactant conditions affect the growth of magnesium hydroxide produced from magnesium chloride hexahydrate and sodium hydroxide.

Table 2. Reaction conditions under which each magnesium hydroxide samples was prepared.

Sample	Magnesium Compound Solution	Basic Solution	Average Reaction Temperature/ ^oC
1	$MgCl_2.6H_2O$ (0.6 M, 60 cm^3)	NH_4OH (1.2 M, 60 cm^3)	25
2	$MgCl_2.6H_2O$ (1.2 M, 60 cm^3)	NH_4OH (0.6 M, 60 cm^3)	25
3	$MgCl_2.6H_2O$ (0.6 M, 60 cm^3)	NH_4OH (2.4 M, 60 cm^3)	24
4	$MgCl_2.6H_2O$ (2.4 M, 60 cm^3)	NH_4OH (0.6 M, 60 cm^3)	24
5	$MgCl_2.6H_2O$ (1.2 M, 60 cm^3)	NH_4OH (1.2 M, 60 cm^3)	22
6	$MgCl_2.6H_2O$ (0.6 M, 60 cm^3)	NH_4OH (1.2 M, 60 cm^3)	51
7	$MgCl_2.6H_2O$ (0.6 M, 60 cm^3)	NH_4OH (1.2 M, 60 cm^3)	38
8	$MgCl_2.6H_2O$ (0.6 M, 60 cm^3)	NH_4OH (1.2 M, 60 cm^3)	10

9	$Mg(NO_3)_2.6H_2O$ (0.6 M, 60 cm^3)	NH_4OH (1.2 M, 60 cm^3)	23
10	$MgSO_4.6H_2O$ (0.6 M, 60 cm^3)	NH_4OH (1.2 M, 60 cm^3)	22
11 [a]	$MgCl_2.6H_2O$ (0.6 M, 60 cm^3)	NH_4OH (1.2 M, 60 cm^3)	24
12 [b]	$MgCl_2.6H_2O$ (0.6 M, 60 cm^3)	NH_4OH (1.2 M, 60 cm^3)	23
13 [c]	$MgCl_2.6H_2O$ (0.6 M, 60 cm^3)	NH_4OH (1.2 M, 60 cm^3)	22
14	$MgSO_4.6H_2O$ (0.6 M, 60 cm^3)	NaOH (1.2 M, 60 cm^3)	24
15	$Mg(NO_3)_2.6H_2O$ (0.6 M, 60 cm^3)	NaOH (1.2 M, 60 cm^3)	23
16	1.2 M, 60 cm^3, 0.072 mol.	2.4 M, 60 cm^3, 0.144 mol.	22
17	2.4 M, 60 cm^3, 0.144 mol.	1.2 M, 60 cm^3, 0.072 mol.	20
18	1.2 M, 60 cm^3, 0.072 mol.	4.8 M, 60 cm^3, 0.288 mol.	20
19	2.4 M, 60 cm^3, 0.144 mol.	0.6 M, 60 cm^3, 0.036 mol.	23
20	1.2 M, 60 cm^3, 0.072 mol.	1.2 M, 60 cm^3, 0.072 mol.	24
21	1.2 M, 60 cm^3, 0.072 mol.	2.4 M, 60 cm^3, 0.144 mol.	50
22	1.2 M, 60 cm^3, 0.072 mol.	2.4 M, 60 cm^3, 0.144 mol.	40
23	1.2 M, 60 cm^3, 0.072 mol.	2.4 M, 60 cm^3, 0.144 mol.	10
24 [a]	1.2 M, 60 cm^3, 0.072 mol.	2.4 M, 60 cm^3, 0.144 mol.	22

25 [b]	1.2 M, 60 cm^3, 0.072 mol.	2.4 M, 60 cm^3, 0.144 mol.	20
26 [d]	1.2 M, 60 cm^3, 0.072 mol.	2.4 M, 60 cm^3, 0.144 mol.	24.9

a – No agitation, b – 72 hours agitation, c – Rate of addition of reactants = 5 ml/min, d-Reactants completely added within 30 s.

2.2.2 Analysis of magnesium hydroxide products

The products formed were collected under vacuum with the use of a Simax S4 sinter funnel (porosity of sinter disc, 16 to 10 µm). The products were then re-dispersed in Milli Q water (200 ml). Water was chosen as the solvent to wash off any impurities on the magnesium hydroxide samples as magnesium hydroxide is sparingly soluble in water whereas any conceivable impurities are all very readily soluble in water. The product was ground with use of a pestle and mortar prior to analysis.

2.2.2.1 SEM and TEM analysis

SEM analysis was undertaken on the dried sample using a Zeiss EVO 60 instrument. The ground sample must be carbon sputter coated in an Edwards High Vacuum, (model E12E2) prior to SEM analysis.

TEM analysis was also carried out using a Jeol 2010 electron microscope with a lanthanum hexaboride crystal filament to produce the electron beam at 200 kV. To prepare the sample for the TEM, the crushed powder was suspended in water and sonicated. 5 µl of this was added to a carbon coated copper grid. The water was left to evaporate. If the original powder had been used as opposed to the suspensions, it would not have adhered itself to the grid and would have been unable to stay on the grid under the vacuum of the TEM.

2.2.2.2 XRD analysis

XRD analysis was used when identifying the sample and to note the crystalline structure of the product. A PANalytical EMPYREAN instrument was used operating with copper Kα1 radiation, 0.15408 nm. 2θ values in the range of 5^o – 70^o were measured. A photograph of an XRD sample holder containing an $Mg(OH)_2$ sample can be seen in Figure 21.

Figure 21. Photograph to show how a sample should appear when packed in the sample holder properly prior to XRD analysis.

2.2.2.3 Fourier Transform-Infrared analysis

Fourier transform-infrared analysis was carried out when identifying synthesised products. A Thermo Fisher, Nicolet iS5 FT-IR Spectrometer was used to carry out this analysis. A small mass of the sample was secured into place by the clamping device on the instrument and data shall be collected, as shown in Figure 22.

Figure 22. Illustration of how magnesium hydroxide powder is secured into place when FT-IR is carried out.

2.2.3 Preparation of magnesium hydroxide dispersions

Each of the dispersions referenced in this thesis was sonicated by the same method. In order to observe the properties of the magnesium hydroxide samples in water, magnesium hydroxide dispersions from the 26 samples were prepared. Each of the magnesium hydroxide samples was dispersed into Milli-Q water. The dispersions were of 0.2 wt. % and 100 ml in volume. They were sonicated for 1 minute at 30 % amplitude using a Branson Digital Sonifier, sonic probe tip 0.6 mm in diameter. The natural pH of each of the dispersions was measured with a Jenway 3510 pH meter at around 24 ^{o}C and was established to be in the region of pH 10.5. The dispersions were cloudy/ milky in appearance.

It was necessary to dilute the dispersions to around 0.02 wt. % magnesium hydroxide in order to analyse the samples using a Malvern Zetasizer ZS-Nanoseries instrument. In order to assess the effect of salt, stock solutions of different concentrations of NaCl were first produced by dissolving an appropriate mass of NaCl in 1 L Milli-Q water. The series of stock solutions of NaCl included concentrations of 10^{-3} M, 10^{-2} M, 10^{-1} M, 0.2 M and 0.5 M. Magnesium hydroxide (sample 19) dispersions (0.1 wt. %, 10 mL) with different concentrations of NaCl solution as the continuous phase were then formed by adding the appropriate NaCl solution to a constant mass of magnesium hydroxide followed by sonication.

2.2.4 Analysis of magnesium hydroxide dispersions

2 ml of each dispersion was added to a disposable cuvette in preparation to be analysed with a Malvern Zetasizer ZS-Nanoseries instrument in order to measure particle diameter and zeta potential.

2.2.4.1 Particle diameter measurements

The Malvern Zetasizer ZS-Nanoseries instrument uses dynamic light scattering to measure the Brownian motions of particles in a sample, which means the refractive index of magnesium hydroxide is important. DLS is achieved by illuminating the particles with a red laser (633 nm) and analysing the intensity fluctuations in the scattered light. Small particles scatter light to a greater extent than large particles. As particles scatter light, a speckle pattern will form with light and dark regions. The light regions are a result of constructive interference of signals, dark regions are a result of destructive interference. As the particles in the sample move, the correlation between signals will reduce. This is the characteristic used to measure the size. If

particles are large, the correlation between signals would reduce more slowly as large particles do not scatter light as efficiently as small particles.

The Stokes- Einstein equation links particle diameter with Brownian motion [87],

$$D = \frac{kT}{6\pi R\eta} \qquad (6)$$

where D is the diffusion coefficient, k is Boltzmann's constant, T is temperature, η is the viscosity of the solution and R is the hydrodynamic radius of the particle.

2.2.4.2 Zeta potential measurements

The Malvern Zetasizer ZS-Nanoseries instrument is able to measure the electrophoretic mobility of the particles, obtained by electrophoresis and measuring the velocity of the particles via laser Doppler velocity. Henry's equation is applied to calculate the zeta potential of the particles [88].

$$U_E = \frac{2\varepsilon z f(ka)}{3\eta} \qquad (7)$$

where U_E is the electrophoretic mobility, ε is the dielectric constant of solvent, z is the zeta potential, f(ka) is the Henry's function and η is the viscosity of dispersant.

The instrument has two settings in order to set the value of f(ka). If an aqueous dispersant with a moderate electrolyte content (electrolyte concentration including and exceeding 10^{-3} M) and the universal dip cell is used, the Smoluchowski approximation should be selected [89]. The f(ka) value is then set at 1.5. If a non-aqueous sample is being measured, the Hückel approximation should be used which sets f(ka) to 1.0. In this experiment, the Smoluchowski setting was selected. Laser doppler velocimetry is used to measure U_E. This measures the flow of tiny particles in a stream of fluid and in the Malvern Zetasizer ZS-Nanoseries this is measured via DLS.

2.2.5 Preparation of emulsions

All emulsions referenced in this thesis were prepared by adding the appropriate oil phase (5 ml) to a magnesium hydroxide aqueous dispersion of the appropriate magnesium hydroxide concentration (5 ml). The emulsions were homogenised for 2 minutes at 13,000 rpm with the use of an Ultra Turrax homogeniser with a low diameter rotor (8 mm). The rotor of the homogeniser was moved vertically through the emulsion by hand in order to homogenise the emulsion completely.

2.2.5.1 Isooctane-in-water emulsions

For each of the 26 magnesium hydroxide samples prepared, isooctane-in-water emulsions (1:1 volume ratio) were formed. Magnesium hydroxide concentration of each emulsion remained constant in this series of emulsions at 1.0 wt. % (with respect to entire emulsion). This was calculated to be around 0.0845 g magnesium hydroxide.

2.2.5.2 Isooctane-in-water emulsions with varied [$Mg(OH)_2$]

Appropriate masses of magnesium hydroxide samples 17, 22 and 24 were measured and isooctane-in-water emulsions (1:1 volume ratio) were formed. For each of the three magnesium hydroxide samples, emulsions with varied magnesium hydroxide concentration were formed. This included emulsions of 0.5 wt. %, 1.0 wt. %, 2.0 wt. %, 3.0 wt. %, 4.0 wt. % and 5.0 wt. % magnesium hydroxide.

2.2.5.3 Isooctane-in-water emulsions with added electrolyte

Isooctane-in-water (1:1 volume ratio) emulsions with varied [NaCl] were also formed. This series of emulsions contained [NaCl] of 0 M, 10^{-3} M, 10^{-2} M, 10^{-1} M, 0.2 M and 0.5 M. Magnesium hydroxide concentration remained constant at 1.0 wt. % for each of the emulsions.

2.2.5.4 Isooctane-in-water emulsions at varied temperature

An isooctane-in-water emulsion (1:1 volume ratio, 1.0 wt. % magnesium hydroxide concentration) was formed at room temperature, 21.4 ^{o}C. The emulsion was then stored at controlled temperatures for 24 hours with the use of a Grant LTD – 6 water bath. These temperatures included 10 ^{o}C, 30 ^{o}C, 40 ^{o}C, 50 ^{o}C, 60 ^{o}C and room temperature.

2.2.5.5 MMA-in-water emulsions

For each of the magnesium hydroxide samples formed from $MgCl_2$. $6H_2O$ and NaOH (samples 16-26) in this experiment, MMA-in-water emulsions (1:1 volume ratio) were formed. Magnesium hydroxide concentration of each emulsion remained constant in this series of emulsions at 1.0 wt. % (with respect to entire emulsion). This was calculated to be around 0.0975 g magnesium hydroxide.

2.2.5.6 MMA-in-water emulsions with added electrolyte

MMA-in-water (1:1 volume ratio) emulsions with varied [NaCl] were also formed. This series of emulsions contained emulsions with [NaCl] of 0 M, 10^{-3} M, 10^{-2} M, 10^{-1} M, 0.2 M and 0.5 M. Magnesium hydroxide concentration remained constant at 1.0 wt. % for each of the emulsions.

2.2.5.7 Variation of isooctane fraction in mixtures with MMA

From magnesium hydroxide sample 19, 1 wt. %, Pickering emulsions were formed between an isooctane/MMA oil phase and a Milli- Q water phase (phase volume 1:1). The oil phase was prepared using desired volumes of both isooctane and MMA. Each of the oil phases prepared were 5 cm^3 in total volume and was added to the appropriate magnesium hydroxide aqueous dispersion. The volume fraction of isooctane was calculated by,

$$\Phi\text{iso} = \frac{volume\ of\ isooctane}{volume\ of\ total\ oil} \qquad (8)$$

2.2.6 Characterisation of emulsions

2.2.6.1 Stability of the emulsions

Each of the emulsions formed was allowed to settle to see if they had been successfully stabilised by the magnesium hydroxide particles or if phase separation was evident. Photographs of the emulsions were taken using a digital camera after different time periods to see how they aged. The stability of the o/w emulsions shall be discussed in terms of droplet diameter and values of f_O and f_W, where f_O is the fraction of oil liberated from the emulsion and f_W is the fraction of water liberated from the emulsion.

$$f\text{o} = \frac{volume\ of\ oil\ liberated\ at\ time}{volume\ of\ oil\ initially} \qquad (9)$$

$$f\text{w} = \frac{volume\ of\ water\ liberated\ at\ time}{volume\ of\ water\ initially} \qquad (10)$$

2.2.6.2 Optical microscopy

A single drop of each emulsion was placed onto a microscope slide and observed with the use of an Olympus BX51 optical microscope, transmission mode, two days after emulsions were formed. Images were taken using a DP50 digital camera fitted to the microscope. ImageJ was used to analyse subsequent micrographs and determine the average droplet size of each emulsion.

2.2.6.3 Malvern Mastersizer 2000

In order to support the mean droplet diameter determined from optical micrographs, Mastersizer 2000 instrument was used. Once the small volume sample dispersion unit had been cleaned, 150 ml of Milli- Q water was added. 150 μl of emulsion was placed in the water within the small volume sample dispersion unit with the use of a micropipette. The Malvern dispersion unit controller was set to 400 rpm as measurements of the droplets were being taken. Because the Malvern Mastersizer 2000 is reliant on light diffraction in order to obtain results, the refractive index of the dispersed phase (isooctane) and the continuous phase (Milli-Q water) were important. Values of each were measured and placed into the Mastersizer 2000 software before measurements were taken. The light source used was a red, laser light (λ = 633 nm).

2.2.6.4 Cryo-SEM

Cryo – SEM was carried out on emulsion from sample 17 at 5.0 wt.% to show the presence of magnesium hydroxide particles in the continuous water phase. A drop of the emulsion was deposited on a 12 mm aluminium SEM stub and layered so that it protruded from the surface of the stub, This was submerged in liquid nitrogen and frozen at -140 ^{o}C with use of a Quorum Technologies Ltd. PP3010T system. The sample was transferred to the sample stage where a blade was used to fracture the emulsion to produce a new surface. The sample was then coated in platinum and insterted into the Zeiss EVO 60 SEM chamber at -170 ^{o}C using a beam voltage of 15 kV.

2.2.6.5 Drop test

The drop test was conducted on each of the emulsions in order to determine emulsion type. This involved using a Pasteur pipette to add a small amount of each emulsion into a container of water and a container of isooctane respectively. If the emulsion was O/W, the emulsion

would disperse in the water and sediment in the oil. If the emulsion was W/O, it would disperse in the oil or sit above water, due to differences in densities.

2.2.7 Contact angle measurements

Samples of raw brucite were cut using a Metkon Geoform saw supplied by Kemet International. The samples were cut so that they had two near parallel, flat surfaces and were around 1 cm in thickness, as shown in Figure 23. The saw yielded a smooth brucite surface. Once cut, the flat surfaces were rinsed with water and allowed to dry in air. The surfaces were then left untouched in order to keep them clean.

Figure 23. An image of raw brucite upon cutting. (a) image of the smooth, clean surface. (b) image displaying the thickness of the brucite sample

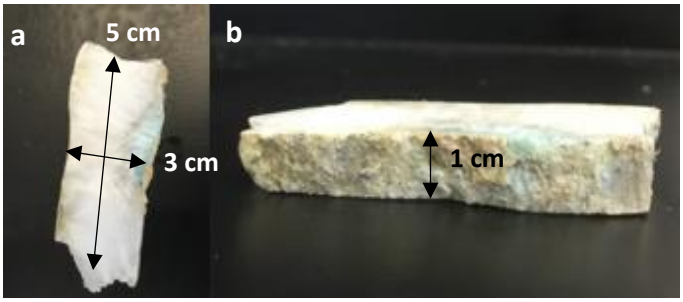

Contact angles were measured using a Kruss DSA10 shape analysis instrument. The magnesium hydroxide sample was placed in a cell and a water drop (10 µl) was deposited under air. This gave the advancing contact angle $\theta_{a,w}$. Two different procedures were used in order to obtain liquid-liquid contact angle measurements. In the first method, a drop of water (10 µl) was injected onto the surface of the magnesium hydroxide sample in air and the cell was then filled with isooctane. This provided the advancing contact angle, $\theta_{w,o}$. In order to obtain the other liquid- liquid contact angle, $\theta_{o,w}$, the cell was first filled with isooctane and then a water drop (10 µl) was deposited onto the surface of the magnesium hydroxide. This procedure was repeated with the use of MMA in place of isooctane.

In order to measure the receding contact angle in each scenario, the water drop was decreased to the minimum volume possible without causing change in the contact surface area between the substrate and the water drop. This minimum volume was around 5 µl in each case. Each of the measurements were repeated 3 times and an average taken. A repeat of the entire experiment was also conducted using a fresh sample of brucite. Water drops of natural pH and also pH 10.5 were deposited onto the magnesium hydroxide in this experiment.

3. Results

The magnesium hydroxide samples formed in this project have been characterised via SEM, TEM, XRD and FTIR analysis. Zeta potential and particle size of the magnesium hydroxide samples were obtained via analysis of aqueous dispersions. fo and fw values and mean droplet diameter have been recorded for isooctane-in-water emulsions, MMA-in-water emulsions and emulsions with an oil phase comprising of an isooctane-MMA mixture. Contact angle measurements of water drops on a brucite substrate were also taken. The findings of these tests are to be outlined in this section of the thesis.

3.1 Characterisation of $Mg(OH)_2$ samples

3.1.1 SEM and TEM analysis

SEM and TEM analysis was carried out on magnesium hydroxide samples formed from ammonium hydroxide in order to note differences in particle size or morphology. Figures 24 – 36 show both SEM and TEM images for magnesium hydroxide samples 1 – 13 respectively. Figure 37 shows variation of particle diameter of the 13 samples.

Figure 24. (a) SEM image and (b) TEM image of magnesium hydroxide powder sample 1, synthesised from magnesium chloride hexahydrate (0.6 M) and ammonium hydroxide (1.2 M) with agitation (2.5 hours) at room temperature.

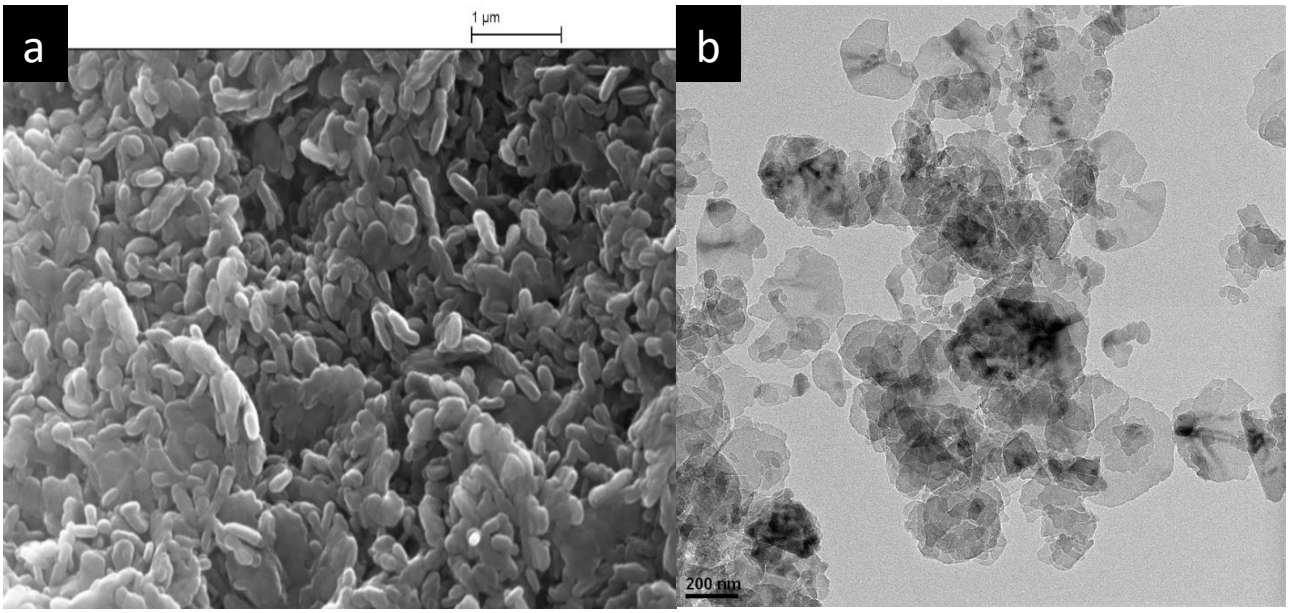

Figure 25. (a) SEM image and (b) TEM image of magnesium hydroxide powder sample 2, synthesised from magnesium chloride hexahydrate (1.2 M) and ammonium hydroxide (0.6 M) with agitation (2.5 hours), at room temperature.

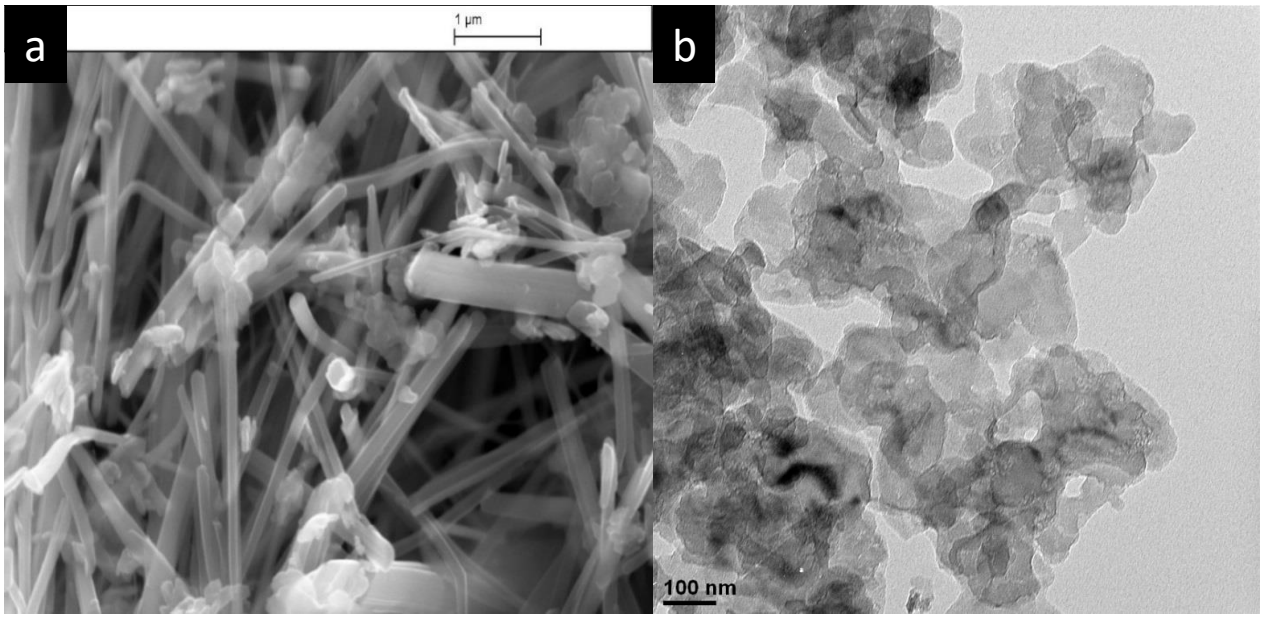

Figure 26. (a) SEM image and (b) TEM image of magnesium hydroxide powder sample 3, synthesised from magnesium chloride hexahydrate (0.6 M) and ammonium hydroxide (2.4 M) with agitation (2.5 hours), at room temperature.

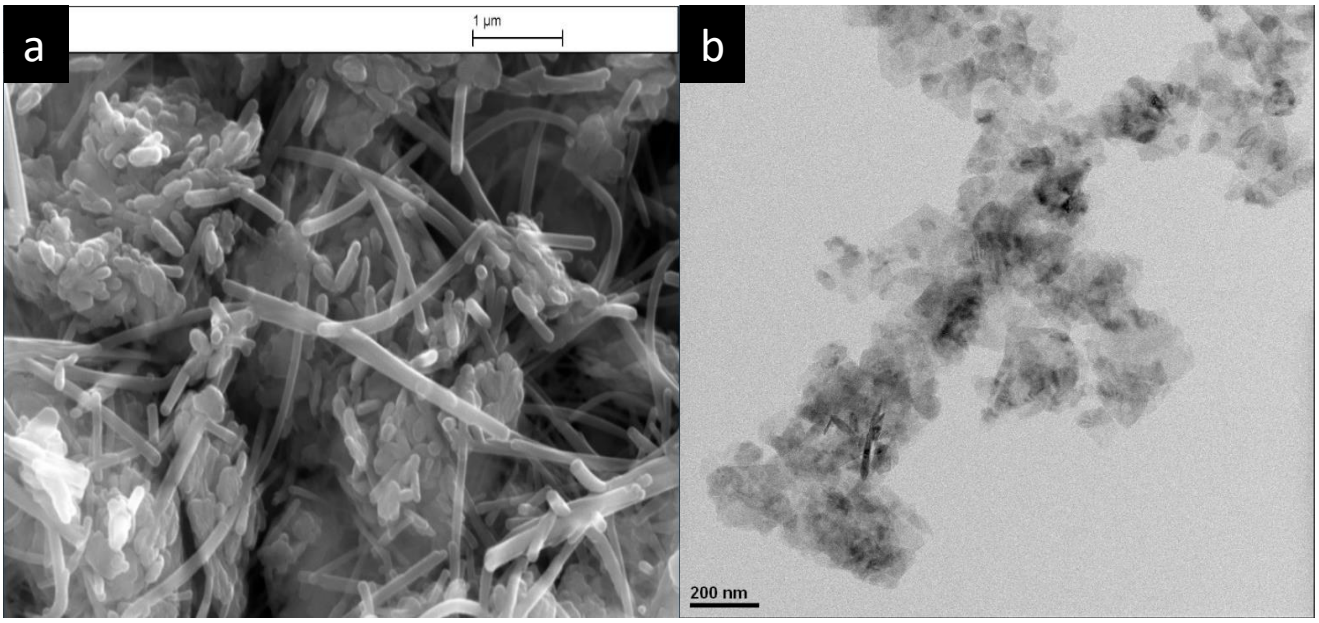

Figure 27. (a) SEM image and (b) TEM image of magnesium hydroxide powder sample 4, synthesised from magnesium chloride hexahydrate (2.4 M) and ammonium hydroxide (0.6 M) with agitation (2.5 hours), at room temperature.

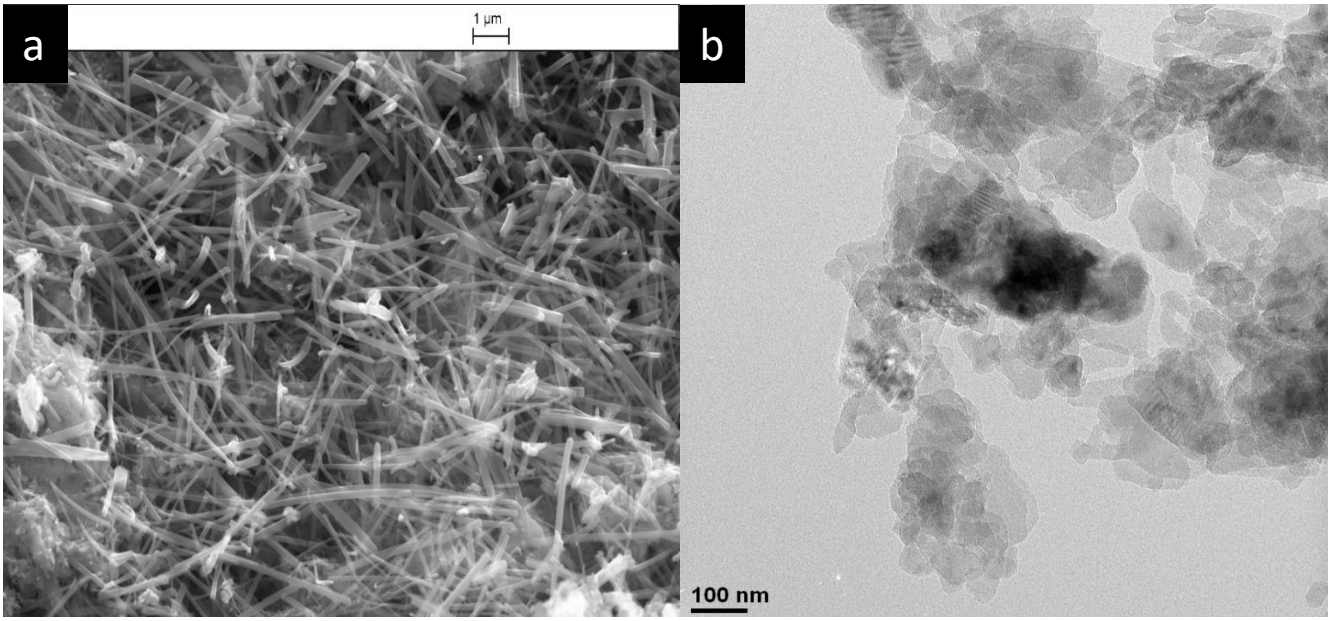

Figure 28. (a) SEM image and (b) TEM image of magnesium hydroxide powder sample 5, synthesised from magnesium chloride hexahydrate (1.2 M) and ammonium hydroxide (1.2 M) with agitation (2.5 hours), at room temperature.

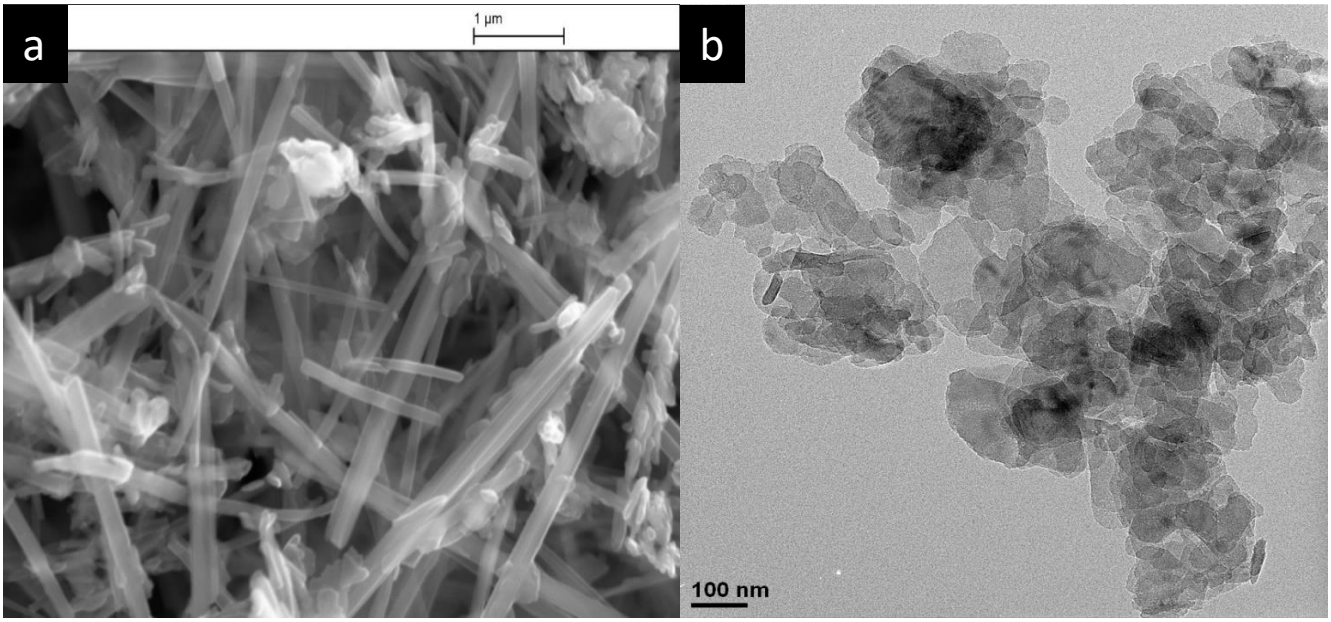

Figure 29. (a) SEM image and (b) TEM image of magnesium hydroxide powder sample 6, synthesised from magnesium chloride hexahydrate (0.6 M) and ammonium hydroxide (1.2 M) with agitation (2.5 hours), at 50 ºC.

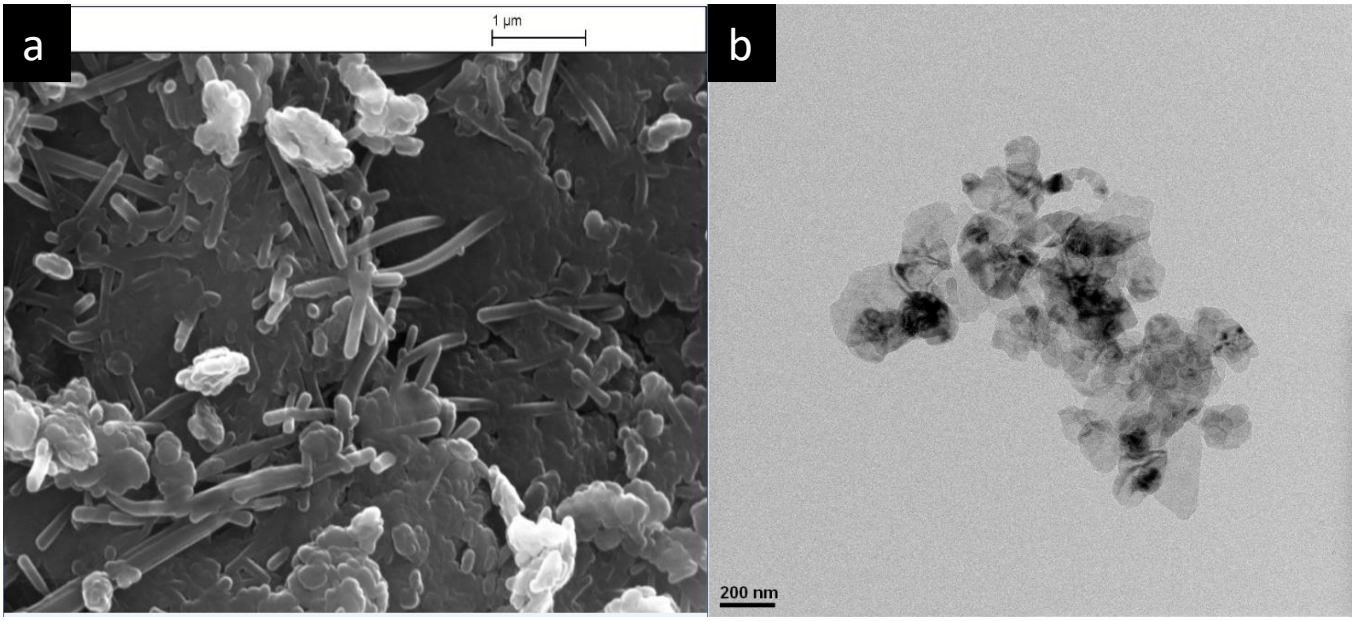

Figure 30. (a) SEM image and (b)TEM image of magnesium hydroxide powder sample 7, synthesised from magnesium chloride hexahydrate (0.6 M) and ammonium hydroxide (1.2 M) with agitation (2.5 hours), at 40 ºC.

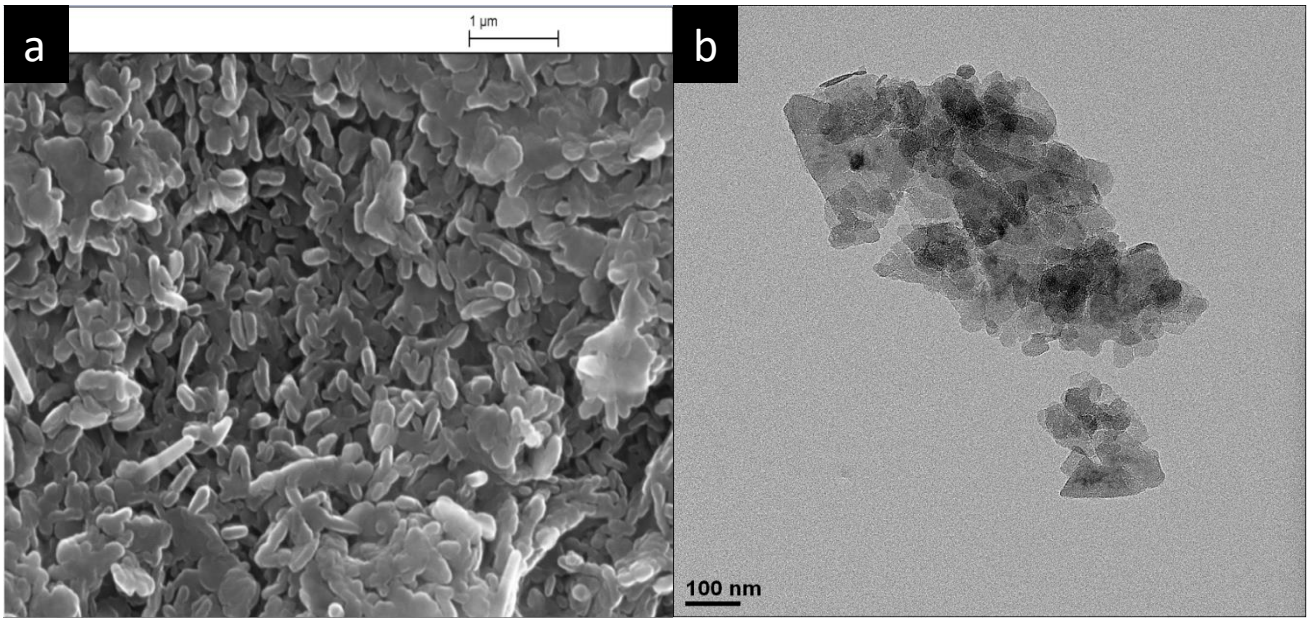

Figure 31. (a) SEM image and (b) TEM image of magnesium hydroxide powder sample 8, synthesised from magnesium chloride hexahydrate (0.6 M) and ammonium hydroxide (1.2 M) with agitation (2.5 hours), at 10 ^{o}C.

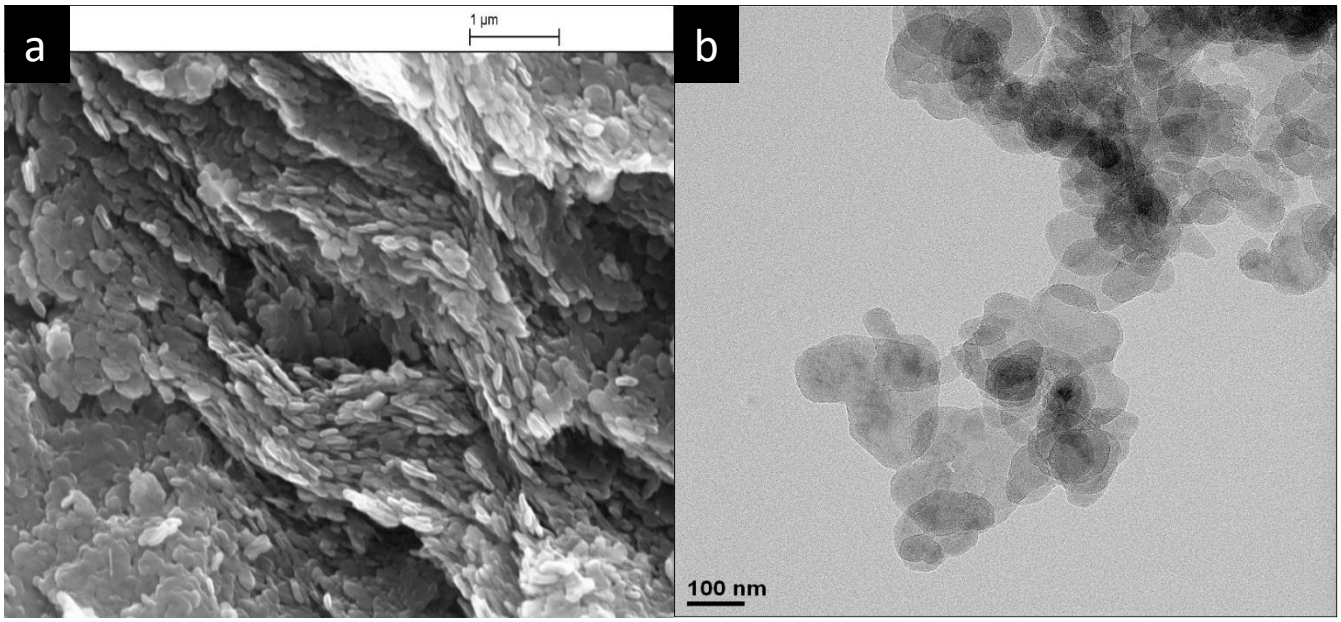

Figure 32. (a) SEM image and (b) TEM image of magnesium hydroxide powder sample 9, synthesised from magnesium nitrate hexahydrate (0.6 M) and ammonium hydroxide (1.2 M) with agitation (2.5 hours), at room temperature.

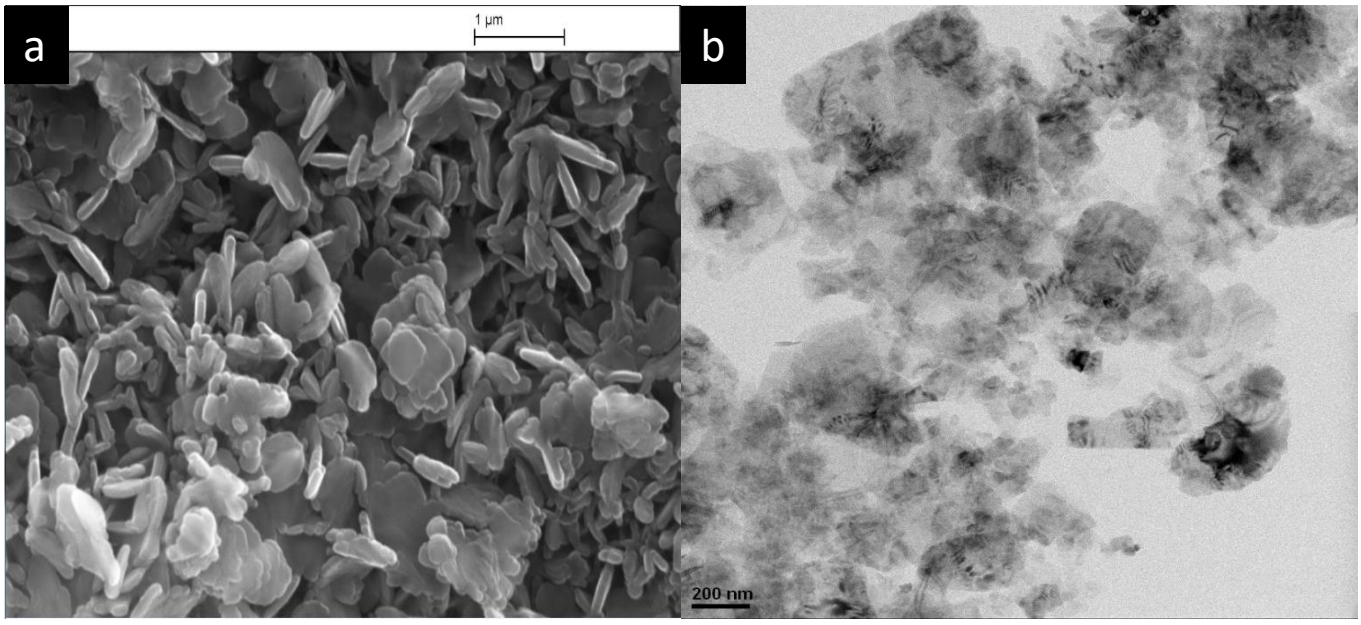

Figure 33. (a) SEM image and (b) TEM image of magnesium hydroxide powder sample 10, synthesised from magnesium sulfate hexahydrate (0.6 M) and ammonium hydroxide (1.2 M) with agitation (2.5 hours), at room temperature.

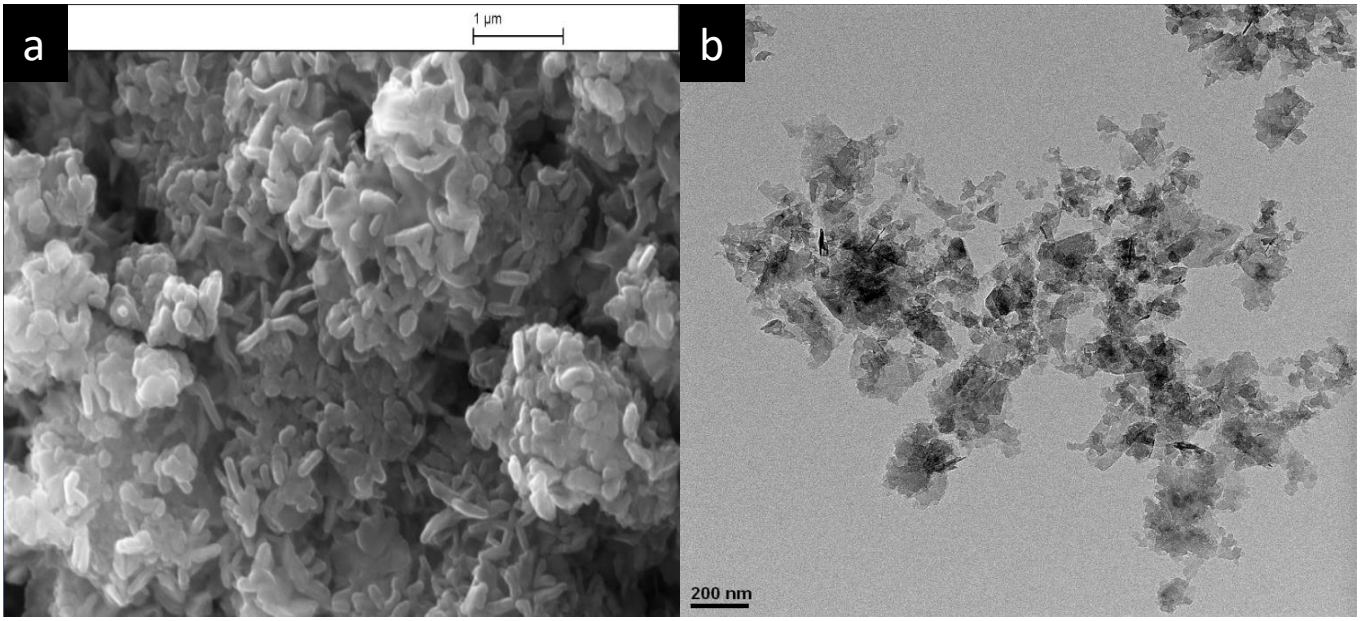

Figure 34. (a) SEM image and (b) TEM image of magnesium hydroxide powder sample 11, synthesised from magnesium chloride hexahydrate (0.6 M) and ammonium hydroxide (1.2 M), no agitation, at room temperature.

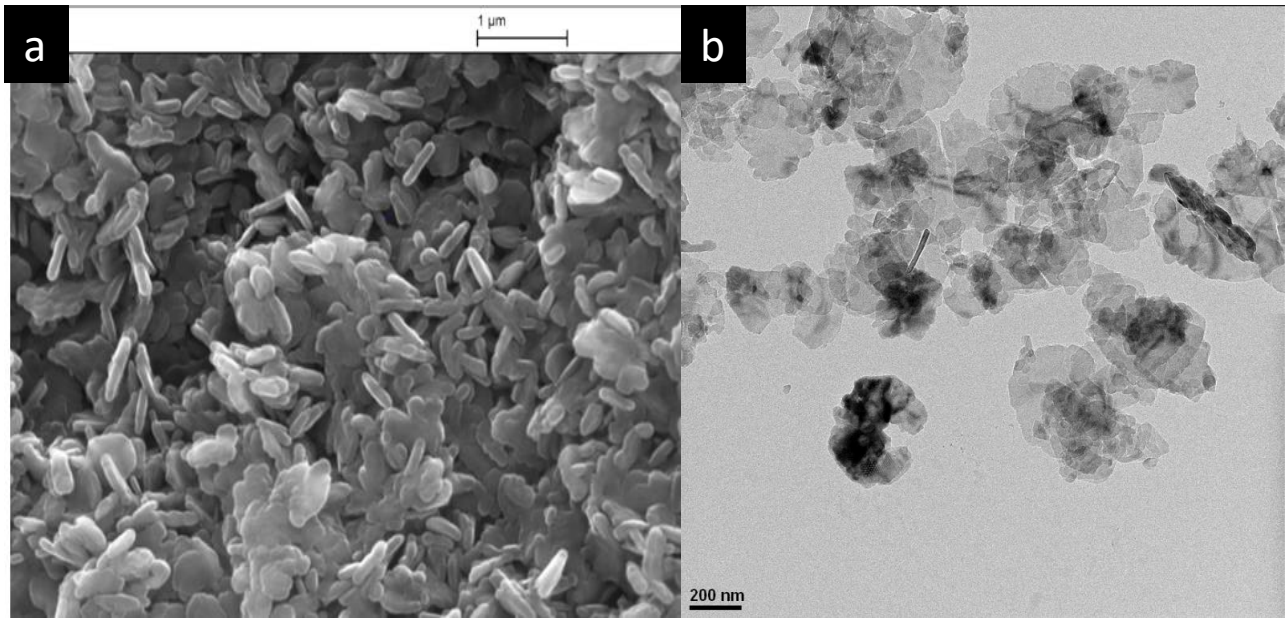

Figure 35. (a) SEM image and (b) TEM image of magnesium hydroxide powder sample 12, synthesised from magnesium chloride hexahydrate (0.6 M) and ammonium hydroxide (1.2 M) with agitation (3 days), at room temperature.

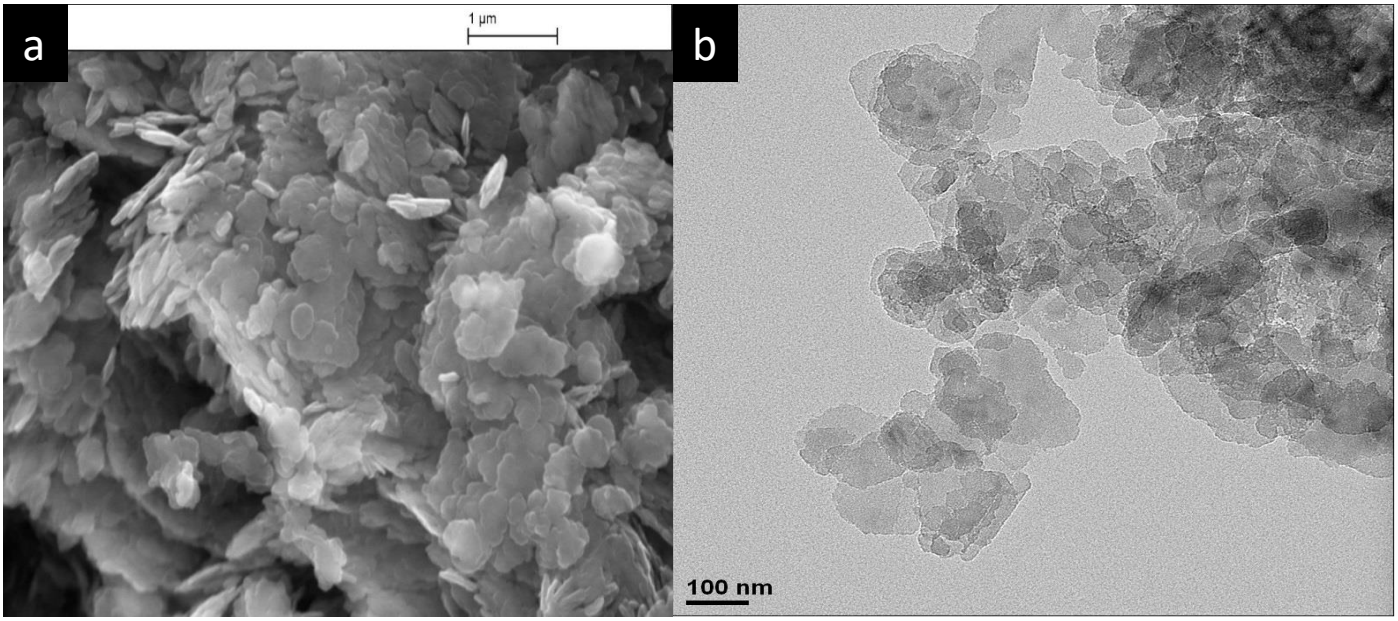

Figure 36. (a) SEM image and (b) TEM image of magnesium hydroxide powder sample 13, synthesised from magnesium chloride hexahydrate (0.6 M) and ammonium hydroxide (1.2 M) with agitation (2.5 h), at room temperature. Reactants added at a slower rate.

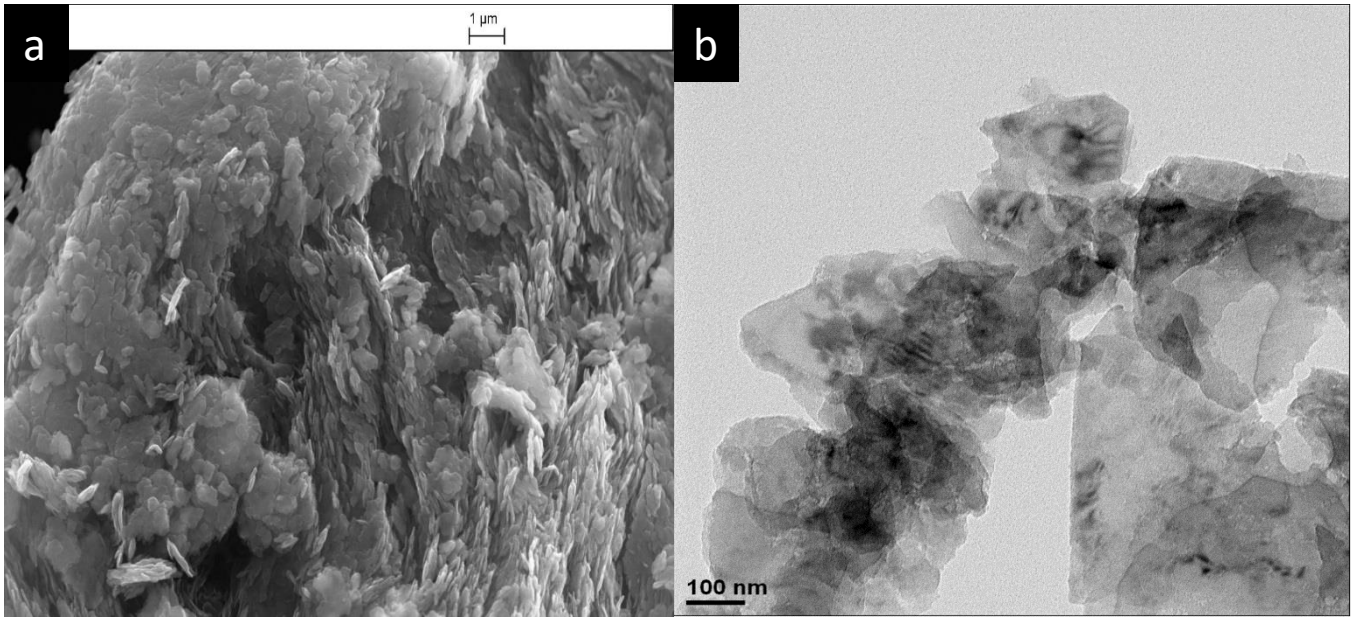

Figure 37. Mean particle diameter/ length of powdered magnesium hydroxide samples formed from a weak base via analysis of SEM micrographs.

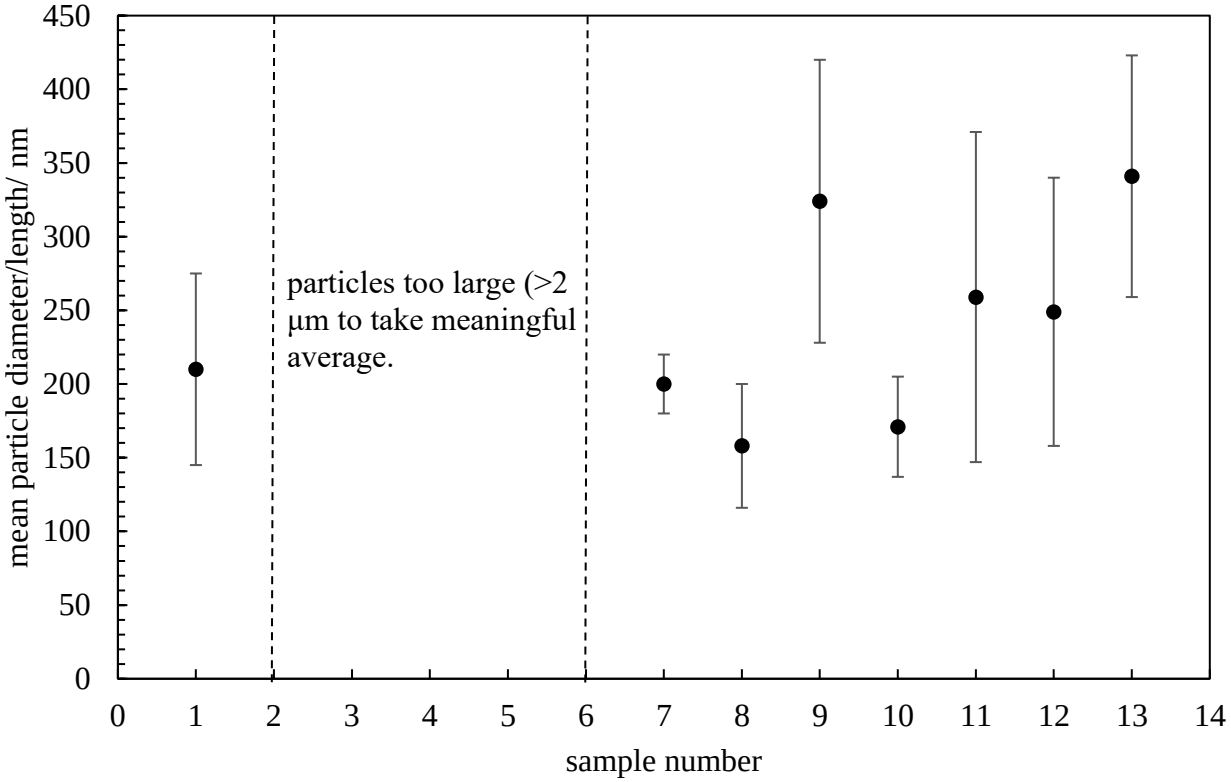

SEM micrographs of the 13 magnesium hydroxide samples were analysed with the use of ImageJ software in order to assess average particle dimensions. When viewing platelets, diameter was recorded. When viewing rods, length of particle was measured. Upon observing SEM micrographs of magnesium hydroxide samples 1-13, it would appear that there are two main categories in terms of morphology and length/ diameter. Samples 1, 7, 8, 9, 10, 11, 12 and 13 are very similar, with mean particle diameter/ length being between 150 nm and 350 nm for each of the samples and morphology being a mixture of rods and platelets. Samples 2, 3, 4, 5 and 6 would fall into the same category as they are much larger than the other samples mentioned and consist of very long rods and highly agglomerated platelets. SEM micrograph of sample 1 shows rods and platelets, similar to the findings of Lv *et al.* under very similar reaction conditions [7]. Sample 2-5, where either OH^- or Mg^{2+} ions are in excess all display very large rod-like particles, in the region of 2 µm and also large agglomerates of platelets. Because the particles are so long, it is difficult to view exactly where they begin and end and therefore, the length readings for the particles in magnesium hydroxide samples 2-5 lack accuracy. The longer particles and large agglomerates present in samples 2-5 could be due to an increased

nucleation rate due to increased supersaturation of either OH^- or Mg^{2+} ions leading to small crystals agglomerating to form large particles and reduce their surface energy.

The rate of heterogeneous nucleation is [90],

$$\frac{dN}{dt} = NoZ\beta` \exp\left(-\frac{dG}{kT}\right) \exp(-\frac{T}{\tau}) \qquad (11)$$

where N_o is the number of available sites for heterogeneous nucleation, Z is de Zeldovich non-equilibrium factor, k is Boltzmann constant (J K^{-1}), β' is rate at which the atoms are being added to the critical nucleus (s^{-1}), T is absolute temperature (K), τ is the incubation time (s), dN is change number of molecules per unit volume, dG is the Gibbs energy of formation of a critical spherical nucleus (J) and R_c is the radius of the critical spherical nucleus (m).

The above equation could also explain why sample 6, formed at 50 ^oC, also contains long, rod-like particles as an increase in temperature also increases the rate of nucleation. The fact that sample 7 displays small platelets indicates that this temperature is not high enough to impact on morphology. When the temperature is decreased from room temperature to 10 ^oC, this also does not affect particle size or morphology as small platelets are observed.

TEM micrographs do not show these large, rod–like particles. This could either be because said particles are broken up during the sonication process, or simply because the particles are too large to be observed by TEM, which has instead shown particles with diameters in the range of 150 – 250 nm.

The absence of agitation did not appear to affect particle size or morphology as the rods and platelets seen in sample 11 strongly resemble sample 1. When the reaction time was increased to 3 days, particles were more likely to adopt a platelet-like morphology as no rod-like particles formed under these conditions. Decreasing rate of addition of reactants also did not appear to affect particle size or morphology as the particles of sample 13 did not differ greatly from the particles of sample 1.

The magnesium hydroxide samples synthesised from NaCl were also assessed via SEM and TEM, see Figures 38–50. Variation of particle diameter/ length (depending on whether morphology is platelet or rod-like) between magnesium hydroxide samples 14–26 can be seen in Figure 51.

Figure 38. (a) SEM image and (b) TEM image of magnesium hydroxide powder sample 14, synthesised from magnesium nitrate hexahydrate (0.6 M) and sodium hydroxide (1.2 M) with agitation (2.5 h), at room temperature.

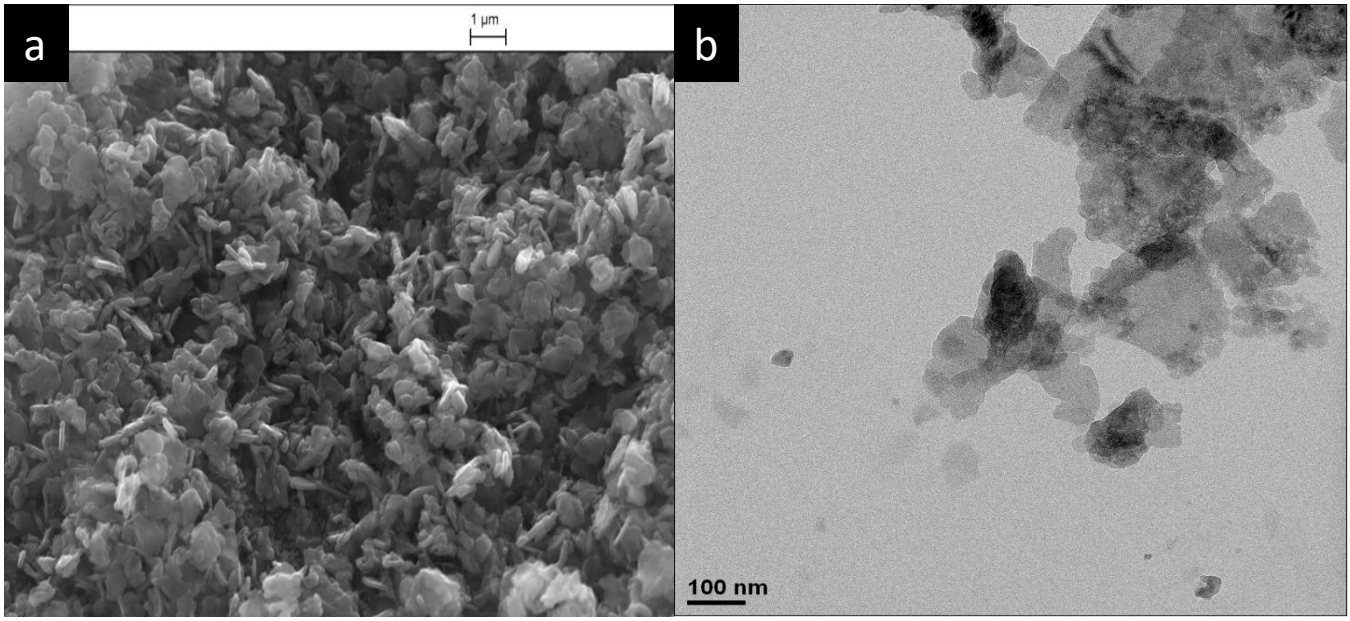

Figure 39. (a) SEM image and (b) TEM image of magnesium hydroxide powder sample 15, synthesised from magnesium sulfate hexahydrate (0.6 M) and sodium hydroxide (1.2 M) with agitation (2.5 h), at room temperature.

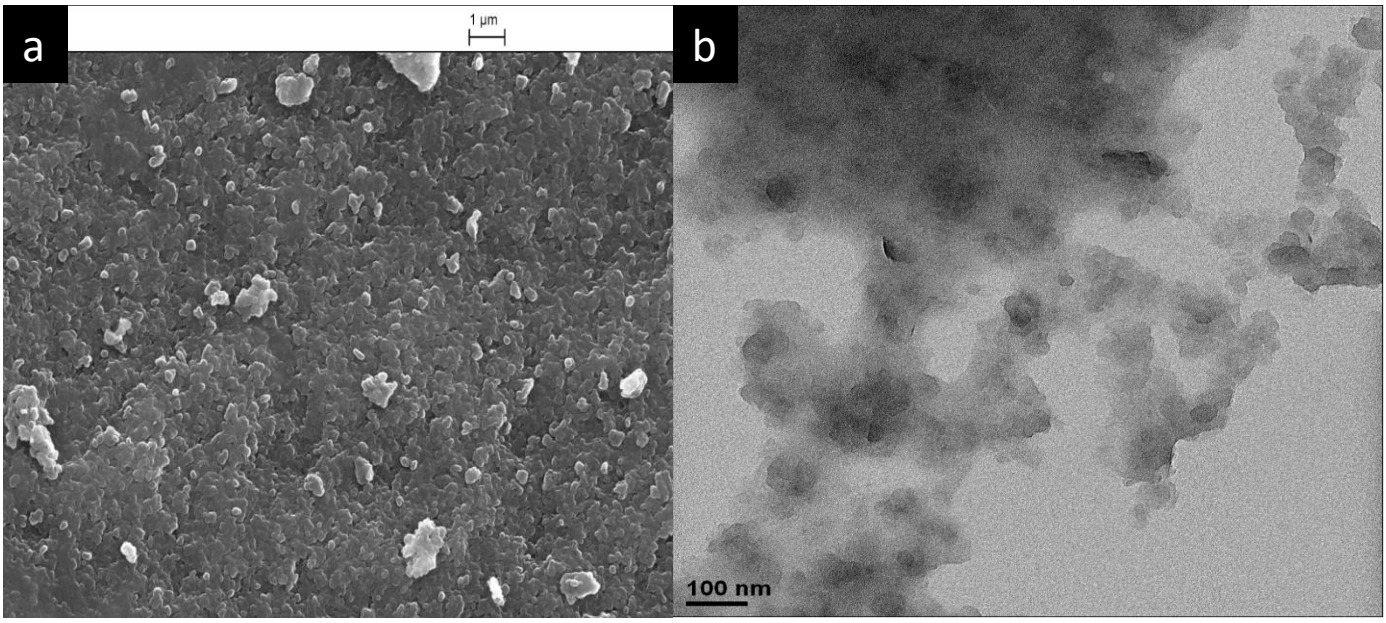

Figure 40. (a) SEM image and (b) TEM image of magnesium hydroxide powder sample 16, synthesised from magnesium chloride hexahydrate (0.6 M) and sodium hydroxide (1.2 M) with agitation (2.5 h), at room temperature.

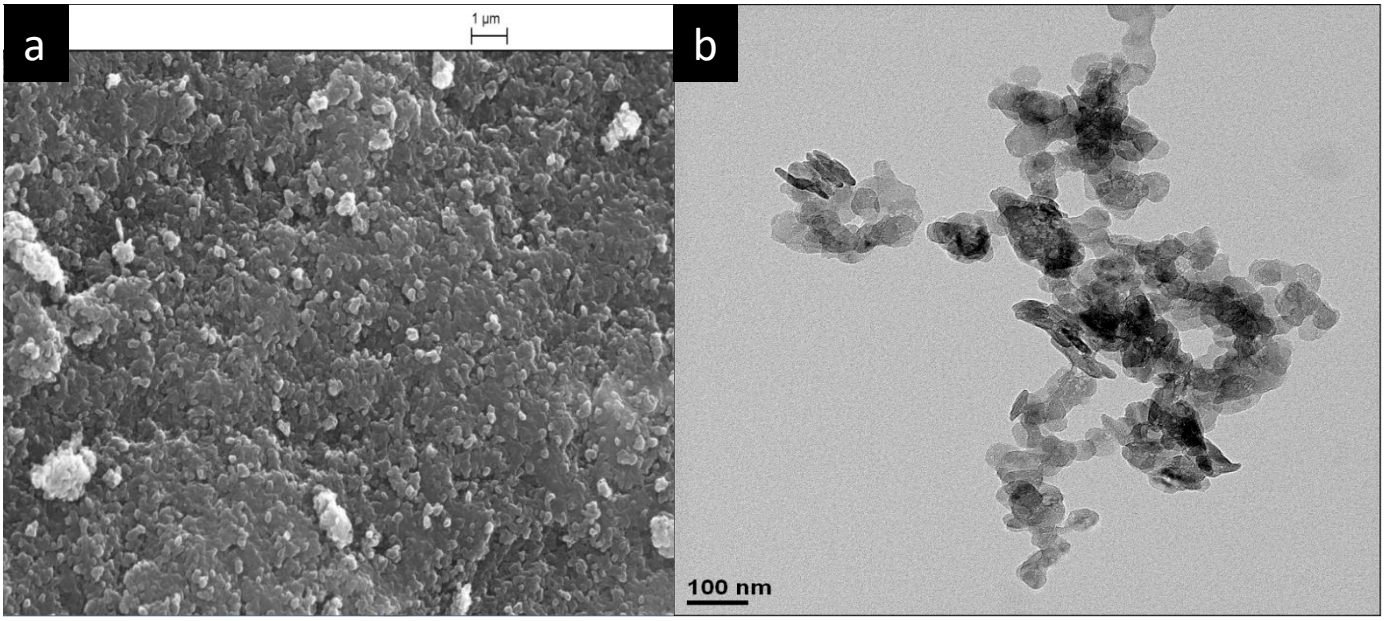

Figure 41. (a) SEM image and (b) TEM image of magnesium hydroxide powder sample 17, synthesised from magnesium chloride hexahydrate (1.2 M) and sodium hydroxide (0.6 M) with agitation (2.5 h), at room temperature.

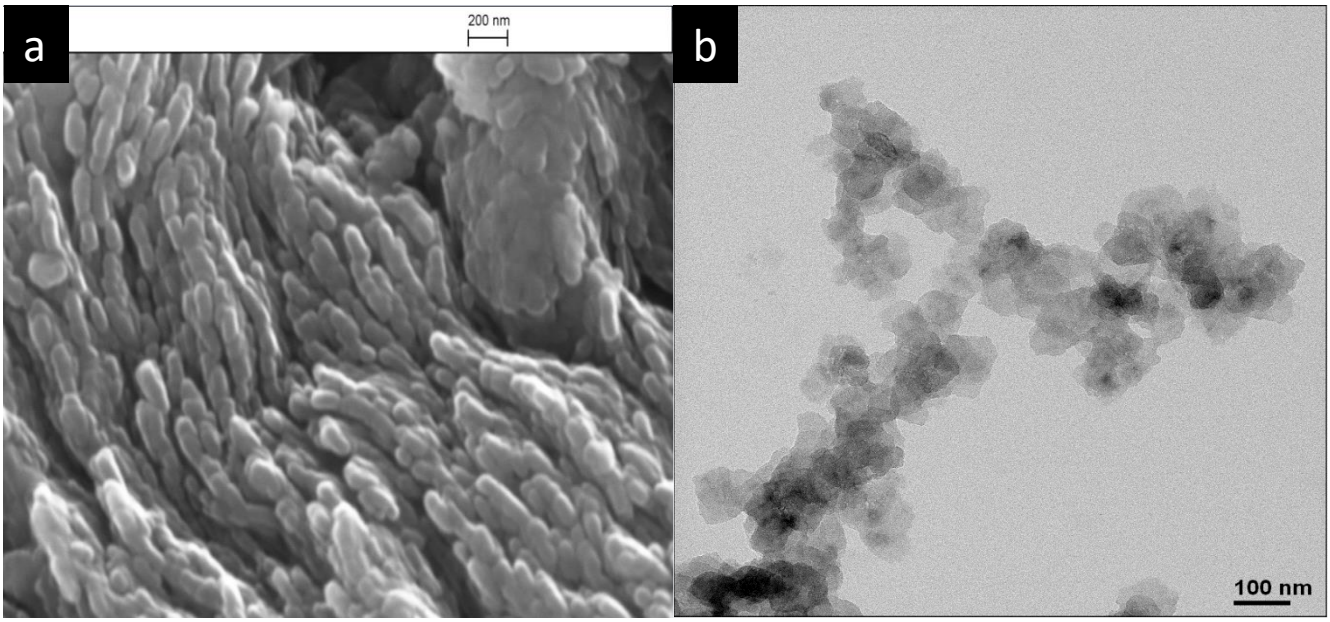

Figure 42. (a) SEM image and (b) TEM image of magnesium hydroxide powder sample 18, synthesised from magnesium chloride hexahydrate (0.6 M) and sodium hydroxide (2.4 M) with agitation (2.5 h), at room temperature.

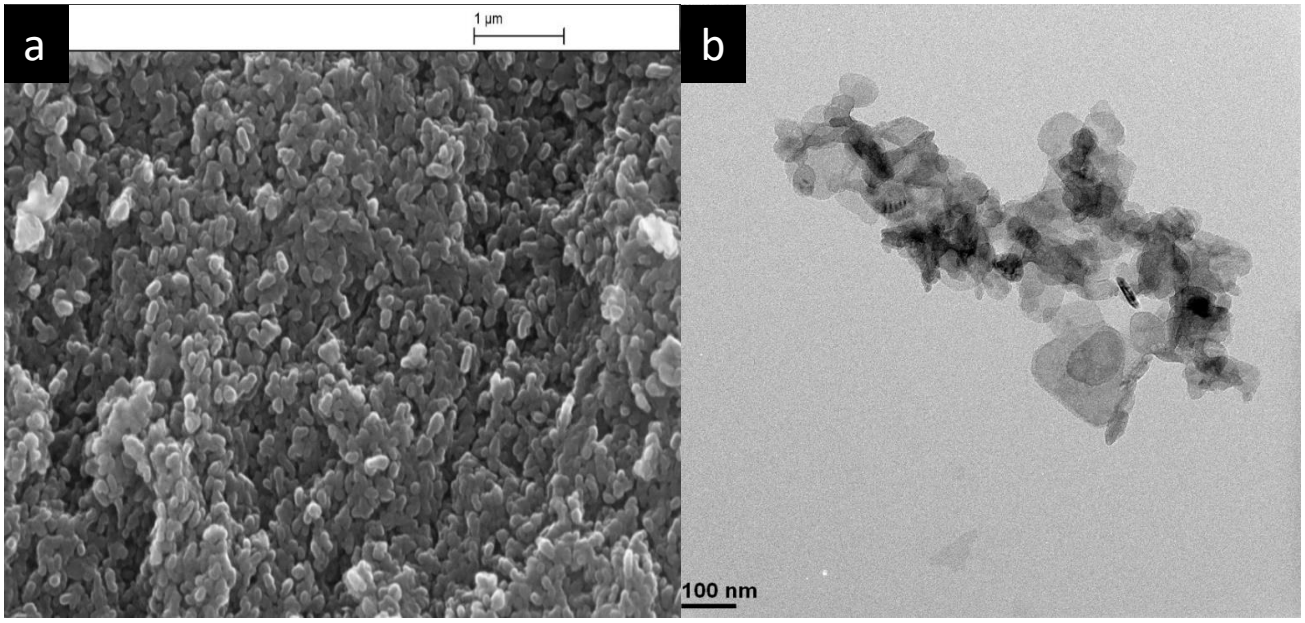

Figure 43. (a) SEM image and (b) TEM image of magnesium hydroxide powder sample 19, synthesised from magnesium chloride hexahydrate (2.4 M) and sodium hydroxide (0.6 M) with agitation (2.5 h), at room temperature.

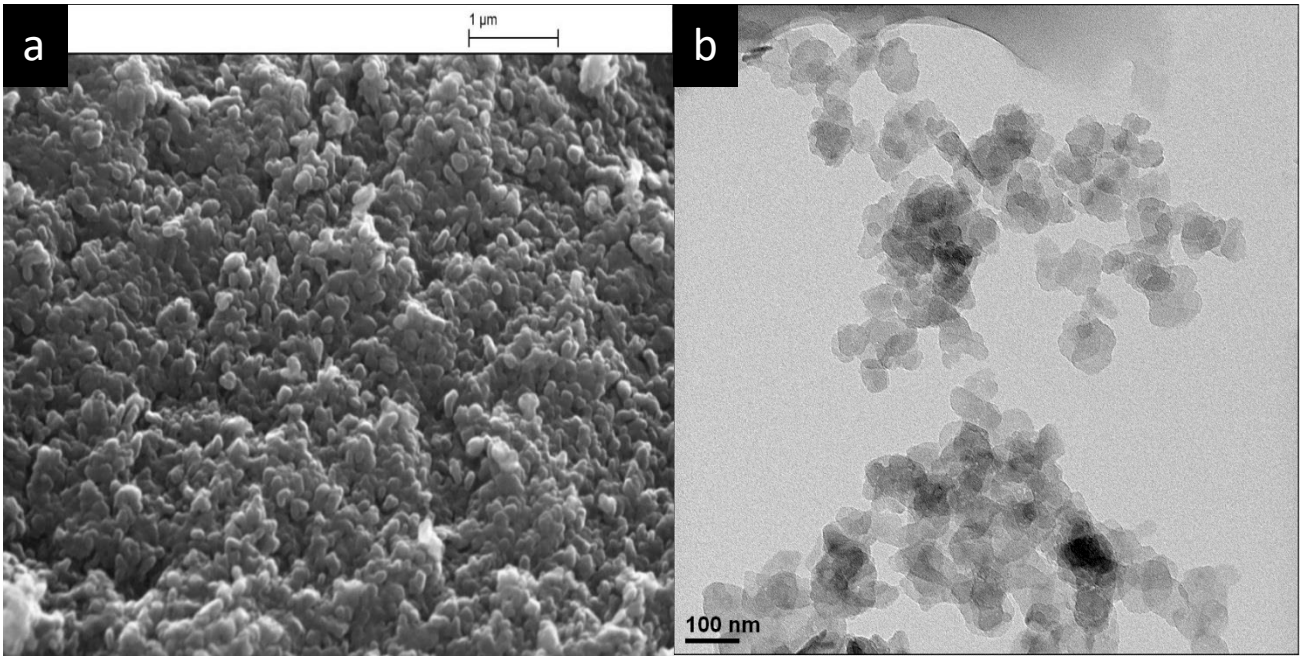

Figure 44. (a) SEM image and (b) TEM image of magnesium hydroxide powder sample 20, synthesised from magnesium chloride hexahydrate (1.2 M) and sodium hydroxide (1.2 M) with agitation (2.5 h), at room temperature.

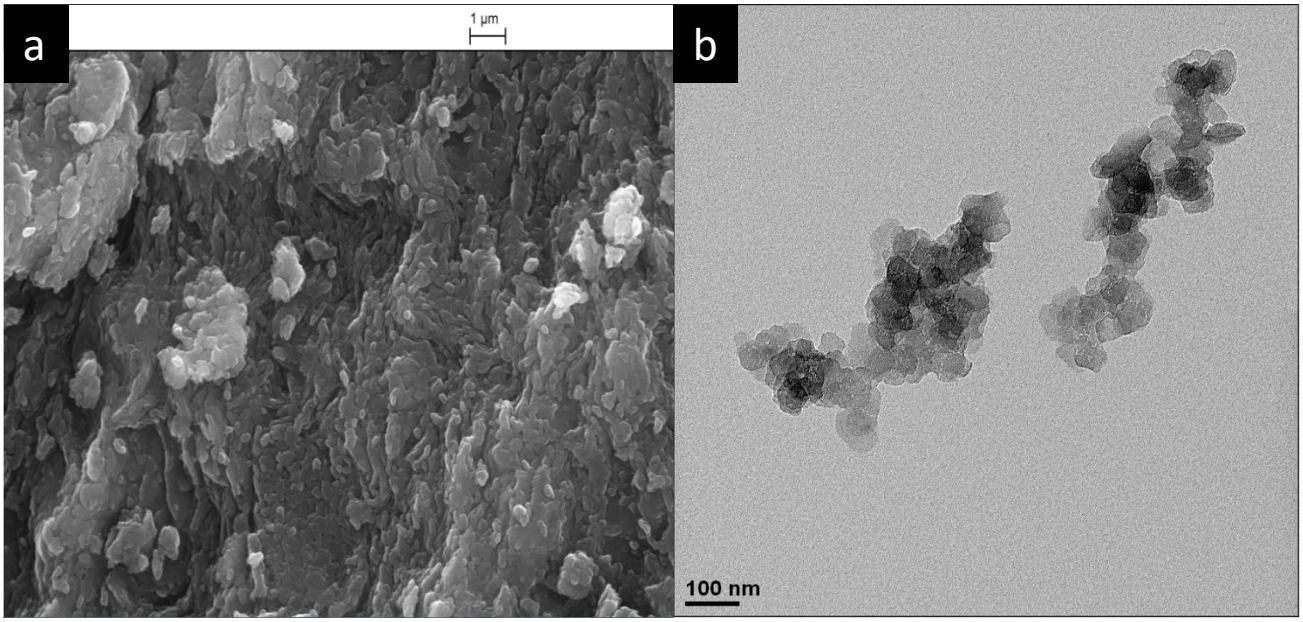

Figure 45. (a) SEM image and (b) TEM image of magnesium hydroxide powder sample 21, synthesised from magnesium chloride hexahydrate (0.6 M) and sodium hydroxide (1.2 M) with agitation (2.5 h), at 50 ºC.

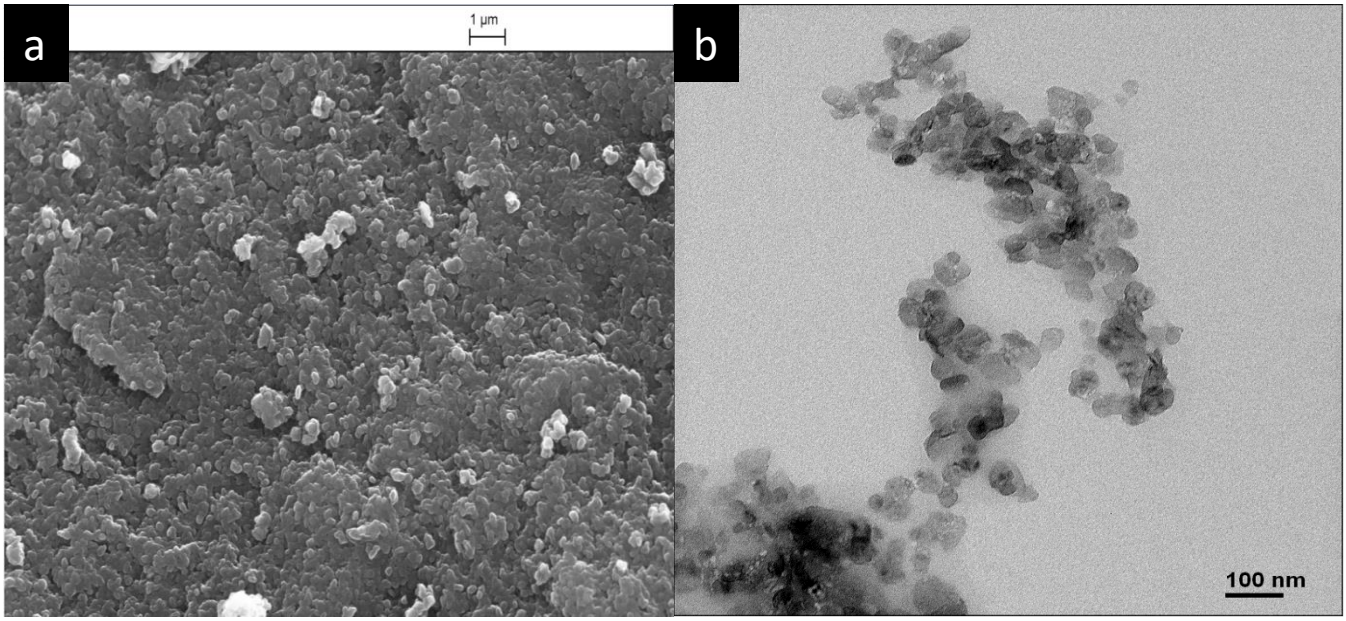

Figure 46. (a) SEM image and (b) TEM image of magnesium hydroxide powder sample 22, synthesised from magnesium chloride hexahydrate (0.6 M) and sodium hydroxide (1.2 M) with agitation (2.5 h), at 40 ^{o}C.

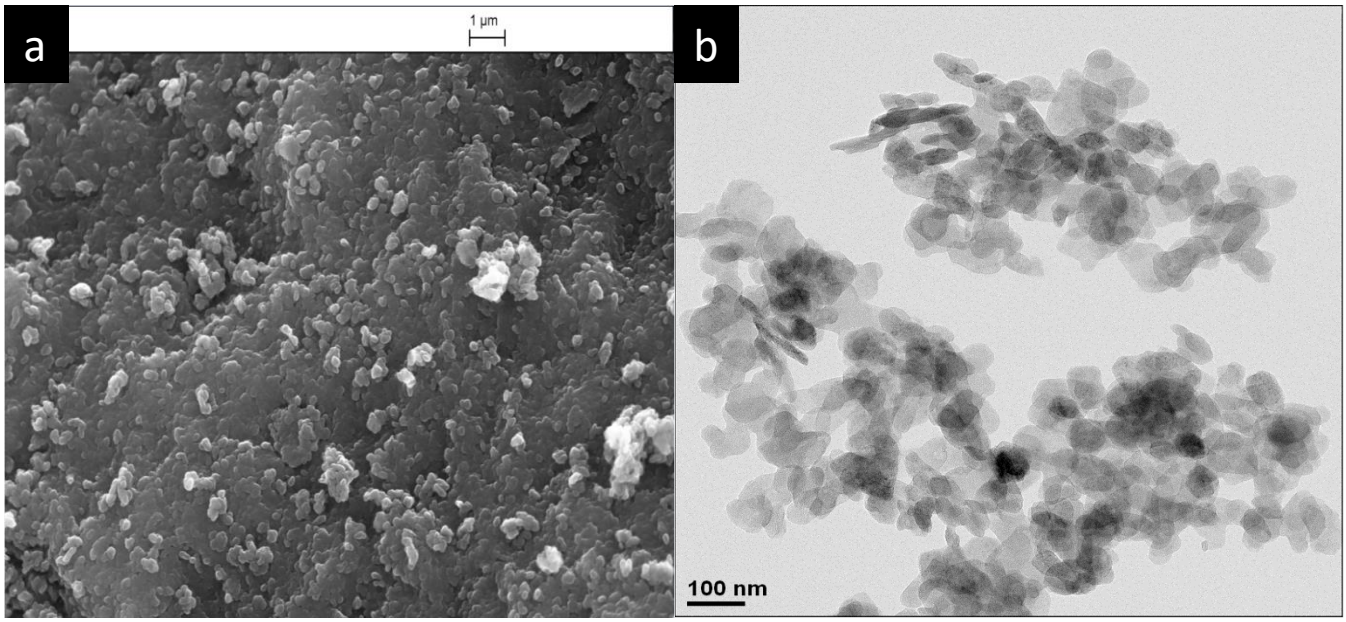

Figure 47. (a) SEM image and (b) TEM image of magnesium hydroxide powder sample 23, synthesised from magnesium chloride hexahydrate (0.6 M) and sodium hydroxide (1.2 M) with agitation (2.5 h), at 10 ^{o}C.

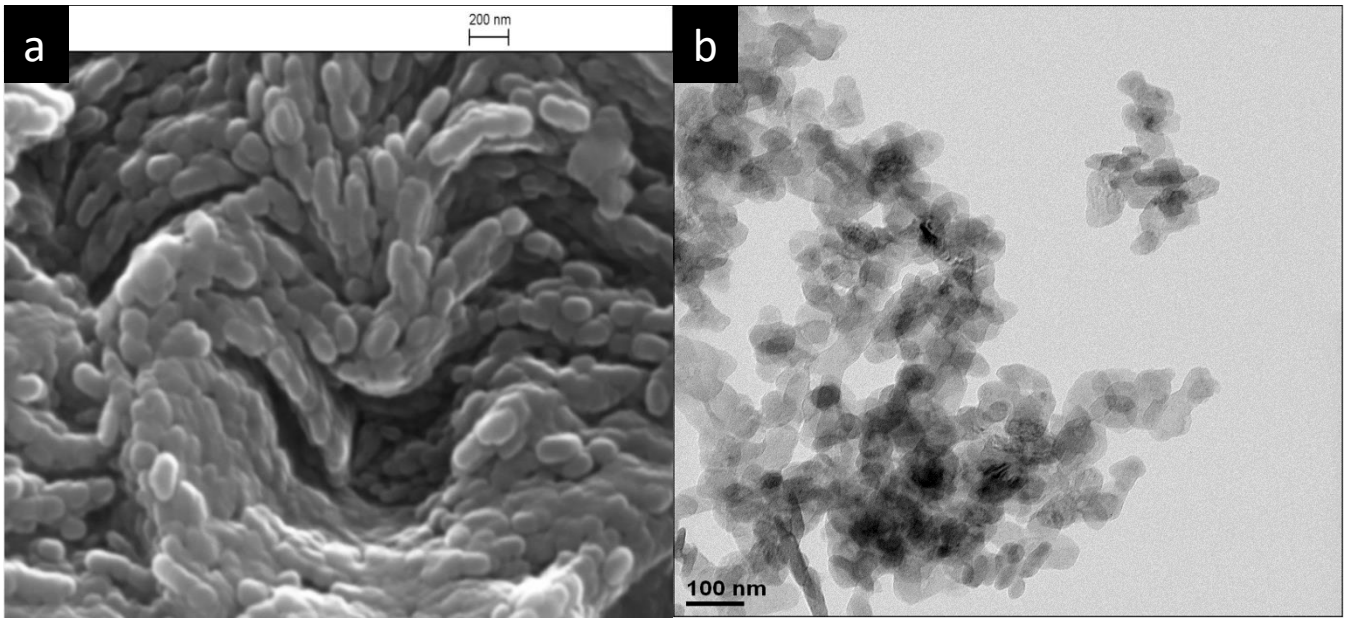

Figure 48. (a) SEM image and (b) TEM image of magnesium hydroxide powder sample 24, synthesised from magnesium chloride hexahydrate (0.6 M) and sodium hydroxide (1.2 M), no agitation, room temperature.

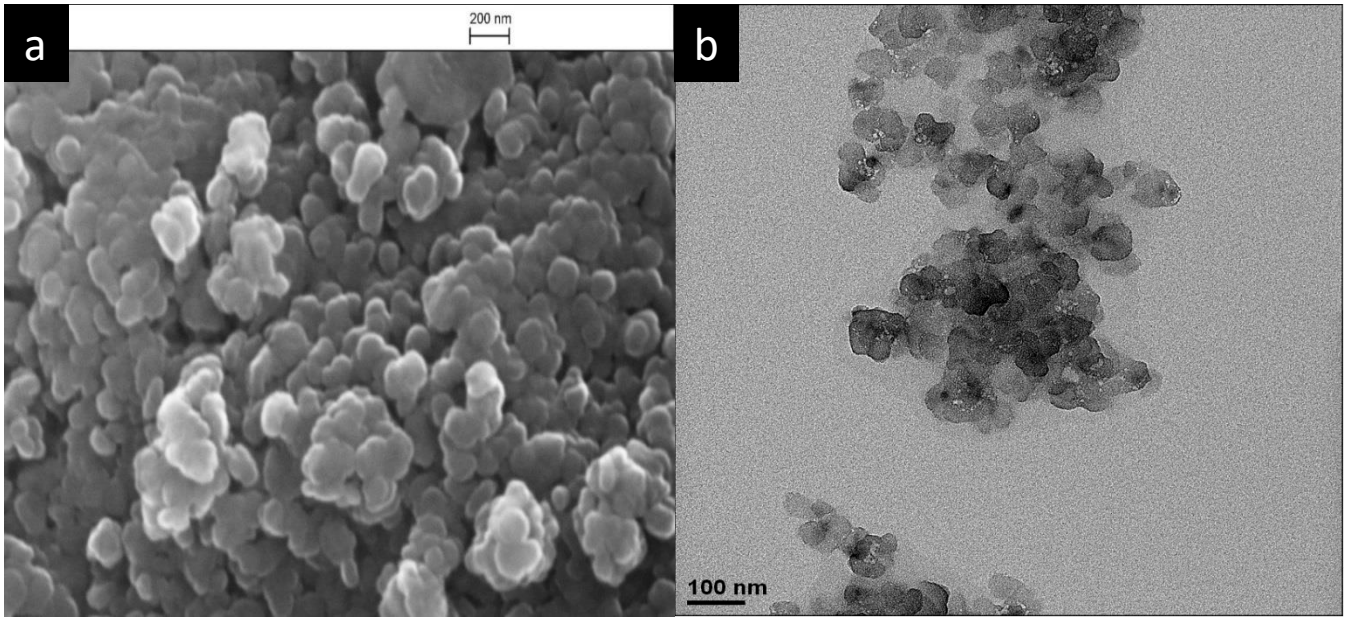

Figure 49. (a) SEM image and (b) TEM image of magnesium hydroxide powder sample 25, synthesised from magnesium chloride hexahydrate (0.6 M) and sodium hydroxide (1.2 M) with agitation (3 days), room temperature.

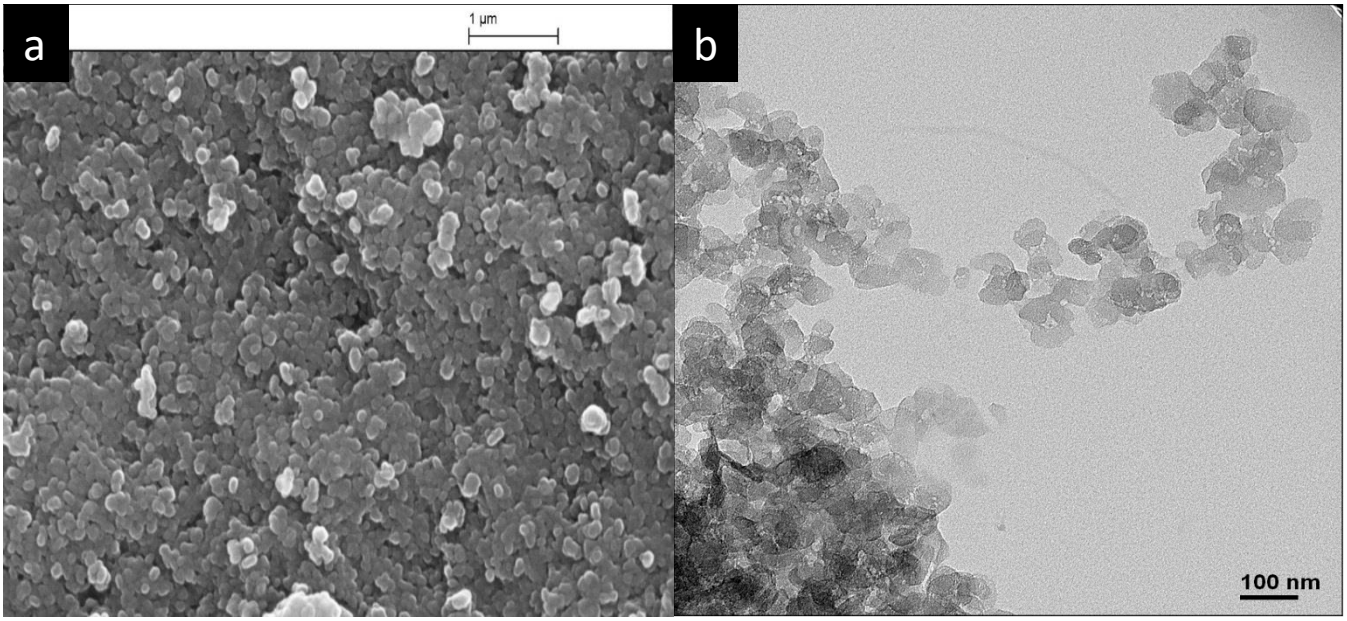

Figure 50. (a) SEM image and (b) TEM image of magnesium hydroxide powder sample 26, synthesised from magnesium chloride hexahydrate (0.6 M) and sodium hydroxide (1.2 M) with agitation (2.5 h), room temperature. Fast rate of addition of reactants.

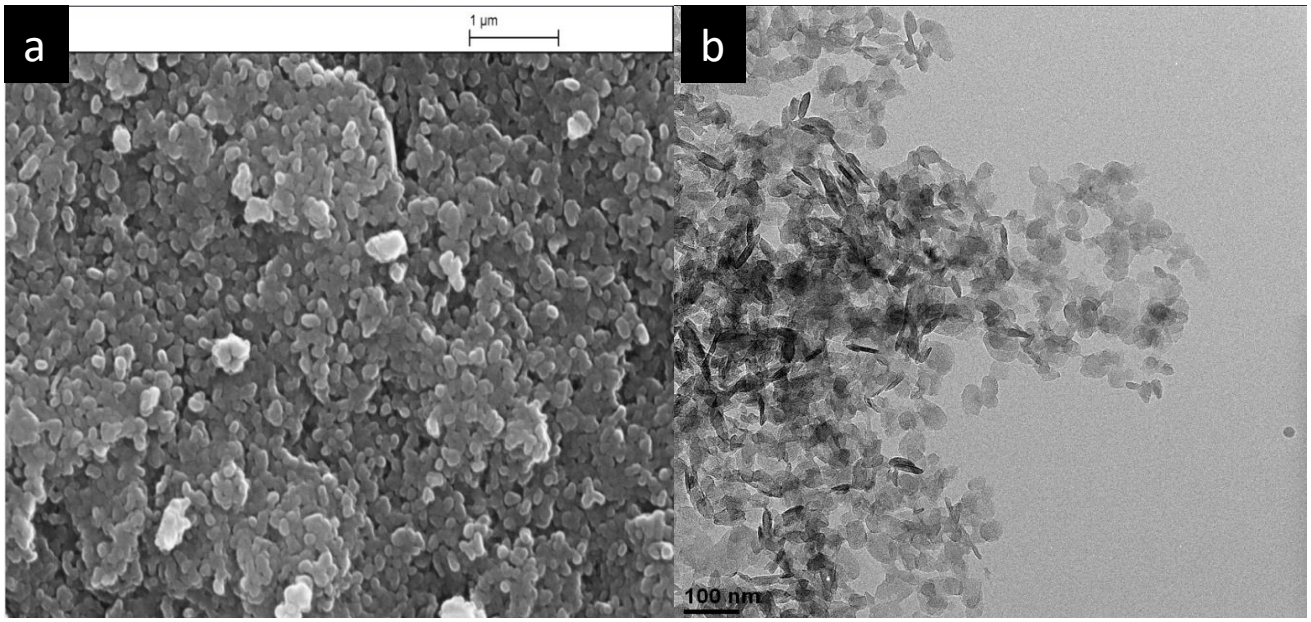

Figure 51. Mean particle diameter/ length of powdered magnesium hydroxide samples, formed from a strong base, via analysis of SEM micrographs.

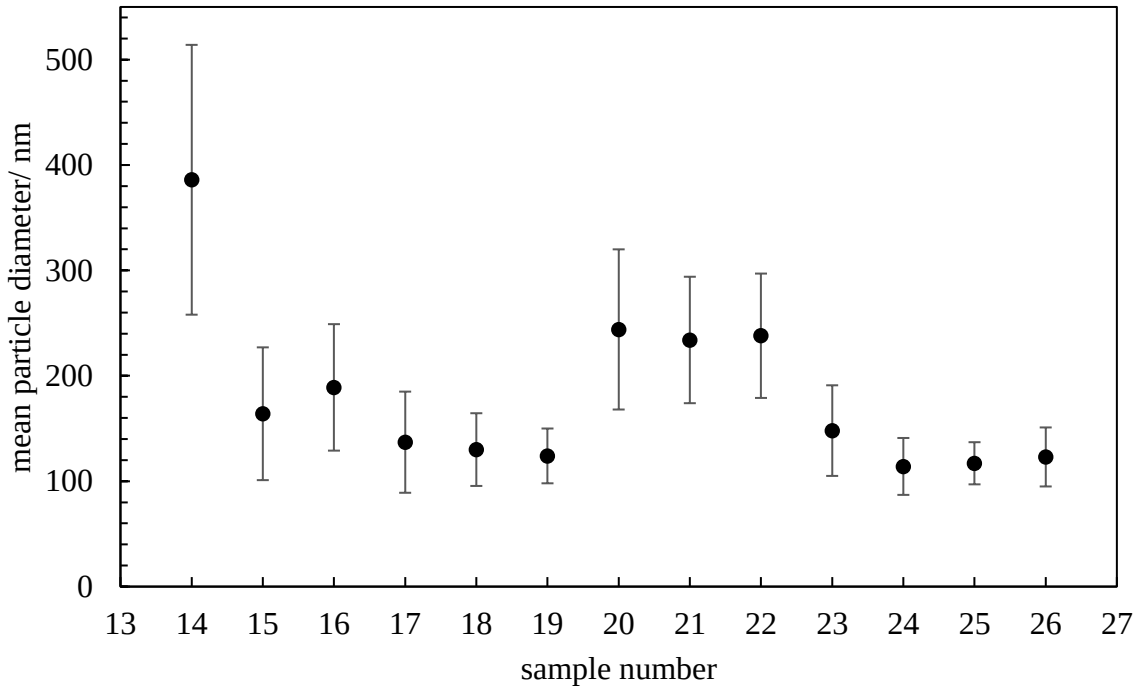

Particles formed from NaOH do not vary greatly when reaction conditions are varied and the samples possess a number of common characteristics. The same variation in particle morphology and size are not as evident in comparison to particles formed from NH_4OH, the particles in samples 14-26 are very similar to samples 1, 7, 8, 9, 10, 11, 12 and 13. Despite an excess of Mg^{2+} ions during the synthesis of samples 17, 19 and 20, the long rods formed under similar conditions when NH_4OH was used as the base are not seen. One theory for this could be when a strong base is used to synthesise $Mg(OH)_2$, pH increases past the isoelectric point of magnesium hydroxide leading to the forming magnesium hydroxide particles having a negative charge. This negative charge attracts the dissociated Na^+ ions which hinder the growth of the crystals, leading to smaller particles. This effect is also noted in the work of Henrist e*t al.*[12].

3.1.2 XRD analysis

XRD analysis suggested initial impurities in samples synthesised when Mg^{2+} was in excess or from NaOH when samples were washed with 10 ml Milli-Q water. However, impurities were removed when particles were redispered. The XRD patterns formed for each of the magnesium hydroxide samples in this experiment each suggested a hexagonal crystal structure, arising as a result of the octahedral anions magnesium hydroxide forms. This pattern is widely seen in the literature and is accepted as the official XRD pattern of magnesium hydroxide, shown in Figure 52 along with the XRD pattern for sample 16 produced in this study for reference.

The literature values for the d-spacing for 001 peaks and 110 peaks are 0.4767 nm ($2\theta = 18.59$ °) and 0.1574 nm ($2\theta = 58.56$ °) respectively, and were used as references when comparing XRD patterns of samples prepared here [23]. d-spacing values can be calculated with the use of Bragg's equation,

$$2d\ sin\theta = n\lambda \qquad (12)$$

where θ is the scattering angle, d is the spacing between layers of atoms, n is an integer and λ is the wavelength of the X – ray.

The d-spacing values for 001 and 110 peaks agreed with values found in the literature, with values ranging from d(001) = 0.4679 nm to 0.47914 nm and d(110) = 0.1574 – 0.1575, further proof that magnesium hydroxide was indeed synthesised.

Figure 52. XRD stick reference pattern for standard magnesium hydroxide (JCPDS 00-044-1482) [91] (blue) with XRD pattern for magnesium hydroxide sample 16, synthesised from magnesium chloride hexahydrate (0.6 M) and sodium hydroxide (1.2 M) with agitation (2.5 h) at room temperature (black).

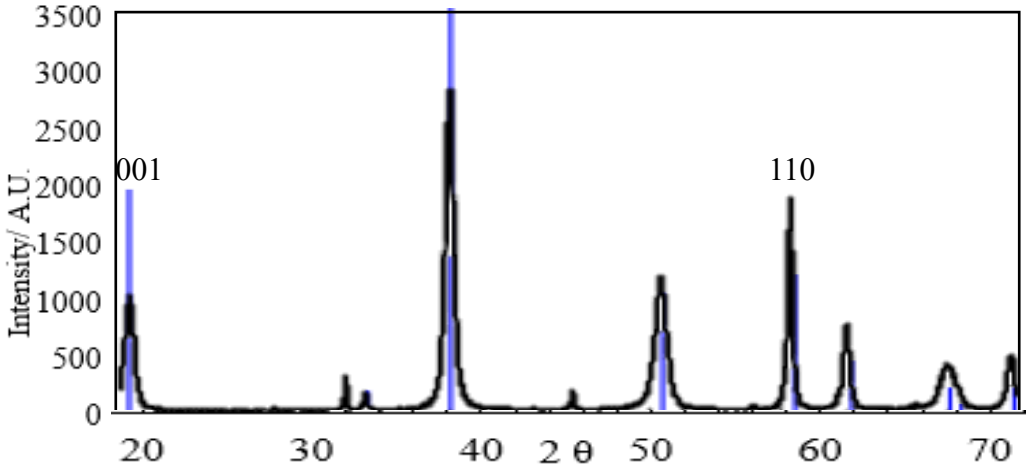

One of the main differences witnessed in XRD patterns for samples prepared here to some patterns found in the literature is the intensity of the 001 peak. For the majority of the samples formed, the 001 peak is less intense than the 110 peak, evident in Figure 52 with sample 16.

The sample which had an XRD pattern with a more intense 001 peak than 110 peak was sample 25, which was produced from a reaction which was allowed to run for 3 days, relevant XRD pattern shown in Figure 53.

Figure 53. XRD pattern for magnesium hydroxide sample 25, synthesised from magnesium chloride hexahydrate (0.6 M) and sodium hydroxide (1.2 M) with agitation (3 days) room temperature.

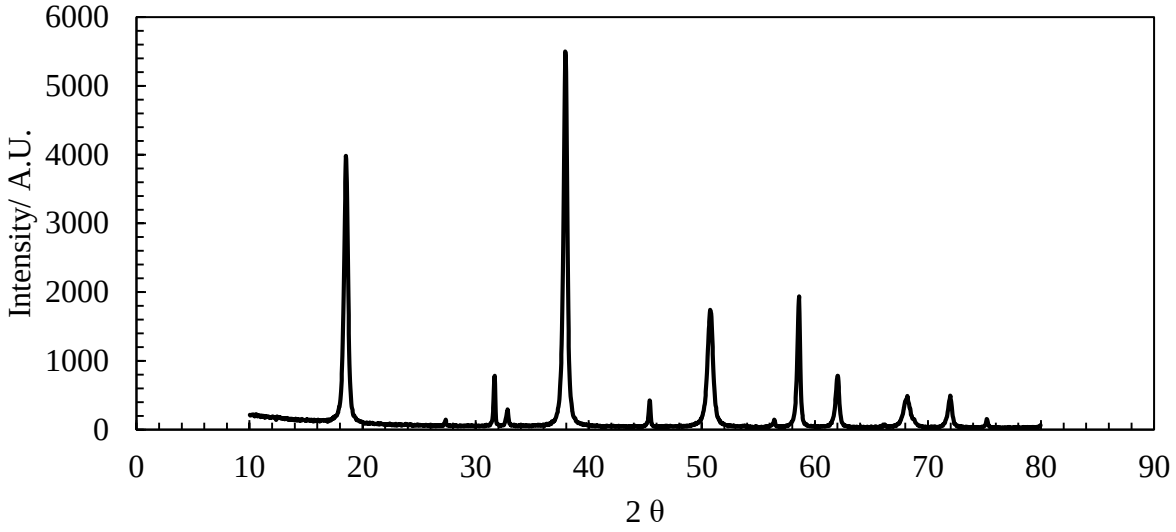

This could suggest that the magnesium hydroxide crystals develop more slowly in the 001 direction than in the 110 direction. In the literature, it is suggested that when the 001 peak is less intense than the 110 peak, the samples are more likely to undergo agglomeration [12].

The XRD patterns for the remaining magnesium hydroxide samples can be found in Appendices 1 – 26. The XRD patterns of samples 4 and 18 are also notable as peaks from impurities are present in the region of 20°-35°. It is thought that these peaks have arisen from magnesium chloride hexahydrate impurities, as these samples were both formed via reactions where magnesium chloride hexahydrate was in excess.

3.1.3 FT-IR analysis

FR-IR analysis was carried out on each of the magnesium hydroxide samples prepared, example given in Figure 54. The spectrum for each $Mg(OH)_2$ sample was similar to those found in the literature. Each of the spectra had the 5 peaks expected for a sample of magnesium hydroxide. Absorption bands at around 3693 cm^{-1} were assigned to O-H stretching vibrations, which are also represented by the very broad peak at 3300 – 3400 cm^{-1}. The absorption peak at around 1630 cm^{-1} was assigned to the bending vibration of the Mg-O bond and the peak at 1430 cm^{-1} represents the bending vibration of O-H bonds. The peak at around 500 cm^{-1} is attributed to lattice vibrations of Mg – O [92].

Figure 54. FT-IR spectrum for magnesium hydroxide sample 19, synthesised from magnesium chloride hexahydrate (2.4 M) and sodium hydroxide (0.6 M) with agitation (2.5 hours) at room temperature.

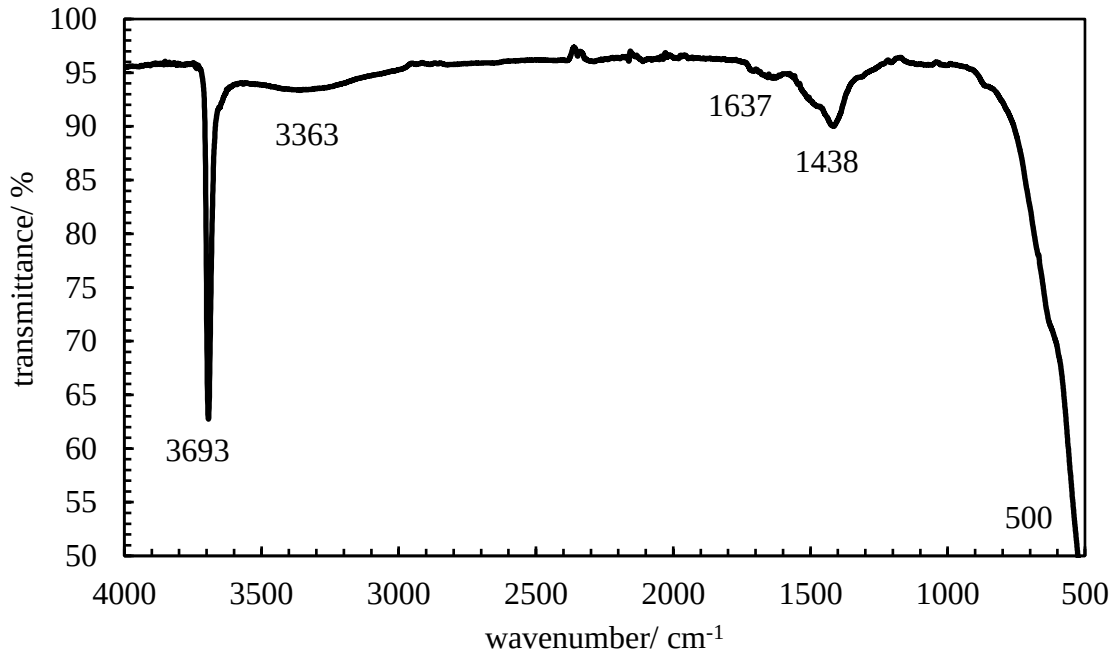

The spectra for the other samples can be found in Appendices 27 – 52.

3.2 Aqueous dispersions

When using the Malvern Zetasizer ZS-Nanoseries instrument to assess particle diameter and zeta potential of magnesium hydroxide particles, dispersions of very low magnesium hydroxide concentration were required. This was because, in dispersions of high magnesium hydroxide concentration, sedimentation of particles occurred very quickly due to magnesium hydroxide being much more dense than water (2.36 g cm^{-3}) [98]. As magnesium hydroxide concentration decreases, the rate of sedimentation also decreases.

Each of the dispersions, 0.2 wt. % of $Mg(OH)_2$, formed from the 26 magnesium hydroxide samples in this experiment appeared milky/ cloudy. There was no apparent difference in turbidity between them when observed by eye. Once the dispersions had been diluted to an appropriate concentration (0.02 wt. %) to, the sample was clear and colourless, evident in Figure 55.

Figure 55. (a) Aqueous dispersion of magnesium hydroxide sample 1, 0.2 wt. %, directly following. (b) Aqueous dispersion of magnesium hydroxide sample 1, 0.02 wt. %, directly following sonication.

As the Malvern Zetasizer ZS–Nanoseries measures the mean particle diameter of a dispersion, it produces a Z-average of the data it records. The Z-average is the weighted mean hydrodynamic size of the particles in the sample measured by dynamic light scattering. When measuring particle diameter or zeta potential, the Zetasizer produces a distribution curve of the results, as can be seen in Figures 56 and 57.

The refractive index of magnesium hydroxide is 1.559 [93].

Figure 56. Distribution curve of Z-average particle diameter of sample 16, 0.02 wt. % magnesium hydroxide aqueous dispersion at 25 ºC and natural pH, 10.5.

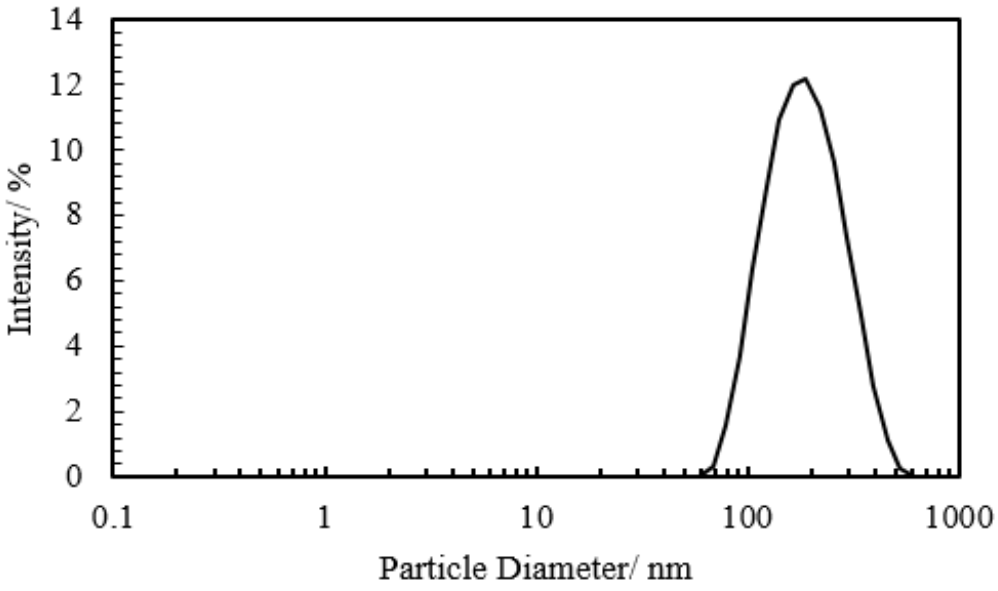

Figure 57. Distribution curve of zeta potential of magnesium hydroxide sample 20, 0.02 wt. % magnesium hydroxide aqueous dispersion at 25 ºC and natural pH, 10.5.

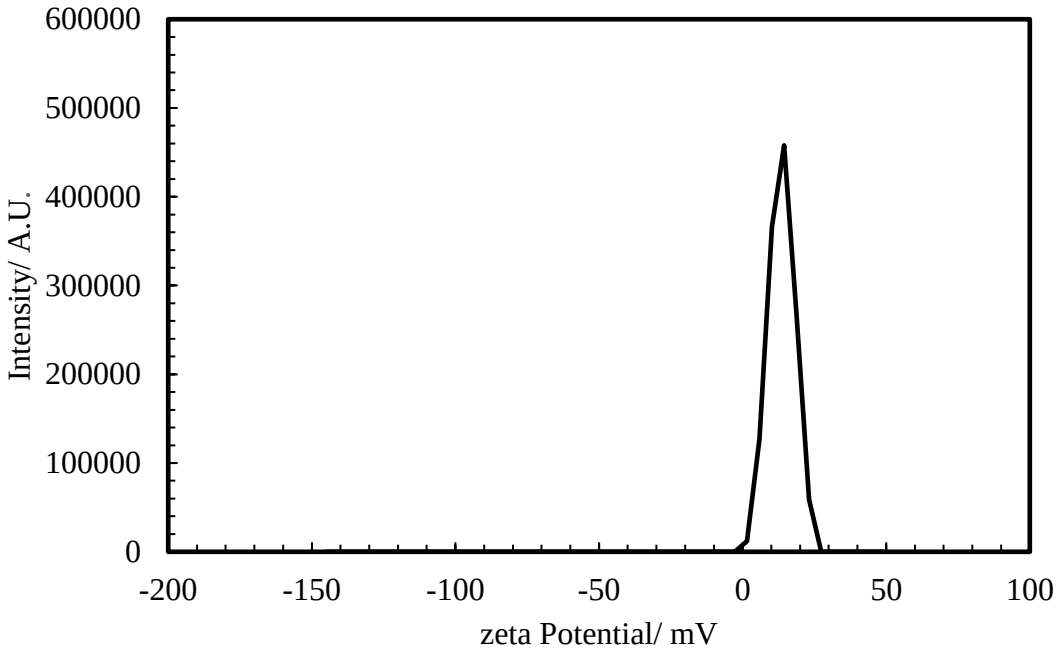

For each of the 26 magnesium hydroxide samples, aqueous dispersions were formed and the mean particle diameter and zeta potential was measured, shown in Figures 58 and 59 for samples 1 – 13 and Figures 60 and 61 for samples 14 – 26.

Figure 58. Mean particle diameter for 0.02 wt.% aqueous dispersions of magnesium hydroxide samples synthesised from a weak base (samples 1-13). Measurements were taken at 25 ^{o}C and natural pH, 10.5.

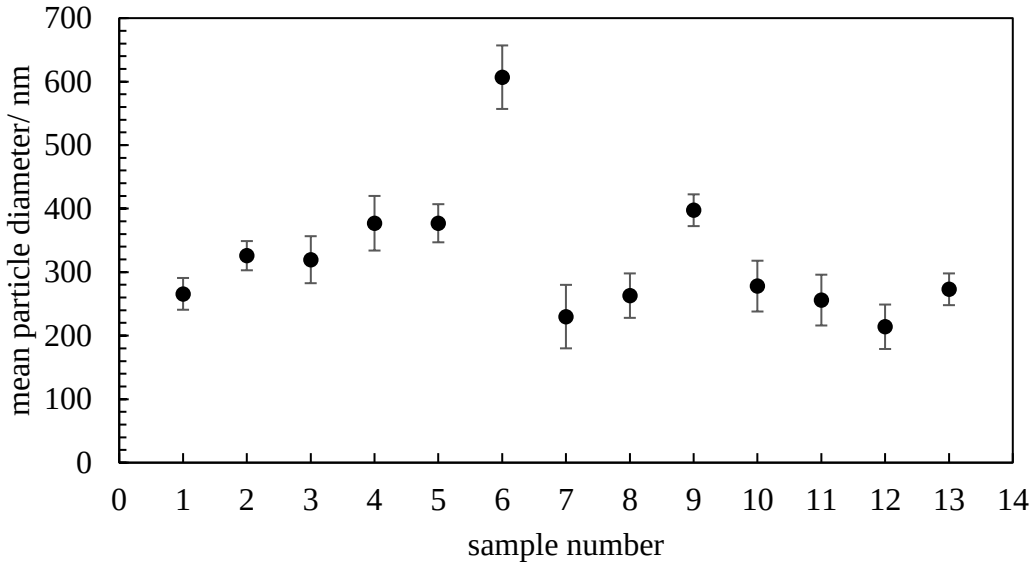

Figure 59. Mean zeta potential for 0.02 wt.% aqueous dispersions of magnesium hydroxide samples synthesised from a weak base (samples 1-13). Measurements were taken at 25 ^{o}C and natural pH, 10.5.

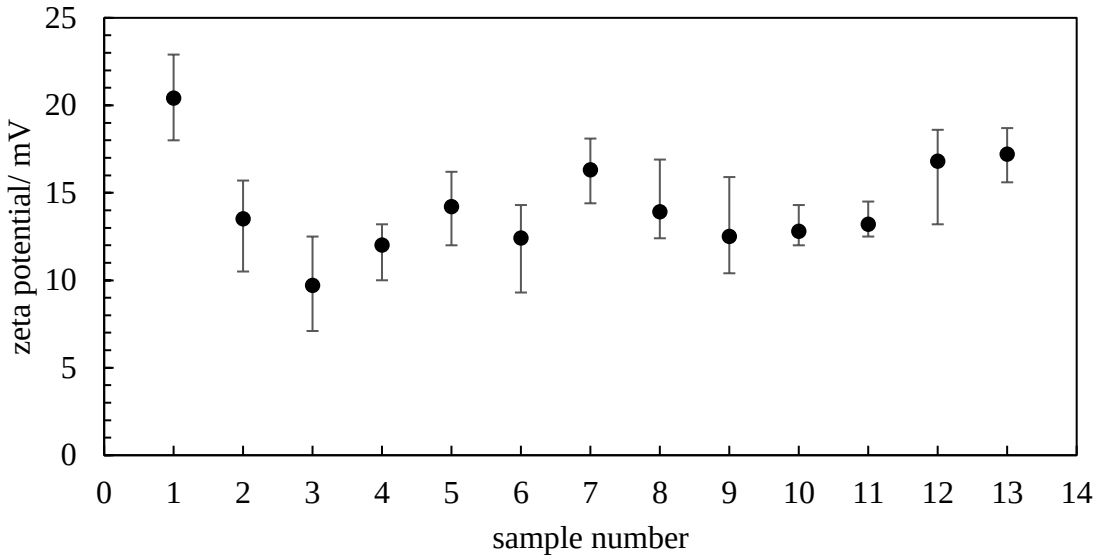

Figure 60. Mean particle diameter measurements for 0.02 wt.% aqueous dispersions of magnesium hydroxide samples synthesised from a strong base (samples 14-26). Measurements were taken at 25 ºC and natural pH, 10.5.

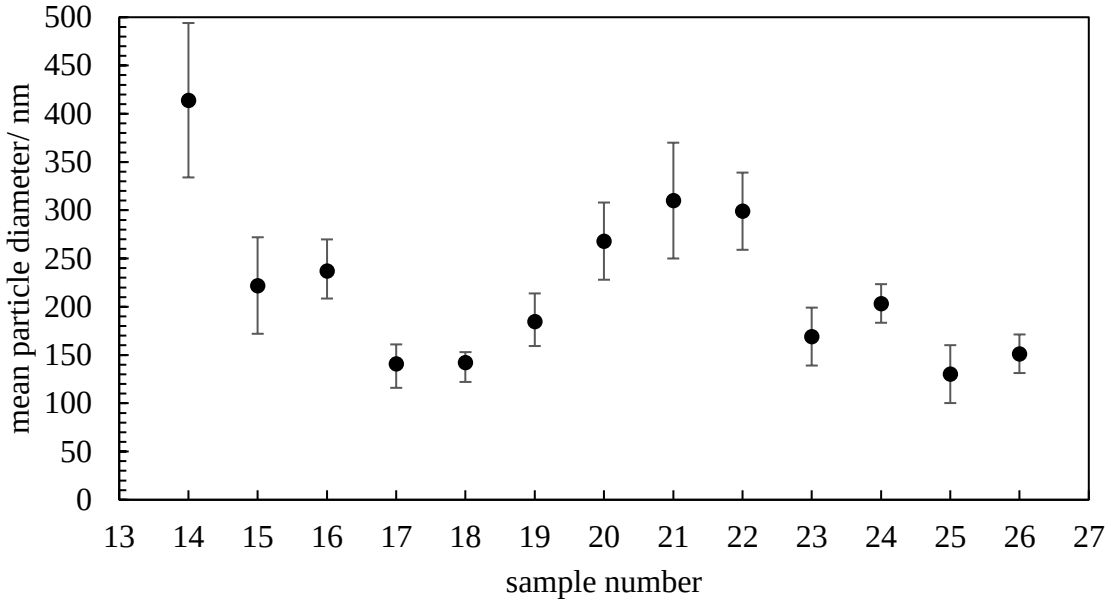

Figure 61. Mean zeta potential measurements for 0.02 wt.% aqueous dispersions of magnesium hydroxide samples synthesised from a weak base (samples 14-26). Measurements were taken at 25 ºC and natural pH 10.5.

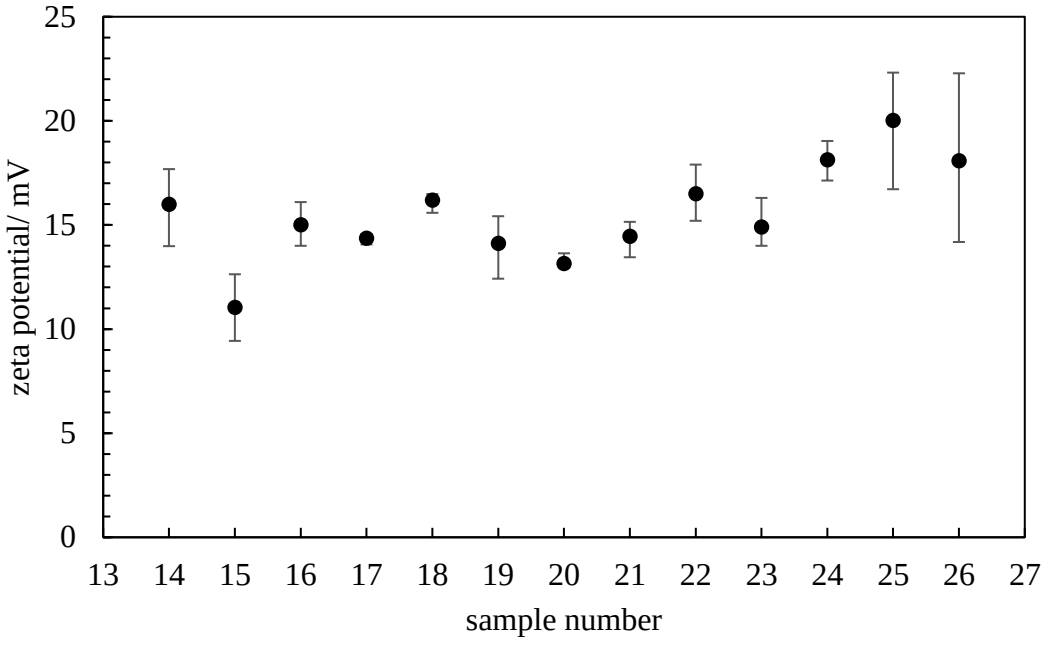

Primary particle diameter was successfully measured by using the Malvern Zetasizer ZS-Nanoseries to analyse magnesium hydroxide dispersions with concentration of 0.02 wt. %. Particle diameter measurements were in agreeance with those obtained from SEM micrographs. For example, particle diameter for sample 1 from SEM was around 210 nm, and was found to be around 240 nm through dynamic light scattering. The particle diameter measured for sample 26 from SEM and dynamic light scattering were also identical. However, the measurements recorded with use of the Malvern Zetasizer may be slightly inaccurate as the DLS method assumes all particles are spherical. This is not true for the particles in the majority of the magnesium hydroxide samples.

There is no apparent correlation between the zeta potential of magnesium hydroxide particles and the reaction conditions they were synthesised under. The average zeta potential value for the samples synthesised from a strong base, + 15.5 mV ± 5 mV, was slightly greater than the average zeta potential value for samples synthesised from a weak base, + 14.2 mV ± 6 mV. However, this slight difference can be considered negligible due to the uncertainty within the zeta potential recorded for each sample. The maximum zeta potential value was of sample 1 which was around + 21 mV. The minimum zeta potential value was of sample 3, which was around +10 mV. The zeta potential values for magnesium hydroxide samples formed in this study are in agreeance with those recorded by Tan *et al.* [6] at similar values of pH.

When an electrolyte is introduced to the aqueous dispersions of magnesium hydroxide, the electrostatic repulsion between particles is reduced [56, 60]. NaCl was dissolved in water before magnesium hydroxide was added. In theory, this should lead to increased agglomeration of particles in the dispersion as the van der Waals forces of attraction overcome the repulsive forces which arise due to the like charges of the particles. Flocs of particles subsequently form. The dispersions with added electrolytes formed in this study support this theory.

In the series of dispersions which contained varied [NaCl], the turbidity of the dispersions immediately following sonication did not appear to increase with salt concentration. However, an increased rate of sedimentation could be observed in NaCl dispersions as opposed to dispersions from Milli–Q water.

Figure 62. Aqueous dispersions of magnesium hydroxide sample 22, 0.2 wt. %, containing different concentrations of NaCl immediately after dispersion. [NaCl]/ M: (a) 0. (b) 10^{-3}. (c) 10^{-2}. (d) 10^{-1}. (e) 0.2. (f) 0.5.

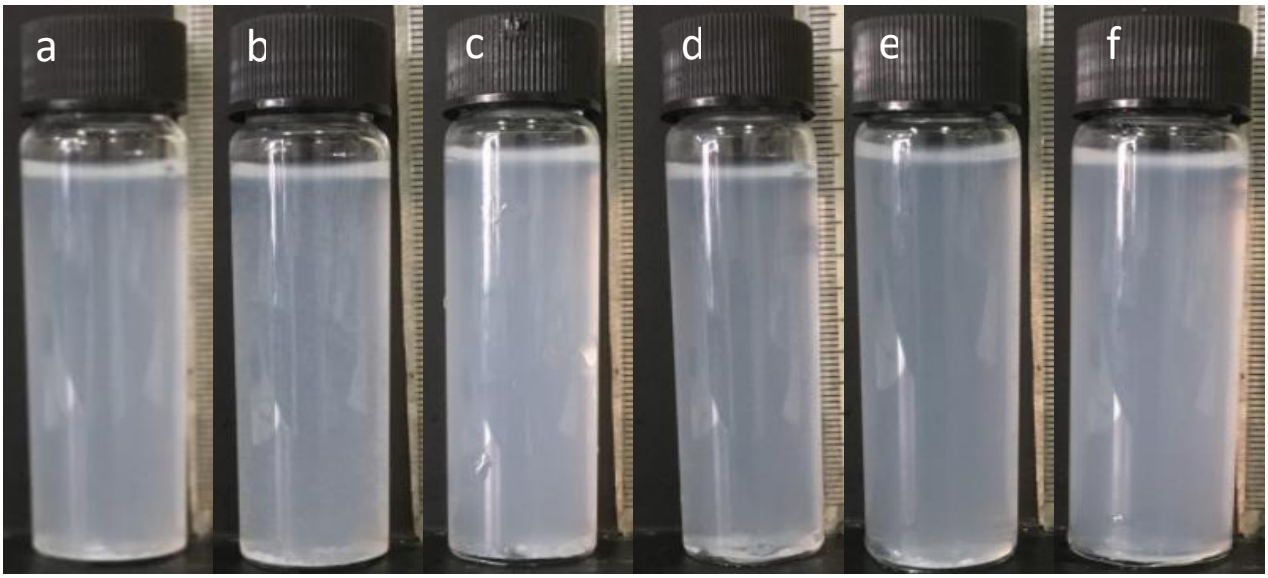

Figure 63. Aqueous dispersions of magnesium hydroxide sample 22, 0.2 wt. %, containing different concentrations of NaCl 2 minutes after dispersion. [NaCl]/ M: (a) 0. (b) 10^{-3}. (c) 10^{-2}. (d) 10^{-1}. (e) 0.2. (f) 0.5.

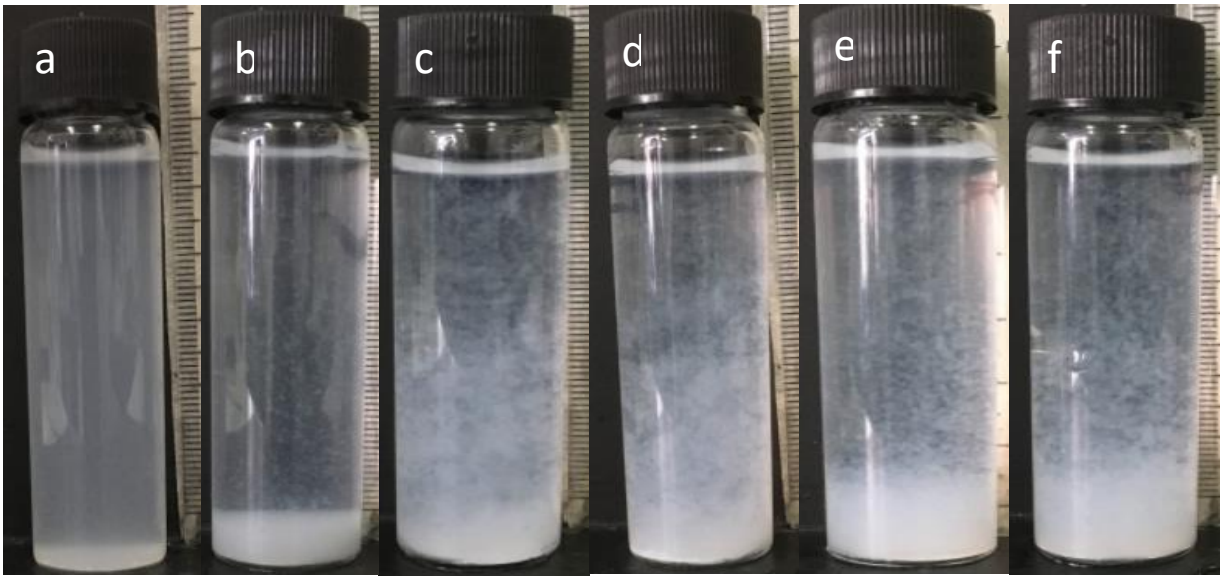

Size measurements by light scattering, Figure 64, also showed that agglomeration of particles increases with [NaCl]. The faster rate of sedimentation in dispersions containing NaCl can be explained by the Stokes equation due to their increased apparent size.

Figure 64. Mean particle diameter of $Mg(OH)_2$ sample 19, 0.02 wt. %, as a function of [NaCl].

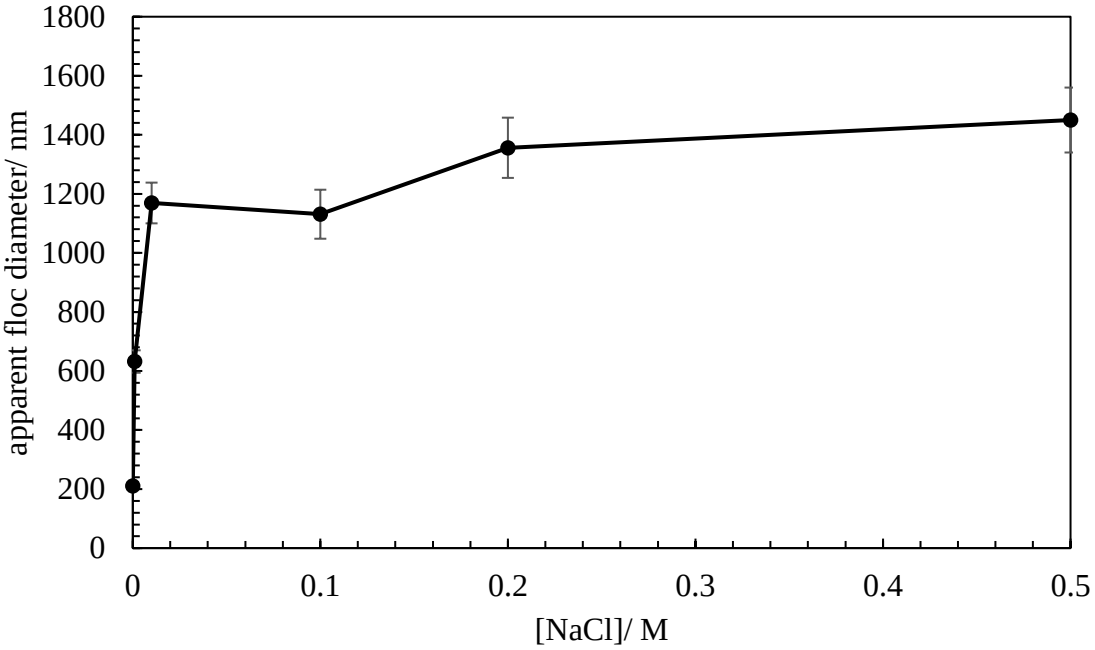

3.3 Isooctane-in-water emulsions

3.3.1 Emulsions stabilised by 26 different magnesium hydroxide Samples

Isooctane-in-water emulsions have been stabilised successfully by $Mg(OH)_2$ particles of different size, morphology and zeta potential. All emulsions of isooctane-in-water remained stable and showed very little variation in f_O, f_W or mean droplet diameter beyond 48 hours since homogenisation. Emulsions from magnesium hydroxide samples synthesised from NH_4OH, samples 1 – 13, shall be discussed first and then the emulsions stabilised by magnesium hydroxide samples synthesised from NaOH, sample 14 – 26 shall follow. Each of the isooctane-in-water emulsions produced were o/w systems. The appearance of the emulsions formed from samples 1 – 7 are shown in the photographs of Figure 65. The clear, top layer of each system is isooctane which has been liberated from the emulsion. The white layer directly below any liberated isooctane is the layer of emulsion. The clear layer below the emulsion is water and any particles which did not adsorb at the interface sediment at the bottom of the container, which can be seen as a white layer. Optical micrographs of each emulsion, from samples 1 – 7 can be seen in Figure 66. Figures 67 and 68 contain photos of emulsions from samples 8 – 13 and their respective optical micrographs. Figure 70 shows f_o and f_w of the emulsions from samples 1 – 13 and Figure 71 shows the mean droplet diameter for these emulsions.

Figure 65. Photographs of isooctane-in-water emulsions (volume 1:1) 100 days after homogenisation. The emulsions were stabilised by 1.0 wt.% of various magnesium hydroxide samples, synthesised from a weak base. (a) **S**ample 1, (b) sample 2, (c) sample 3, (d) sample 4, (e) sample 5, (f) magnesium hydroxide sample 6, (g) sample 7.

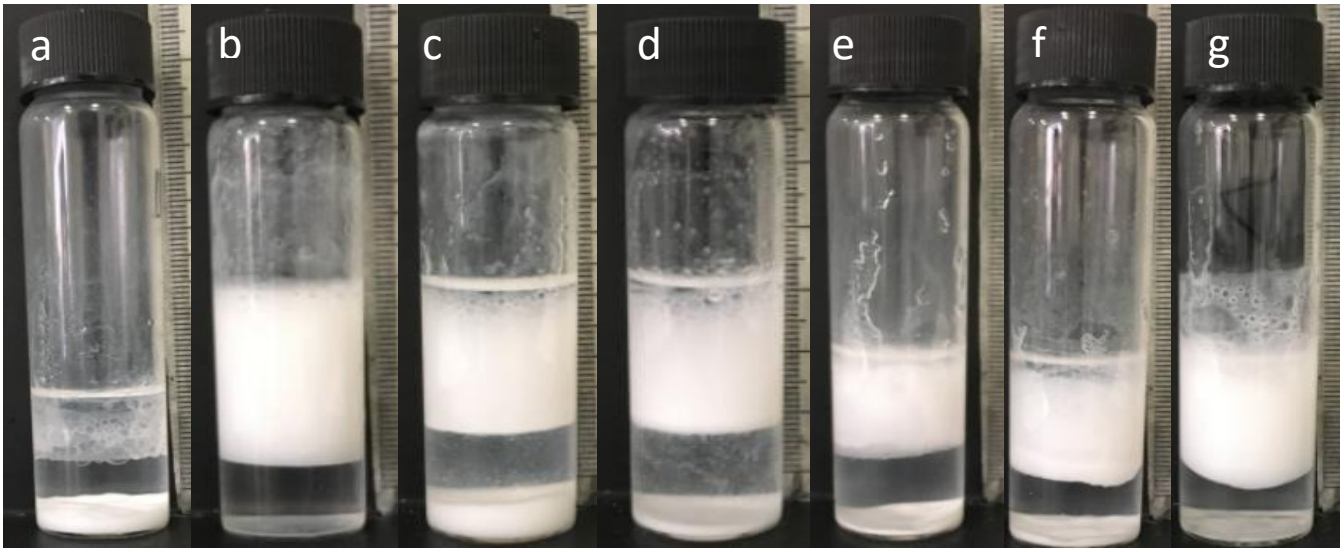

Figure 66. Optical micrographs of isooctane-in-water emulsions (volume 1:1) 2 days after homogenisation. The emulsions were stabilised by 1.0 wt.% of various magnesium hydroxide samples, synthesised from a weak base. (a) **S**ample 1, (b) sample 2, (c) sample 3, (d) sample 4, (e) sample 5, (f) magnesium hydroxide sample 6, (g) sample 7.

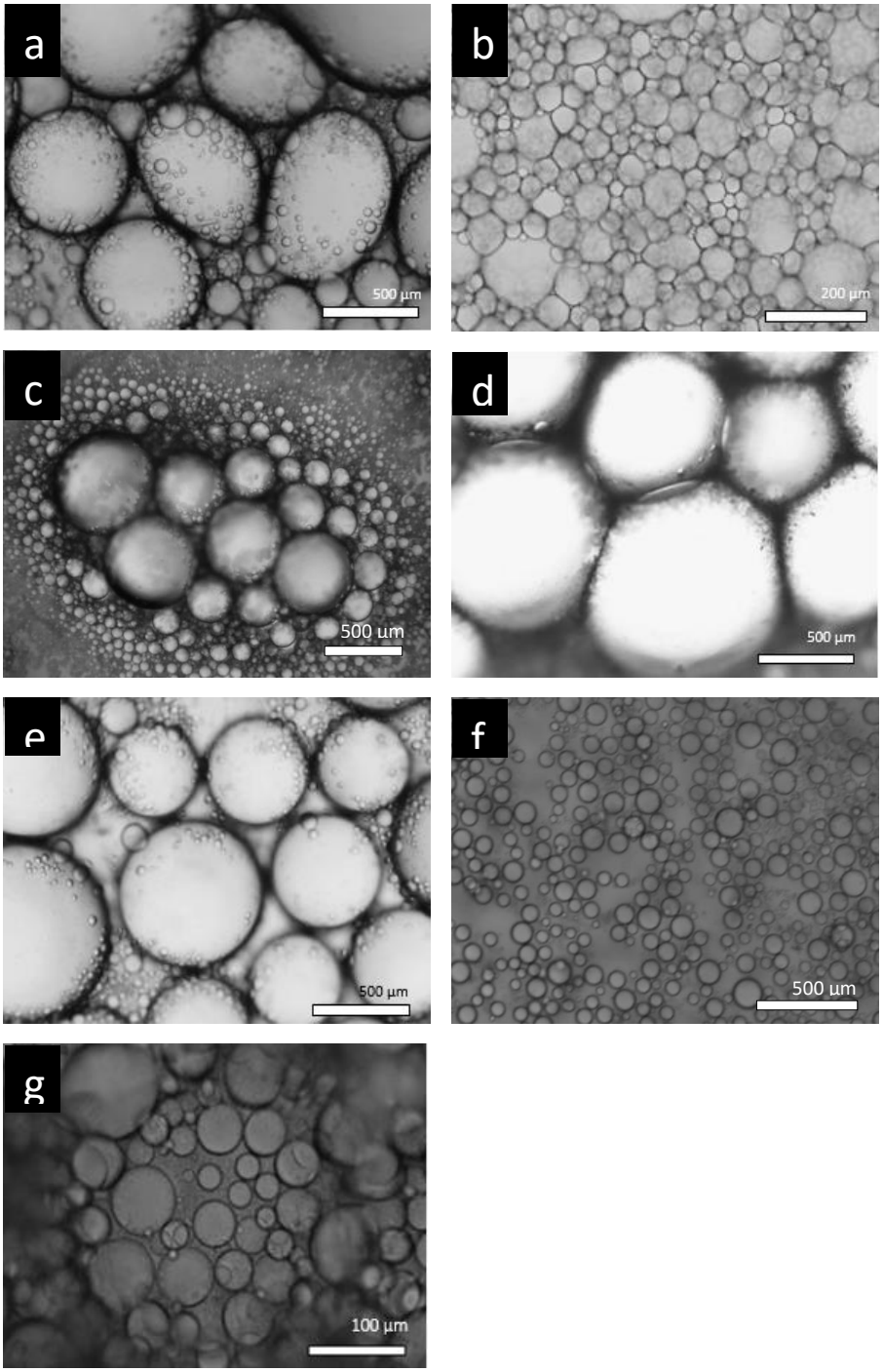

Figure 67. Photographs of isooctane-in-water emulsions (volume 1:1) 100 days after homogenisation. The emulsions were stabilised by 1.0 wt.% of various magnesium hydroxide samples, synthesised from a weak base. (a) Sample 8, (b) sample 9, (c) sample 10, (d) sample 11, (e) sample 12, (f) magnesium hydroxide sample 13.

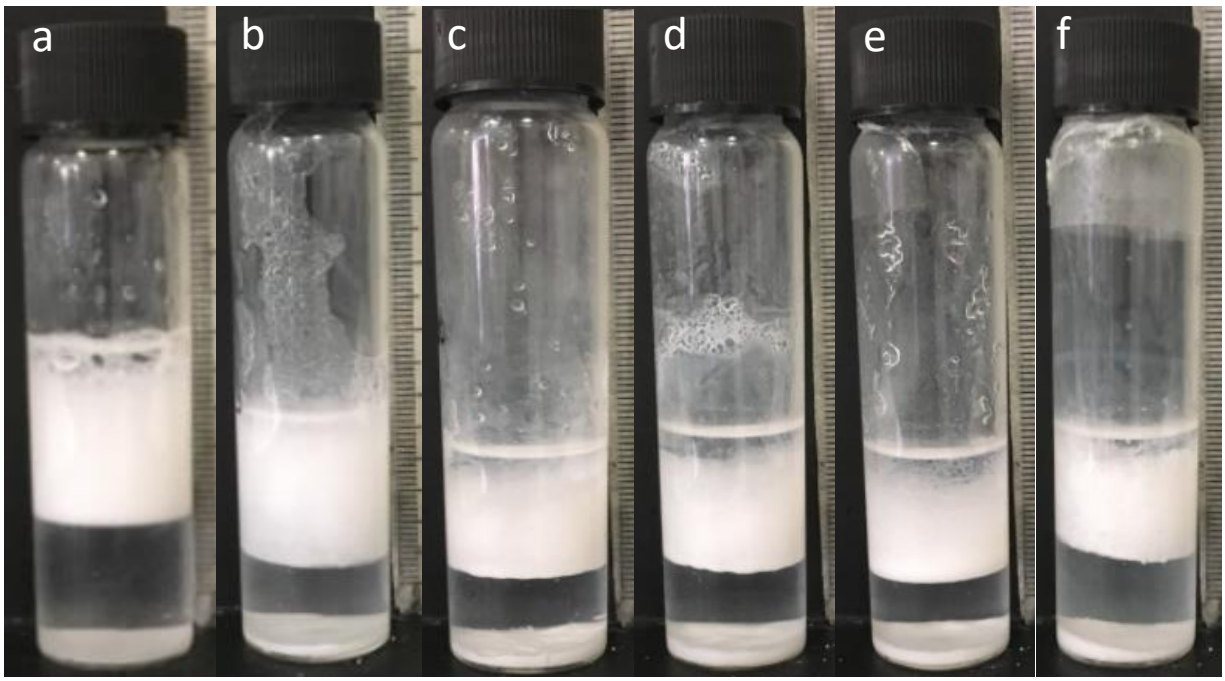

Figure 68. Optical micrographs of isooctane-in-water emulsions (volume 1:1) 2 days after homogenisation. The emulsions were stabilised by 1.0 wt.% of various magnesium hydroxide samples, synthesised from a weak base. (a) Sample 8, (b) sample 9, (c) sample 10, (d) sample 11, (e) sample 12, (f) magnesium hydroxide sample 13.

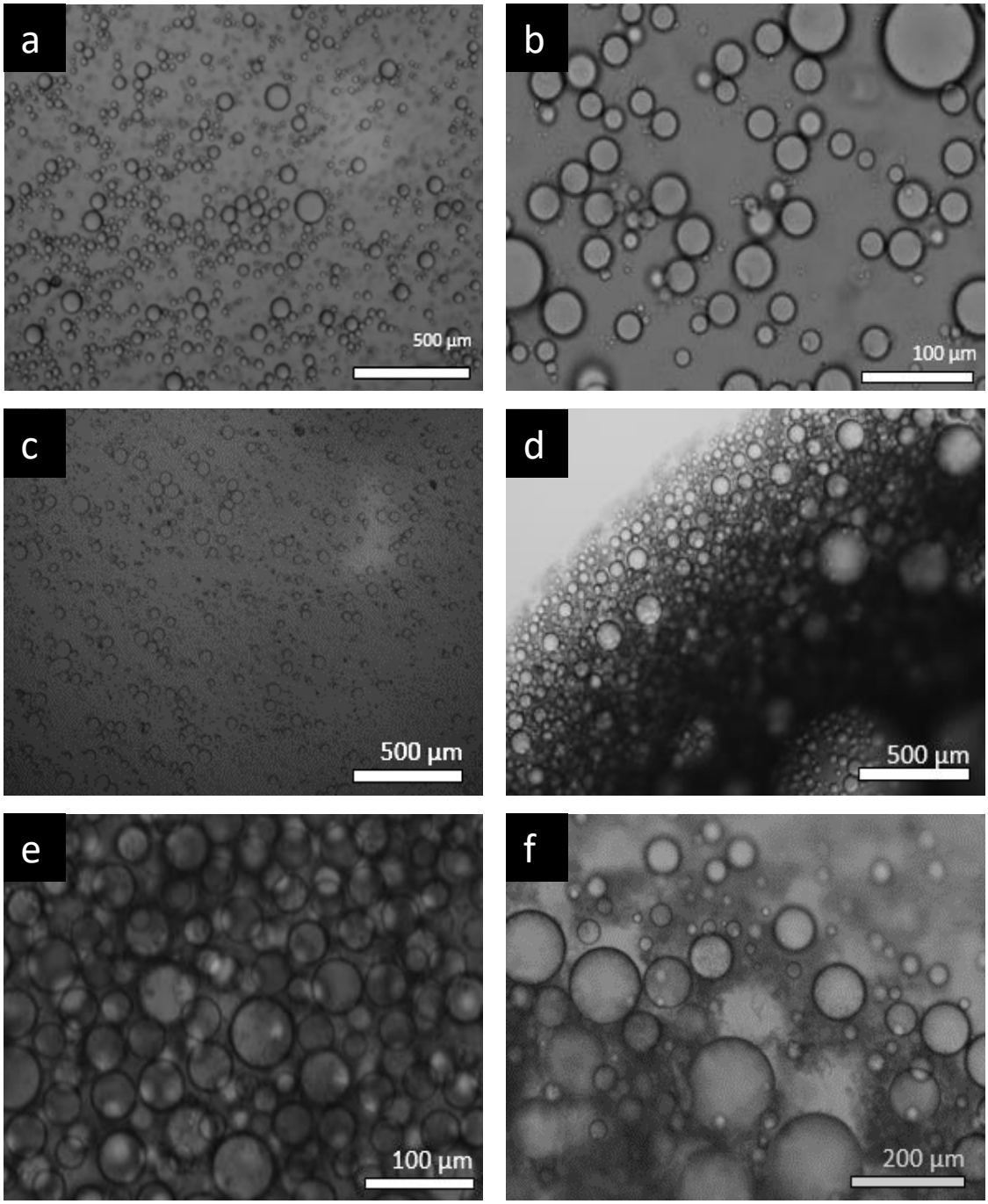

Figure 69. Variation of f_O and f_W values of isooctane-in-water emulsions (1:1 volume) stabilised by different magnesium hydroxide samples which were synthesised under different reaction conditions from a weak base. 1 wt.% $Mg(OH)_2$, 100 days after homogenisation.

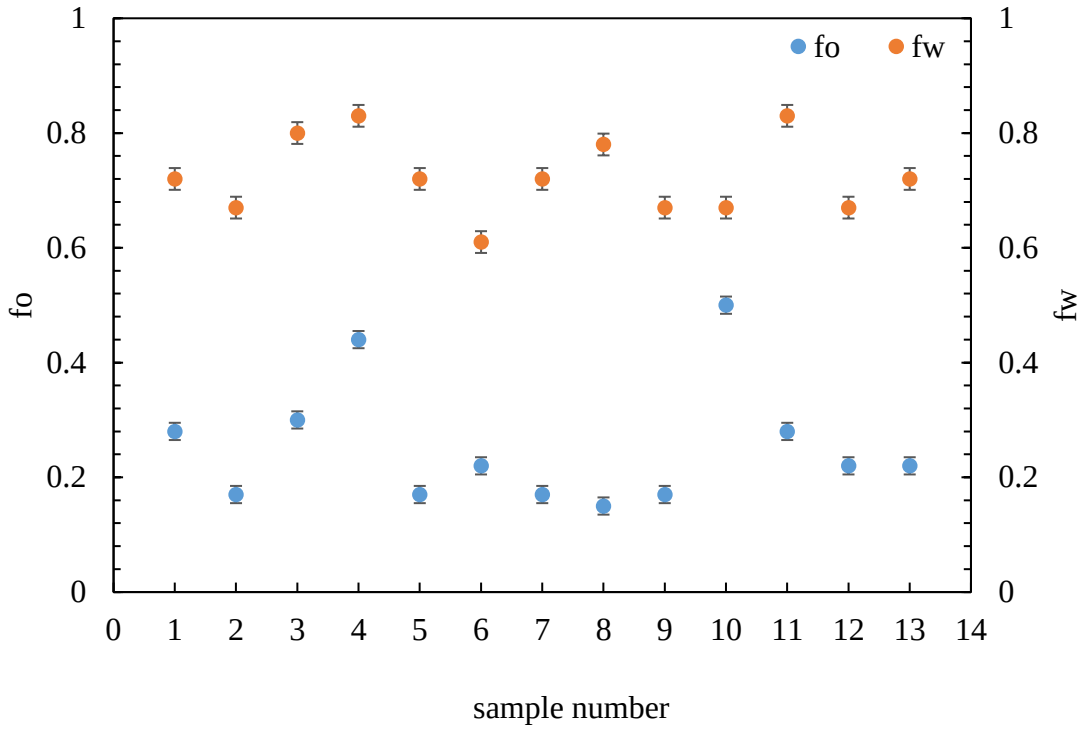

For f_o and f_w, the maximum limit = 1 and minimum limit = 0. When f_o or f_w = 1, the emulsion is completely stable to coalescence or creaming respectively. When f_o or f_w = 0, complete phase separation has occurred.

Figure 70. Mean droplet diameter of isooctane-in-water emulsions (1:1 volume) stabilised by different magnesium hydroxide samples which were synthesised under different reaction conditions, from a weak base. 1 wt. % $Mg(OH)_2$, 100 days after homogenisation. Measurements from microscopy.

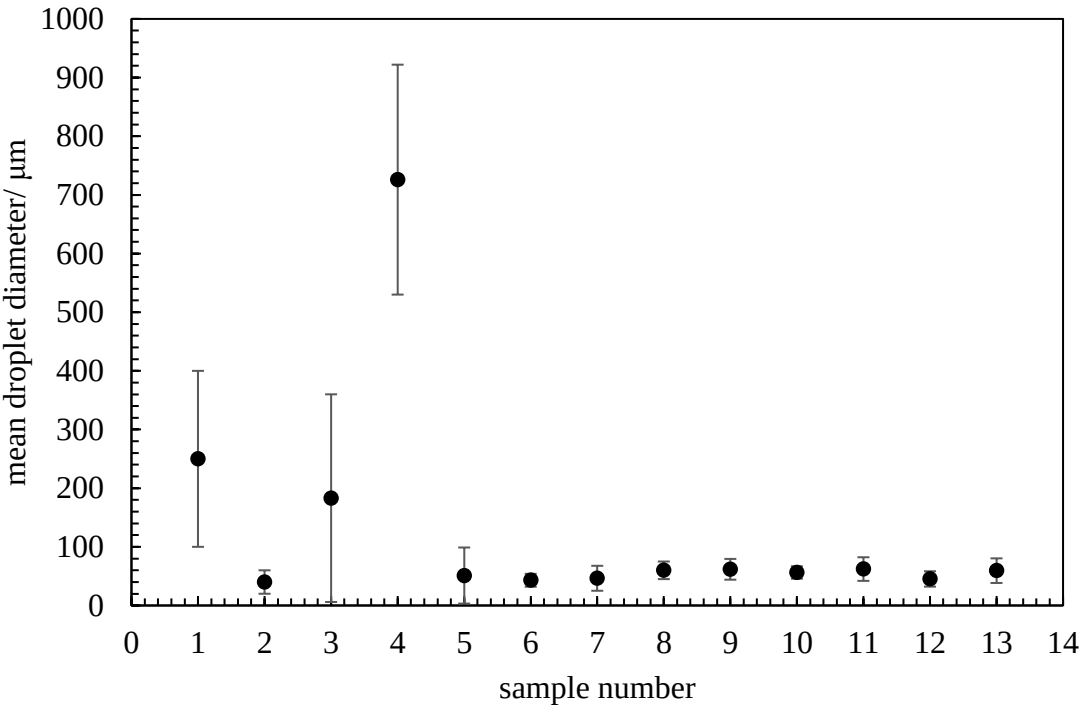

In this series of emulsions, emulsion 4 was the least stable in terms of coalescence and creaming, indicated by high f_O, (0.44) and f_W, (0.83), values, seen in Figure 67. Emulsion 10 was also unstable in terms of f_O. The mean droplet diameter of emulsion 4, 726 µm, was also much greater than the average droplet size for the emulsions in this series, 130 µm, shown in Figure 68. The average f_O and f_W values were 0.25 and 0.72 respectively. It would appear from this set of results that morphology is not an important factor in determining how successful magnesium hydroxide particles are as emulsifiers. Sample 2 and sample 4 have a similar morphology, but sample 2 is one of the most successful stabilisers as $f_O = 0.17$, $f_W = 0.67$ and the mean droplet diameter is 40 µm, whereas sample 4 is the least successful. Sample 8, a sample which possesses a small, rod-like morphology has similar potential to sample 2 in terms of producing stable emulsions, despite a completely different size and morphology of particles. When viewing this series of isooctane-in-water emulsions, there is no obvious correlation

between particle diameter/length and emulsion stability in terms of mean droplet diameter and fO and f_W values, as shown in Figure 71 and 72.

Figure 71. f_O and f_W of isooctane-in-water emulsions (1:1 volume) stabilised by magnesium hydroxide. 1 wt. % $Mg(OH)_2$, 100 days after homogenisation as a function of mean particle length of different magnesium hydroxide samples formed from a weak base.

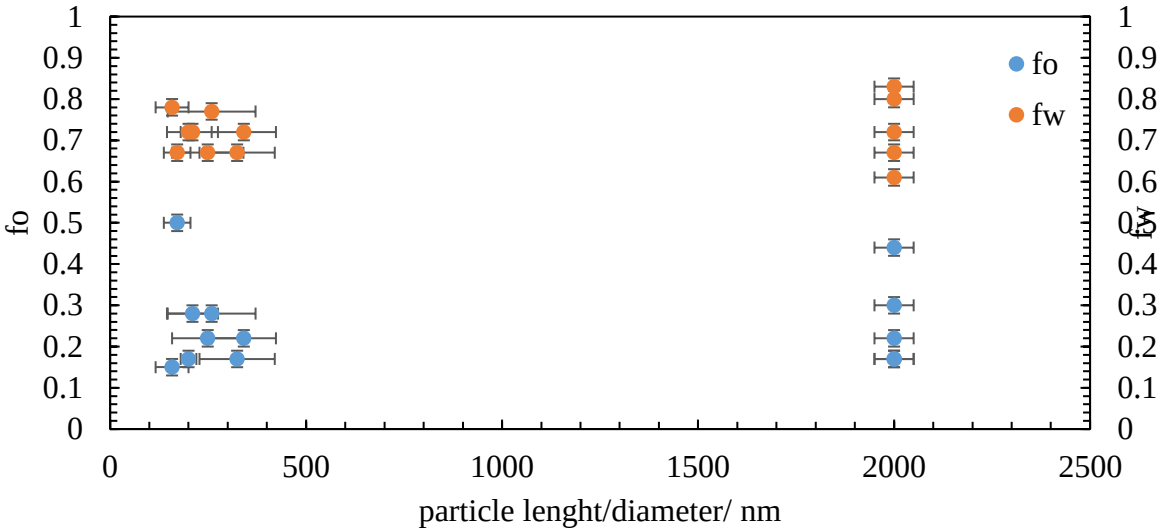

Figure 72. Mean droplet diameter of isooctane-in-water emulsions (1:1 volume) stabilised by magnesium hydroxide. 1 wt. % $Mg(OH)_2$, 100 days after homogenisation as a function of mean particle length of different magnesium hydroxide samples formed from a weak base. Droplet diameter measurements determined from optical microscopy.

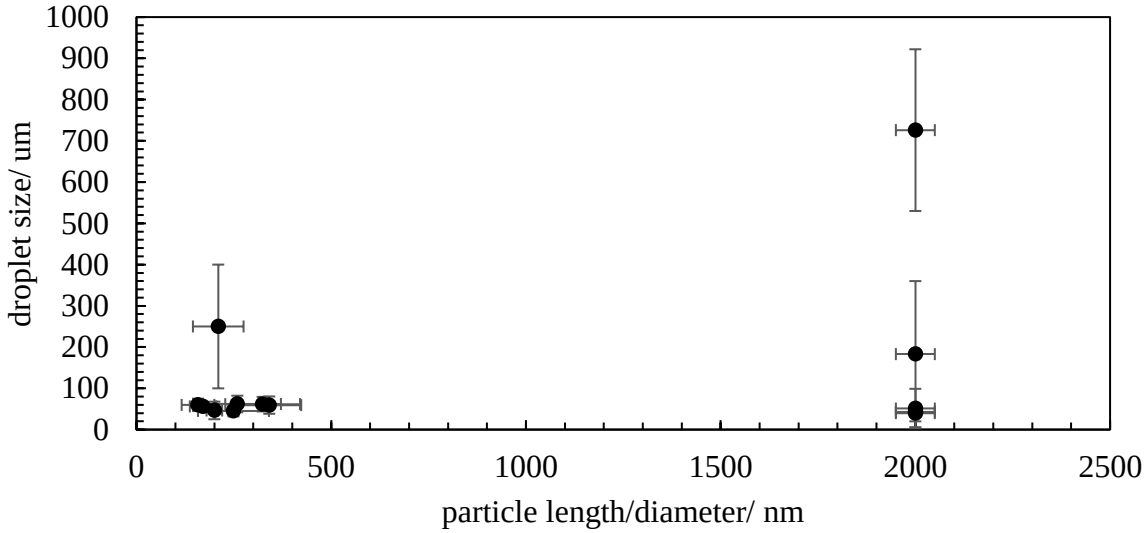

There is also no apparent correlation between zeta potential of magnesium hydroxide particles and isooctane-in-water emulsion stability when observing this series of emulsions in terms of mean droplet diameter and f_O and f_W values, as shown in Figures 73 and 74.

Figure 73. f_O and f_W of isooctane-in-water emulsions (1:1 volume) stabilised by magnesium hydroxide. 1 wt. % $Mg(OH)_2$, 100 days after homogenisation as a function of zeta potential of different magnesium hydroxide samples formed from a weak base.

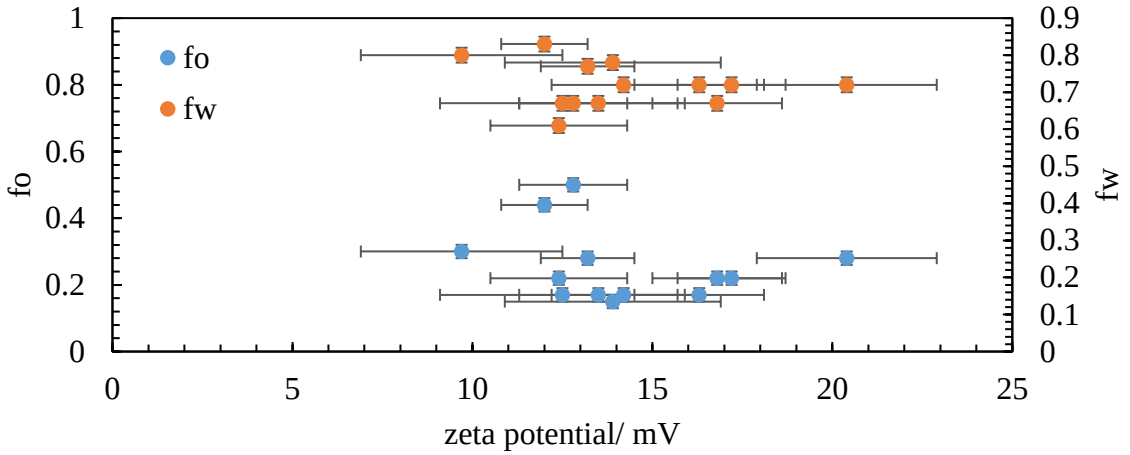

Figure 74. Mean droplet diameter of isooctane-in-water emulsions (1:1 volume) stabilised by magnesium hydroxide. 1 wt. % $Mg(OH)_2$, 100 days after homogenisation as a function of zeta potential of different magnesium hydroxide samples formed from a weak base. Droplet diameter measurements determined from optical microscopy.

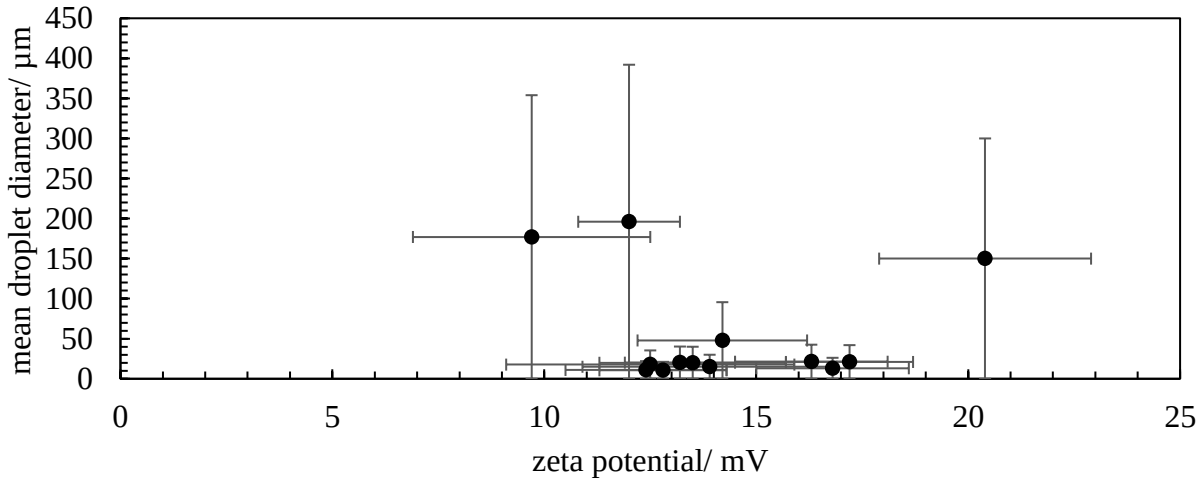

The appearance of the emulsions formed from samples 14 – 20 (samples formed from NaOH) are shown in the photographs of Figure 75. Optical micrographs of each emulsion, from samples 14 – 20 can be seen in Figure 76. Figure 77 and 78 contain photos of emulsions from samples 21 – 26 (samples formed from NaOH) and their respective optical micrographs. Figure 79 shows f_o and f_w of the emulsions from samples 14 – 26 and Figure 80 shows the mean droplet diameter for these emulsions.

Figure 75. Photographs of isooctane-in-water emulsions 100 days upon homogenisation. The emulsions were stabilised by 1.0 wt.% of various magnesium hydroxide samples, synthesised from a strong base. (a) **S**ample 14, (b) sample 15, (c) sample 16, (d) sample 17, (e) sample 18, (f) sample 19, (g) sample 20.

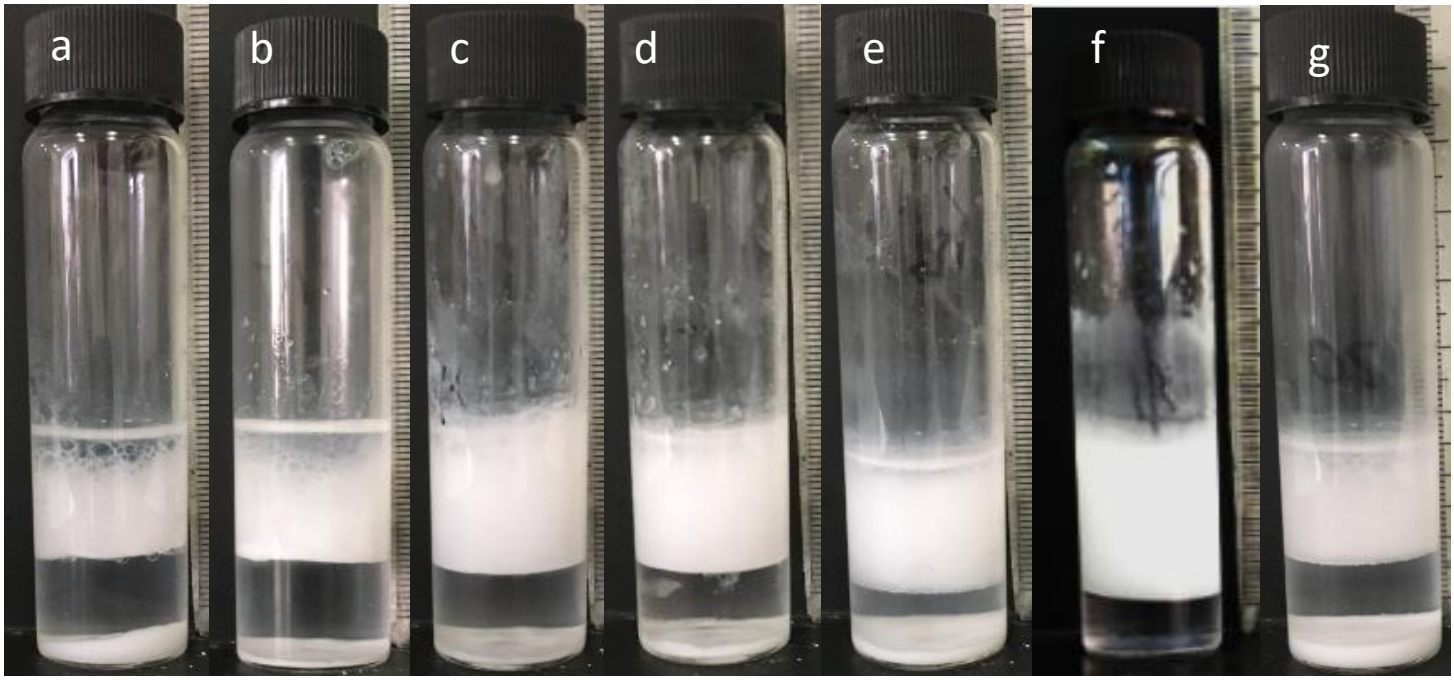

Figure 76. Optical micrographs of emulsions of isooctane-in-water emulsions (volume 1:1) 2 days after homogenisation. The emulsions were stabilised by 1.0 wt. % of various magnesium hydroxide samples synthesised from a strong base. (a) **S**ample 14, (b) sample 15, (c) sample 16, (d) sample 17, (e) sample 18, (f) sample 19, (g) sample 20.

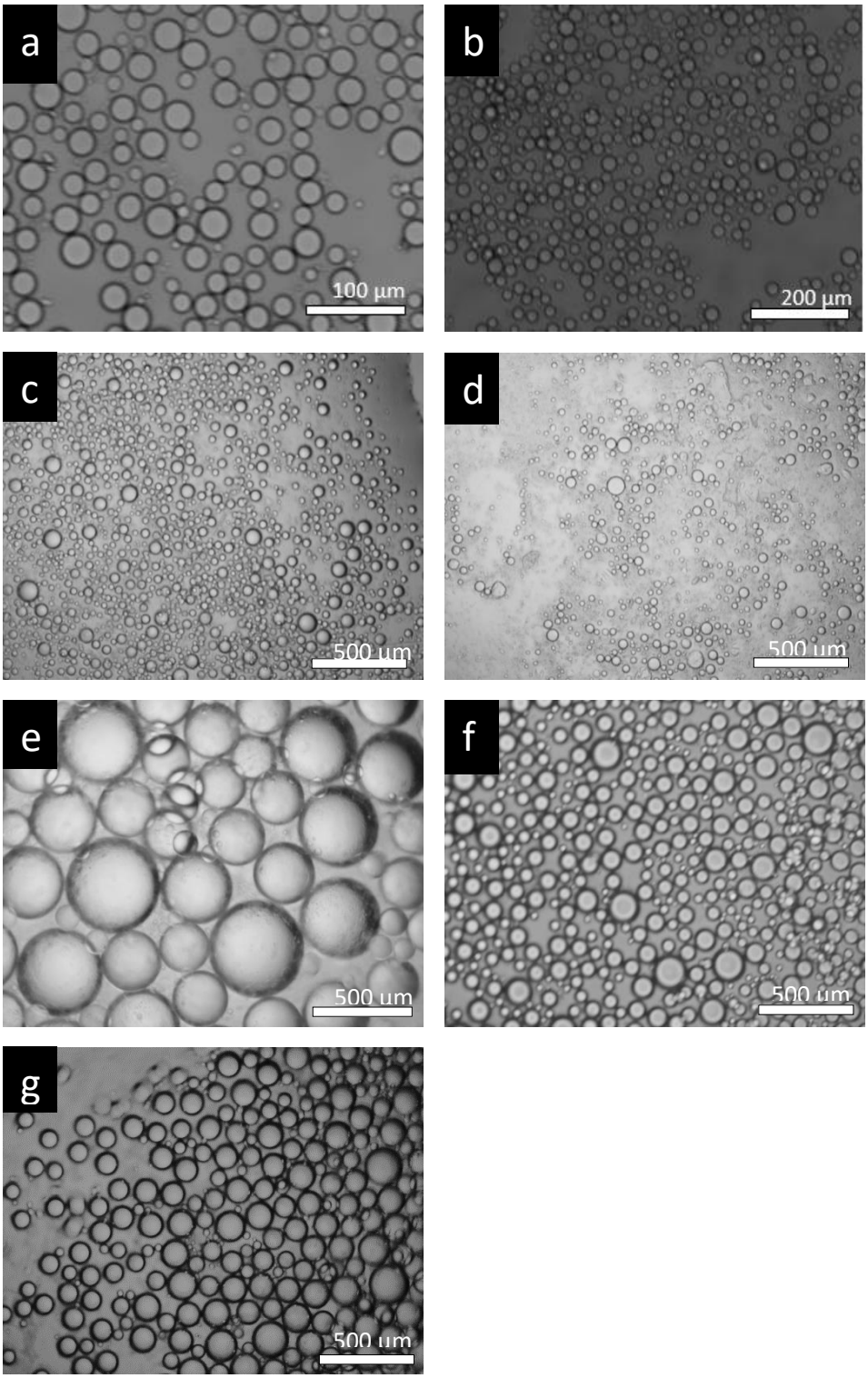

Figure 77. Photographs of isooctane-in-water emulsions, 100 days after homogenisation. The emulsions were stabilised by 1.0 wt.% of various magnesium hydroxide samples, synthesised from a weak base. (a) **S**ample 21, (b) sample 22, (c) sample 23, (d) sample 24, (e) sample 25, (f) sample 26.

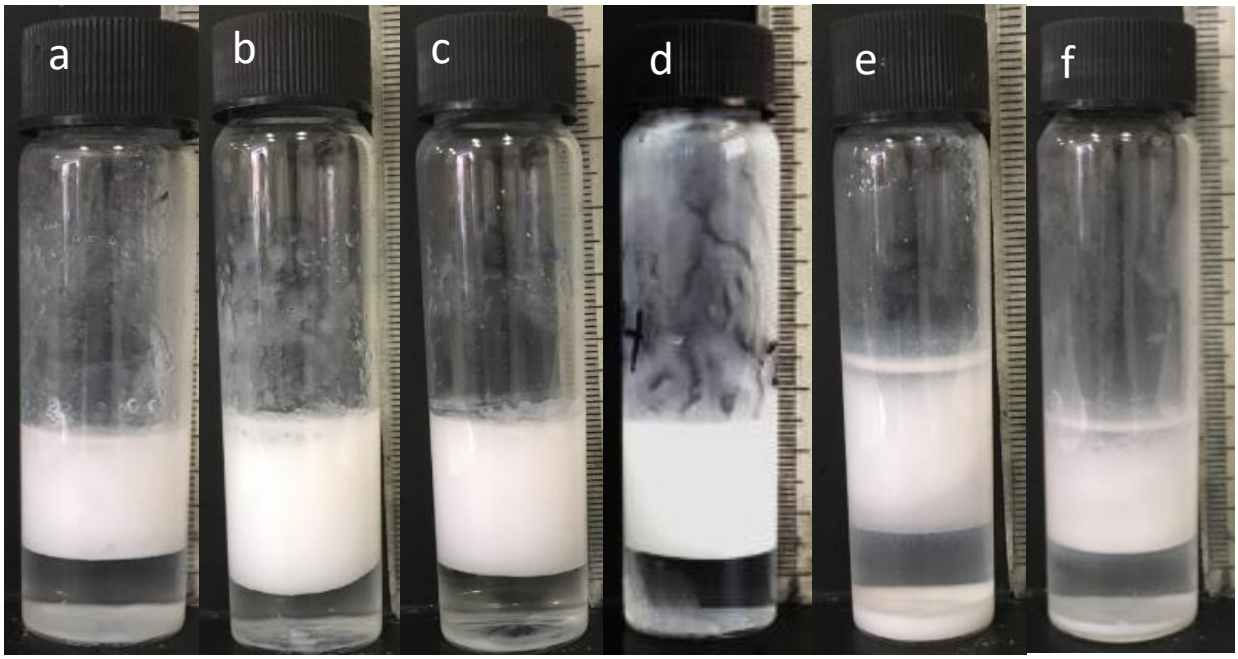

Figure 78. Optical micrographs of emulsions of isooctane – in – water emulsions (volume 1:1) 2 days after homogenisation. The emulsions were stabilised by 1.0 wt. % of various magnesium hydroxide samples synthesised from a strong base. (a) **S**ample 21, (b) sample 22, (c) sample 23, (d) sample 24, (e) sample 25, (f) sample 26.

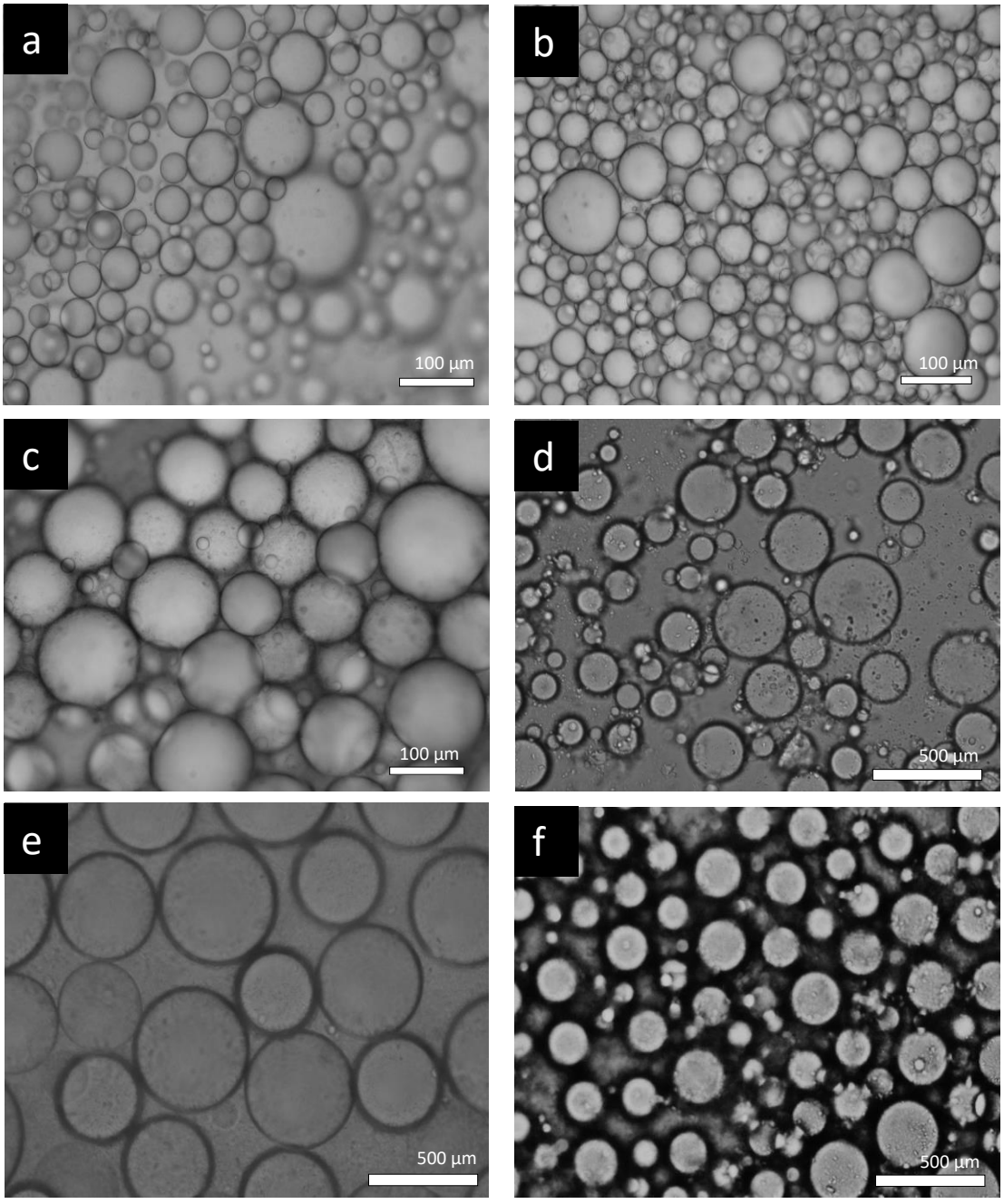

Figure 79. Variation of f_O and f_W of isooctane – in – water emulsions (1:1 volume) stabilised by different magnesium hydroxide samples which were synthesised under different reaction conditions, from a strong base. 1 wt.% $Mg(OH)_2$, 100 days after homogenisation.

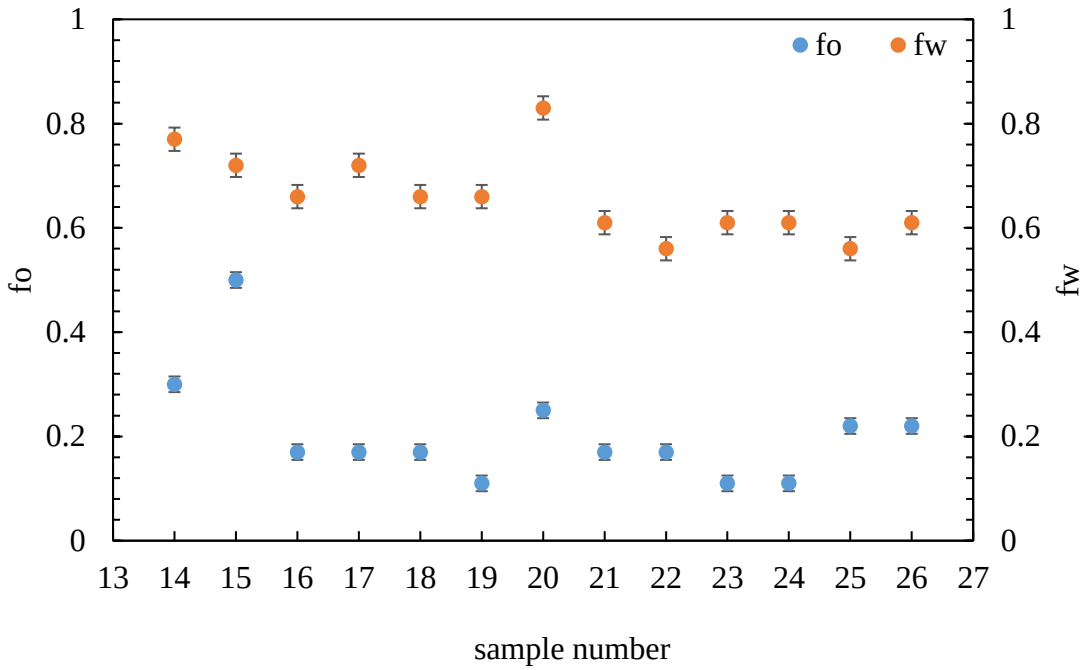

Figure 80. Mean droplet diameter of isooctane – in – water emulsions (1:1 volume) stabilised by different magnesium hydroxide samples which were synthesised under different reaction conditions, from a strong base. 1 wt.% $Mg(OH)_2$, 100 days after homogenisation, from microscopy.

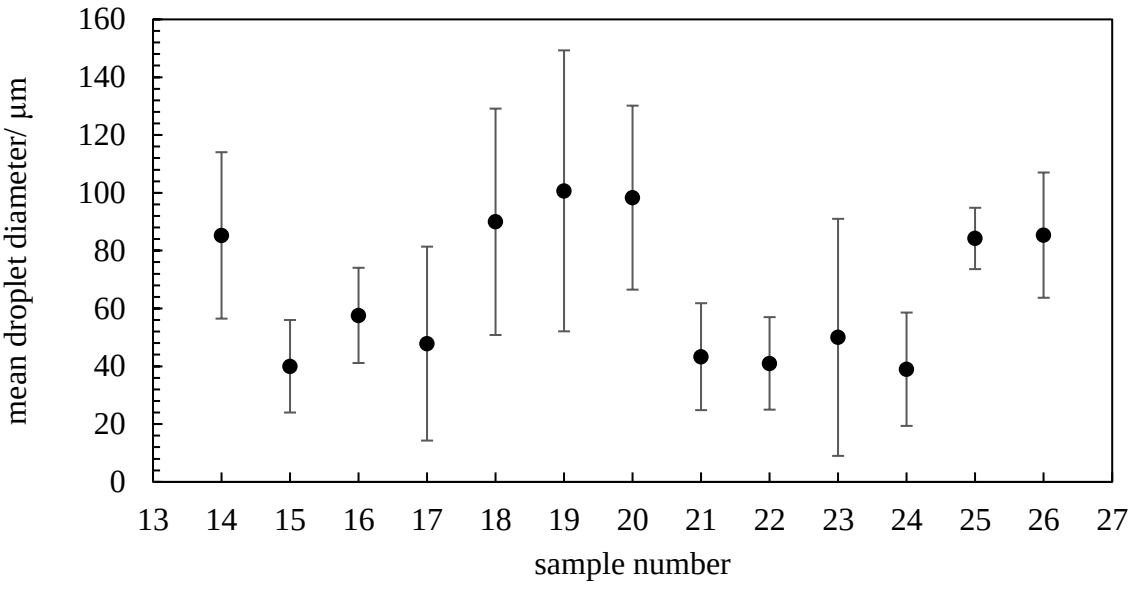

The emulsions produced from magnesium hydroxide samples 14-26 appeared to show little variation in terms of stability to coalescence and creaming. The mean droplet diameter did not vary to the same extent as in the series of emulsions produced from magnesium hydroxide samples synthesised from a weak base and f_O and f_W values also appeared to be more constant. Sample 20 appeared to be less effective at stabilising the emulsion than the other samples, which is indicated by a high f_O value and also increased sedimentation levels. However, the mean droplet diameter for emulsion from sample 20 is comparable to the other emulsions in this series. The isooctane–in–water emulsions formed from sample 14- 26 appeared to produce slightly more stable emulsions with respect to both coalescence and creaming in comparison to the emulsions from $Mg(OH)_2$ samples 1-13.

There was also no correlation between zeta potential/ particle length/diameter and isooctane-in-water emulsion stability when stabilised by magnesium hydroxide particles formed from a strong base, shown in Figures 81-84 in terms of f_O and f_W values and droplet diameter.

Figure 81. f_O and f_W of isooctane – in – water emulsions (1:1 volume) stabilised by magnesium hydroxide. 1 wt. % $Mg(OH)_2$, 100 days after homogenisation as a function of zeta potential of different magnesium hydroxide samples formed from a strong base.

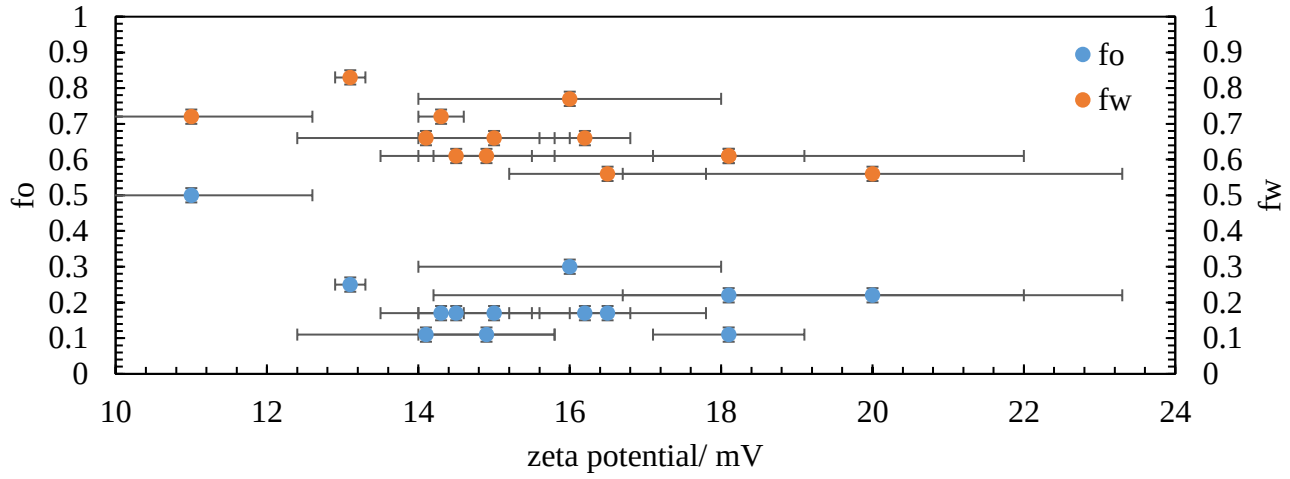

Figure 82. Mean droplet diameter of isooctane-in-water emulsions (1:1 volume) stabilised by magnesium hydroxide. 1 wt. % $Mg(OH)_2$, 100 days after homogenisation as a function of zeta potential of different magnesium hydroxide samples formed from a strong base. Droplet diameter measurements determined from optical microscopy.

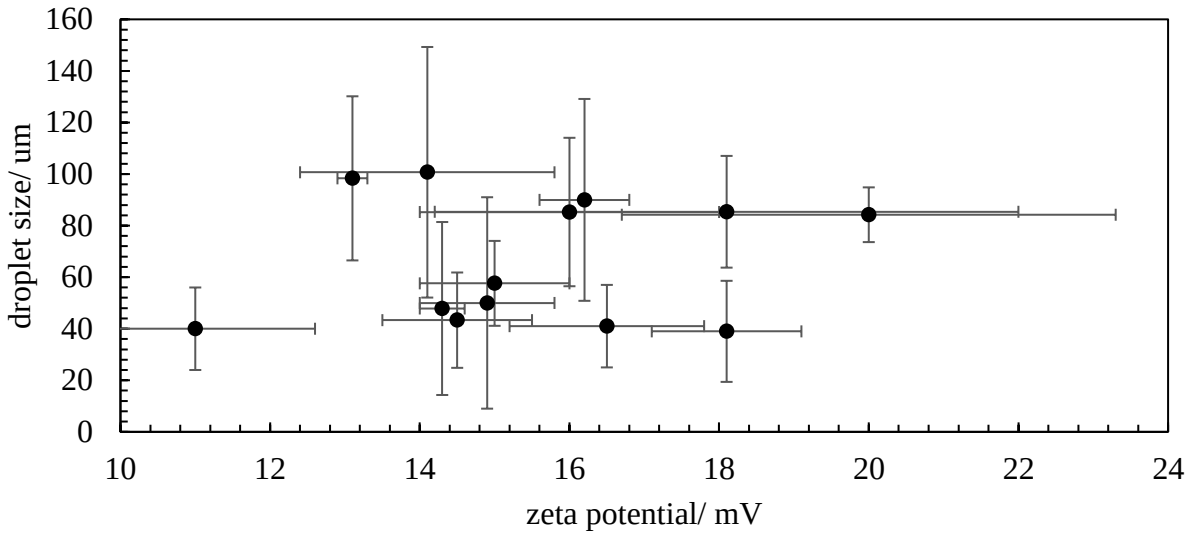

Figure 83. f_O and f_W of isooctane-in-water emulsions (1:1 volume) stabilised by magnesium hydroxide. 1 wt. % $Mg(OH)_2$, 100 days after homogenisation as a function of mean particle length of different magnesium hydroxide samples formed from a strong base.

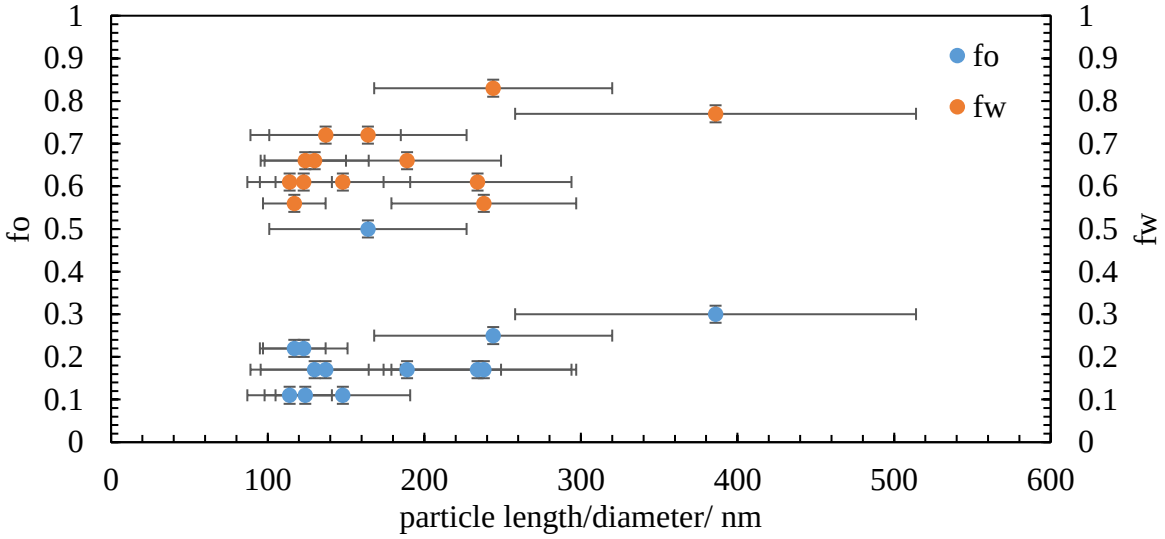

Figure 84. Mean droplet diameter of isooctane-in-water emulsions (1:1 volume) stabilised by magnesium hydroxide. 1 wt. % $Mg(OH)_2$, 100 days after homogenisation as a function of mean particle length of different magnesium hydroxide samples formed from a strong base. Droplet diameter measurements determined from optical microscopy.

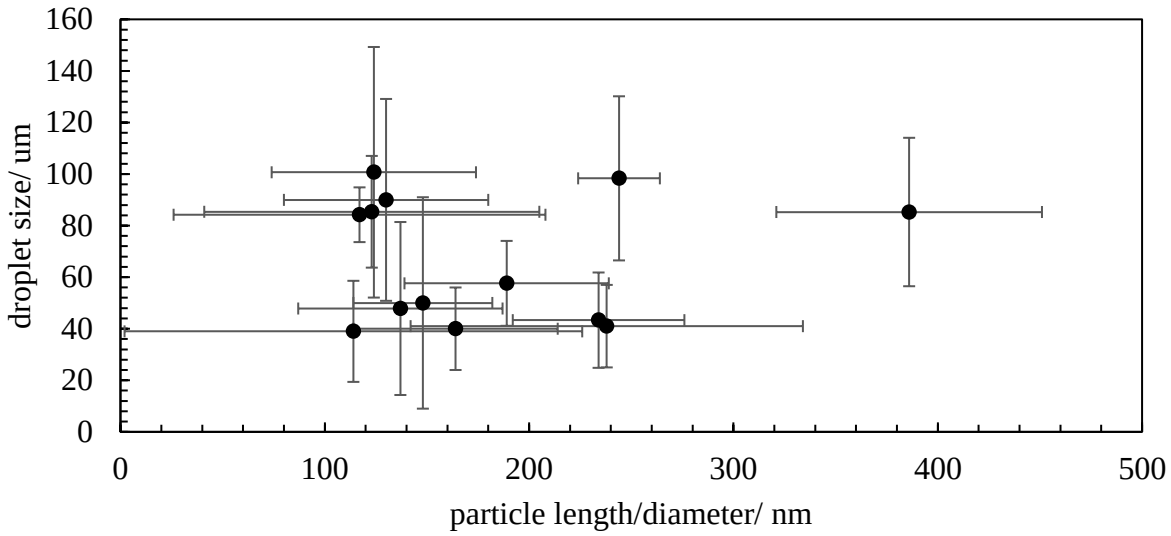

For isooctane-in-water emulsions, creaming occurred rather quickly due to the significant density difference between isooctane (density = 0.69194 g/cm^3 at 20 ^{o}C) and water [93].

The sponsors of this research project, AkzoNobel are particularly interested in the colloidal characteristics of magnesium hydroxide samples formed from magnesium chloride hexahydrate and sodium hydroxide. Therefore, the magnesium hydroxide samples which proved to be better Pickering emulsifiers in the original isooctane-in-water emulsions (1:1 volume, 1 wt.% $Mg(OH)_2$) have been used in further experiments. For example, isooctane-in-water Pickering emulsions containing different concentrations of magnesium hydroxide particles were formed from samples 17, 22 and 24 in order to assess the effect of magnesium hydroxide concentration on emulsions stability. The stability of isooctane-in-water emulsions, stabilised by sample 22 were also assessed as a function of storage temperature and concentration of added electrolyte. Sample 22 was explored further as the original isooctane-in-water emulsion from this sample had the lowest f_O and f_W values.

3.3.2 Isooctane-in-water emulsions with varied concentration of $Mg(OH)_2$

Particles act to stabilise emulsion droplets in a number of ways depending on particle concentration. In theory, when the particle concentration is high, the surface of the droplets will be completely encased by the emulsifying particles. The close packed nature of the particles bound to the surface of the droplet means a physical barrier forms around the droplets, providing steric and electrostatic repulsion. Also, at high particle concentrations, the stability of the thin film of continuous phase which forms between droplets, and requires a greater capillary force to break. Networks of particles can also form between droplets of an emulsion. As particle concentration increases initially, stability to coalescence will also increase as more particles bind at the interface. However, after a certain concentration of particles, stability to coalescence will remain constant. This is because there is no longer space at the interface for additional particles to adsorb to. The additional particles will enter the continuous phase. As particle concentration increases, the emulsion becomes more viscous, which results in greater stability to creaming, which can be explained by the Stokes equation,

$$v = \frac{d^2(p_1 - p_2)g}{18n} \qquad (13)$$

where v is the rate of sedimentation or velocity of the sphere, d is the diameter of the sphere, p_1 is the particle density, p_2 is the medium density, n is the viscosity of the medium and g is the gravitational force.

To investigate the effect of magnesium hydroxide concentration on emulsion stability, series of emulsions were produced containing different concentrations of sample 17, 22 and 24. This is because these samples were effective stabilisers in isooctane-in-water emulsions of 1 wt.% $Mg(OH)_2$.

Photographs of emulsions of different particle concentration can be seen in Figure 85 (sample 17), Figure 87 (sample 22) and Figure 89 (sample 24). Their respective optical micrographs are shown in Figure 86, 88 and 90. f_O and f_W for each of these emulsions are shown in figure 91. See Figure 92 – 94 for mean droplet diameter measurements for each of the emulsions.

Figure 85. Emulsions of isooctane and Milli-Q water (1:1 volume) stabilised by magnesium hydroxide sample 17 42 days after homogenisation. (a) 0.5 wt.%, (b) 1 wt.%, (c) 2 wt.%, (d) 3 wt.%, (e) 4 wt.%, (f) 5 wt.%.

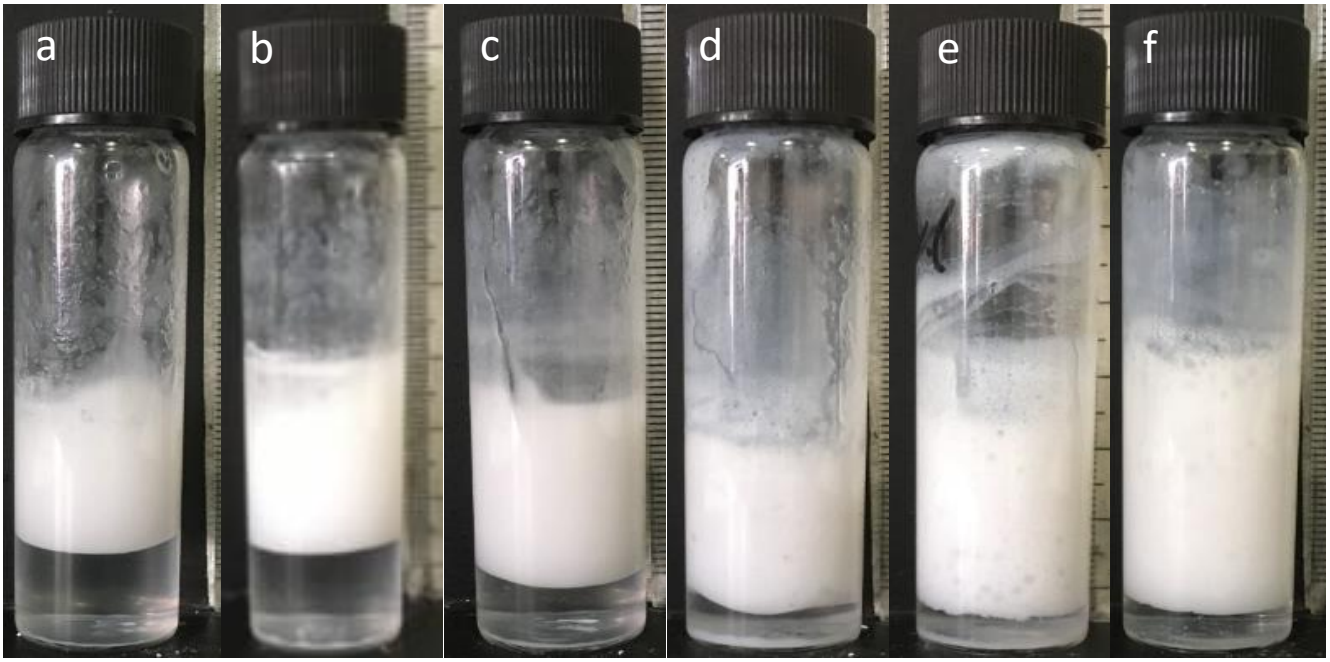

Figure 86. Optical micrographs of emulsions of isooctane and Milli-Q water (1:1 volume) formed at room temperature stabilised by magnesium hydroxide sample 17. Images 48 hours after homogenisation. (a) 0.5 wt.%, (b) 1 wt.%, (c) 2 wt.%, (d) 3 wt.%, (e) 4 wt.%, (f) 5 wt.%.

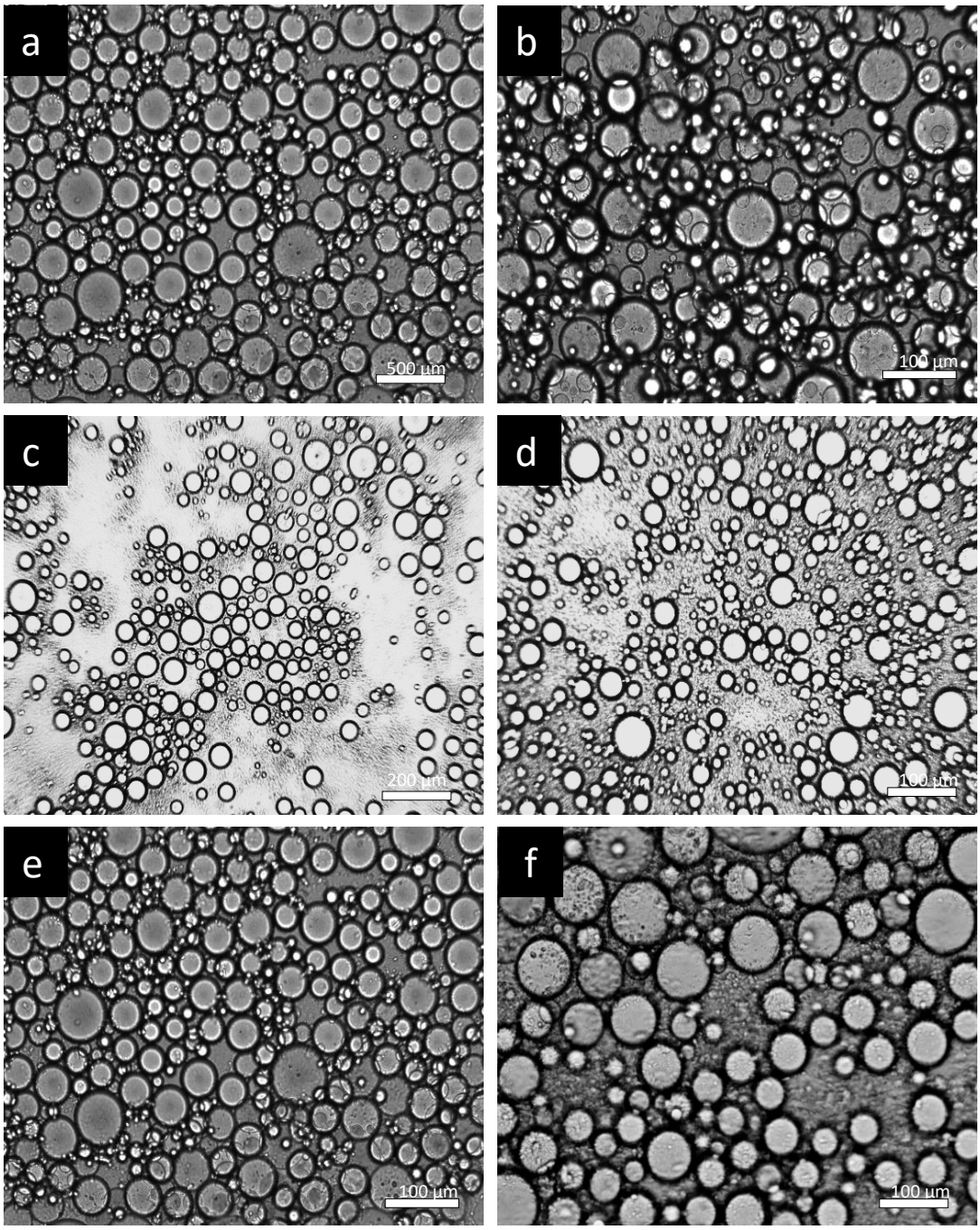

Figure 87. Emulsions of isooctane and Milli-Q water (1:1 volume) stabilised by magnesium hydroxide sample 22 42 days after homogenisation. (a) 0.5 wt.%, (b) 1 wt.%, (c) 2 wt.%, (d) 3 wt.%, (e) 4 wt.%, (f) 5 wt.%.

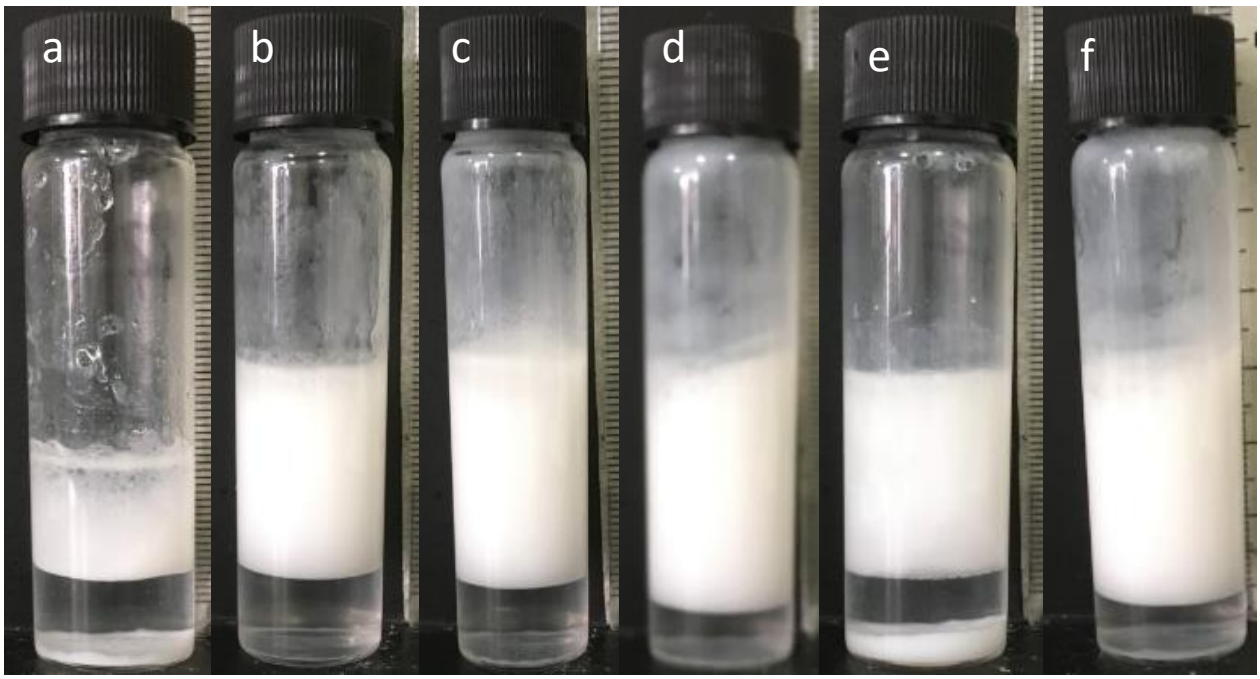

Figure 88. Optical micrographs of emulsions of isooctane and Milli-Q water (1:1 volume) formed at room temperature stabilised by magnesium hydroxide sample 22. Images 48 hours after homogenisation. (a) 0.5 wt.%, (b) 1 wt.%, (c) 2 wt.%, (d) 3 wt.%, (e) 4 wt.%, (f) 5 wt.%.

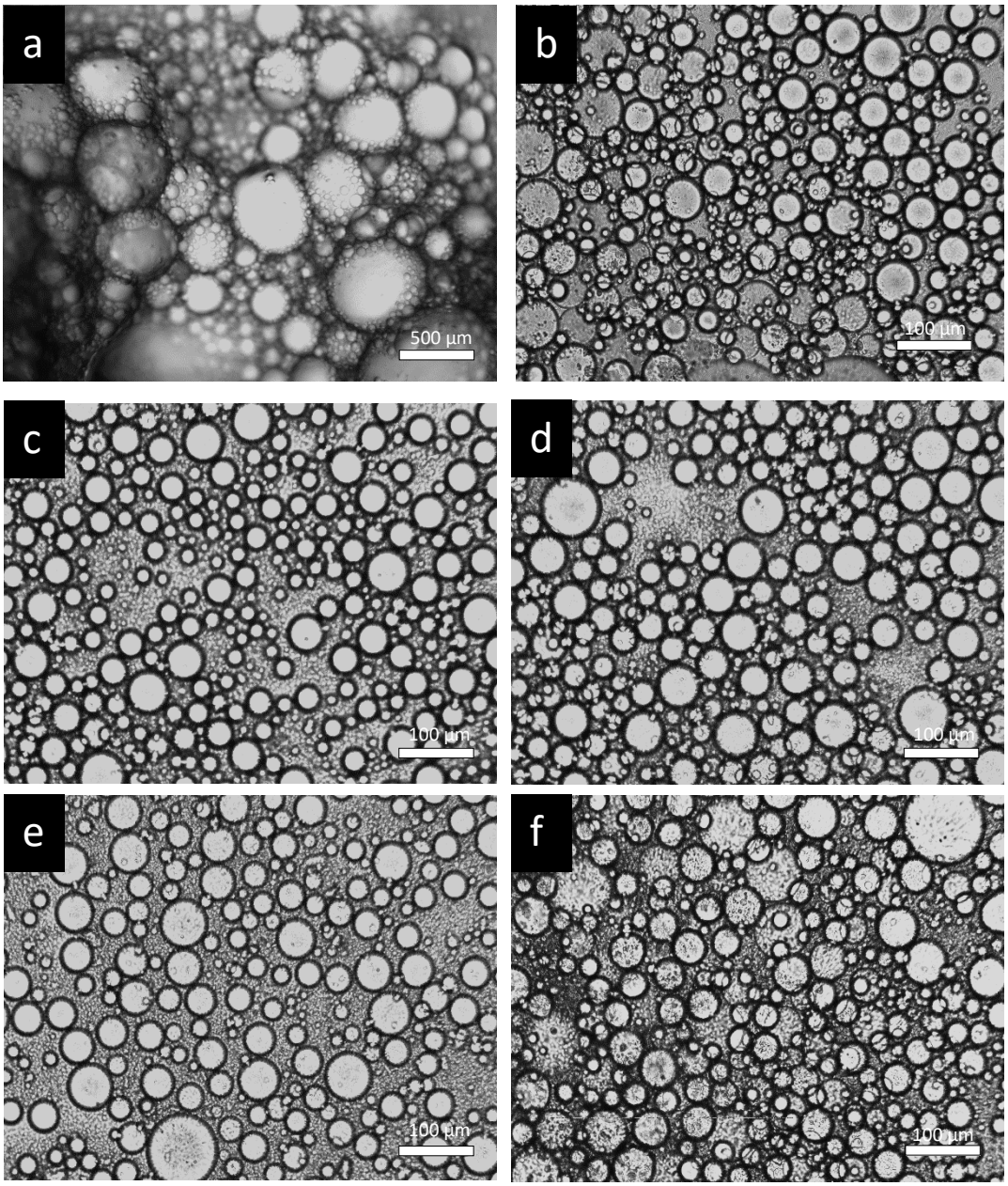

Figure 89. Emulsions of isooctane and Milli-Q water (1:1 volume) stabilised by magnesium hydroxide sample 24 42 days after homogenisation. (a) 0.5 wt.%, (b) 1 wt.%, (c) 2 wt.%, (d) 3 wt.%, (e) 4 wt.%, (f) 5 wt.%.

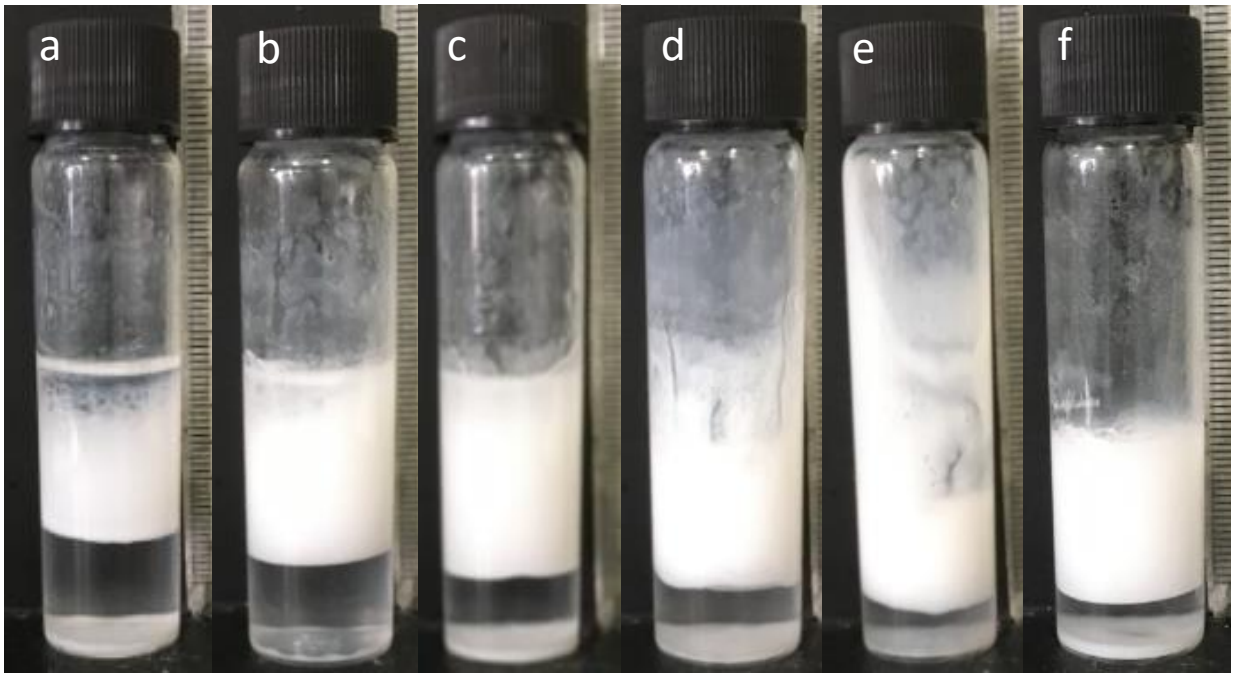

Figure 90. Emulsions of isooctane and Milli-Q water (1:1 volume) stabilised by magnesium hydroxide sample 24 48 hours after homogenisation. (a) 0.5 wt.%, (b) 1 wt.%, (c) 2 wt.%, (d) 3 wt.%, (e) 4 wt.%, (f) 5 wt.%.

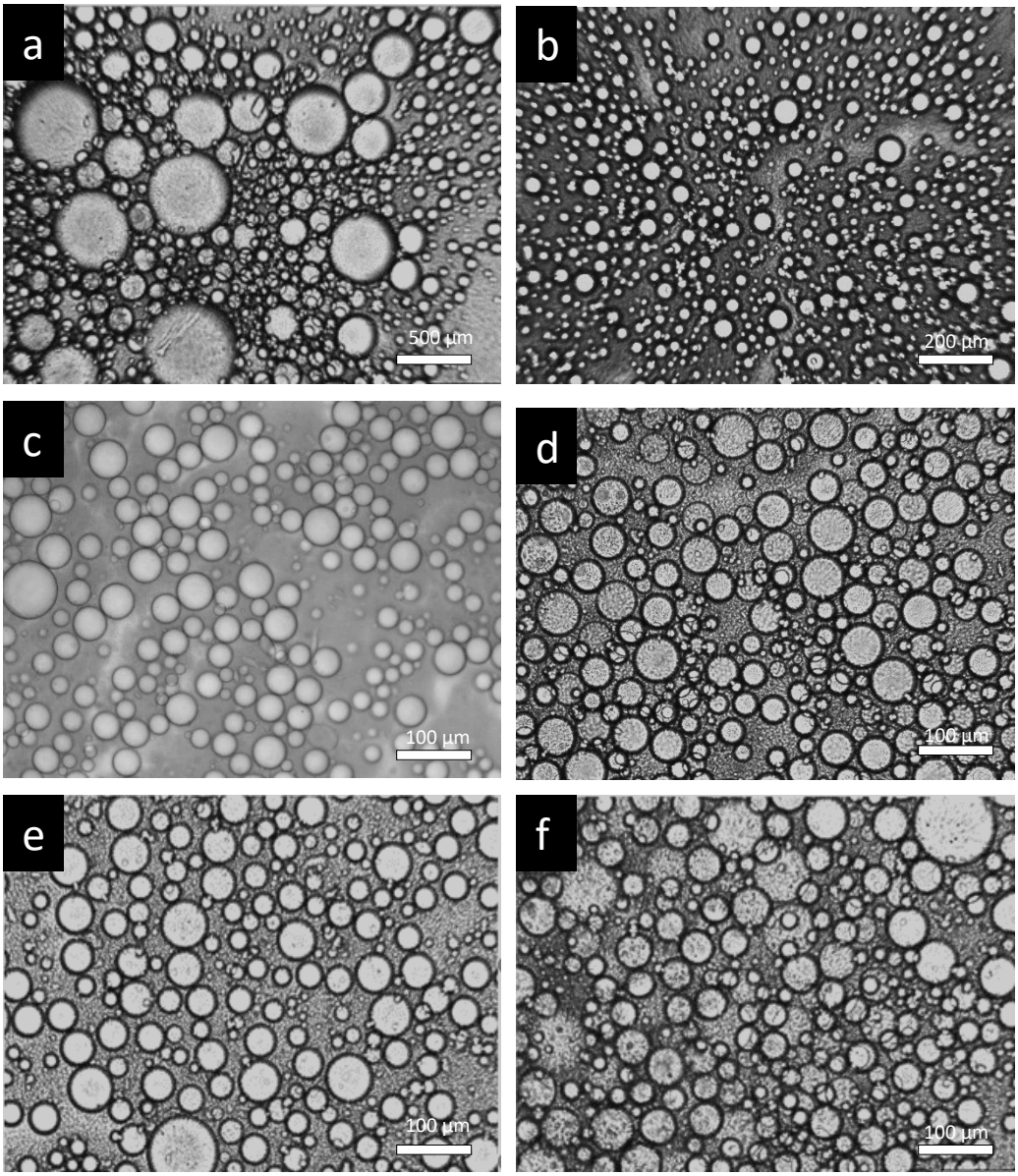

Figure 81. Variation of f_O and f_W as a function of magnesium hydroxide concentration in isooctane-in-water emulsions (1:1 volume). 40 days after homogenisation for 3 different samples.

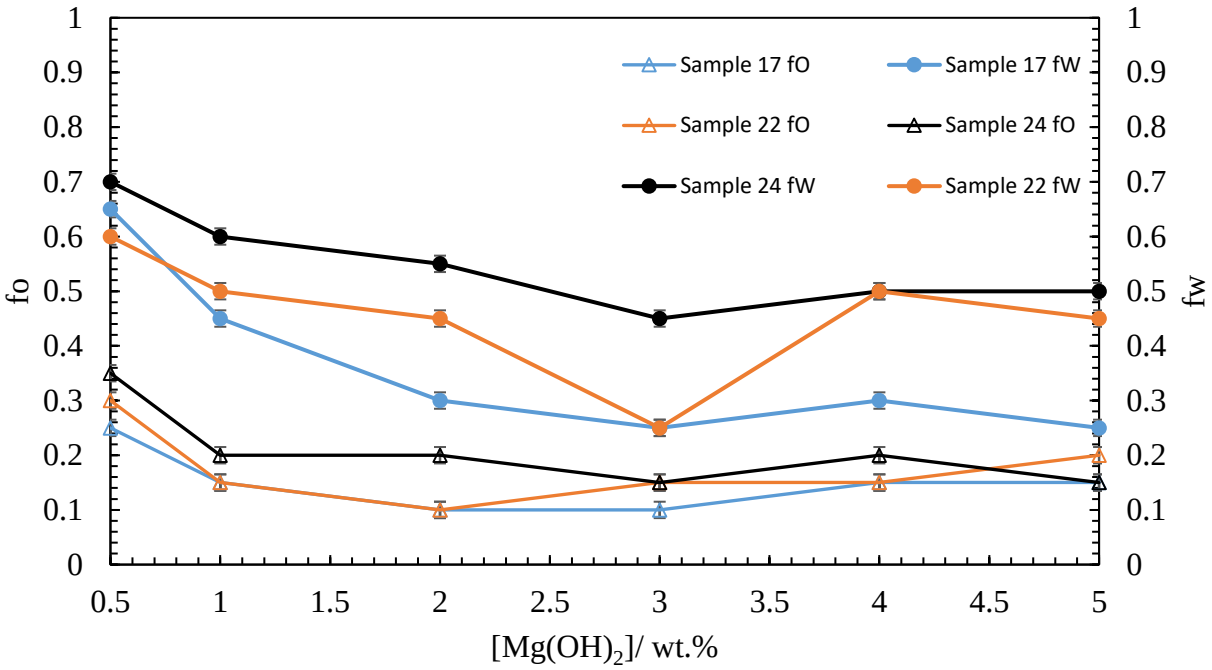

Figure 92. Variation of mean droplet diameter with particle concentration for isooctane-in-water emulsions (1:1 volume) stabilised by 3 samples of magnesium hydroxide after 48 hours, from microscopy.

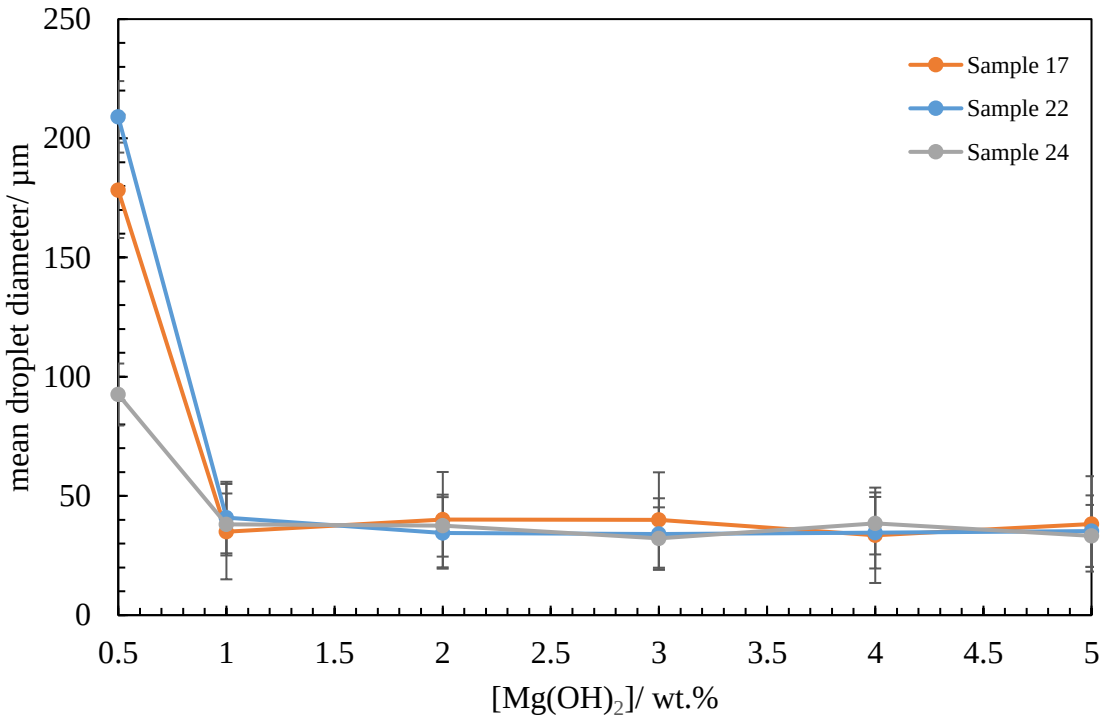

Figure 93. Variation of d(0.5) values (a percentile indicating half of the droplet diameters are smaller than the given value) with particle concentration for isooctane-in-water emulsions (1:1 volume) stabilised by 3 samples of magnesium hydroxide 45 days after homogenisation from light diffraction.

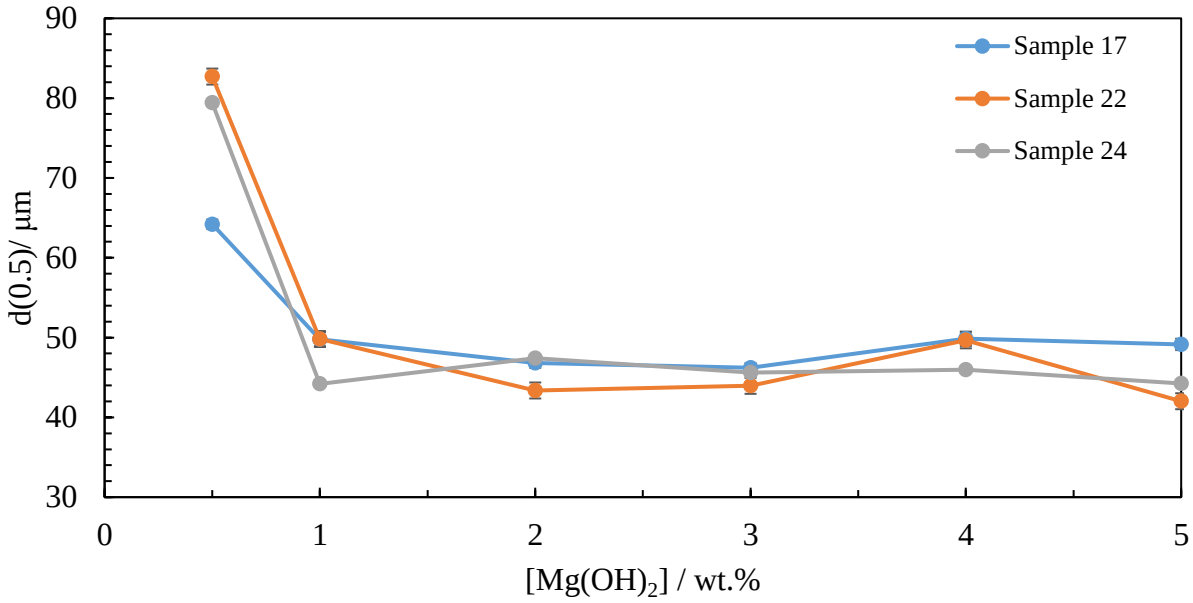

Figure 94. Variation of D[4,3] values (mean weighted volume of the droplets) with particle concentration for isooctane-in-water emulsions (1:1 volume) stabilised by 3 samples of magnesium hydroxide 45 days after homogenisation, from light diffraction.

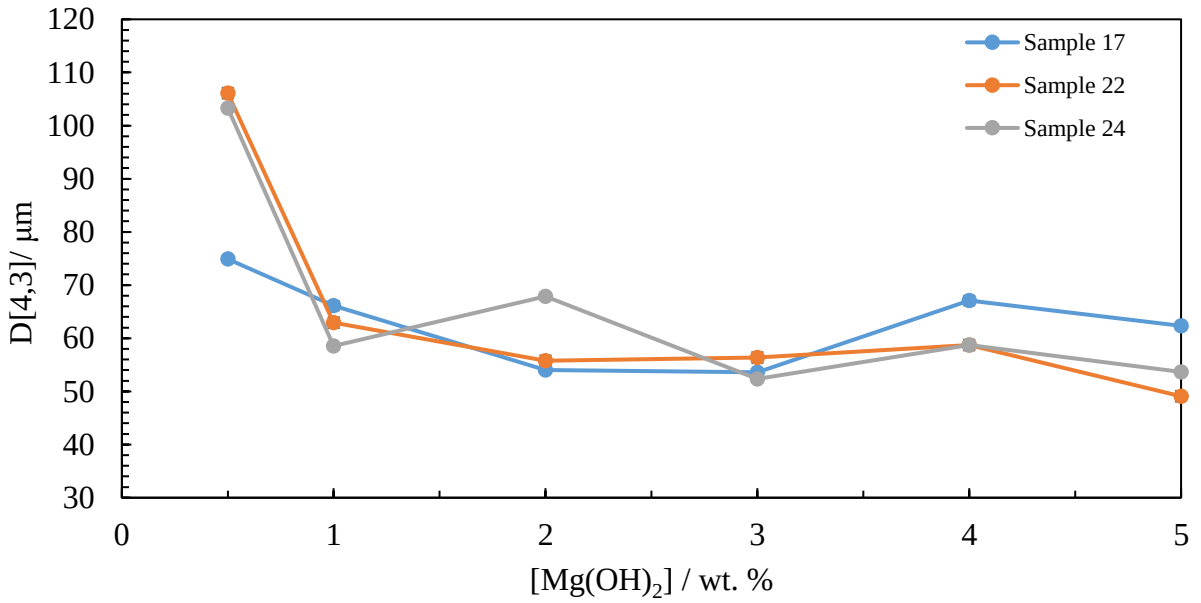

As previously seen in the literature [94], there was an initial increase in stability to coalescence, followed stability to coalescence remaining constant beyond a certain particle concentration. For each of the series of emulsions prepared at different magnesium hydroxide concentration, f_O decreased as particle concentration was increased from 0.5 wt.% to 1 wt.%. For example, sample 24 at 0.5 wt.% f_O was 0.35, which decreased to 0.2 when magnesium hydroxide concentration was increased to 1 wt.%. Beyond 1.0 wt.% $Mg(OH)_2$, f_O remained fairly constant. Generally remaining within the range of 0.2 ± 0.05 as shown in Figure 84. This trend in stability to coalescence was also evident in the mean droplet diameter values, which sharply decreased from between 100 µm – 200 µm at 0.5 wt.% to around 40 µm for magnesium hydroxide concentration 1.0 wt.% and above.

The expected trend was also observed in terms of stability to creaming. As magnesium hydroxide concentration increased, viscosity of the emulsions also increased, due to an increased solid content being present in the emulsion, leading to a decrease in rate of creaming. This is reflected by f_W values in Figure 89. The emulsion stabilised by sample 22 at 3.0 wt.% had a particularly low f_W value of 0.3. This could perhaps be anomalous as it does not follow the trend within the series of emulsions stabilised by sample 22. The f_W value of 0.6 for the emulsion stabilised by sample 22 at 4.0 wt.% is slightly higher than expected due to unexplained sedimentation of particles seen in Figure 80 (e) which is perhaps due to human error during homogenisation of this emulsion. Droplet diameter was apparently unaffected and followed the expected trend.

The mean droplet diameter measurements from light scattering, Figures 93 and 94 were in agreement with measurements based on optical micrographs.

Figure 95 suggests that at high magnesium hydroxide concentration, there is no longer room for particles to adsorb at the isooctane – water interface as it indicates the presence of $Mg(OH)_2$ in the continuous water phase which is typically amorphous and smooth. The carbon shown in the EDX spectrum is due to isooctane droplets, Oxygen is mainly attributed to the presence of water and Mg is from the magnesium hydroxide. Pt is present due to the coating of the sample.

Figure 95. Cryo-SEM images of isooctane-in-water emulsion from magnesium hydroxide sample 17 at 5.0 wt.% and accompanying EDX spectrum.

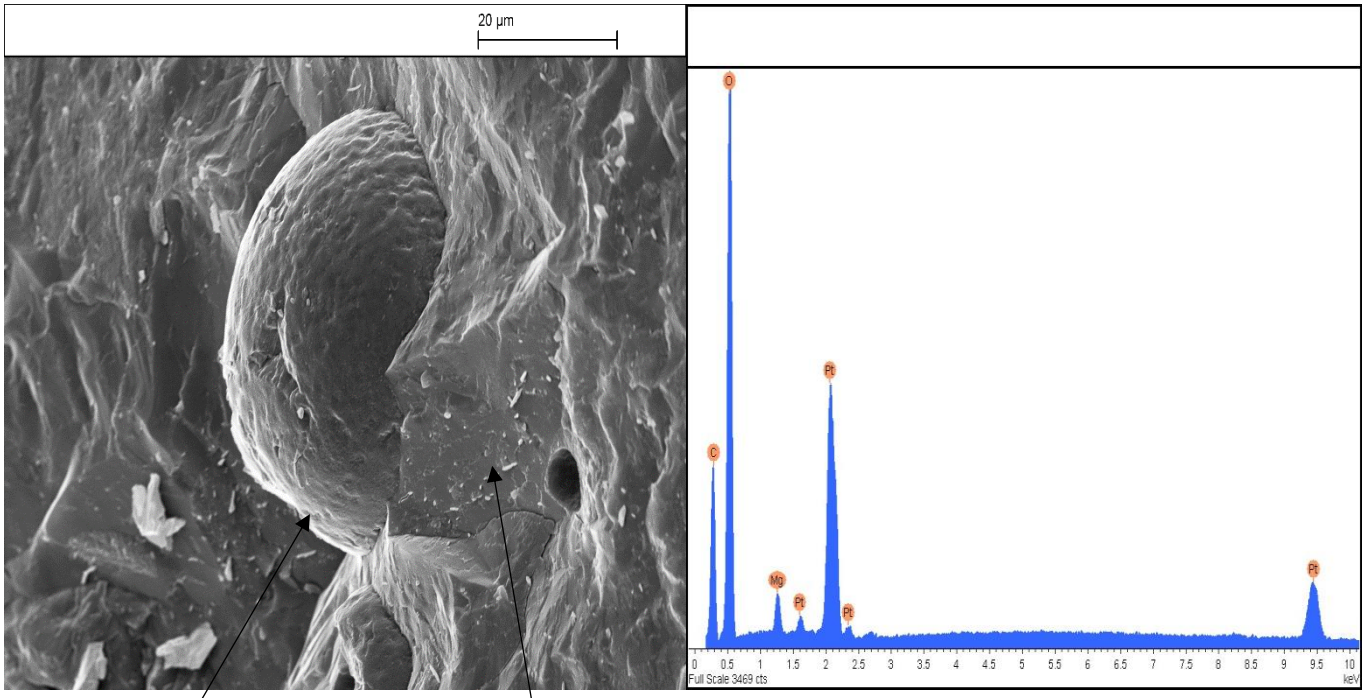

3.3.3 Stability of isooctane-in-water emulsions containing NaCl

As [NaCl] increased from 0 M to 0.2 M, stability to coalescence increased overall, shown in Figure 96-Figure 99. This could be due to the weak flocculation leading to a more dense film of particles forming around the droplets [95]. The particles then provide increased steric and electrostatic repulsion which prevents coalescence. However, as [NaCl] increased further from 0.2 M to 0.5 M, stability to coalescence appeared to level off. This could indicate 0.2 M NaCl is the optimum concentration in terms of emulsion stability to coalescence. There was very little difference between floc size when [NaCl] was 0.2 M and 0.5 M as floc diameter was measured to be 1131 nm and 1356 nm respectively, Figure 65. When the concentration of electrolyte is increased too much, flocs may be too large to improve stability to coalescence, as they do not adsorb at the interface quickly during homogenisation. Values of f_W displayed little variation as a function of [NaCl]. This is because the major factors affecting creaming, density difference of the two phases, mean droplet diameter and viscosity did not appear to vary to a great extent.

Figure 96. Emulsions of isooctane and NaCl solutions of varied concentration (1:1 volume ratio) formed from magnesium hydroxide sample 22 at 1.0 wt.% 30 days after homogenisation. [NaCl]/ M is: (a) 0, (b) 10^{-3}, (c) 10^{-2}, (d) 10^{-1}, (e) 0.2, (f) 0.5.

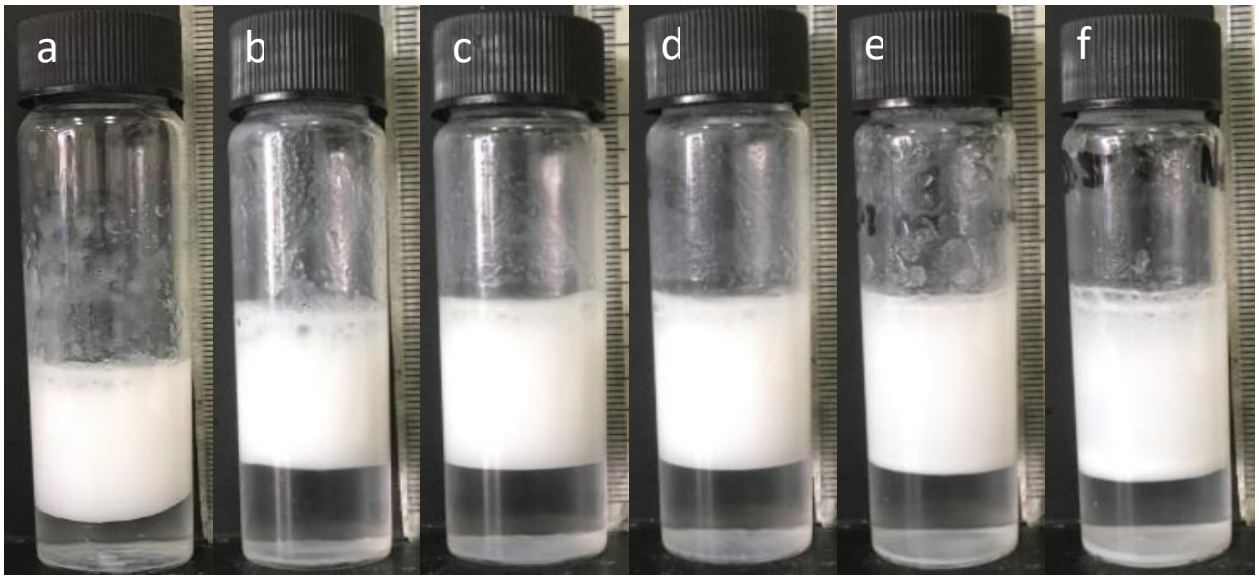

Figure 97. Optical micrographs of emulsions of isooctane and NaCl solutions of varied concentration (1:1 volume ratio) formed from magnesium hydroxide sample 22 at 1.0 wt.% 48 hours after homogenisation. [NaCl]/ M is: (a) 0, (b) 10^{-3}, (c) 10^{-2}, (d) 10^{-1}, (e) 0.2, (f) 0.5.

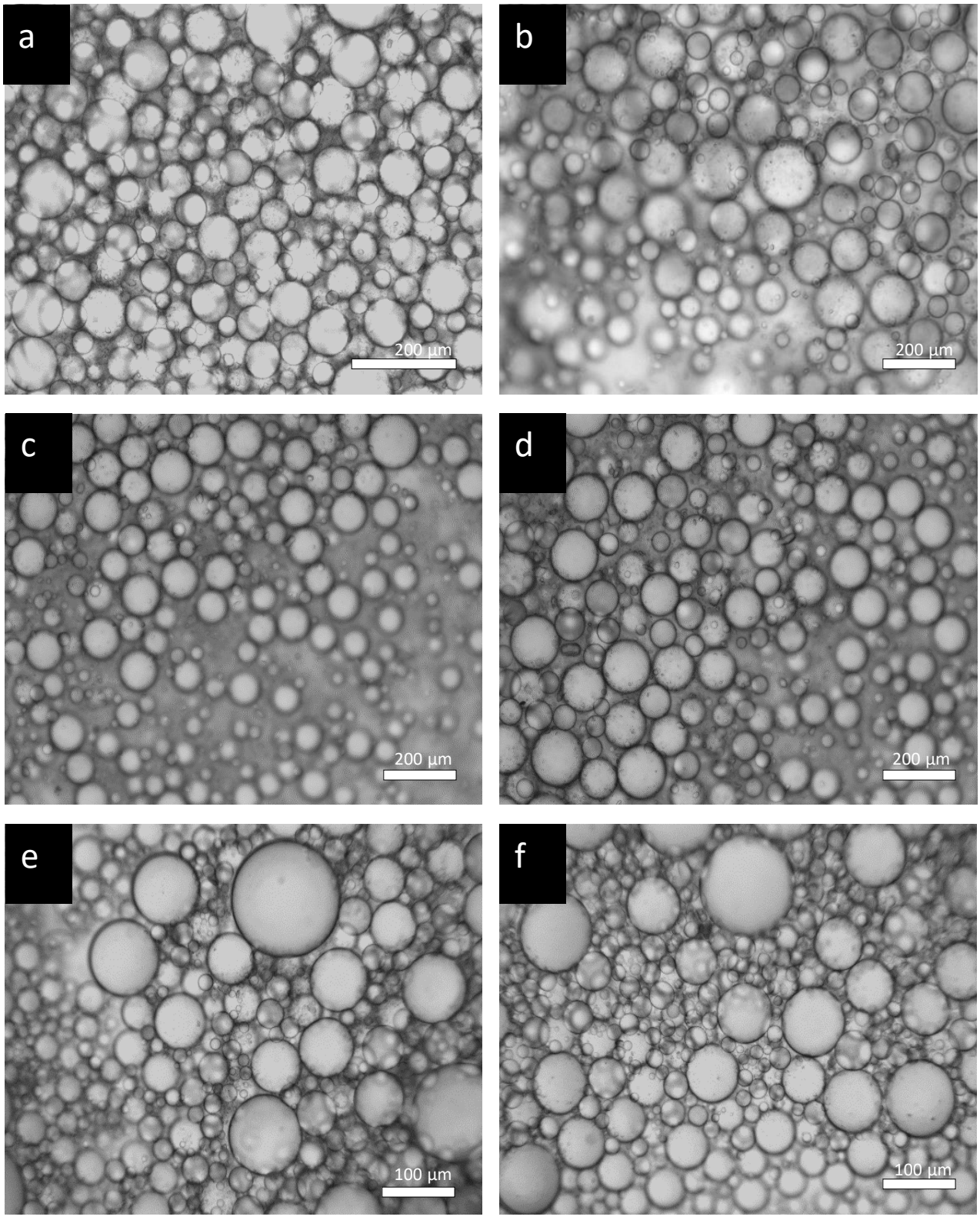

Figure 98. Variation of f_O and f_W as a function of [NaCl] in isooctane-in-water emulsions (1:1 volume) stabilised by $Mg(OH)_2$ sample 22 at 1.0 wt.%. 30 days after homogenisation.

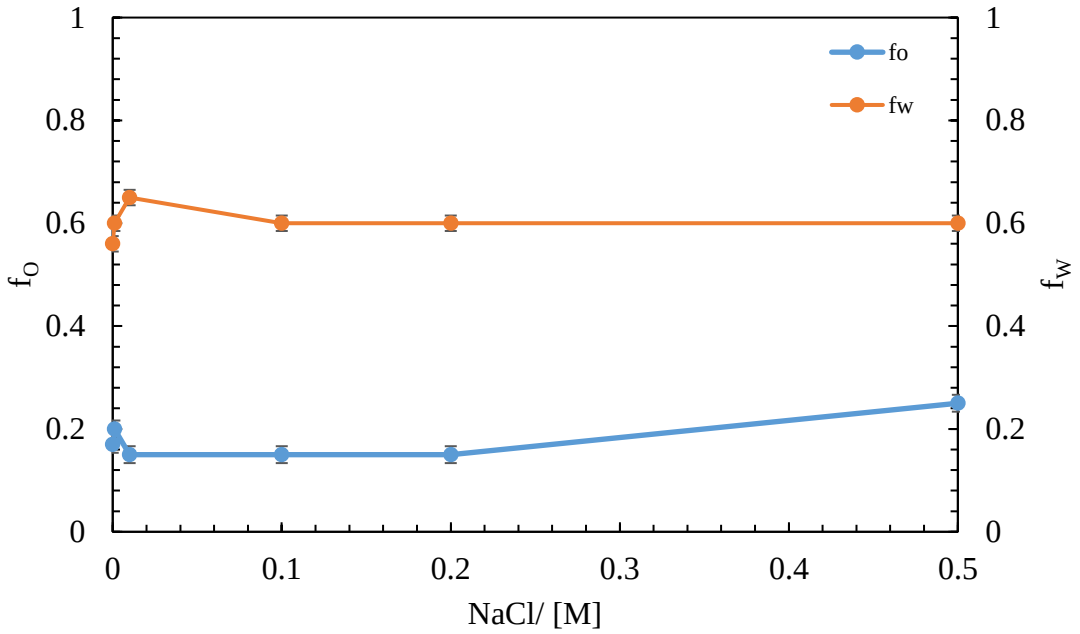

Figure 99. Variation of mean droplet diameter with [NaCl] for isooctane-in-water emulsions (1:1 volume) stabilised by $Mg(OH)_2$ sample 22 at 1.0 wt.% 48 hours after homogenisation by microscopy.

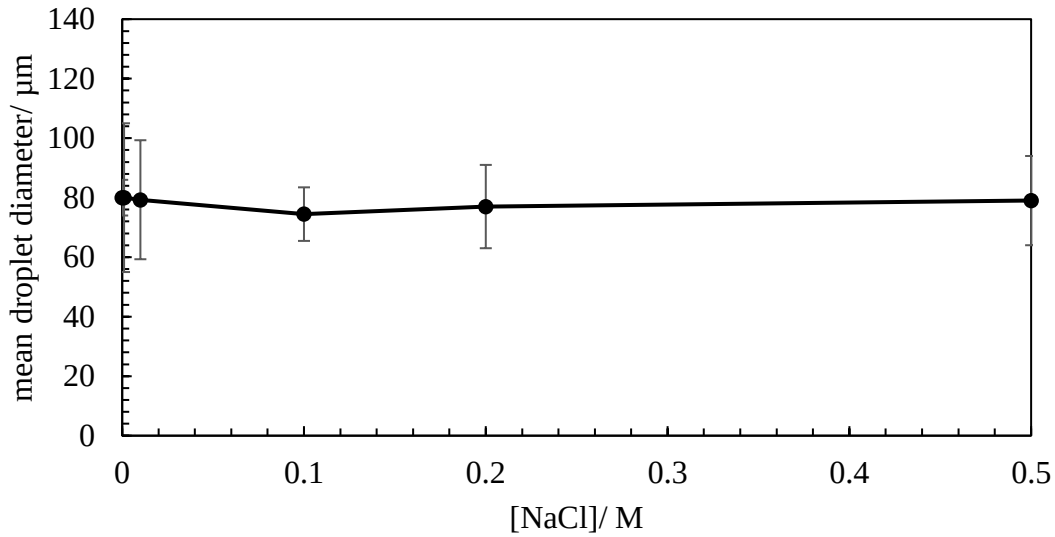

3.3.4 Isooctane-in-water emulsions and temperature

Isooctane-in-water emulsion stability was assessed as a function of storage temperature. An isooctane-in-water emulsion was prepared from sample 22 at 1.0 wt.% at room temperature and was heated/ cooled to a control temperature for 24 hours. Photographs of the emulsion after being stored at different temperatures can be seen in Figure 100, with optical micrographs of their respective droplets in Figure 101. As temperature increased from 10 ^{o}C to 40 ^{o}C, stability to coalescence did not change. Despite the fact droplets are more likely to collide as temperature increases due to possessing greater thermal energy at elevated temperatures, there may not have been enough energy supplied to remove the particles from the isooctane – water interface. This means the particles continued to provide steric and electrostatic repulsion between droplets preventing coalescence. However, beyond 40 ^{o}C, f_O values increased slightly indicating some coalescence had occurred, seen in Figure 102. Sedimentation also slightly increased beyond this temperature, suggesting that some particles had been removed from the interface which promoted coalescence of emulsion droplets due to decreased levels of repulsion. There is no apparent change in droplet size, evident in Figure 103. Due to magnesium hydroxide having a very high melting point, 350 ^{o}C, it is not surprising that very little variation was seen from 10 ^{o}C – 60 ^{o} C. In previous studies [96], it was suggested that the emulsion begins to destabilise at a temperature where the particles begin to melt and desorb from the interface.

Figure 100. Isooctane-in-water emulsions (1:1 volume) stabilised by magnesium hydroxide sample 22 at 1.0 wt. %, stored at a controlled temperature for 24 hours. (a) 10 ^{o}C, (b) 20 ^{o}C, (c) 30 ^{o}C, (d) 40 ^{o}C, (e) 50 ^{o}C, (f) 60 ^{o}C.

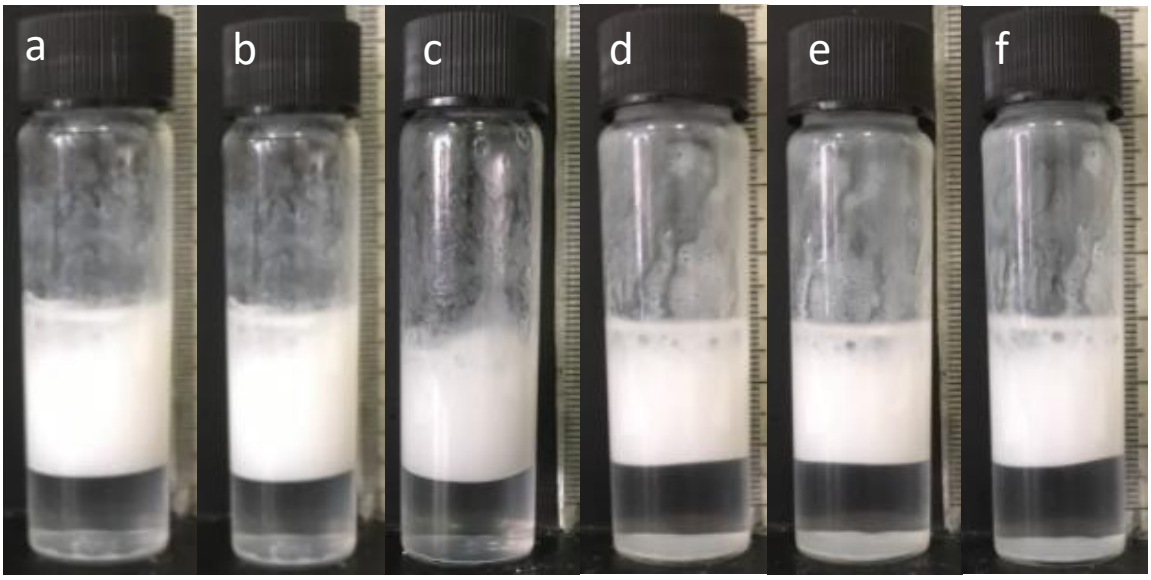

Figure 101. Optical micrographs of isooctane-in-water emulsions (1:1 volume) stabilised by magnesium hydroxide sample 22 at 1.0 wt. %, stored at a controlled temperature for 24 hours. (a) 10 ºC, (b) 20 ºC, (c) 30 ºC, (d) 40 ºC, (e) 50 ºC, (f) 60 ºC.

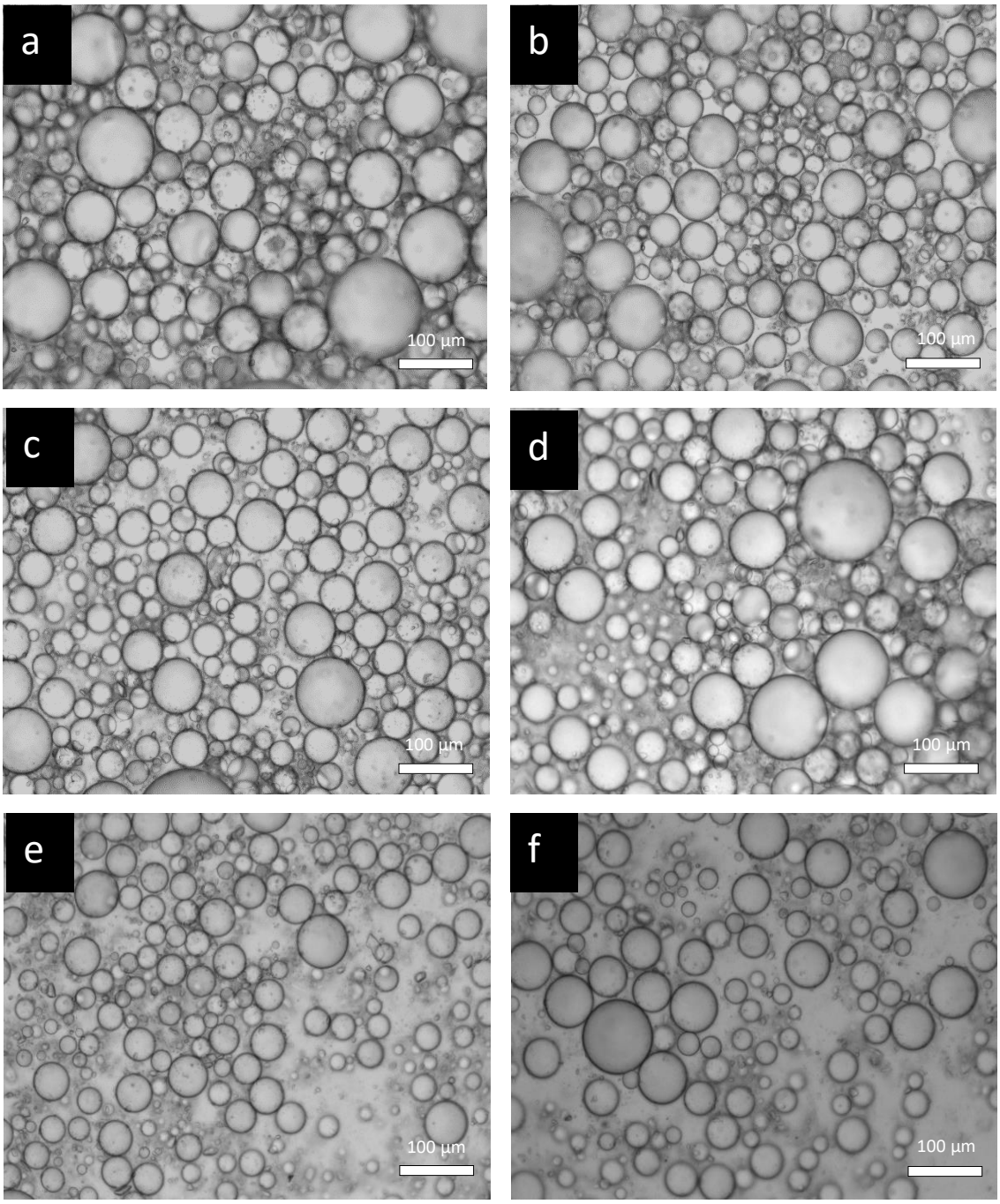

Figure 102. Variation of f_O and f_W of isooctane-in-water emulsions (1:1 volume) stabilised by magnesium hydroxide sample 22 at 1.0 wt.% as a function of temperature after preparation (emulsion stored at a controlled temperature for 24 hours).

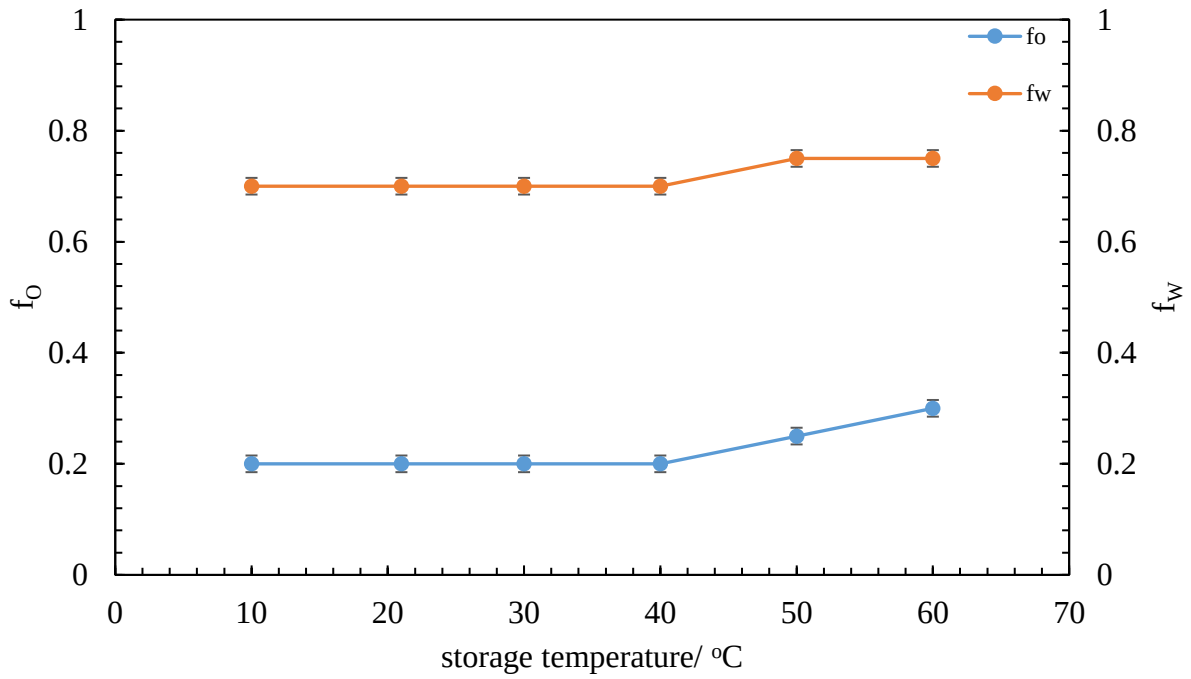

Figure 103. Mean droplet diameter of isooctane-in-water emulsion (1:1 volume) stabilised by magnesium hydroxide sample 22 at 1.0 wt.% as a function of temperature after preparation (emulsion stored at a controlled temperature for 24 hours).

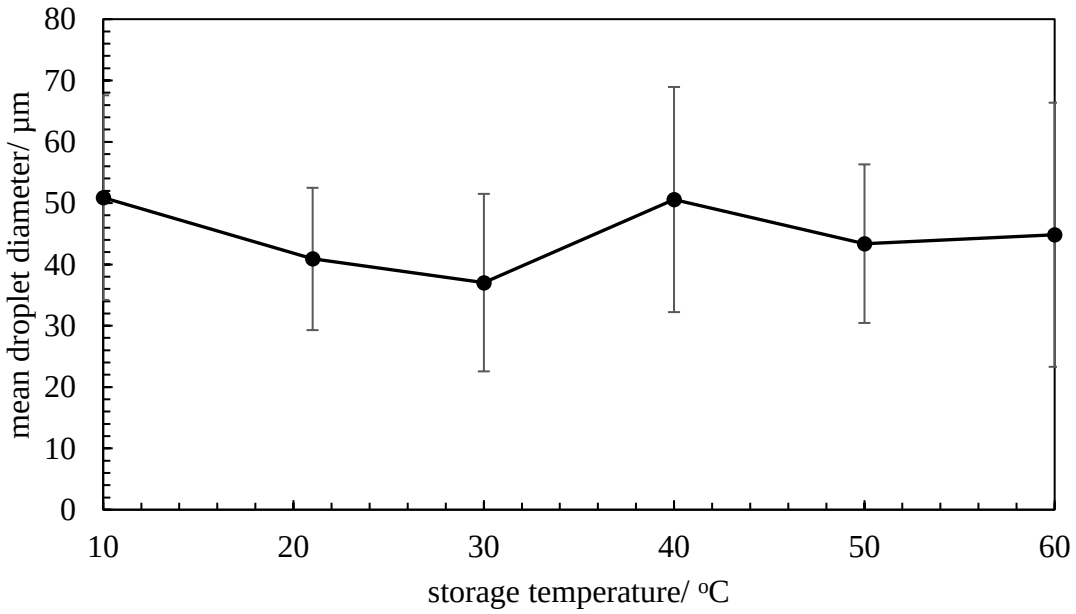

3.4 MMA-in-water emulsions

Initially, it appeared as though a good emulsion had formed between MMA and water. For emulsions with isooctane, creaming occurs within seconds due to a relatively high density difference between isooctane and water. This was not the case with MMA as the emulsion remained as a single cloudy phase for a number of minutes as MMA has a significantly higher density, 0.9337 g/cm^3 at 25 ^{o}C [97], than isooctane. The MMA-in-water emulsion from sample 22 can be seen immediately after homogenisation as an example in Figure 104.

Figure 104. MMA-in-water emulsion stabilised by sample 22 at 1.0 wt.% immediately after homogenisation.

However, as time since homogenisation elapsed, emulsions of MMA-in-water soon began to quickly destabilise. Sedimentation of magnesium hydroxide particles occurs, quickly followed by coalescence of the oil phase, forming a layer of MMA as the top layer of the system. The droplets become visible by eye at around 30 minutes – 1 hour after homogenisation and typically, within 48 hours, complete phase separation of emulsions occurred. MMA-in-water emulsions from magnesium hydroxide samples 19 and 22 remained past 48 hours. Figure 105 shows the MMA-in-water emulsions forty- eight hours after homogenisation.

Figure 105. Photographs of MMA-in-water emulsions (volume 1:1) 48 hours after homogenisation. The emulsions were stabilised by 1.0 wt.% of various magnesium hydroxide samples, synthesised from magnesium chloride hexahydrate and sodium hydroxide. (a) Sample 16, (b) sample 17, (c) sample 18, (d) sample 19, (e) sample 20, (f) magnesium hydroxide sample 21, (g) sample 22, (h) sample 23, (i) sample 24, (j) sample 25, (k) sample 26.

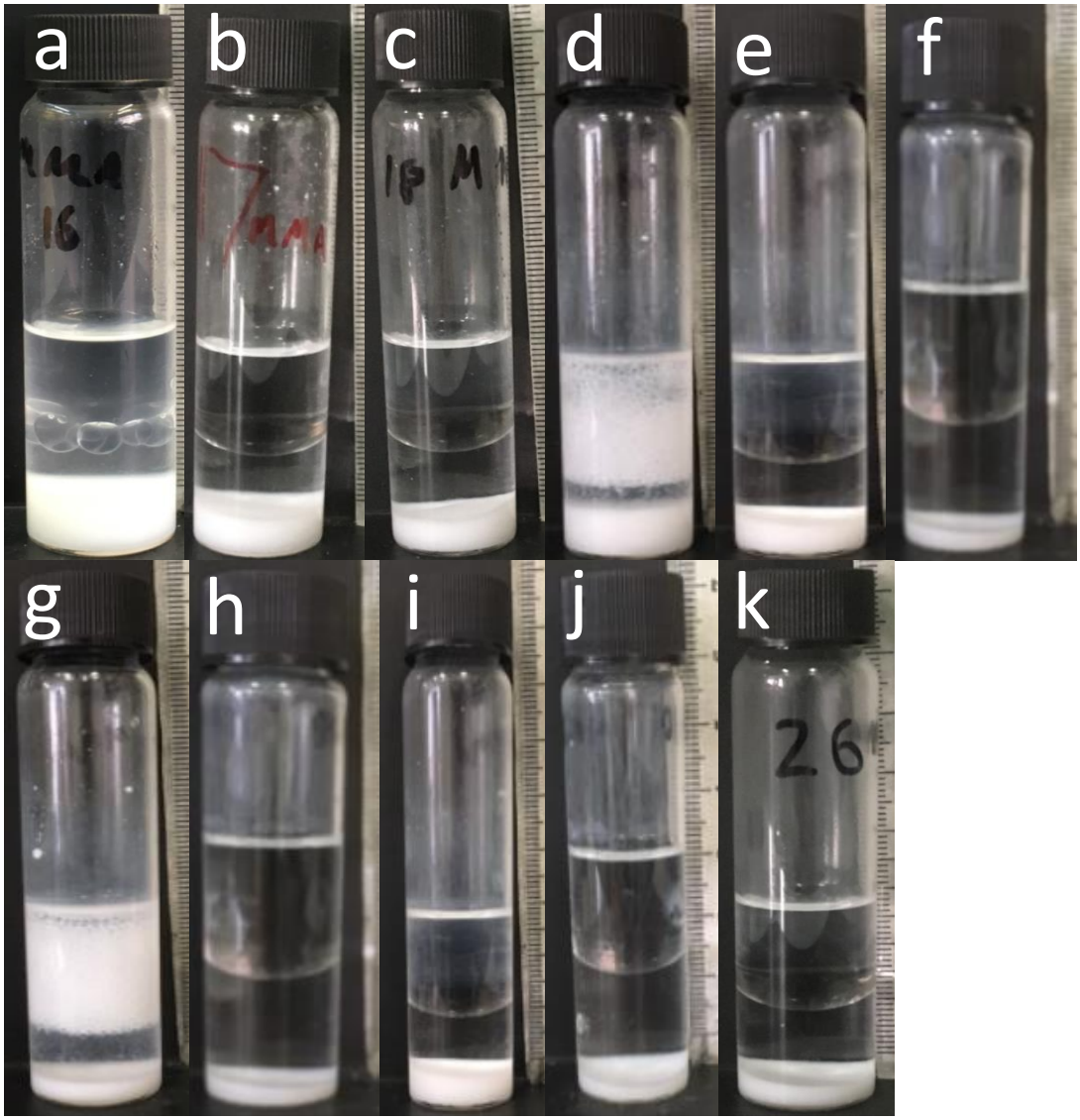

However, for all MMA-in-water emulsions in this series, complete phase separation occurred within 7 days after homogenisation. The MMA-in-water emulsions formed could be so poor due to MMA being somewhat polar and therefore partially water soluble, solubility of MMA = (0.016 g/ml in water at 20 ^{o}C [97]). This is not a problem for isooctane-in-water emulsions as isooctane is considered to be insoluble in water.

Although MMA has a higher liquid surface tension (0.028 N/m [98]) than isooctane (0.016 N/m [99]) MMA has a much lower interfacial tension against water (0.019 N/m [98]) than isooctane (0.058 N/m [100]). Equation 2 states that as interfacial tension increases, more energy is required to remove the $Mg(OH)_2$ particles from the interface. This may also be a factor leading to isooctane-in-water emulsions having a better long-term stability than MMA-in-water emulsions when stabilised by $Mg(OH)_2$. It is not thought that contact angle affected long-term stability as o,w and w,o values were similar when isooctane and MMA were used as the oil, based on the results of this study. o,w and w,o contact angle measurements carried out in this study were Long-term stability of MMA-water emulsions is often not discussed in literature.

3.4.1 MMA-in-water emulsions with added electrolyte

When electrolytes were added to the MMA-in-water emulsions, long-term stability slightly increased. As [NaCl] increases, very little variation in f_W was observed. f_O values decrease from 0.5 to 0.35, which can be noted in figure 106 and figure 107. Figure 62 shows that as [NaCl] increases from 10^{-2} M to 0.2 M, the mean particle diameter increases from 1169 nm to 1356 nm. The agglomerated particles at increased [NaCl] could form a thicker layer of particles at the interface and this could reduce the rate of dissolution of MMA in water. f_W values are larger than expected when considering the height of the emulsion layer remaining. This could be due to some of the MMA dissolving already, which increases the height of the layer of water. There was no obvious correlation between [NaCl] and mean droplet diameter, which can be observed in Figure 107 and 109.

The emulsions continued to destabilise with time. Thirty days after homogenisation, all of the emulsions had completely phase separated, evident in Figure 110.

Figure 106. MMA-in-water emulsions (1:1 volume) with varied [NaCl] stabilised by $Mg(OH)_2$ sample 22 at 1.0 wt.% 48 hours after homogenisation. [NaCl]/ M: (a) 0, (b) 10^{-3}, (c) 10^{-2}, (d) 10^{-1} M, (e) 0.2, (f) 0.5.

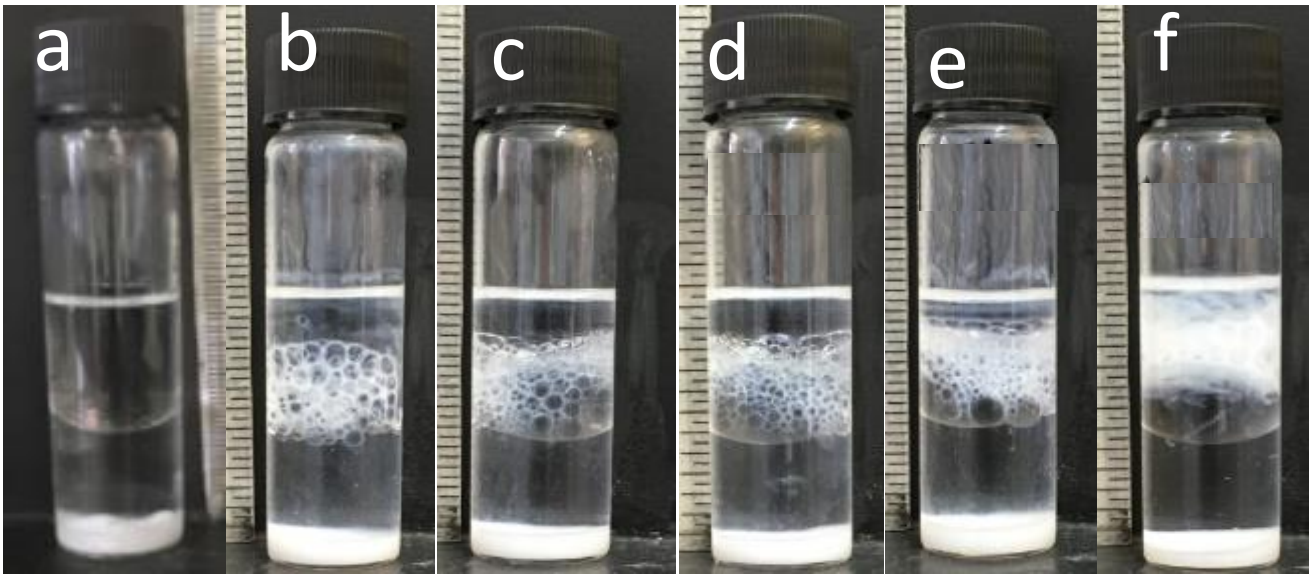

Figure 107. Optical micrographs of emulsions between MMA and NaCl solutions of varied concentration (1:1 volume ratio, formed from magnesium hydroxide sample 22, 1.0 wt. %) 48 hours upon homogenisation. **a.** [NaCl] = 10^{-3} M, **b.** [NaCl] = 10^{-2} M, **c.** [NaCl] = 10^{-1} M, **d.** [NaCl] = 0.2 M, **e.** [NaCl] = 0.5 M, 15 days after homogenisation (taken from centre of emulsion layer).

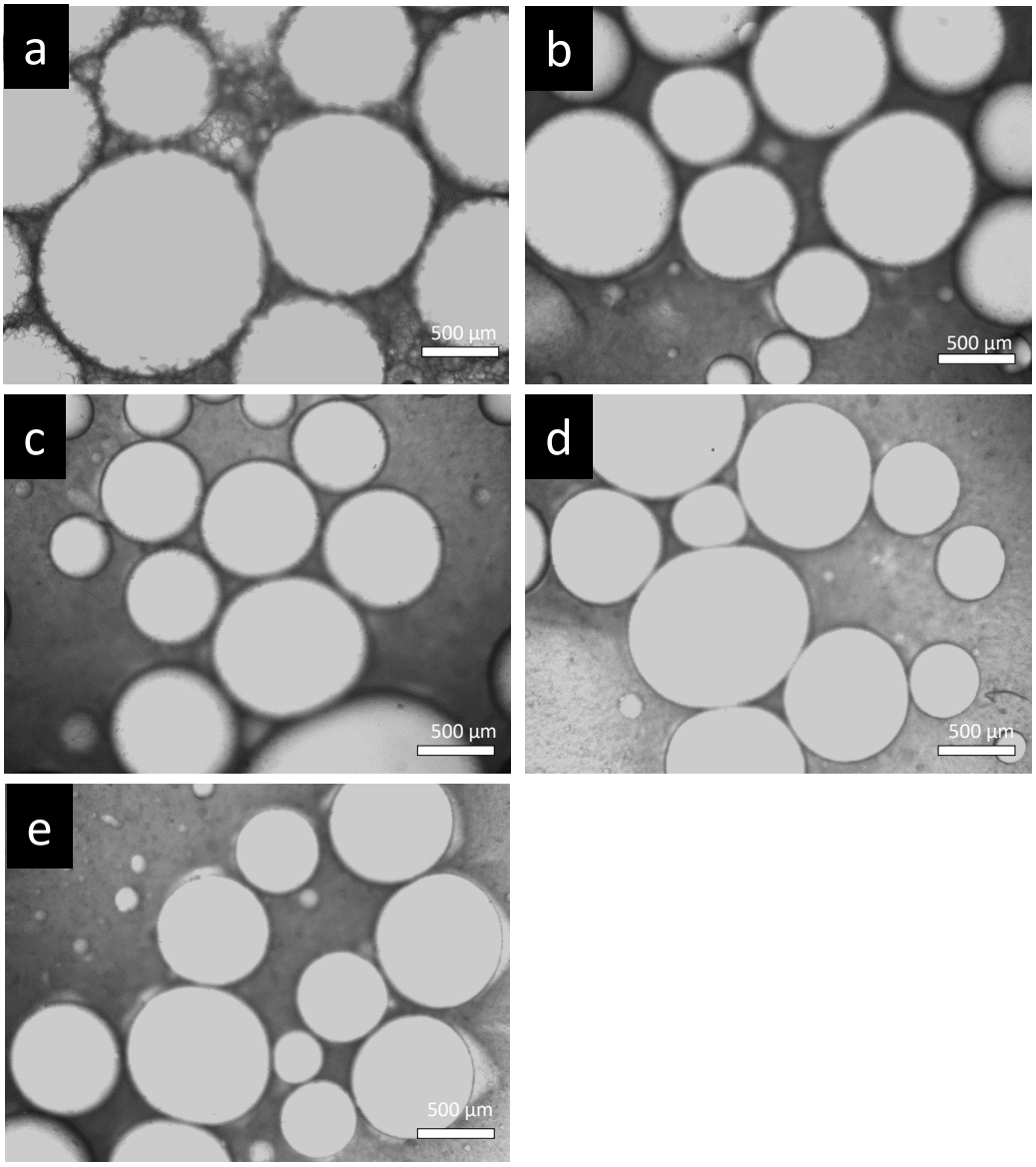

Figure 108. f_O and f_W as a function of [NaCl] in MMA-in-NaCl solution (aq.) emulsions (1:1 volume), stabilised by $Mg(OH)_2$ sample 22, 1.0 wt. %. 48 hours after homogenisation.

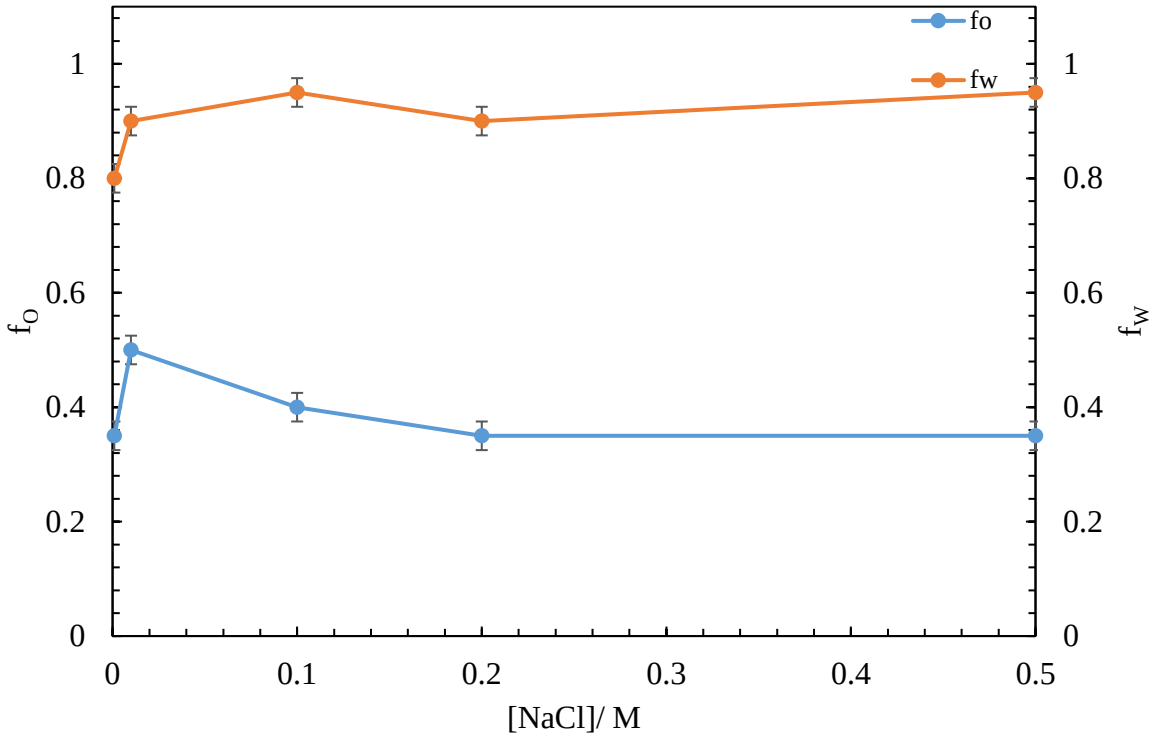

Figure 109. Variation of mean droplet diameter with [NaCl] for MMA-in-NaCl solution (aq.) emulsions (1:1 volume) stabilised by $Mg(OH)_2$ sample 22, 1.0 wt. %, 48 hours after homogenisation, by microscopy.

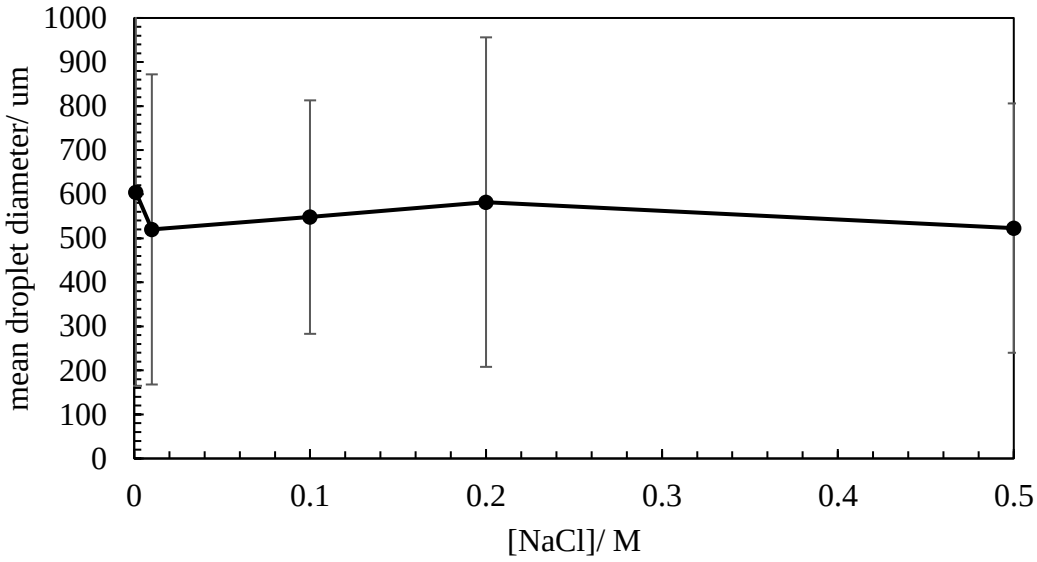

Figure 110. MMA-in-water emulsions (1:1 volume) with varied [NaCl], stabilised by $Mg(OH)_2$ sample 22, 1.0 wt.%, 48 hours after homogenisation. **a.** [NaCl] = 0 M, **b.** [NaCl] = 10^{-3} M, **c.** [NaCl] = 10^{-2} M, **d.** [NaCl] = 10^{-1} M, **e.** [NaCl] = 0.2 M, **f.** [NaCl] = 0.5 M, 30 days after homogenisation.

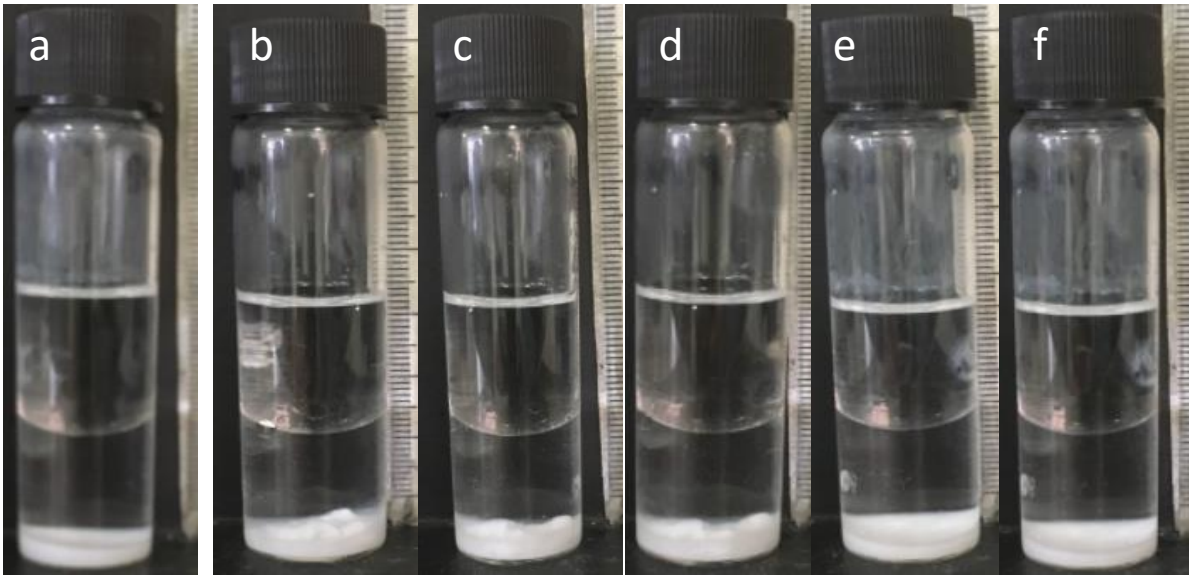

3.5 Variation of isooctane fraction in mixtures with MMA

Emulsions with different mixtures of isooctane and MMA as their oil phase were prepared. Emulsion stability to coalescence and creaming increased as fraction of isooctane, ϕiso, increased. Which is evident from the increased volume of oil and water liberated from the emulsions at lower ϕiso, seen in Figure 104. At Φiso 0 and 0.1, complete phase separation quickly occurred. At ϕiso = 0.2, the emulsion did not phase separate but was of poor quality and the diameter of the oil droplets were very large and were visible to the eye. As ϕiso of the oil phase increases, the droplet diameter decreases, seen in Figures 105, 106 and 108, indicating that the emulsion becomes more stable to coalescence. This was expected due to magnesium hydroxide particles successfully stabilising emulsions of water and isooctane (1:1 volume), but not so successful in stabilising emulsions of water and MMA (1:1 volume). Between ϕiso = 0.3 ϕiso – 0.5, the mean droplet diameter was almost constant at around 325 μm. From ϕiso = 0.5–0.9, the mean droplet diameter decreased in an almost linear fashion, from 325 μm to around 50 μm. At ϕiso = 1, the mean droplet diameter was around 47 μm. As ϕiso increases, the emulsions become more stable which is evident from the mean droplet diameter and f_O/f_W values decreasing, evident in the photographs of Figure 104 and also Figure 107.

According to the Stokes equation, eq. 11, there are 3 main factors to take into account when considering the rate of creaming in this experiment. These are difference in density between oil phase and aqueous phase, difference in viscosity and the difference in mean droplet diameter. As ϕiso decreases, the difference in density between oil phase and aqueous phase also decreases. However, despite this, as ϕiso decreases, the stability of the emulsions to creaming also decreases. This suggests that the mean droplet diameter has a greater effect on emulsion stability in terms of creaming than difference in density between the two phases in this experiment. As ϕiso increases, droplet diameter decreases.

Figure 111. Photographs of emulsions containing Milli-Q water and an oil phase containing different ratios of isooctane and MMA (1:1 volume ratio with respect to oil: water) stabilised by sample 22 at 1 wt.%, 38 days after homogenisation ϕiso: (a) 0, (b) 0.1, (c) 0.2, (d) 0.3, (e) 0.4, (f) 0.5, (g) 0.6, (h) 0.7, (i) 0.8, (j) 0.9, (k) ϕiso 1.0.

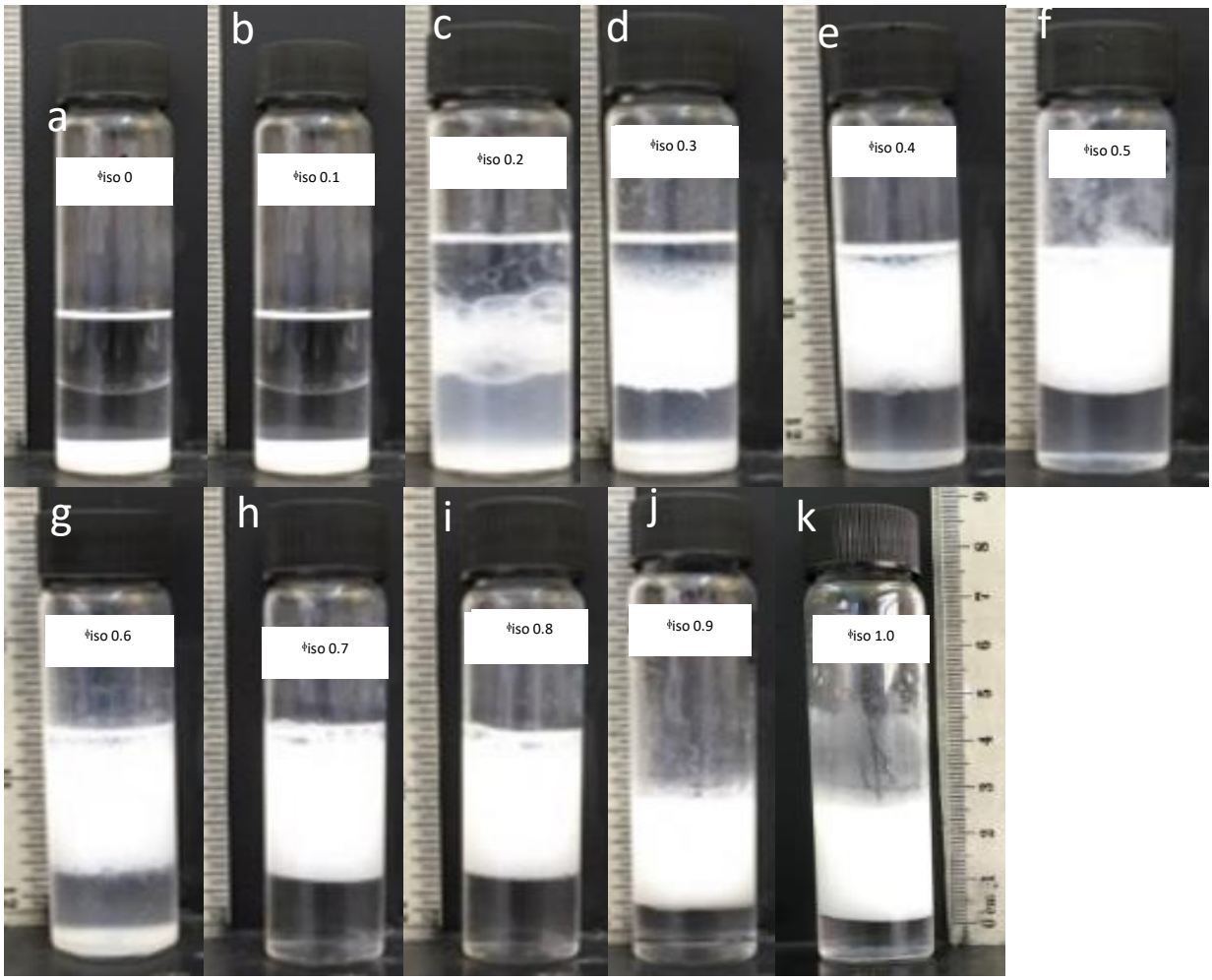

Figure 112. Optical micrographs of emulsions of emulsions containing Milli-Q water and an oil phase containing different ratios of isooctane and MMA (1:1 volume ratio with respect to oil: water) stabilised by sample 22 at 1 wt.%, 48 hours after homogenisation Φiso: (a) 0.2, (b) 0.3, (c) 0.4, (d) 0.5.

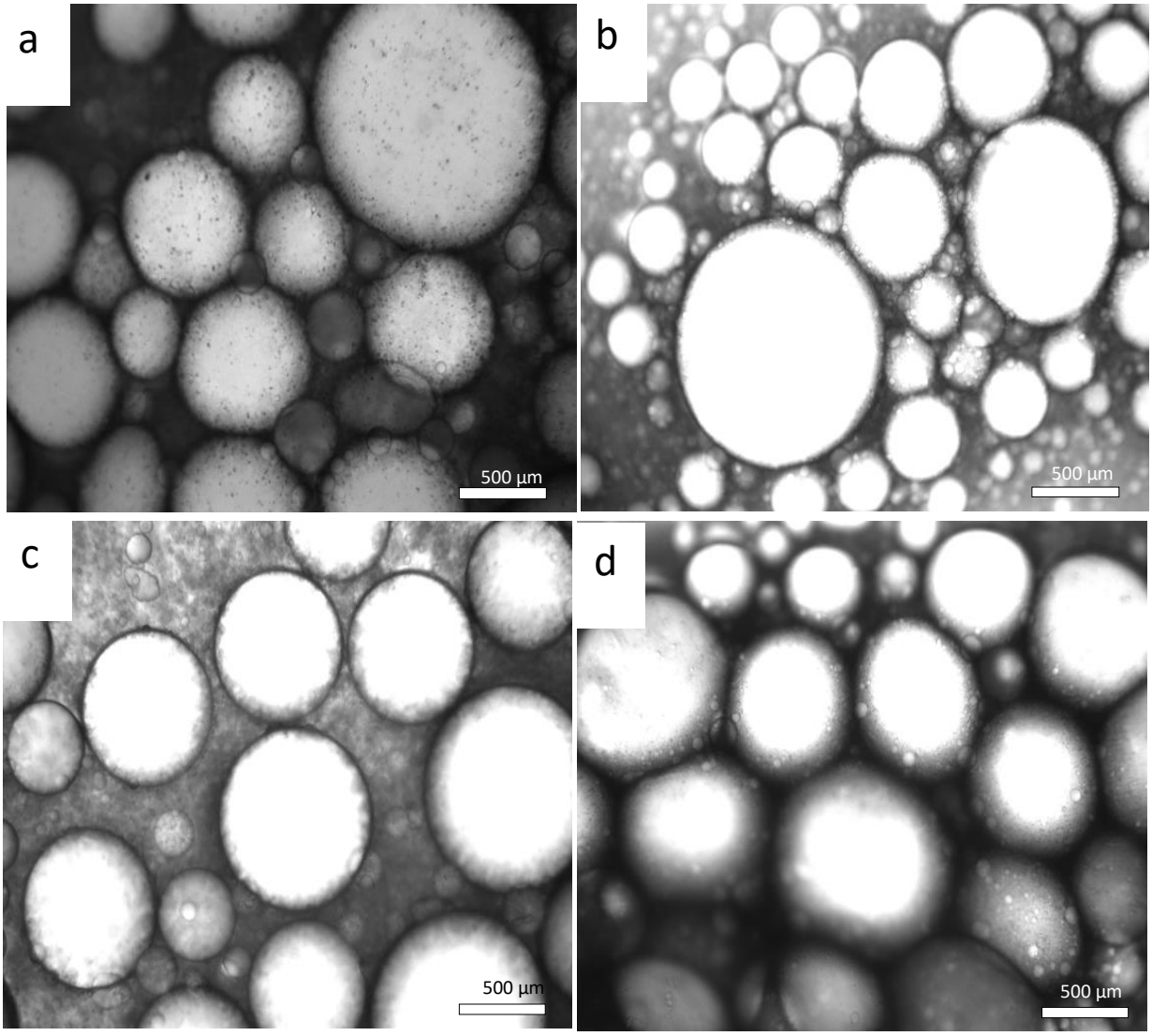

Figure 113. Optical micrographs of emulsions of emulsions containing Milli-Q water and an oil phase containing different ratios of isooctane and MMA (1:1 volume ratio with respect to oil: water) stabilised by sample 22 at 1 wt.%, 48 hours after homogenisation Φiso: (a) 0.6, (b) 0.7, (c) 0.8, (d) 0.9.

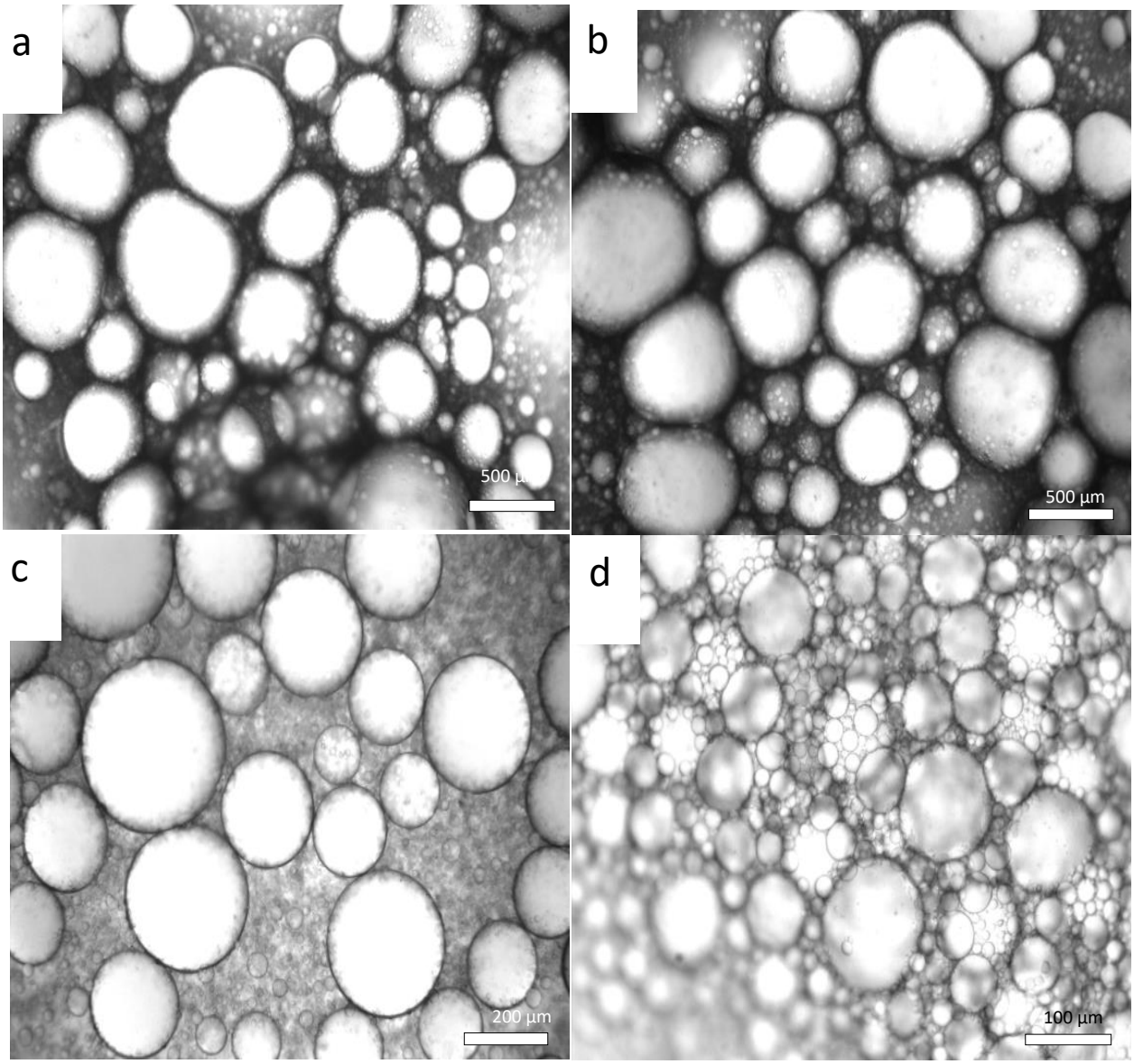

Figure 114. Variation of f_O and f_W as a function of Φiso of the oil phase for oil-in-water emulsions (1:1 volume) where isooctane is mixed with MMA stabilised by 1 wt.% of magnesium hydroxide sample 19 40 days after homogenisation.

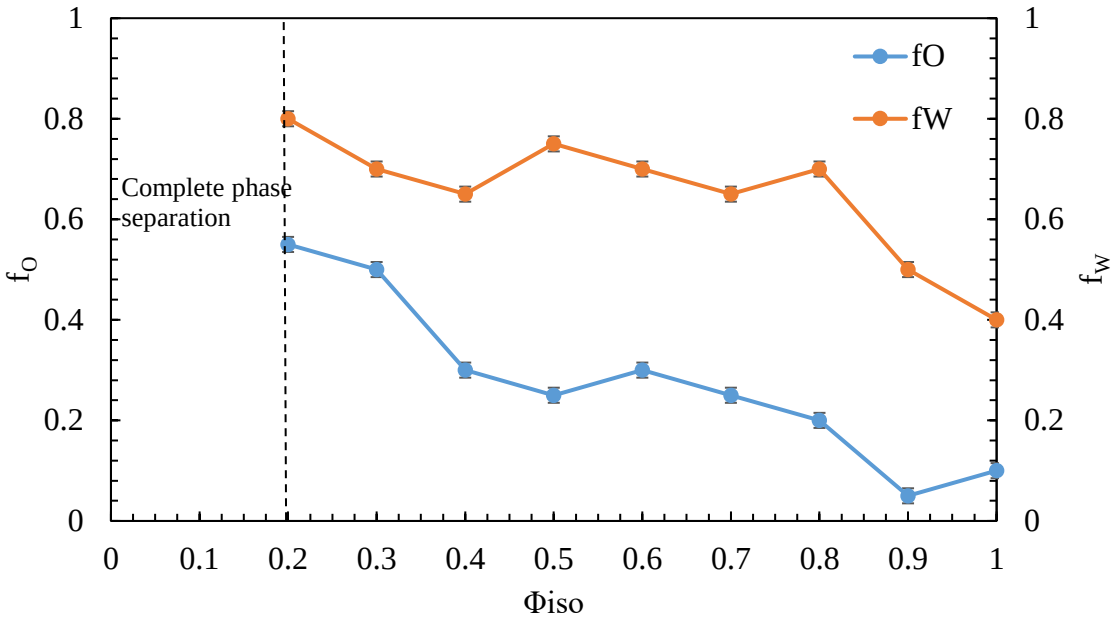

Figure 115. Variation of mean droplet diameter with Φiso for oil-in-water emulsions (1:1 volume) where isooctane is mixed with MMA stabilised by 1 wt. % of magnesium hydroxide sample 19 48 hours after homogenisation from microscopy.

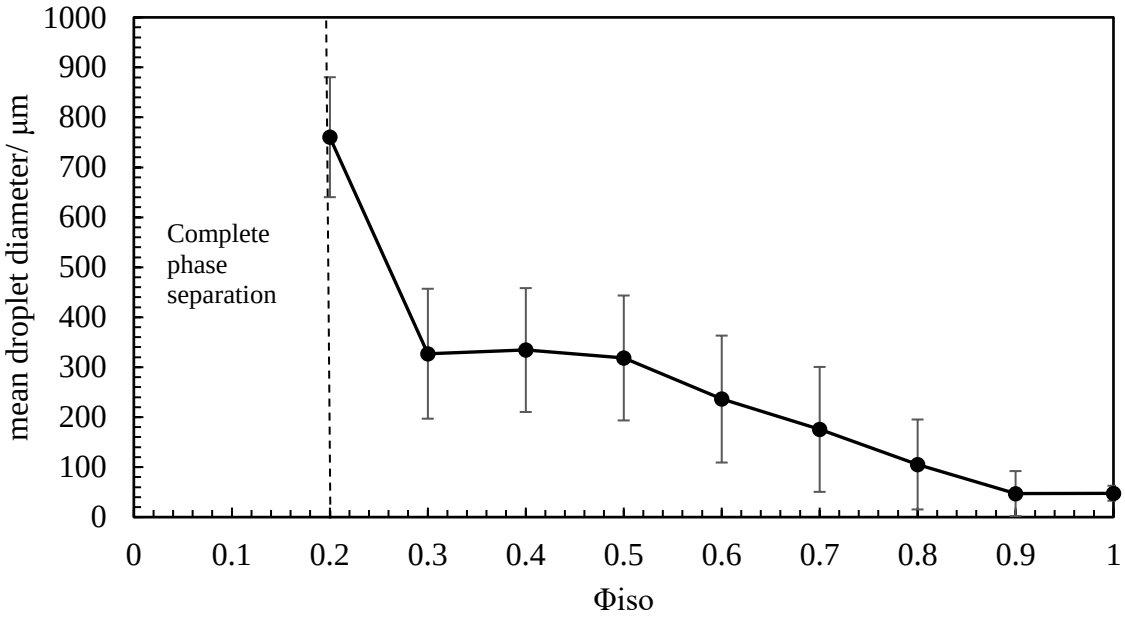

3.6 Contact angle measurements

Contact angle measurements of water drops on brucite were taken in different conditions. Brucite was chosen as it was easy to cut and yield a fresh, flat surface. $\theta_{a,w}$, $\theta_{w,o}$ and $\theta_{o,w}$ of a water drop at neutural pH were recorded and are presented in Table 3 and Table 5. Contact angles were also recorded for a water drop of pH 10.5 on brucite, seen in Table 4 and 6. During the experiment the oil used was also varied. Both isooctane (Tables 3 and 4) and MMA (Tables 5 and 6) were used.

Table 3. Average contact angles taken where brucite is the substrate. The droplet is 10 µl Milli-Q water (neutral pH) and the oil is isooctane.

	$\theta_{a,w}$	$\theta_{w,o}$	$\theta_{o,w}$
Advancing contact angle/ ^{o} (± 5^{o})	64.3	42.0	83.1
Receding contact angle/ ^{o} (± 5^{o})	44.5	27.1	72.0

Table 4. Average contact angles taken where brucite is the substrate. The droplet is 10 µl Milli-Q water (pH 10.5) and the oil is isooctane.

	$\theta_{a,w}$	$\theta_{w,o}$	$\theta_{o,w}$
Advancing contact angle/ ^{o} (± 5^{o})	73.3	45.6	84.9
Receding contact angle/ ^{o} (± 5^{o})	49.6	31.1	70.3

Table 5. Average contact angles taken where brucite is the substrate. The droplet is 10 µl Milli-Q water (neutral pH) and the oil is MMA.

	$\theta_{a,w}$	$\theta_{w,o}$	$\theta_{o,w}$
Advancing contact angle/ ^{o} (± 5^{o})	64.3	49.2	79.8
Receding contact angle/ ^{o} (± 5^{o})	44.5	33.4	66.5

Table 6. Average contact angles taken where brucite is the substrate. The droplet is 10 µl Milli-Q water (pH 10.5) and the oil is MMA.

	$\theta_{a,w}$	$\theta_{w,o}$	$\theta_{o,w}$
Advancing contact angle/ ^{o} (± 5^{o})	73.3	46.3	83.5
Receding contact angle/ ^{o} (± 5^{o})	49.6	32.7	74.6

The $\theta_{a,w}$ values recorded in this experiment support the fact that magnesium hydroxide is partially hydrophobic and therefore will stabilise oil-in-water emulsions. Different pH of the water droplet did not appear to make a great difference on the contact angle. This could be that once the water has been placed on the brucite, pH increases from neutral pH to around 10.5, which is the pH of a magnesium hydroxide aqueous dispersion. Contact angles recorded for $\theta_{w,o}$ and $\theta_{o,w}$ did not change greatly when MMA was used in place of isooctane as the oil. Considering the fact that isooctane produces stable emulsions with Milli-Q water, and MMA produces very unstable emulsions, this is somewhat surprising. The difference in stability is not due to differences in contact angle.

The $\theta_{w,o}$ are the most relevant here to show how magnesium hydroxide is behaving in the emulsions formed in this project, because the magnesium hydroxide sample first contacts the water, not the oil, during the preparation of each of the emulsions.

However, the contact angle measurements taken here may be doubtful as it was expected that $\theta_{w,o}$ values would be greater than $\theta_{a,w}$. Perhaps the low values of $\theta_{w,o}$ seen here are due to oil penetrating the brucite, having an adverse effect on contact angles.

4. Conclusions and Future Work

When Mg^{2+} ions or OH^- ions were in excess in the formation of magnesium hydroxide, large, rod-like particles which were around 2 μm in length were formed. This was also true for magnesium hydroxide formed at 50 ^oC. The other magnesium hydroxide samples formed from a weak base in this experiment were around 150 – 200 nm in diameter and possessed platelet and rod-like morphologies. The magnesium hydroxide samples formed from a strong base were not as strongly affected by reaction conditions and all of the particles had a diameter of around 100 – 200 nm. Each of the magnesium hydroxide particles had a zeta potential in the range of 16 mV ±5 mV and there was no apparent correlation between reaction conditions and zeta potential of particles.

The different samples of magnesium hydroxide all produced isooctane-in-water emulsions. There was no apparent link between particle size and morphology and emulsion stability. Isooctane-in-water emulsions did not destabilise beyond 48 hours after homogenisation.

When magnesium hydroxide concentration was varied in isooctane-in-water emulsions, f_W decreased with increasing magnesium hydroxide concentration. An initial decrease of f_O was observed when magnesium hydroxide concentration was increased from 0.5 wt. % to 1.0 wt. %, beyond this point f_O values levelled off. When NaCl was introduced to isooctane-water systems, stability to coalescence slightly increased. Indicated by a decreasing f_O value. This trend continued as [NaCl] increased to 0.2 M. Beyond this point, stability to coalescence appeared to remain constant until 0.5 M. Increasing temperature had very little effect on emulsion stability.

MMA-in-water emulsions showed very poor long-term stability, completely destabilising within 7 days following homogenisation. When NaCl was introduced to the system, long-term stability was increased. The emulsions destabilised in around 30 days following evidence of deterioration.

When different ratios of isooctane and MMA were used as the oil phase of emulsions, the emulsion containing a greater fraction of isooctane were more stable.

Suggestions of future work include noting the effect of added electrolytes in systems containing both isooctane and MMA in the oil phase. It would also be interesting to note the effect on emulsion stability of varied volume of oil: volume of water. Adding a surfactant to the systems may also be of interest.

5. References

[1] M. A. Shah and F. M. Al-Marzouki, A simple safe method for preparation of $Mg(OH)_2$ nanorods in ambient air, *Int. J. Nano Dim*., 2011, **2**, 111- 116.

[2] https://wonderworlds.org/mineral/brucite.htm (Accessed on 16/08/17)

[3] S. Zhang, F. Cheng, Z. Tao, F. Gao and J. Chen, Removal of nickel ions from wastewater by $Mg(OH)_2$/ MgO nanostructures embedded in Al_2O_3 membranes, *J. Alloys Compd*., 2006, **426**, 281-285.

[4] T. E. Larson and A. M. Buswell, Water Softening, *Ind. Eng. Chem.*, 1940, **32**, 132-134.

[5] L. A. Hollingberry,. and R. T. Hull, The thermal decomposition of natural mixtures of huntite and hydromagnesite, *Thermochimica Acta*, 2012, **528**, 45-52.

[6] J. Tan, J. Wang, L. Wang, J. Xu and D. Sun, In Situ formed $Mg(OH)_2$ nanoparticles as pH-switchable stabilisers for emulsions, *J. Colloid Interface Sci*, 2011, **359**, 155-162.

[7] J. Lv, L. Qui and B. Qu, Controlled growth of three morphological structures of magnesium hydroxide nanoparticles by wet precipitation method, *J. Cryst. Growth*, 2004, **267**, 676-684.

[8] D. Chen, L. Zhu, H. Zhang, K. Xu and M. Chen, Magnesium hydroxide nanoparticles with controlled morphologies via wet coprecipitation, *Mater. Chem. Phys.*, 2008, **109**, 224-229.

[9] A. Sierra-Fernandez, L.S. Gomez-Villalba, O. Milosevic, R. Fort and M.E. Rabanal, Synthesis and morpho-structural characterization of nanostructured magnesium hydroxide obtained by a hydrothermal method, *Ceram. Int*., 2014, **40**, 12285-12292.

[10] C. Yan, D. Xue, L. Zou, X. Yan and W. Wang, Preparation of magnesium hydroxide nanoflowers, *J. Cryst. Growth*, 2005, **282**, 448-454.

[11] V. A. Phillips, J. L. Kolbe and H. Opperhauser, Effect of pH on the growth of $Mg(OH)_2$ crystals in an aqueous environment at 60 ^oC, *J. Cryst. Growth*, 1977, **41**, 228- 234.

[12] C. Henrist, J.-P. Mathieu, C. Vogels, A. Rulmont and R. Cloots, Morphological study of magnesium hydroxide nanoparticles precipitated in dilute aqueous solution, *J. Cryst. Growth.*, 2003, **249**, 321–330.

[13] O. Baidukova and E. V. Skorb, Ultrasound-assisted synthesis of magnesium hydroxide nanoparticles from magnesium, *Ultrason. Sonochem.*, 2016, **31**, 423-428.

[14] Y. Li, M. Sui, Y. Ding, G. Zhang, J. Zhuang and C. Wang, Preparation of $Mg(OH)_2$ nanorods, *Adv. Mater.*, 2000, **11**, 818-821.

[15] Y. Ding, G. Zhang, H. Wu, B. Hai, L. Wang and Y. Qian, Nanoscale Magnesium Hydroxide and Magnesium Oxide Powders: Control over Size, Shape, and Structure via Hydrothermal Synthesis, *Chem. Mater.*, 2001, **13**, 435-440.

[16] S. Utamapanya, K. J. Klabunde and J. R. Schlup, Nanoscale metal oxide particles/ clusters as chemical reagents. Synthesis and properties of ultrahigh surface area magnesium hydroxide and magnesium oxide, *Chem. Mater.*, 1991, **3**, 175-181.

[17] J. C. Yu, A. Xu, L. Zhang, R. Song and L. Wu, Synthesis and Characterisation of Porous Magnesium Hydroxide and Oxide nanoplates, *J. Phys. Chem. B,* 2004, **108**, 64- 70.

[18] W. Fan, S. Sun, X. Song, W. Zhang, H. Yu, X. Tan and G. Cao, Controlled synthesis of single-crystalline $Mg(OH)_2$ nanotubes and nanorods via a solvothermal process, *J. Solid State Chem.*, 2004, **177**, 2329-2338.

[19] H. Wu, M. Shao, J. Gu and X. Wei, Microwave-assisted synthesis of fibre- like $Mg(OH)_2$ nanoparticles in aqueous solution at room temperature, *Mater. Lett.*, 2004, **58**, 2166-2169.

[20] L. Yan, J. Zhuang, X. Sun, Z. Deng and Y. Li, Formation of rod-like $Mg(OH)_2$ nanocrystallites under hydrothermal conditions and the conversion to MgO nanorods by thermal dehydration, *Mater. Chem. Phys.*,2002, **76**, 119-122.

[21] R. Giorgi, C. Bozzi, L. Deo, C. Gabbiani, B.W. Ninham and P. Baglioni, Nanoparticles of $Mg(OH)_2$: synthesis and application to paper conservation, *Langmuir,* 2005, **21**,8495–8501.

[22] J. Fagerlund and R. Zevenhoven, An experimental study of $Mg(OH)_2$ carbonation, *Int. J. Greenh. Gas Control*, 2011, **5**, 1406–1412.

[23] J.S. Wu, J. Du and Y.M. Gao, Crystal growth morphology of magnesium hydroxide, *Turk J. Chem.*, 2014, **38**, 402- 412.

[24] X. Li, C. Ma, J. Zhao, Z. Li, S. Xu and Y. Liu, Preparation of magnesium hydroxide nanoplates using a bubbling setup, *Powder Technol.*, 2010, **198**, 292–297.

[25] G.W. Beall, E.-S.M. Duraia, F. E.- Tantawy, F. A.- Hazmi and A.A. Al- Ghamdi, Rapid fabrication of nanostructured magnesium hydroxide and hydromagnesite via microwave-assisted technique, *Powder Technol.*, 2012, **234**, 26–31.

[26] P.S. Das, A. Dey, A.K. Mandal, N. Dey, N. Dey and A.K. Mukhopadhyay, Synthesis of $Mg(OH)_2$ micro/nano flowers at room temperature, *J. Adv. Ceram.*, 2013, **2**, 173–179.

[27] M. Láska, J. Valtýni and P. Fellner, Influence of pH on the crystal size distribution of $Mg(OH)_2$ prepared by the hydration of MgO, *Cryst. Res. Technol*., 1993, **28**, 931–936.

[28] H. Dong, Z. Du, Y. Zhao and D. Zhou, Preparation of surface modified nano$Mg(OH)_2$ via precipitation method, *Powder Technol.*, 2010, **198**, 325–329.

[29] G. Song, S. Ma, G. Tang and X. Wang, Ultrasonic-assisted synthesis of hydrophobic magnesium hydroxide nanoparticles, *Colloids Surf. A*, 2010, **364**, 99–104.

[30] Q. Wang, C. Li, M. Guo, L. Sun and C. Hu, Hydrothermal synthesis of hexagonal magnesium hydroxide nanoflakes, *Mater. Res. Bull.*, 2014, **51**, 35–39.

[31] M. Laska, J. Valtyni and P. Fellner, Influence of pH on the crystal size distribution of $Mg(OH)_2$ prepared by the hydration of MgO, *Res Technol.*, 1993, **28**, 931.

[32] J. Chen, L. Lin, Y. Song, L. Shao, Influence of KOH on the hydrothermal modification of Mg(OH)2 crystals, *J. Cryst. Growth*, 2009, **311**, 2405–2408.

[33] D. Jin, X. Gu, X. Yu, G. Ding, H. Zhu and K. Yao, Hydrothermal synthesis and characterization of hexagonal $Mg(OH)_2$ nano-flake as a flame retardant, *Mater. Chem. Phys.*, 2008, **112**, 962–965.

[34] Q.L. Wu, L. Xiang and Y. Jin, Influence of $CaCl_2$ on the hydrothermal modification of $Mg(OH)_2$, *Powder Technol.*, 2006, **165**, 100–104.

[35] X. Wang, H. Pang, W. Chen, Y. Lin and G. Ning, Controllable fabrication of high purity $Mg(OH)_2$ nanoneedles via direct transformation of natural brucite, *Mater. Lett.*, 2014, **120**, 69–72.

[36] M. A. Shah and F. M. Al- Marzouki, A simple and safe method for preparation of $Mg(OH)_2$ nanorods in ambient air, *Int. J. Nano Dim.* 2011, **2**, 111- 116.

[37] H. Lingyun, Z. Cunlings, M. Xiao, J. Wanquan, Z. Yuan., Z. Yurui and C. Zuyao, Preparation and characterization of $Mg(OH)_2$ nanorods by liquid solid arc discharge technique, *Inorg. Chem. Commun*., 2003, **6**, 229-232.

[38] M. A. Shah and F. M. Marzouki,, Biosafe approach for magnesium oxide nanoflowers at very low temperature, *Int. J. Bionanosci. and Nanotechnol.*, 2010, **1**, 10-16.

[39] R. Sharma, M. J. McKelvy, H. Berat, A. V. G. Chizmeshya and R. W. Carpenter, In- situ nanoscale observations of the $Mg(OH)_2$ dehydroxylation and rehydroxylation mechanisms, *Philos. Mag.*, 2004, **84,** 2711- 2729.

[40] J. W. Mullin, J. D. Murphy, O. Sohnel and G. Spoors, Aging of Precipitated Magnesium Hydroxide, *Ind. Eng. Chem. Res.*, 1989, **28**, 1725- 1730.

[41] X. Wu, G. Hu, B. Wang and Y. Yang, Synthesis and characterization of superfine magnesium hydroxide with monodispersity, *J. Cryst. Growth*, 2008, **310**, 457- 461.

[42] J. D. Ng, B. Lorber, J. Witz, A. Theobald- Dietrich, D. Kern and R. Giege, The crystallization of biological macromolecules from precipitates: Evidence for Ostwald ripening, *J. Cryst. Growth*, 1996, **168,** 50- 62.

[43] R. Boistelle and J. P. Astier, Crystallization mechanisms in solution, *J. Cryst. Growth*, 1988, **90**, 14-30.

[44] J. W. Mullin, Crystallization, 4th Ed., 2001, Butterworth- Heinemann, 182-190, Woburn.

[45] T. Tadros, P. Izquiendo, J. Esquena and C. Solans, Formation and stability of nano-emulsions, *Adv. Colloid Interface Sci.*, 2004, **108**,303-318.

[46] L. Goibier, S. Lecomte, F. Leal- Calderon and C. Faure, The effect of surfactant crystallization on partial coalescence in O/W emulsions, *J. Colloid Interface Sci*, 2017 **500**, 304- 314.

[47] E. N. Schulz, R.E. Ambrusi, D.B. Miraglia, E.P. Schulz, S.G. Garcia, J.L. Rodriguez and P.C. Schulz, Evaluation of oil – in – water emulsions with cationic – anionic surfactants mixtures for potential use in the oil industry, *Colloids Surf. A*, 2016, **490**, 145- 154.

[48] J. R. Karamath, A.A. Vallejo-Cardona, R. Ceron- Camacho, I. N. Zapata- Penasco, V. Garibay- Febles and J. Aburto, Relative performance of several surfactants used for heavy crude oil emulsions as studied by AFM and force spectroscopy, *J. Petrol. Sci. Eng.*, 2015, **135**, 652- 659.

[49] N. Zhang, Y. Fu, G. Chen, D. Liang, A. Abdunaibe, H. Li and J. Hao, Highly concentrated oil-in- water (O/W) emulsions stabilized by cationic surfactants, *Colloids Surf. A*, 2016, **495**, 159- 168.

[50] I. Masalova, R. Foudazi and A. Ya. Malkin, The rheology of highly concentrated emulsions stabilized with different surfactants, *Colloids Surf. A*, 2011, **375**, 76- 86.

[51] M. Kawaguchi, Silicone oil emulsions stabilized by polymers and solid particles, *Adv. Colloid Interface Sci*, 2016, **233**, 186- 199.

[52] S.S. Davis, The properties of emulsions stabilized by mixtures of anionic surfactant and anionic polyelectrolyte, *J. Colloid Interface Sci.*, 1971, **35**, 665.

[53] S. Wang, Y. Shi, Z. Tu, L. Zhang, H. Wang and M. Tian, Influence of soy lecithin concentration of the physical properties of whey protein isolate- stabilized emulsion and microcapsule formation, *J. Food Eng.*, 2017, **207**, 73- 80.

[54] M. Felix, A. Romero and A. Guerrero, Visoelastic properties, microstructure and stability of high- oleic O/W emulsions stabilised by crayfish protein concentrate and xanthan gum, *Food Hydrocolloid*, 2017, **69**, 173- 184.

[55] M. Zhang, A. Wang, J. Li and N. Song, Effect of stearic acid modified HAp nanoparticles in different solvents on the properties of Pickering emulsions and Hap/ PLLA composites, *Mater. Sci. Eng. C*, 2017, **79**, 255- 261.

[56] R. Aveyard, B.P. Binks and J.H. Clint, Emulsions stabilised solely by colloidal particles, *Adv. Colloid Interface Sci.*, 2002, **100- 102**, 503- 546.

[57] W. Ramsden, Separation of Solids in the Surface-Layers of Solutions and 'Suspensions' (Observations on Surface-Membranes, Bubbles, Emulsions, and Mechanical Coagulation). - Preliminary Account, *Proc. Roy. Soc.*, 1901, **72**, 156-164.

[58] S.U. Pickering, Emulsions, *J. Chem. Soc.*, 1907, **91**, 2001- 2021.

[59] C.J. van Oss and R.F. Giese, The hydrophilicity and hydrophobicity of clay minerals, *Clays Clay Miner.*, 1995, **43**, 474 – 477.

[60] B. P. Binks, Particles as surfactants-similarities and differences, *Curr. Opin. Colloid Interface Sci.*, 2002,**7**, 21- 41.

[61] G. T. Barnes and I. R. Gentle, Interfacial Science: An introduction, Oxford University Press Inc., New York, 2005, 8-15.

[62] A. B. D. Cassie, Contact angles, *Discuss. Faraday Soc.*, 1948, **3**, 11.

[63] M. Zanini and L. Isa, Particle contact angles at fluid interfaces: pushing the boundary beyond hard uniform spherical colloids, *J. Phys. Condens. Matter*, 2016, **28**, 313002.

[64] N.V. Churaev, B. V. Derjaguin and V. M. Muller, Surface Forces, Springer, New York, 1987, 293- 310.

[65] http://www.silver-colloids.com/Tutorials/Intro/pcs8.html (accessed 08/06/2017).

[66] I.B Ivanov, K. D. Danov and P. A Kralchevsky, Flocculation and coalescence of micro-size emulsion droplets, *Colloids Surf. A*, 1999, **152**, 161-182.

[67] F. Leal- Calderon and P. Poulin, Progress in understanding emulsion metastability and surface forces, *Curr. Opin. Colloid Interface Sci.*, 1999, **4**, 223- 230.

[68] D.T. Wasan, A.D. Nikolov and F. Aimetti, *Adv. Colloid Interface Sci.*, 2004, **108- 109**, 187- 195.

[69] L. Sagis, Nonequilibrium Thermodynamic Model of water-in- water emulsions, *J. Phys. Chem. C*, 2007, **111**, 3139- 3145.

[70] Y. Hayashi, N. Shinyashiki and S. Yagihara, Dynamical structure of water around bipolymers investigated by microwave dielectric measurements using time domain reflectometry method, *J. Non- Cryst. Solids*, 2002, **305**, 328- 332.

[71] M.B.J. Meinders and T. van Vliet, The role of interfacial rheological properties on Ostwald ripening in emulsions, *Adv. Colloid Interface Sci*., 2004, **108- 109**, 119- 126.

[72] B. P. Binks and T. S. Horozov, Colloidal Particles at Liquid Interfaces, Cambridge University Press, Cambridge, 2006.

[73] B. P. Binks, Colloidal particles at a range of fluid – fluid interfaces, *Langmuir*, 2017, **33**, 6947 – 6963.

[74] B. P. Binks and S. O. Lumsdon, Stability of oil – in – water emulsions stabilised by silica particles, *Phys. Chem. Chem. Phys.*, 1999, **1**, 3007 – 3016.

[75] B. P. Binks and C. P. Whitby, Nanoparticle silica – stabilised oil – in – water emulsions: improving emulsion stability. *Colloids Surf. A*, 2005, **253**, 105 – 115.

[76] N. P. Ashby and B. P. Binks, Pickering emulsions stabilised by Laponite clay particles. *Phys. Chem. Chem. Phys.*, 2000, **2**, 5640 – 5646.

[77] H. Wang, V. Singh and S. H. Behrens, Image charge effects on the formation of Pickering emulsions, *J. Phys. Chem. Lett.*, 2012, **3**, 2986 – 2990.

[78] F. Yang, S. Liu, J. Xu, Q. Lan, F. Wei and D. Sun, Pickering emulsions stabilized solely by layered double hydroxides particles: the effect of salt on emulsion formation and stability, *J. Colloid Interface Sci*., 2006, **302**, 159- 169.

[79] Y. Xu, M. P. Konrad, W. W. Y. Lee, Z. Ye and S. E. J. Bell, A method for promoting assembly of metallic and non-metallic nanoparticles into interfacial monolayer films. *Nano Lett.*, 2016, **16**, 5255 – 5260.

[80] J. I. Amalvy, S. P. Armes, B. P. Binks, J. A. Rodrigues and G-F Unali, Use of sterically – stabilised polystyrene latex particles as a pH – responsive particulate emulsifier to prepare surfactant – free oil – in – water emulsions, *Chem. Commun.*, 2003, 1826 – 1827.

[81] N. Younan, M. Hojeij, L. Ribeaucourt and H. H. Girault, Electrochemical properties of gold nanoparticles assembly at polarised liquid|liquid interfaces, *Electrochem. Commun.*, 2010, **12**, 912- 915.

[82] B. P. Binks, W. Liu and J. A. Rodrigues, Novel stabilization of emulsions via the heteroaggregation of nanoparticles, *Langmuir*, 2008, **24**, 4443 – 4446.

[83] A. M. Bago – Rodriguez, B. P. Binks and T. Sekine, Novel stabilization of Pickering emulsions by soft particles: polyelectrolyte complexes, *Faraday Discuss.*, 2016, **191**, 255 – 285.

[84] B. P. Binks, J. A. Rodrigues and W. J. Frith, Synergistic interaction in emulsions stabilized by a mixture of silica nanoparticles and cationic surfactant, *Langmuir*, 2007, **23**, 3626 – 3636.

[85] Z-G. Cui, L-L. Yang, Y-Z Cui and B. P. Binks, Effects of surfactant structure on the phase inversion of emulsions stabilized by mixtures of silica nanoparticles and cationic surfactant. *Langmuir*, 2010, **26**, 4717 – 4724.

[86] B. P. Binks and D. Yin, Pickering emulsions stabilized by hydrophilic nanoparticles: in situ modification by oil, *Soft Matter*, 2016, **12**, 6858 – 6867.

[87] R. Shrivastava and R.K. Mishra, Transport coefficients and validity of the Stokes-Einstein relation in metallic melts: From excess entropy scaling laws, *Chem. Phys.*, 2017, **493**, 115-119.

[88] M. Kaszuba, J. Corbett, F.M. Watson and A. Jones, High-concentration zeta potential measurements using light-scattering techniques, *Philos. Trans. A Math. Phys. Eng. Sci.*, 2010, **368**, 4439-4451.

[89] S.A. Matveev, A.P. Smirnov and E.E. Tyrtyshnikov, A fast numerical method for the Cauchy problem for the Smoluchowski equation, *J. Comput. Phys.*, 2015, **282**, 23 – 32.

[90] M. Perez, M. Dumont, D. Acevedo-Reyes., Implementation of classical nucleation and growth theories for precipitation, *Acta Mater*., 2008, **56**, 2119-2132.

[91] R. Sailer and G. McCarthy, North Dakota State University, USA, *ICDD Grant-in- Aid* (1992).

[92] F. Li, L. Ye, Y. Li and T. Wu, Investigation into the adsorption of partially hydrolyzed polyacrylamide onto in situ formed magnesium hydroxide particles, *RSC Adv.*, 2016, **6**, 31092.

[93] S. Budavri, *The Merck Index – Encyclopedia of Chemicals, Drugs and Biologicals*, Rahway, NJ: Merck and Co., Inc., 1989, 817-818.

[94] T. S. Horozov and B.P. Binks, Particle-stabilized emulsions: a bilayer or a bridging monolayer? *Angew. Chem. Int. Ed*., 2006, **45**, 773-776.

[95] N.P. Ashby and B.P. Binks, Pickering emulsions stabilised by laponite clay particles, *Phys. Chem. Chem. Phys.*, 2000, **2**, 5640 – 5646.

[96] B.P. Binks and C.P. Whitby, Temperature-dependent stability of water-in-undecanol emulsions, *Colloids Surf. A*, 2003, **224**, 241 – 249.

[97] J.A. Dean, Handbook of Organic Chemistry, McGraw-Hill, New York, 1987, 1-294.

[98] M.A.M. Oliveira, P.A. Melo, M. Nele and J.C. Pinto, Suspension copolymerization of vinyl acetate and methyl methacrylate in the presence of amoxicillin, *Macromol. React. Eng.*, 2012. **6**, 280 – 292.

[99] Y. Pei, J. Qin, X. Li, D. Zhang, K. Wang and Y. Liu, Experimental investigation on free and impingement spray fuelled with methanol, ethanol, isooctane, TRF and gasoline, *Fuel*, 2017, **208**, 174 – 183.

[100] M. Natalia and D.S. Cordeiro, Interfacial tension behaviour of water/ hydrocarbon liquid-liquid interfaces: A molecular dynamics simulation, *Molecular Simulations*, 2003, **29**, 817 – 827.

6. Appendix

Appendix 1. XRD pattern for magnesium hydroxide sample 1.

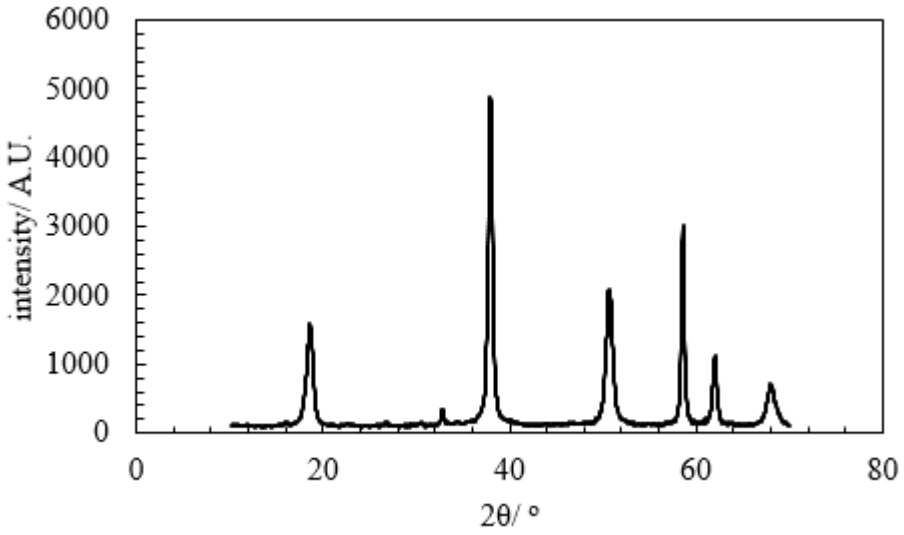

Appendix 2. XRD pattern for magnesium hydroxide sample 2.

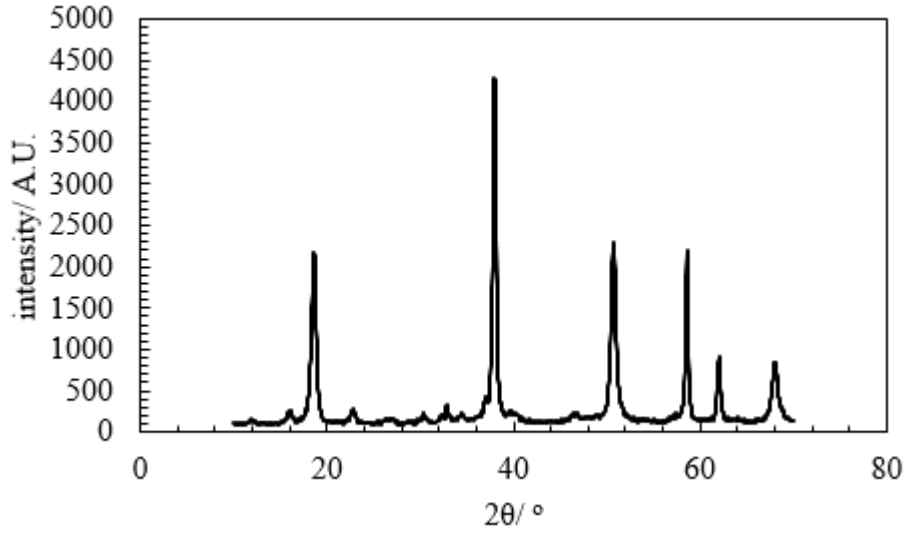

Appendix 3. XRD pattern for magnesium hydroxide sample 3.

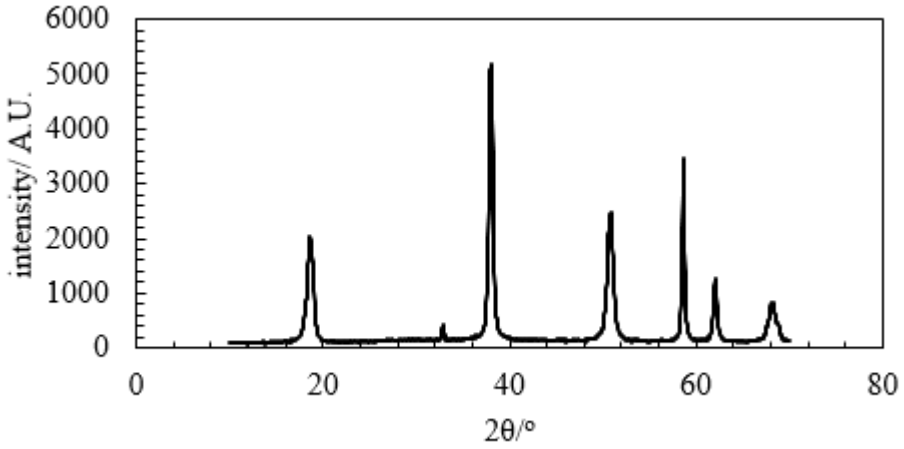

Appendix 4. XRD pattern for magnesium hydroxide sample 4.

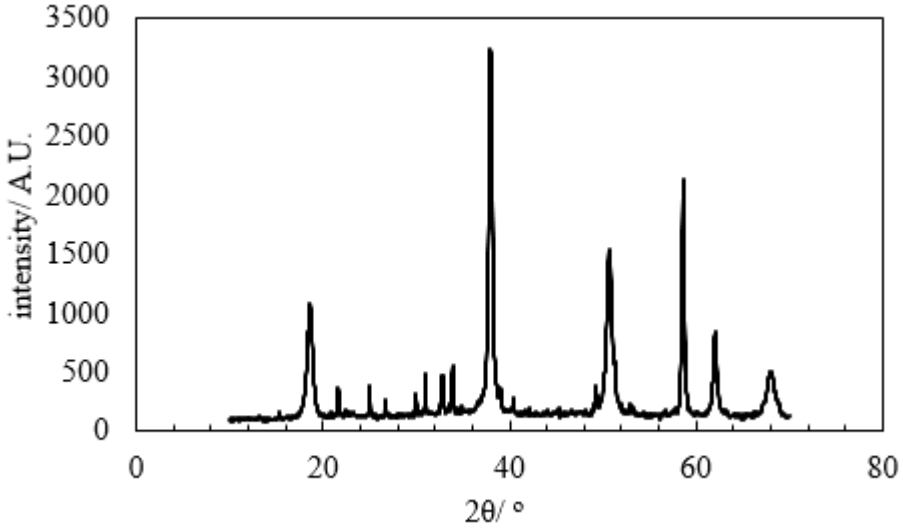

Appendix 5. XRD pattern for magnesium hydroxide sample 5.

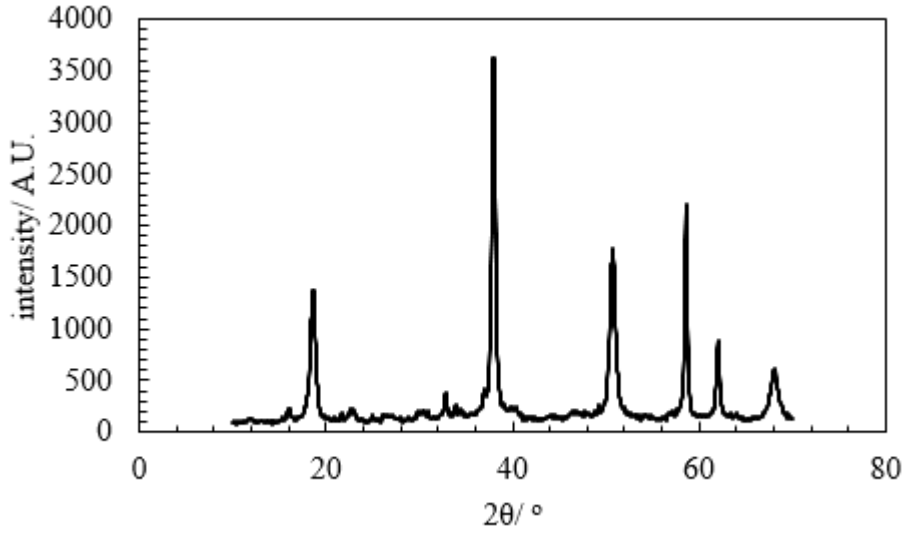

Appendix 6. XRD pattern for magnesium hydroxide sample 6.

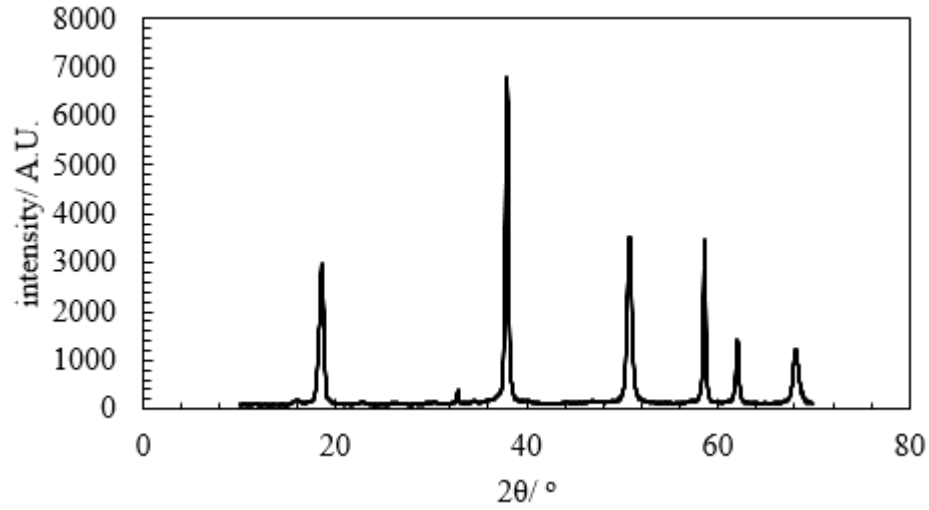

Appendix 7. XRD pattern for magnesium hydroxide sample 7.

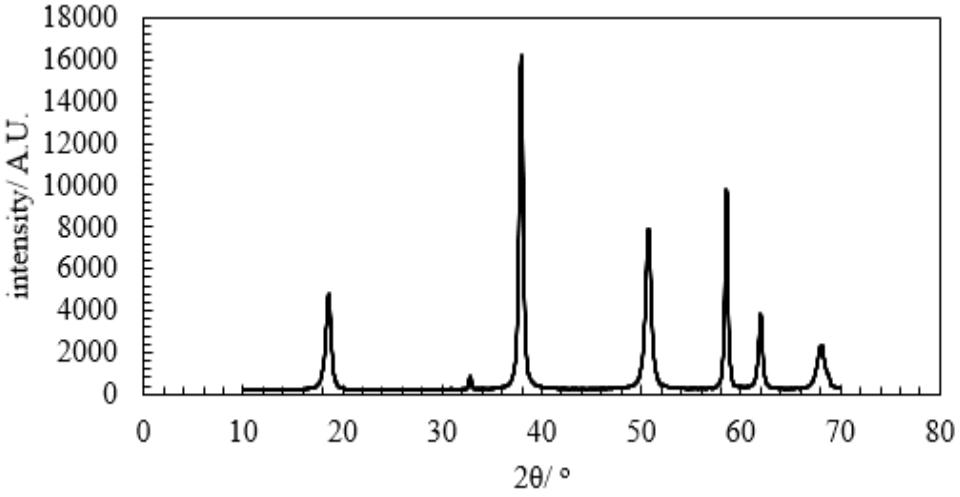

Appendix 8. XRD pattern for magnesium hydroxide sample 8.

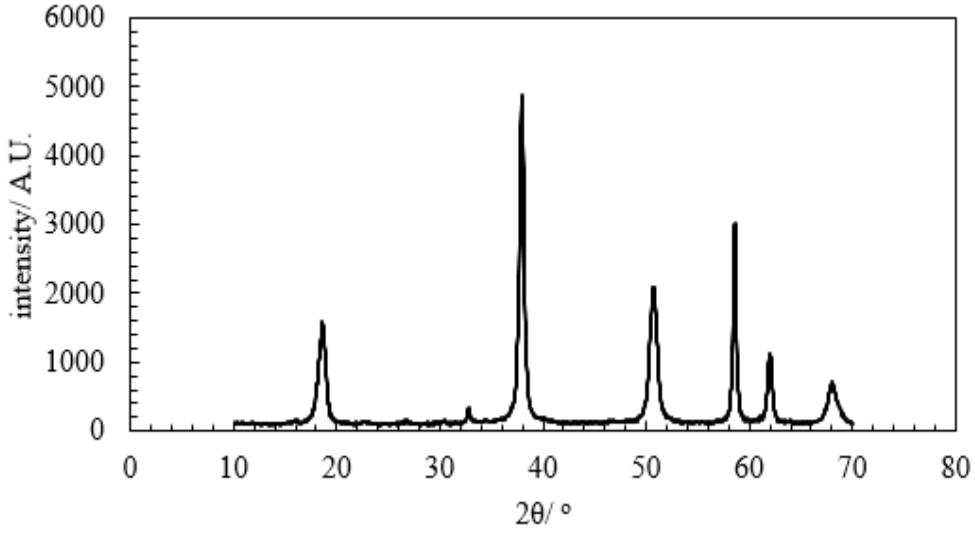

Appendix 9. XRD pattern for magnesium hydroxide sample 9.

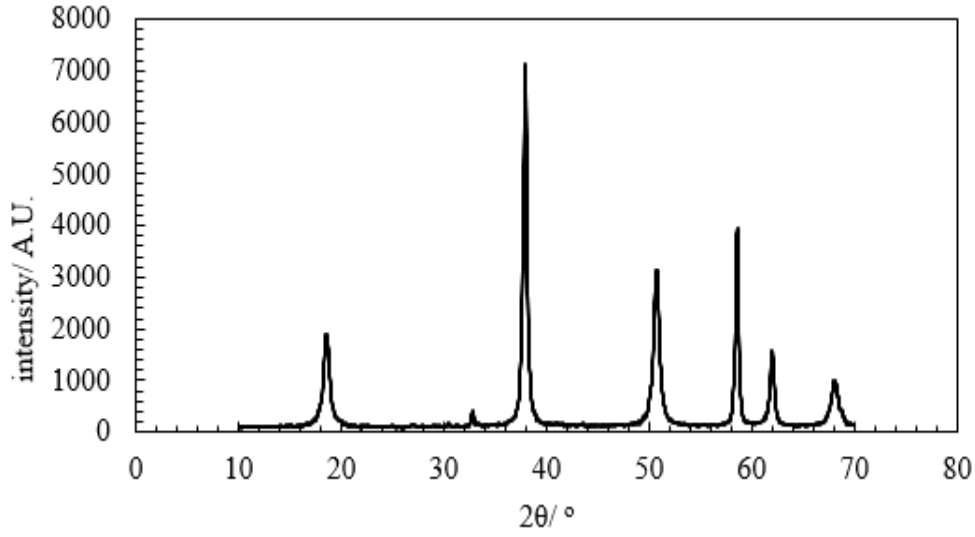

Appendix 10. XRD pattern for magnesium hydroxide sample 10.

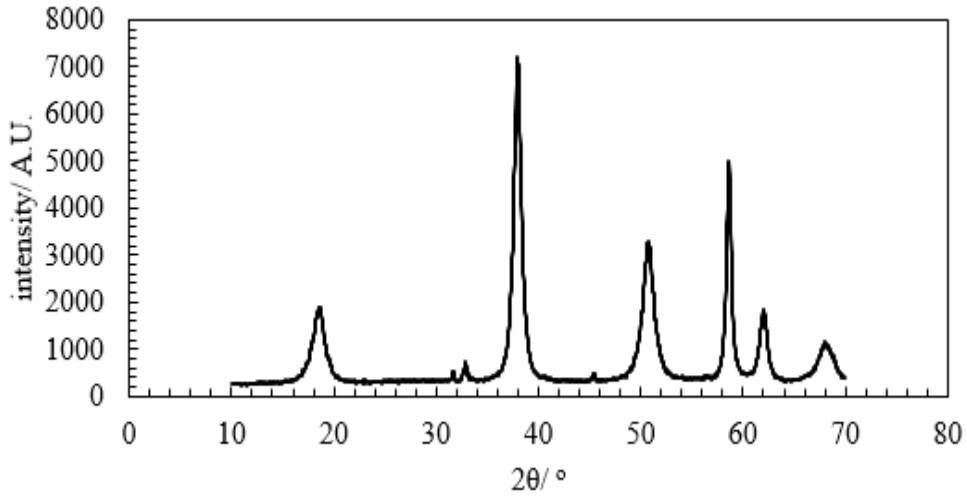

Appendix 11. XRD pattern for magnesium hydroxide sample 11.

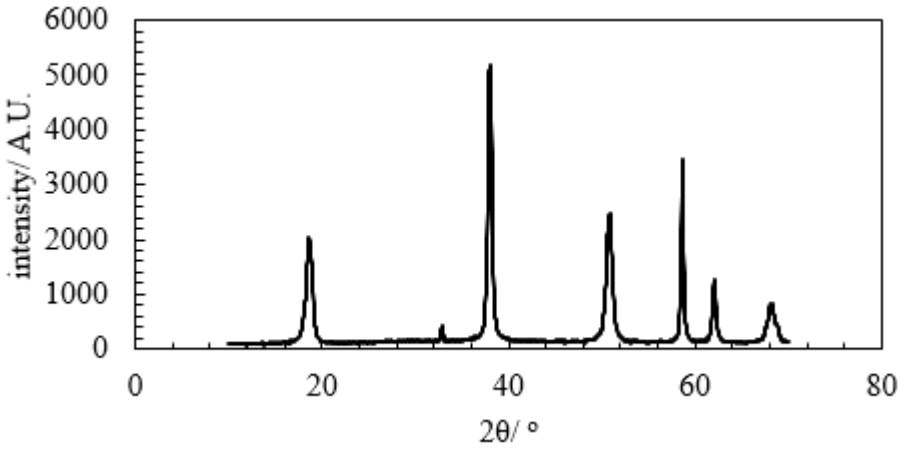

Appendix 12. XRD pattern for magnesium hydroxide sample 12.

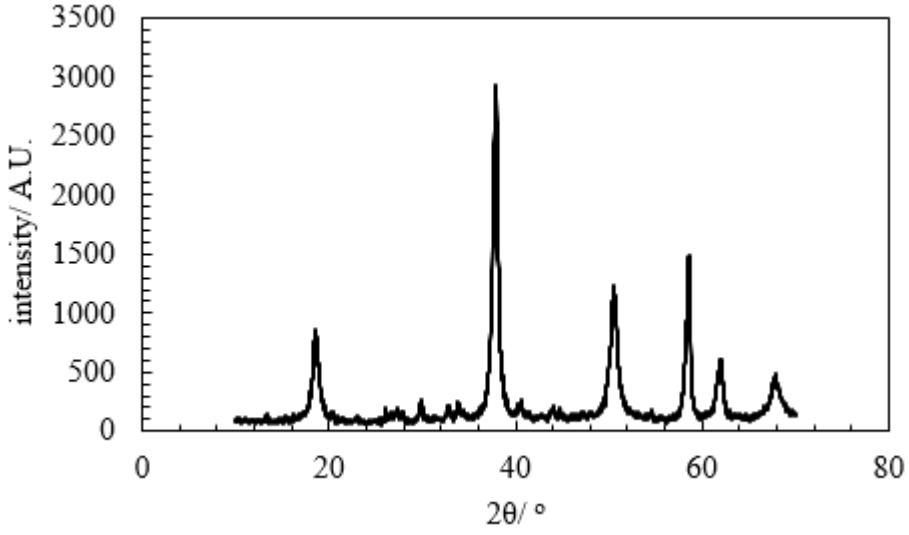

Appendix 13. XRD pattern for magnesium hydroxide sample 13.

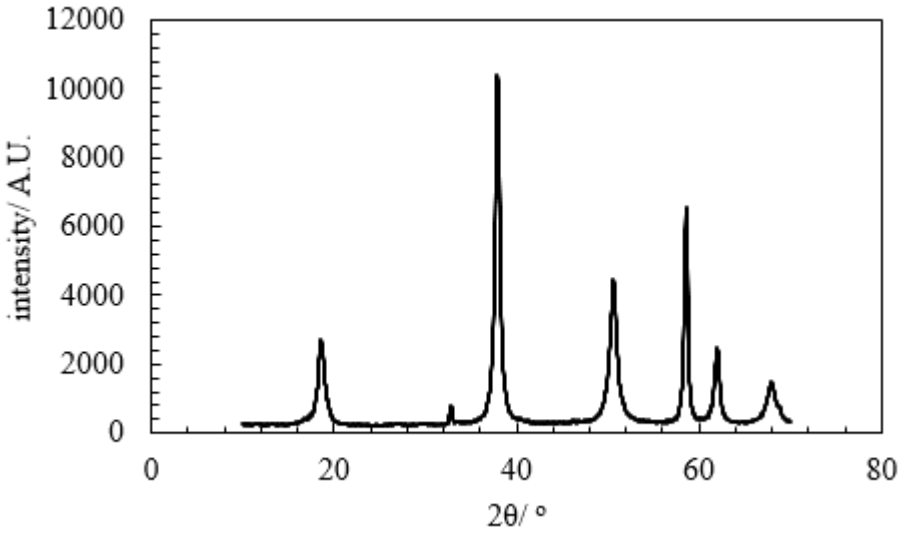

Appendix 14. XRD pattern for magnesium hydroxide sample 14.

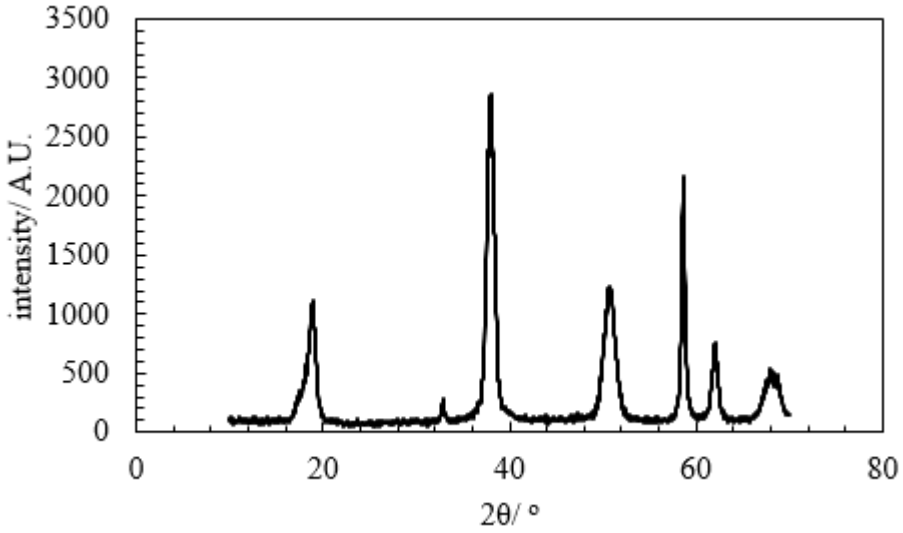

Appendix 15. XRD pattern for magnesium hydroxide sample 15.

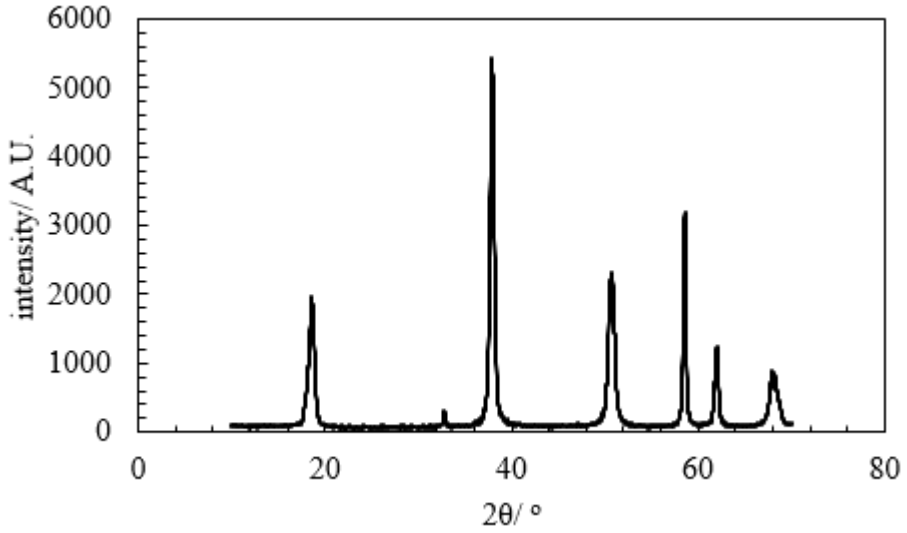

Appendix 16. XRD pattern for magnesium hydroxide sample 16.

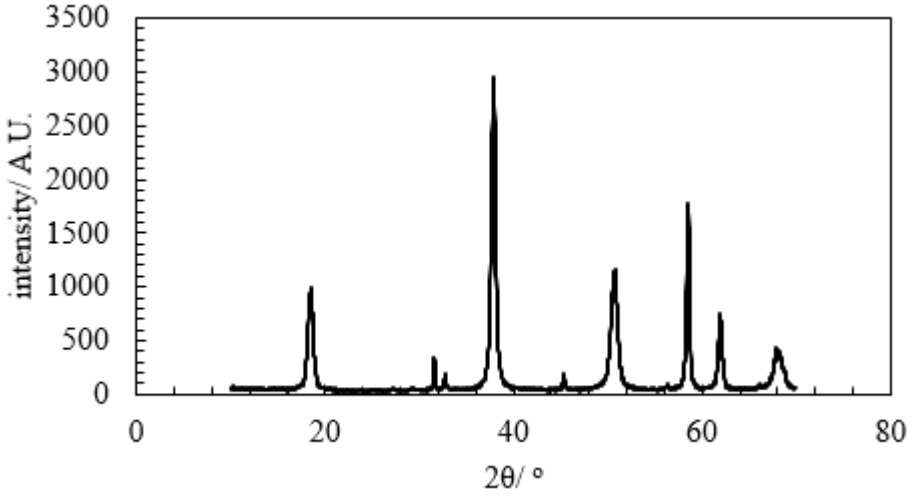

Appendix 17. XRD pattern for magnesium hydroxide sample 17.

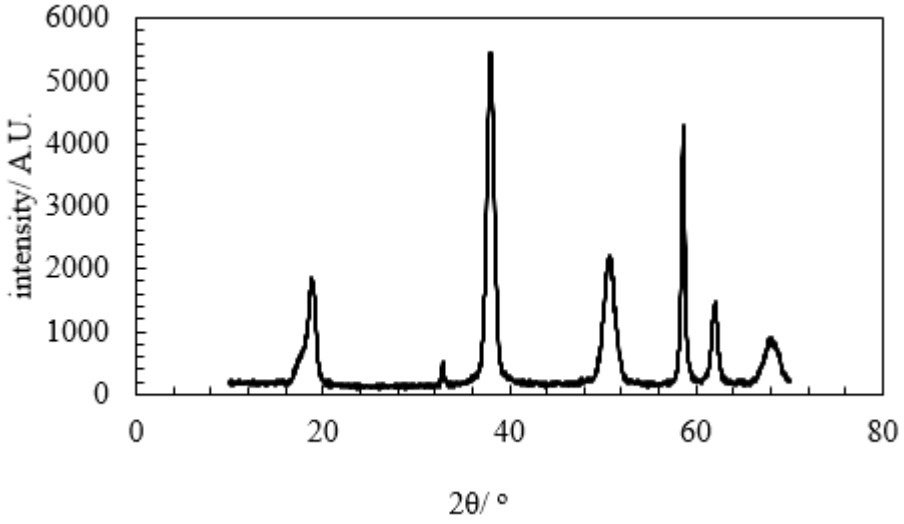

Appendix 18. XRD pattern for magnesium hydroxide sample 18.

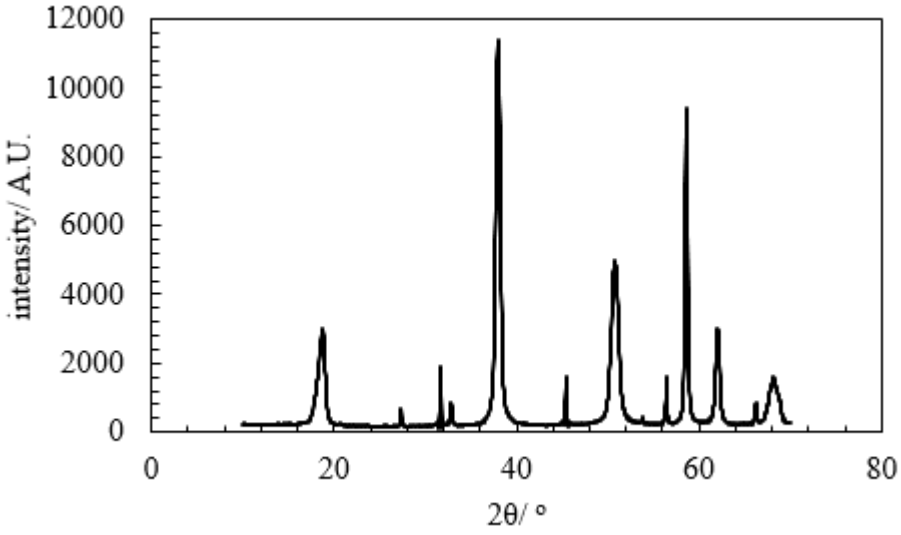

Appendix 19. XRD pattern for magnesium hydroxide sample 19.

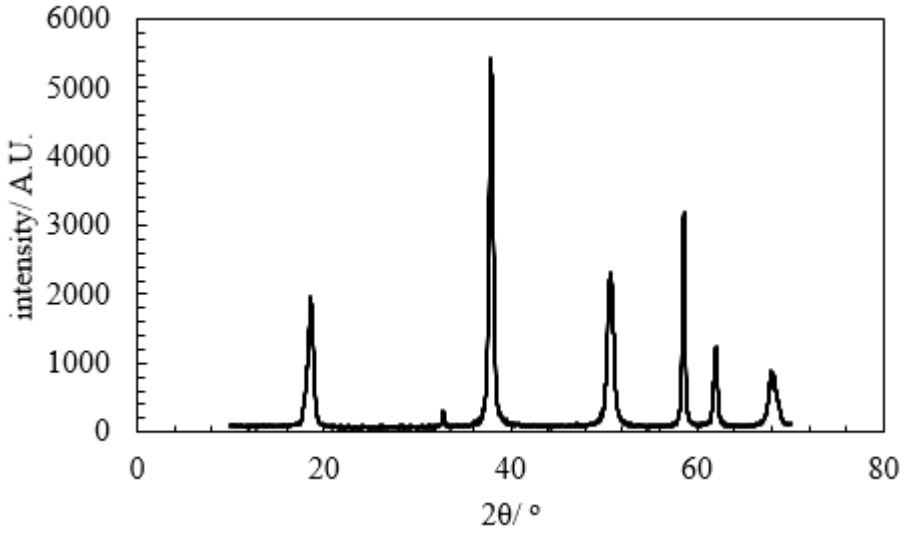

Appendix 20. XRD pattern for magnesium hydroxide sample 20.

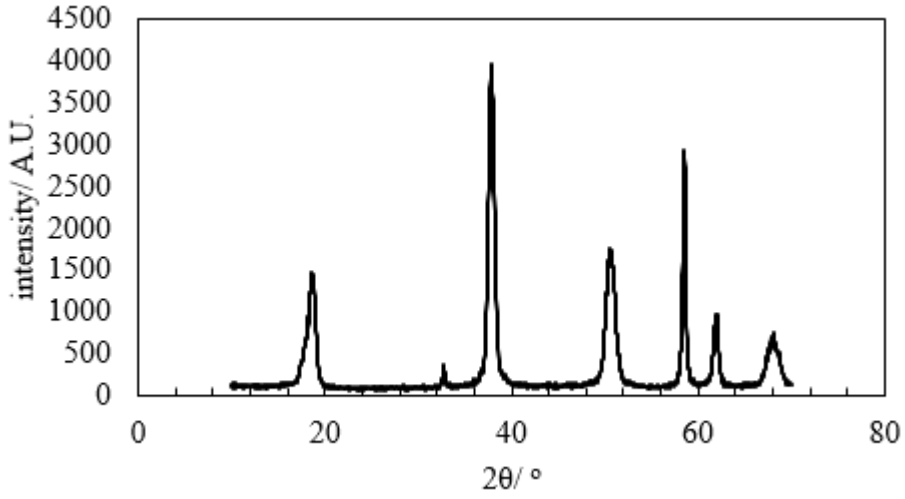

Appendix 21. XRD pattern for magnesium hydroxide sample 21.

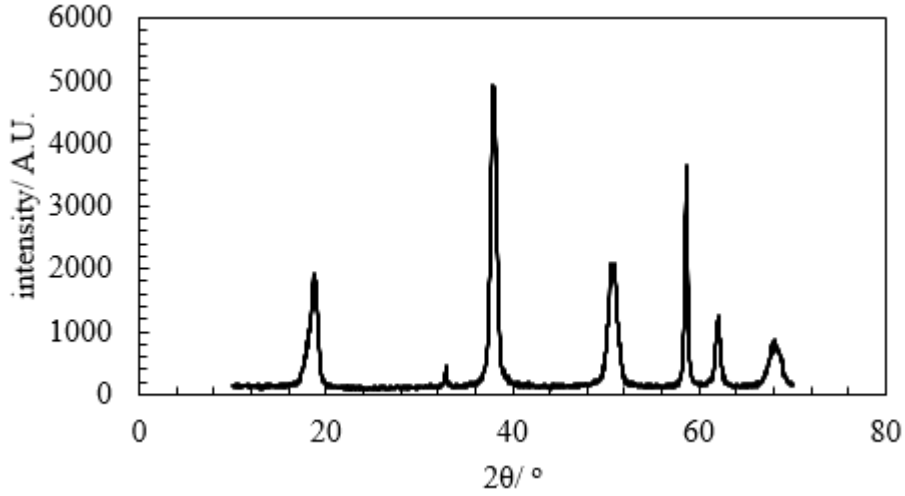

Appendix 22. XRD pattern for magnesium hydroxide sample 22.

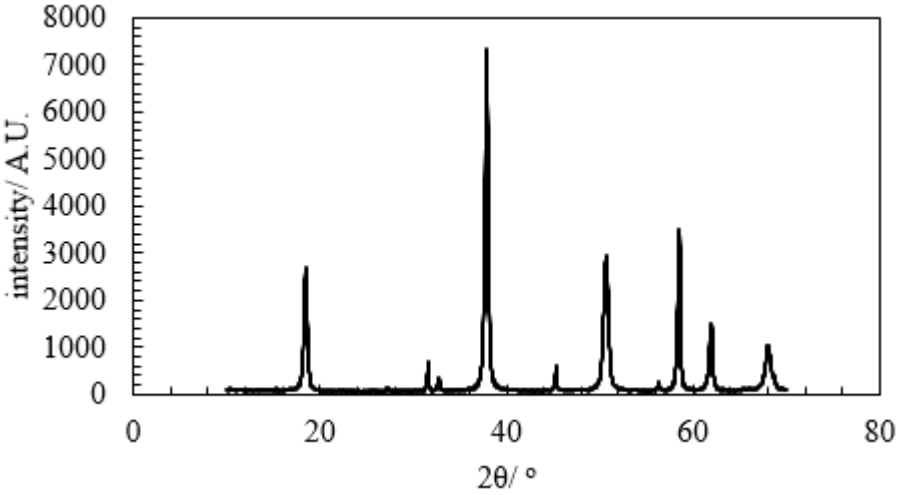

Appendix 23. XRD pattern of magnesium hydroxide sample 23.

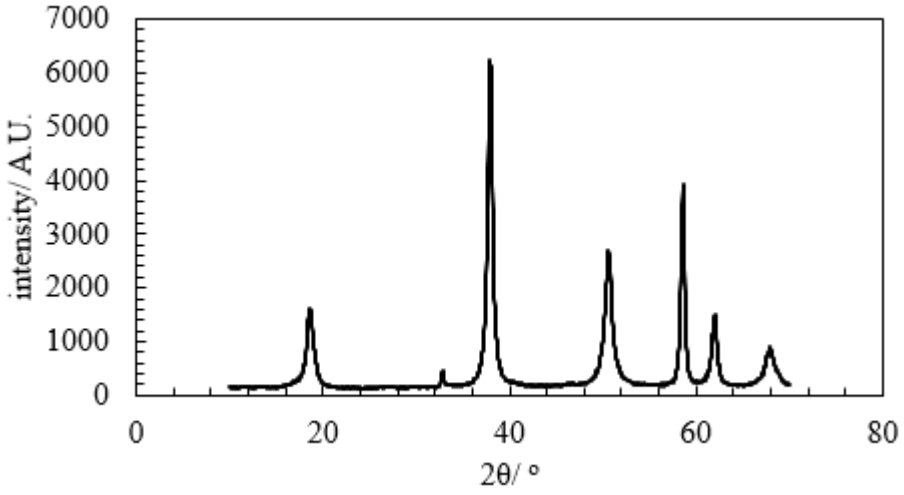

Appendix 24. XRD pattern of magnesium hydroxide sample 24.

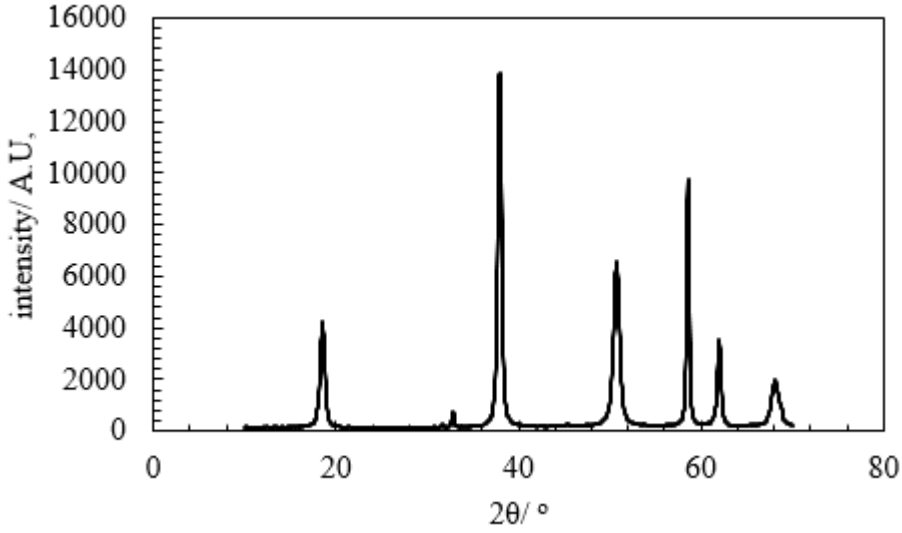

Appendix 25. XRD pattern for magnesium hydroxide sample 25.

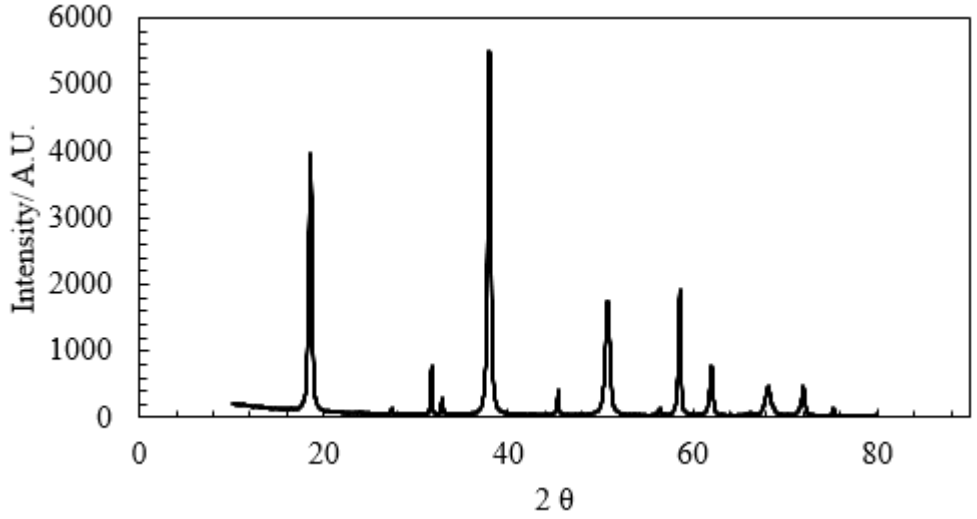

Appendix 26. XRD pattern for magnesium hydroxide sample 26.

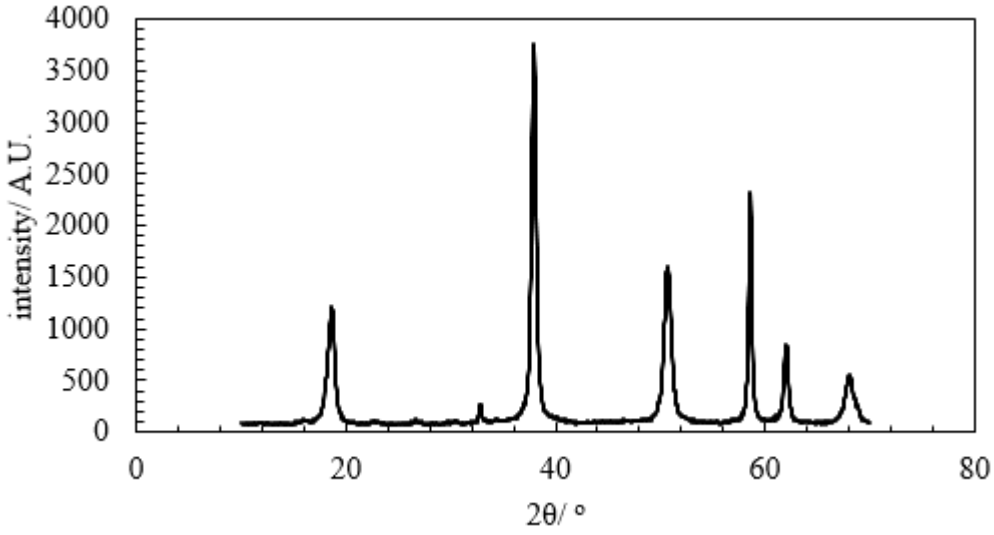

Appendix 27. FT-IR spectrum of magnesium hydroxide sample 1.

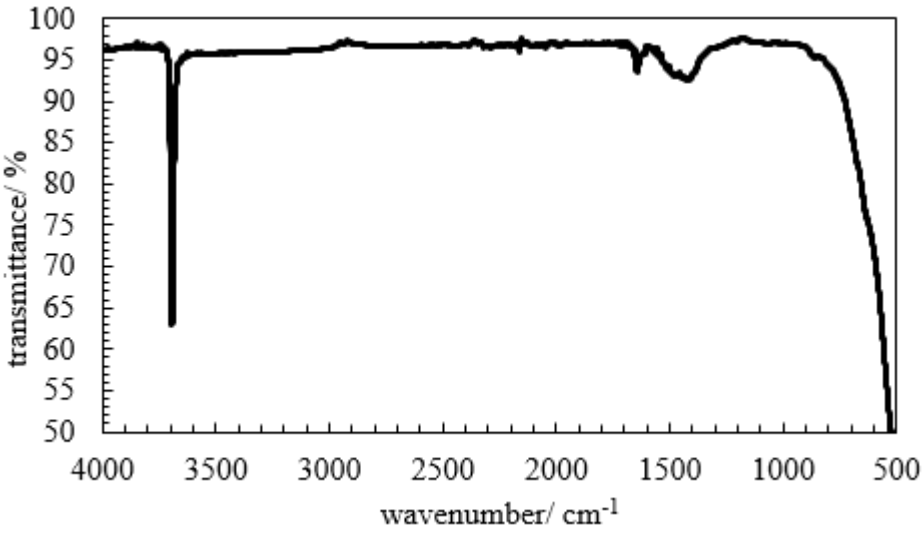

Appendix 28. FT-IR spectrum of magnesium hydroxide sample 2.

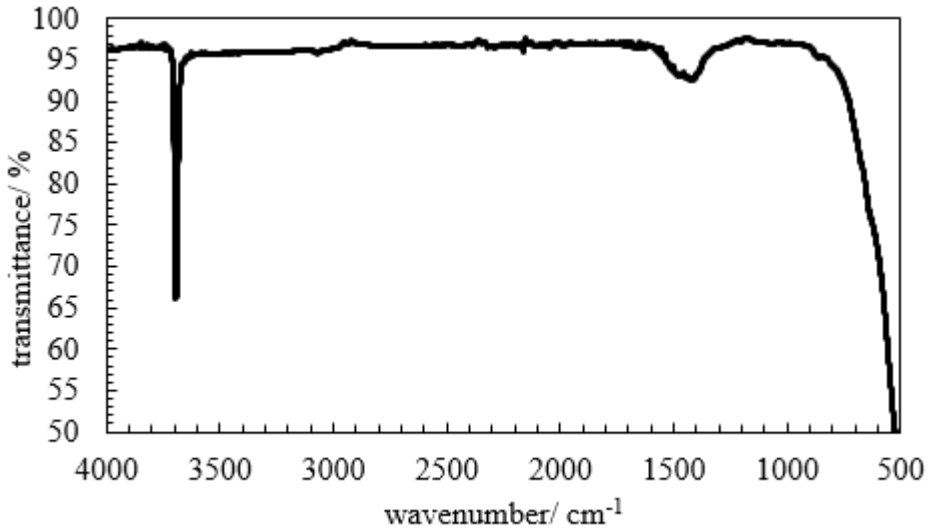

Appendix 29. FT-IR spectrum of magnesium hydroxide sample 3.

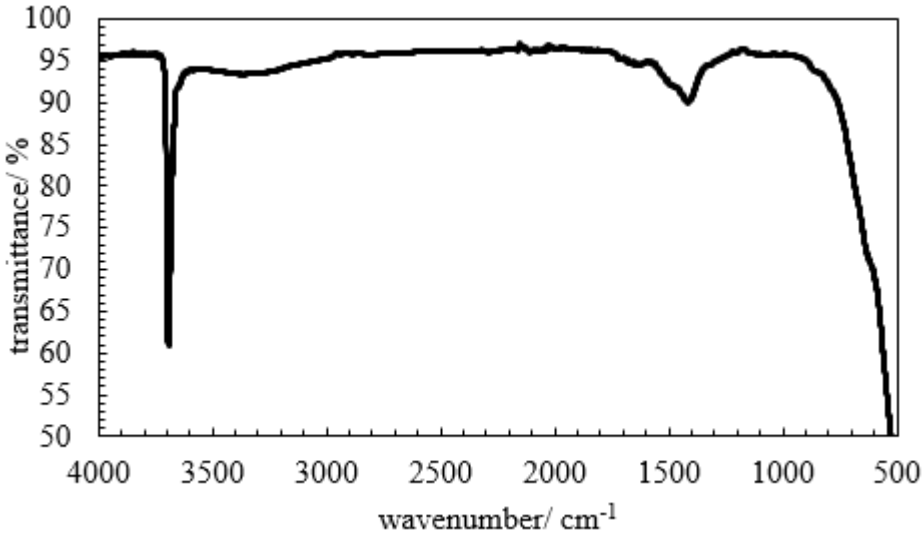

Appendix 30. FT-IR spectrum of magnesium hydroxide sample 4.

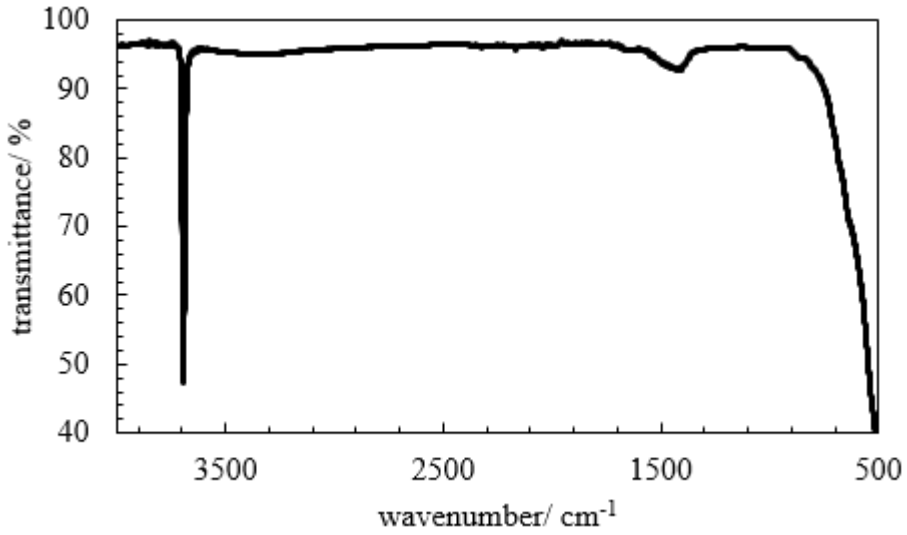

Appendix 31. FT-IR spectrum of magnesium hydroxide sample 5.

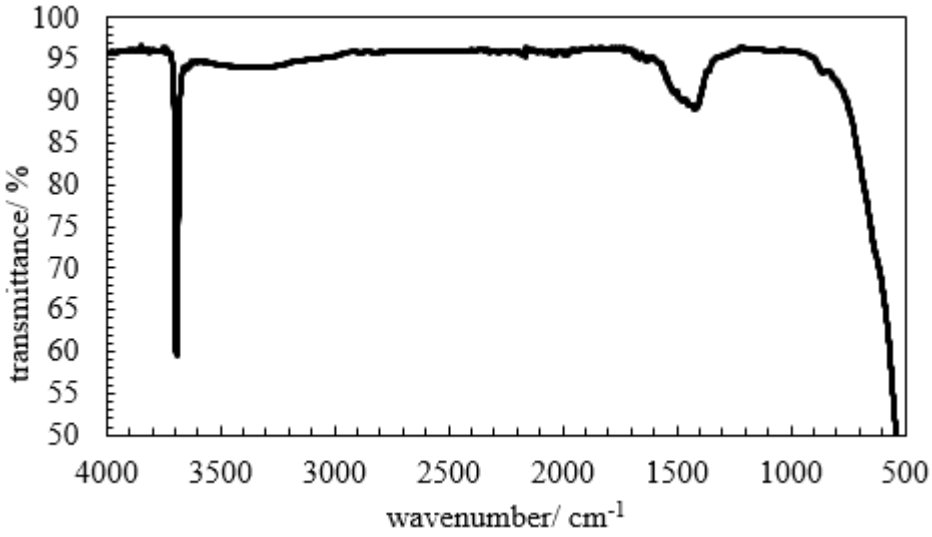

Appendix 32. FT-IR spectrum of magnesium hydroxide sample 6.

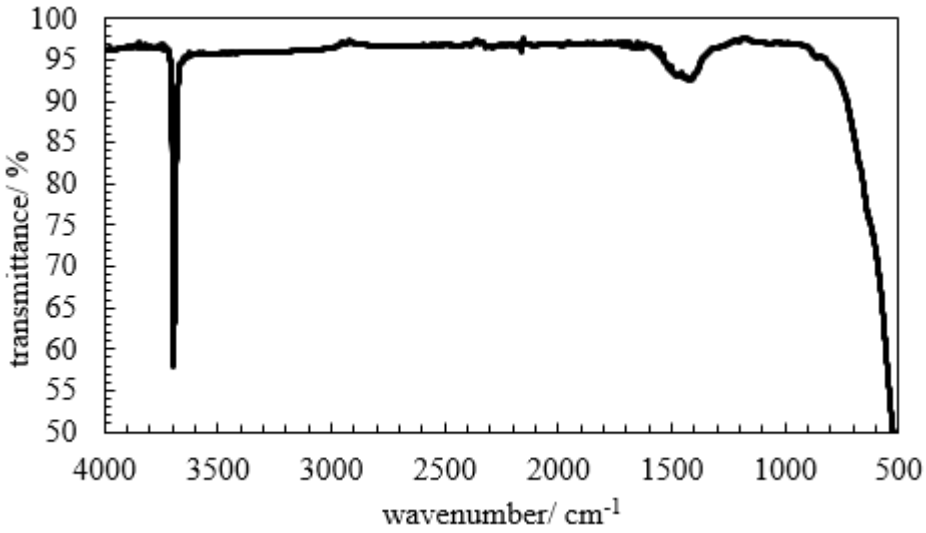

Appendix 33. FT-IR Spectrum of magnesium hydroxide sample 7.

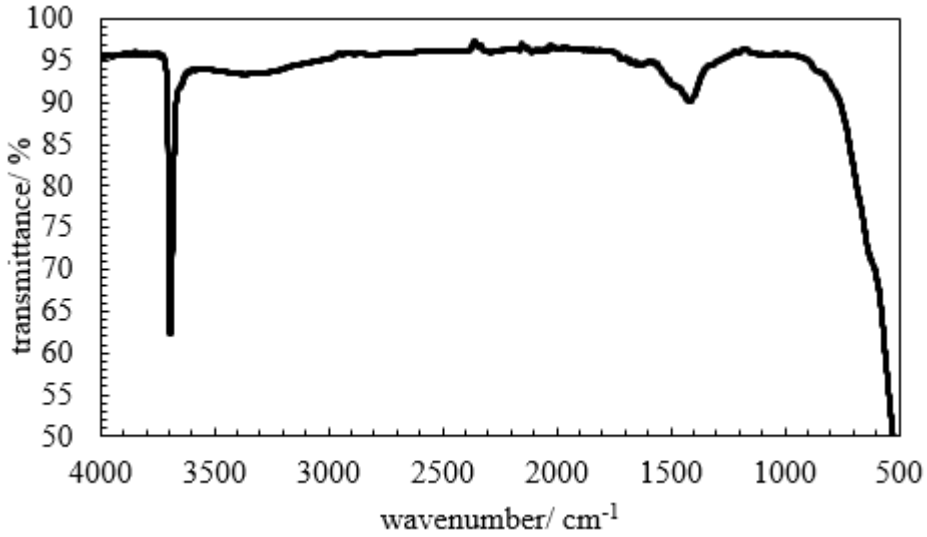

Appendix 34. FT-IR spectrum of magnesium hydroxide sample 8.

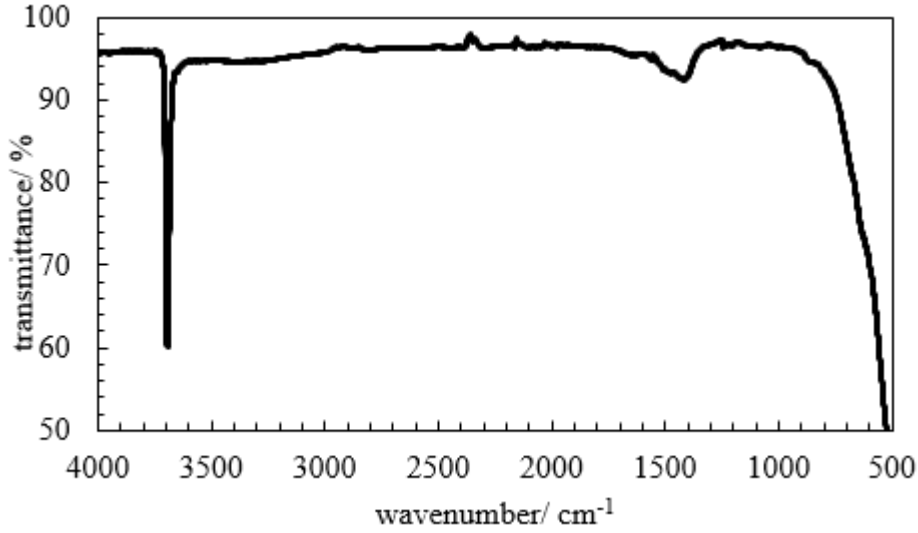

Appendix 35. FT-IR spectrum of magnesium hydroxide sample 9.

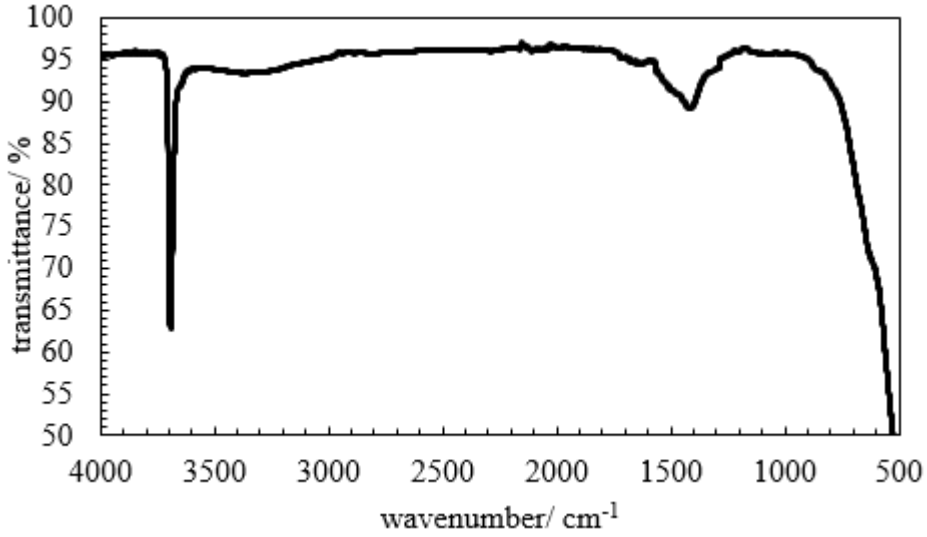

Appendix 36. FT-IR spectrum of magnesium hydroxide sample 10.

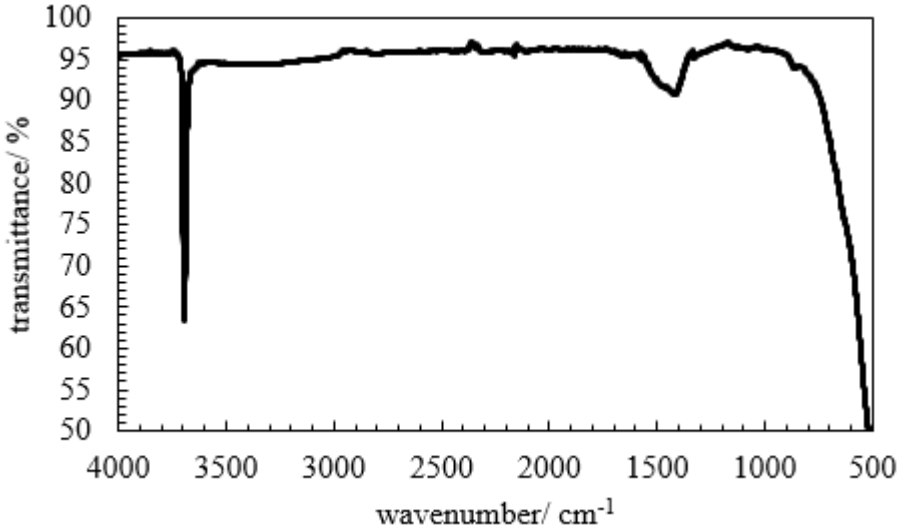

Appendix 37. FT-IR spectrum of magnesium hydroxide sample 11.

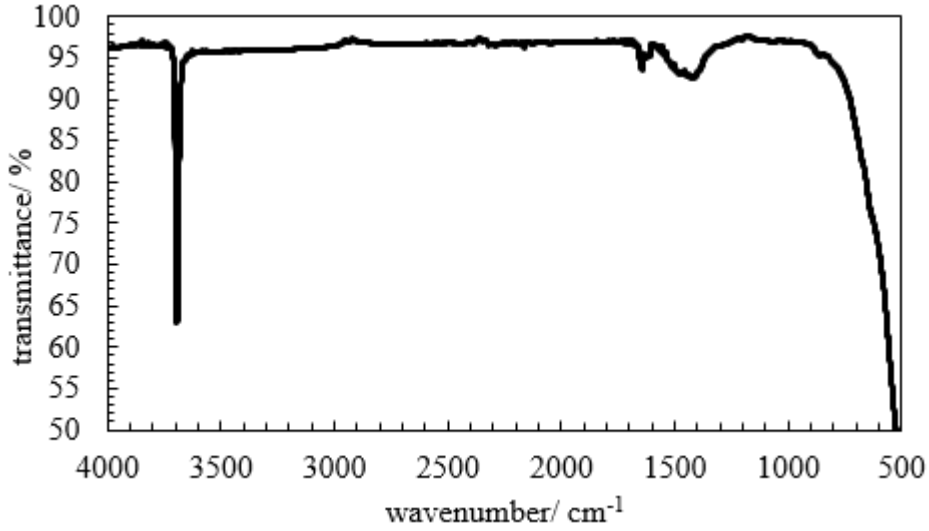

Appendix 38. FT-IR spectrum of magnesium hydroxide sample 12.

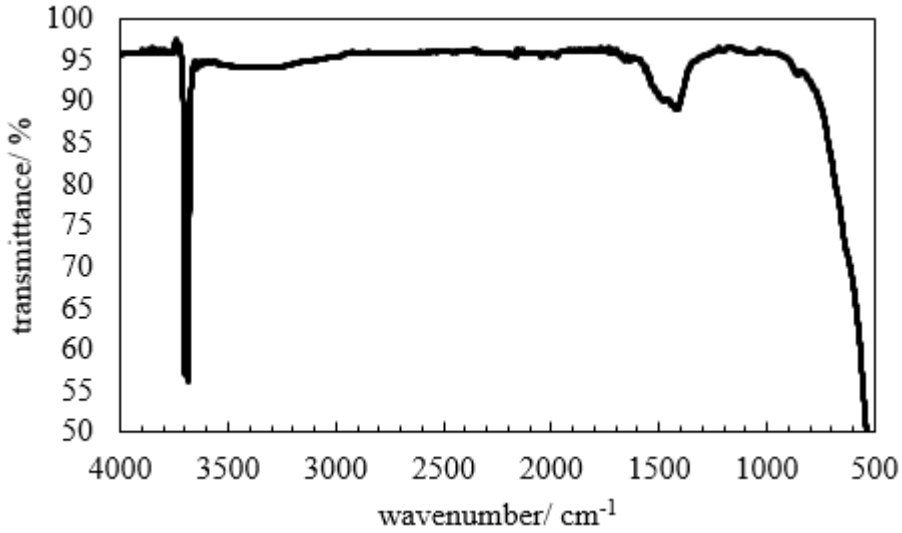

Appendix 39. FT-IR spectrum of magnesium hydroxide sample 13.

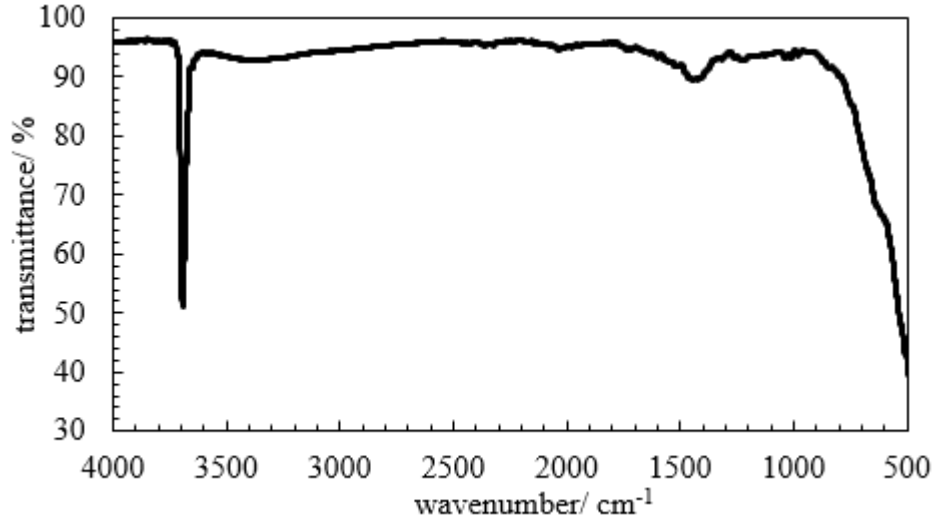

Appendix 40. FT-IR spectrum of magnesium hydroxide sample 14.

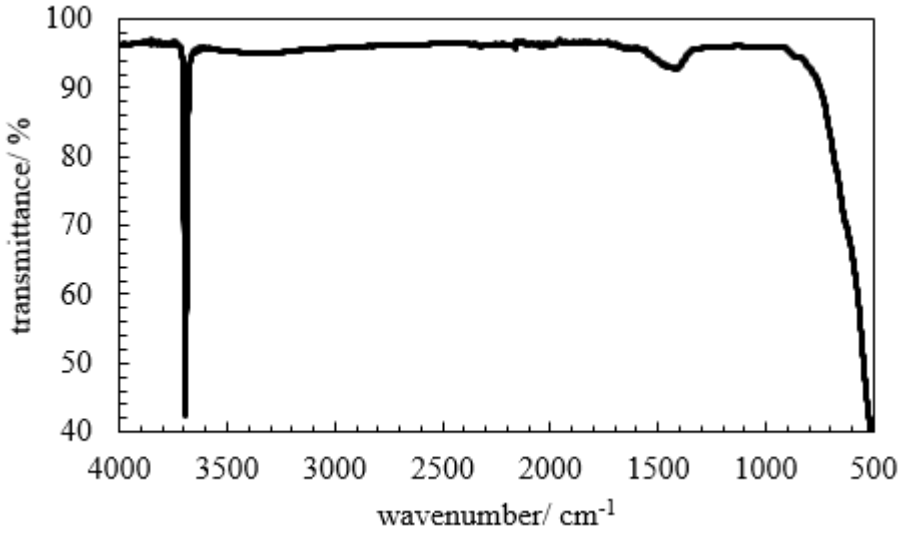

Appendix 41. FT-IR spectrum of magnesium hydroxide sample 15.

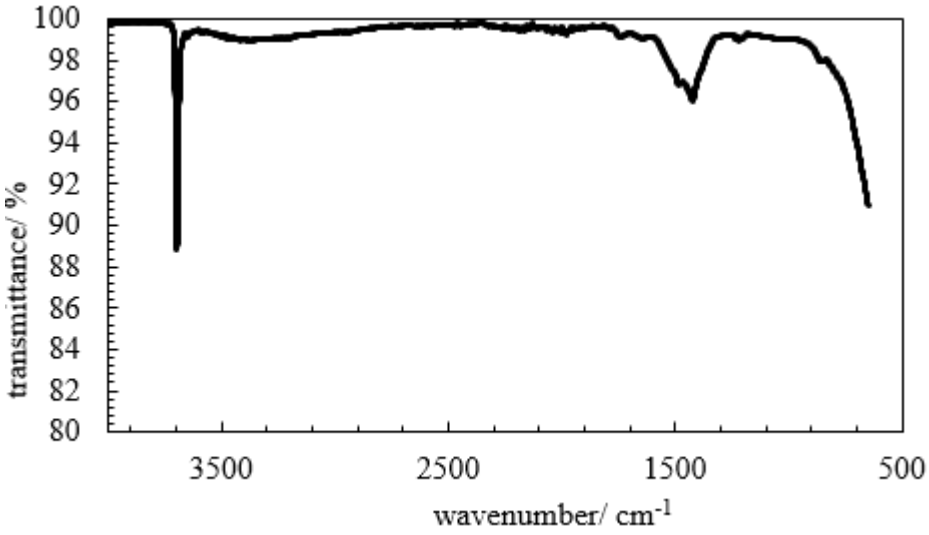

Appendix 42. FT-IR spectrum for magnesium hydroxide sample 16.

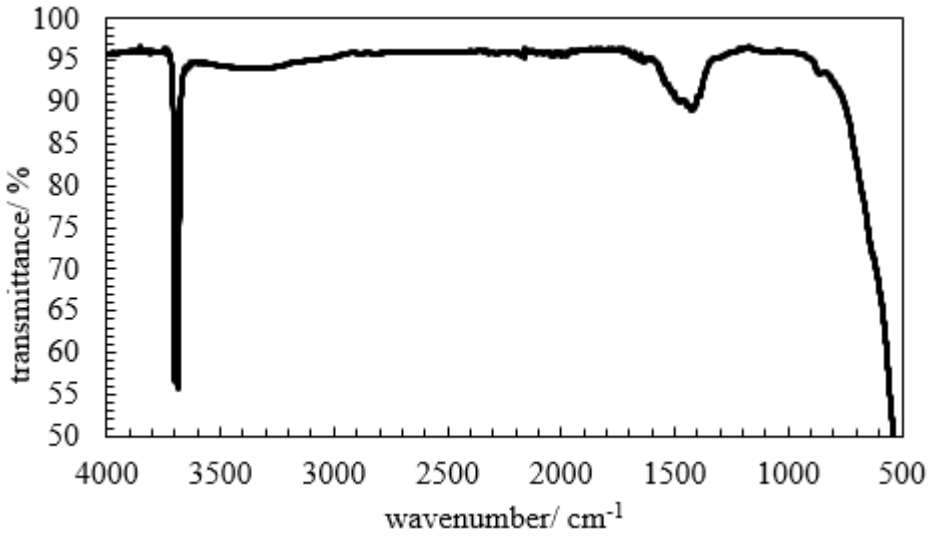

Appendix 43. FT-IR spectrum for magnesium hydroxide sample 17.

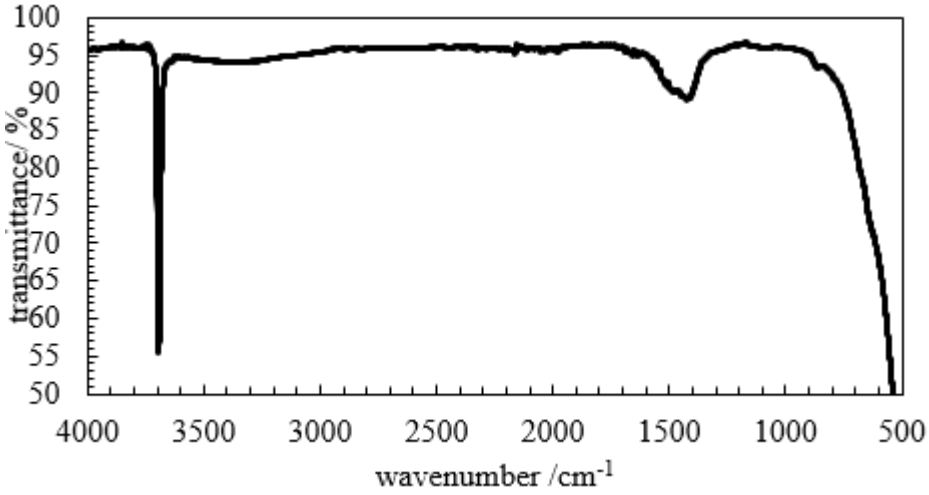

Appendix 44. FT-IR spectrum for magnesium hydroxide sample 18.

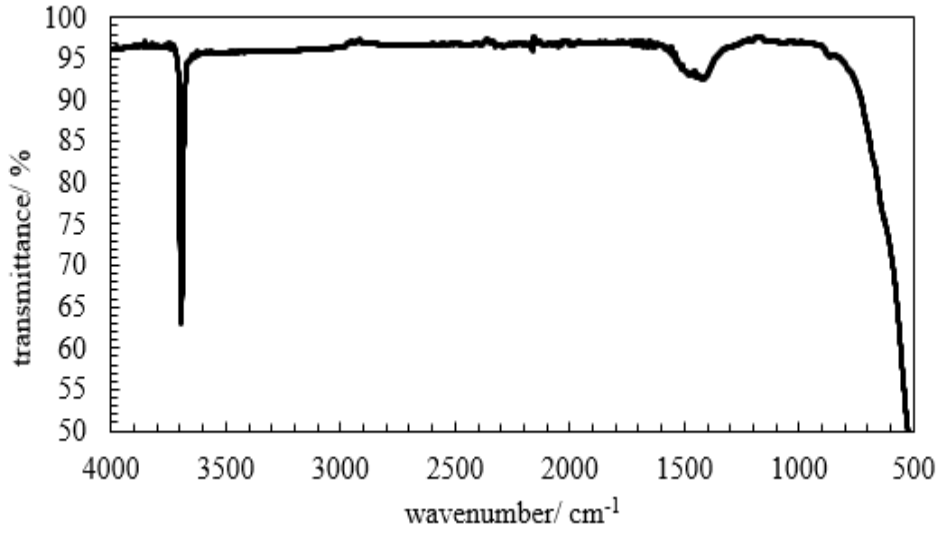

Appendix 45. FT-IR spectrum for magnesium hydroxide sample 19.

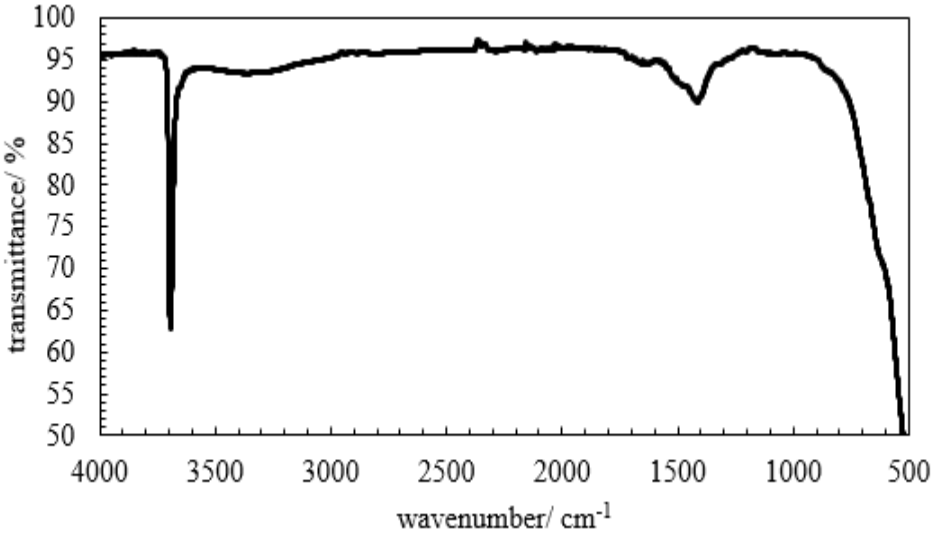

Appendix 46. FT-IR spectrum for magnesium hydroxide sample 20.

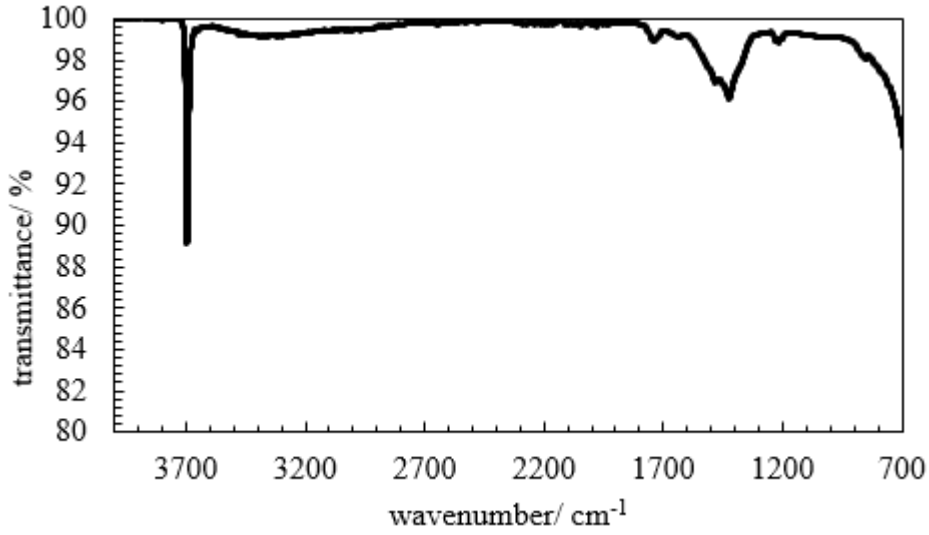

Appendix 47. FT-IR spectrum for magnesium hydroxide sample 21.

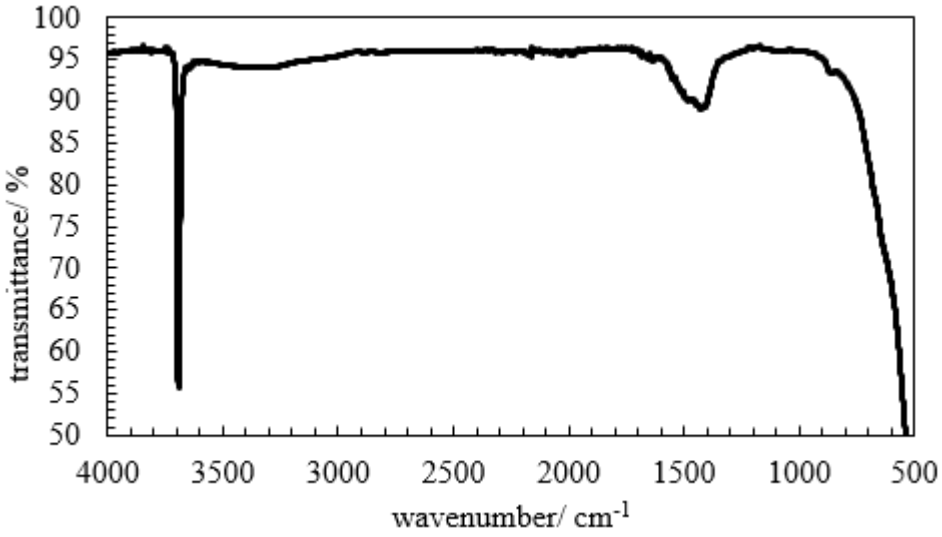

Appendix 48. FT-IR spectrum for magnesium hydroxide sample 22.

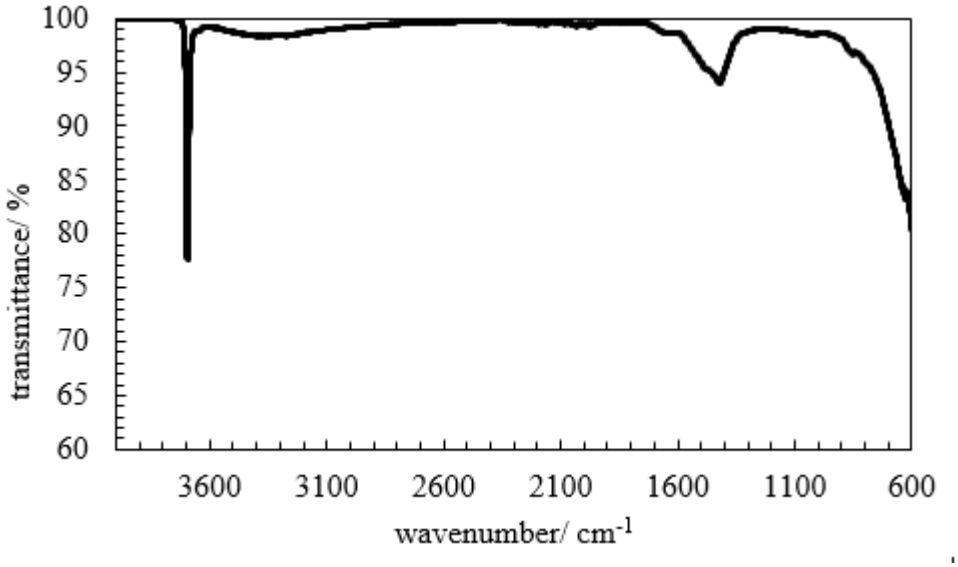

Appendix 49. FT-IR spectrum for magnesium hydroxide sample 23.

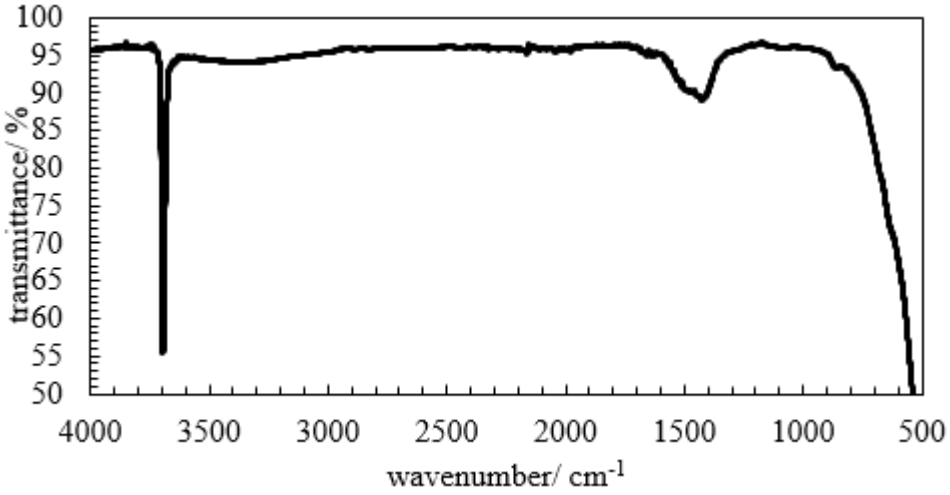

Appendix 50. FT-IR spectrum for magnesium hydroxide sample 24.

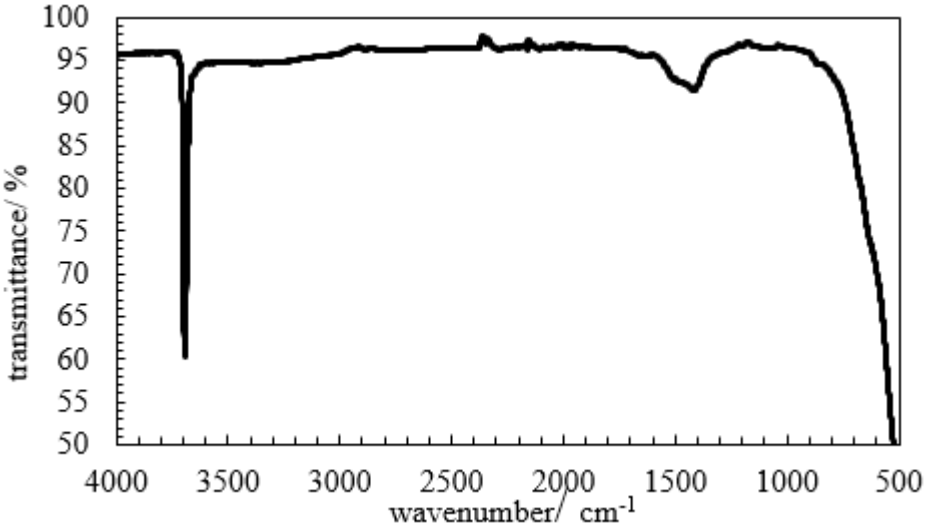

Appendix 51. FT-IR spectrum for magnesium hydroxide sample 25.

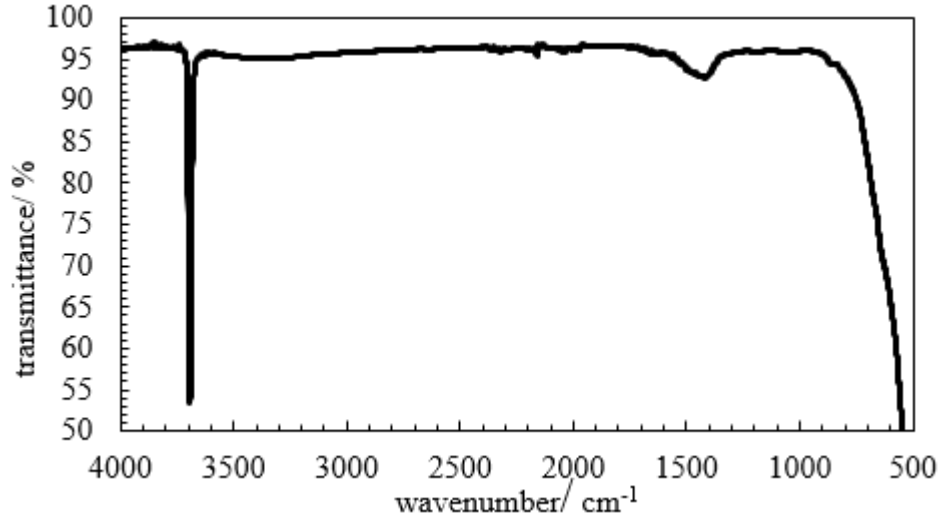

Appendix 52. FT-IR spectrum for magnesium hydroxide sample 26.